REMOTE SENSING AND GIS-BASED ANALYSIS OF HYDROCARBON SEEPS: DETECTION, MAPPING, AND QUANTIFICATION

Dissertation

Zur Erlangung des

Doktorgrades der Naturwissenschaften

(Dr. rer. Nat.)

dem Fachbereich Geowissenschaften

der Universität Bremen

vorgelegt von

Jan-Hendrik Körber

Bremen, Juli 2012

1. Gutachter: Prof. Dr. Gerhard Bohrmann

2. Gutachter: Prof. Dr. Heinrich Villinger

Preface

The research for this thesis was conducted at the 'Marum – Center for Marine Environmental Sciences' and the Department of Geosciences of the University of Bremen. The PhD project was part of the Marum project 'Geo-Biosphere Interactions (GB) 5 – Linking benthic fluxes and ecology of the ocean floor' which is carried out in close cooperation with project 'GB 4 – Structure and dynamic of cold seeps'. Support for conference participations and further education beyond the topic of the thesis was provided by the Bremen International Graduate School for Marine Sciences 'Global Change in the Marine Realm' (GLOMAR). The thesis was started in August 2009, and initially focused on the geophysical and optical mapping of cold seep structures and associated biological communities. The data used for this initial work was acquired during R/V METEOR cruise M74/3 to the Makran accretionary margin offshore Pakistan in 2007. From 2010 on the PhD project focused on exploring the capabilities of satellite imagery to detect oil seeps in the Black Sea. A first introduction to the applied satellite techniques was provided by Prof. Ian MacDonald and Dr. Oscar Garcia-Pineda at the Florida State University, Tallahassee. The satellite images used in this thesis were provided by the European Space Agency within project C1.P7157 which is carried out in cooperation with the Department of Environmental Physics of the University of Bremen. Results of the satellite data analysis were groundtruthed during research cruises with R/V MARIA S. MERIAN (2010) and R/V METEOR (2011) in the eastern Black Sea.

The thesis comprises five chapters. The first chapter provides an introduction to cold seeps and seepage in general. Chapter 2 presents the motivation for and main objectives of the thesis. In Chapter 3, a general overview on satellite and hydroacoustic remote sensing techniques used for the identification and investigation of cold seeps is given. This chapter is followed by a brief introduction to the two study areas this work focused on – the Makran accretionary margin and the Black Sea. Chapter 5 presents the first case study which deals with the methane budget of a cold seep offshore Pakistan, and geological controls of seepage at this site. The sixth chapter presents the second case study. It details seepage processes at two prolific oil seeps in the Black Sea, including estimates of seepage rates and persistency of seepage. The third case study of this work is presented in Chapter 7. It provides an inventory of oil seeps in the Black Sea and an interpretation of geological processes controlling seepage occurrence and variability. The thesis closes with a summary of the main results and perspectives on future work.

Contents

Abbreviations

AOM	Anaerobic oxidation of methane
ASAR	Advanced Synthetic Aperture Radar
AUV	Autonomous underwater vehicle
avi	Audio video interleave
bsl	Below sea level
BSR	Bottom simulating reflector
C_{2+}	Hydrocarbons higher than methane
CH_4	Methane
cmbsf	Centimeter below seafloor
d	Day
$\delta^{13}C$	Carbon stable isotope ratio
δD	Hydrogen stable isotope ratio
°C	Degree Celsius (SI Temperature unit)
EM122	12 kHz echosounder (Kongsberg Maritime ASA)
ESA	European Space Agency
Fig.	Figure
g, Tg	gram, Teragram (10^{12} grams)
GC	Gravity core
geoTIFF	Georeferenced tagged image file format
GHSZ	Gas hydrate stability zone
GIS	Geographic information system
HLS	Horizontally looking sonar
Hz, kHz	Hertz, Kilohertz, SI frequency unit
km^2	Square kilometer
kmbsl	Kilometer below sea level
l	Liter
m^2, m^3	Square meter, cubic meter
MBES	Multibeam echosounder
mbsl	Meter below sea level
MDAC	Methane derived authigenic carbonate
min	Minute
OMZ	Oxygen minimum zone
OSO	Oil slick origin
%, ‰	Percent, per mil
PHF	Primary high frequency
ppb	Parts per billion
ppm	Parts per million
ROV	Remotely operated vehicle
SAR	Synthetic aperture radar
sI	Structure I gas hydrate
sII	Structure II gas hydrate
SLAR	Side-looking aperture radar
SLF	Secondary low frequency
SMOW	Standard mean ocean water
TV-grab	Camera-guided sediment sampling tool
Gt	Gigaton
V-PDB	Vienna-Bee Dee Belemnite
yr, kyrs	Year, 1000 years

Abstract

The aim of this thesis is to contribute to a better understanding of the relevance of deep-sea hydrocarbon seeps in shallow water and atmospheric methane concentrations, and climate. For the detection, detailed mapping, and quantification of hydrocarbon emissions from such seeps, a variety of ship and satellite based methods were employed. These methods are, in this combination, not yet established in marine seep research. On local scale, the relevance of dissolved methane fluxes versus gas bubble fluxes was assessed. On regional scale, new hydrocarbon seeps were identified by satellite imagery. Flux rates and seepage activity were investigated using satellite images as a first approach. The fate of hydrocarbons injected to the hydrosphere was investigated using multibeam echosounder.

The first case study was conducted at the Makran accretionary margin offshore Pakistan at a seep site in 1,025 m depth. A combination of remotely operated vehicle (ROV) -based high-frequency sonar seafloor mapping and video-mosaicking allowed to precisely determine the area of active seepage and occurrence of distinct habitats of chemosynthetic communities. These data served as the base to extrapolate turnover rates of dissolved methane. These were compared to the volume of methane discharged to the hydrosphere as gas bubbles, providing a methane budget for the entire seep area. The results indicate that bubble transport of hydrocarbons to the hydrosphere is by far more important than the flux of dissolved gases. According to current literature, this was only the second study to present a detailed areal methane budget for a deep-sea seep area. Methane that is transferred from the seabed to the hydrosphere might reach the atmosphere by diffusion or bubble flux. To better constrain the volumes of methane that are injected to the water column, the assessment of methane budgets for entire seep areas is crucial. So far, areal flux extrapolations largely rely on local measurements of dissolved or bubble-gas discharge which do not consider areal variations of fluxes. In order to obtain more realistic methane budgets for seepage areas, the here presented combination of hydroacoustic and optical mapping, complemented by local sampling and flux determinations is suggested as primary tool for future investigations of seeps and related methane budget assessments.

While the first study highlighted the importance of gas bubble emissions for the transfer of methane to the hydrosphere two other case studies, conducted in the Black Sea, investigated the transfer of bubbles towards the atmosphere. In contrast to the Makran accretionary margin, the Black Sea has passive margins and is largely anoxic due to limited exchange with the world ocean and methane oxidation. Therefore, deep-water seeps are devoid of higher life in the Black Sea, and the only biological process reducing the discharge of methane to the hydrosphere is the anaerobic oxidation of methane. Gas bubble seepage is a widespread phenomenon in the Black Sea. Yet, previous studies have shown that gas bubbles rapidly dissolve after discharge to the water column. In case bubbles are emitted within the gas hydrate stability zone (GHSZ), they might form dissolution-hampering gas hydrate shells. These decompose upon reaching the upper limit of the GHSZ, making bubbles prone to rapid dissolution. Results from a limited number of studies in other regions suggest that at sites of combined oil and gas seepage, bubbles might be transported to the hydrosphere-atmosphere interface due to dissolution impeding effects of oil coatings around bubbles. Though the Black Sea is considered as potential hydrocarbon area, little was known about the occurrence of oil seepage pre-dating this thesis. The analysis of a large dataset of *Advanced Synthetic Aperture Radar* satellite images allowed identifying several sites of intermittent to persistent oil seepage. For two sites minimum oil discharge rates were estimated. The results show that 360,000 to 1,810,000 l yr^{-1} of oil are transferred from the

seabed to the sea surface. Hydroacoustic techniques were employed to test whether oil transport is coupled to gas bubble emissions. In this work multibeam echosounder were used to image gas emissions (*flares*) to the hydrosphere. The major advantage of multibeam systems for flare imaging, compared to traditionally used single-beam systems, is their wide swath which allows tracing gas bubbles that are horizontally deflected during ascent. These are usually not fully imaged by single-beam systems. The most striking result of these investigations was that gas bubble discharge was evidenced in all expected oil seepage areas, and that the majority of imaged flares rose at least into the mixed layer of the water body. Based on visual observations, it is anticipated that most flares reach the sea surface. Even if the bubbles dissolved in the mixed layer, they could contribute to local atmospheric methane concentrations by diffusion from the surface waters. Further, it is proposed that beside oil coatings around gas bubbles, also formation of structure II gas hydrate shells might prolong bubble lifetimes. Since structure II hydrate is thermodynamically more stable than structure I hydrate, it allows bubbles to rise about 550 m higher. The latter process might be relevant also at seeps that discharge thermogenic gas but no oil.

Detailed seafloor investigations by autonomous underwater vehicle MARUM B-SEAL5000 and remotely operated vehicle MARUM QUEST4000, allowed mapping one site of intensive oil and gas discharge. The results revealed a mounded morphology with a crater-rich morphology of the structure's summit. It is suggested that the heterogeneous seafloor morphology originates from frequent buoyancy-driven rafting of shallow gas hydrate deposits. Hydrate particles floating up to the sea surface were visually observed.

The observed oil seepage was suggested to be related to diapiric movement of fluid-rich sediments. Low oil seepage rates were linked to the presence of shale diapirs and oil migration through fractures and capillaries. Higher seepage rates and more persistent oil seepage were linked to mud diatremes that transport fluid-rich sediments to the seabed.

The major findings of the present work are that bubble gas fluxes are much more relevant than dissolved fluxes for the transfer of methane from the geosphere to the hydrosphere. This is because the latter are largely consumed by anaerobic oxidation of methane and associated chemosynthetic communities. Numerous previous studies indicate that gas bubbles emitted from deep-sea seeps dissolve at depth of several hundreds of meters. Therefore, biogenic methane that is discharged in deep-waters seems to be of no relevance to atmospheric methane concentrations. However, at seeps emitting thermogenic hydrocarbons, the formation of oil coatings or structure II hydrate shells provide a potential mechanism to transport methane from the deep-sea to the atmosphere. Evidence for such seepage is given by oil slicks on the sea surface. Since oil slicks can be conveniently imaged and monitored using satellite techniques, it is suggested to focus future research on these sites when aiming to better constrain the impact of marine hydrocarbon seepage on climate.

Kurzfassung

Das Ziel der vorliegenden Arbeit ist es, zu einem besseren Verständnis des Einflusses von Tiefsee-Methanemissionen auf den Methanhaushalt der Hydrosphäre und Atmosphäre beizutragen. Methan und andere Kohlenwasserstoffe treten natürlicherweise an vielen Stellen am Meeresboden aus. Diese Austrittsstellen werden als *kalte Quellen* bezeichnet. Für das Aufspüren, die Kartierung und die Quantifizierung von Kohlenwasserstoffemissionen solcher kalten Quellen wurden in der vorliegenden Arbeit verschiedene satelliten- und schiffsgestützte Fernerkundungsmethoden angewandt. Die hier vorgestellte Kombination von Fernerkundungsmethoden stellt einen neuen Ansatz zur Erforschung kalter Quellen dar. Kleinräumig wurde, basierend auf optischer und hydroakustischer Kartierung, das Verhältnis von Emissionen gelösten Methans im Vergleich zu Gasblasenemissionen untersucht. Auf regionaler Ebene wurden mittels Satellitenfernerkundung neue, öl- und gasemittierende, kalte Quellen aufgespürt. Emissionsraten und zeitliche Variabilität von Ölemissionen konnten anhand von Satellitenbildern bestimmt werden. Mittels schiffsgestützter Fächerlotkartierung wurde der Transport von methanreichen, öligen Gasblasen durch die Wassersäule untersucht.

Die erste Fallstudie im Rahmen dieser Arbeit wurde an einer kalten Quelle in 1.025 m Wassertiefe am Makran-Kontinentalhang vor Pakistan durchgeführt. Die Kombination von *remotely operated vehicle* (ROV)-gestützter Hochfrequenzsonar-Kartierung und Videomosaiken ermöglichte, den Bereich aktiver Methanemissionen sowie das Vorkommen bestimmter chemotropher Organismen präzise zu bestimmen. Die gewonnenen Daten stellten die Grundlage zur flächenmäßigen Berechung von gelösten Methanemissionen und Methanumsatzraten dar. Diese konnten mit Raten gasförmiger Methanemissionen aus der Literatur verglichen und so ein Methanbudget für die gesamte kalte Quelle berechnet werden. Die Ergebnisse dieser Fallstudie zeigen, dass gelöstes Methan vollständig durch biogeochemische Prozesse am Meeresboden umgesetzt wird, während blasenförmige Emissionen große Mengen an Methan in die Wassersäule transportieren. Nur Methan, das in die Wassersäule gelangt, kann eventuell durch Austauschprozesse in der Grenzschicht zwischen Hydro- und Atmosphäre in die Atmosphäre gelangen. Um genauer bestimmen zu können wie viel Methan tatsächlich von kalten Quellen in Hydro- und Atmosphäre gelangt, ist es entscheidend Methanbudgets, wie sie hier vorgestellt werden, zu bestimmen. Bislang basierten Berechnungen von Kohlenwasserstoffflüssen an kalten Quellen vornehmlich auf punktuellen Messungen, die flächenmäßige Variationen von Flüssen vernachlässigen. Des Weiteren erlauben es traditionelle Beprobungsmethoden nicht, zwischen der relativen Bedeutung von gelösten Flüssen über große Flächen und lokalen Emissionen von gasförmigem Methan zu differenzieren. Die hier vorgestellten hydroakustischen und optischen Kartierungsmethoden in Kombination mit lokalen Methanflussbestimmungen erlauben es, ein differenzierteres Bild von Kohlenwasserstofftransportprozessen zu gewinnen. Diese Methode stellte eine effiziente Möglichkeit dar, um die Bedeutung von kalten Quellen auf den lokalen Methanhaushalt der Hydrosphäre zu erforschen.

Während die erste Fallstudie gezeigt hat, dass durch Gasblasen bei weitem mehr Methan in die Wassersäule transportiert wird als durch Flüsse gelösten Methans, wurde in zwei weiteren Fallstudien im Schwarzen Meer unter anderem der Verbleib von ölumhüllten Gasblasen in der Wassersäule untersucht. Diese Arbeiten sollten Hinweise darauf geben, ob klimarelevante Gase tatsächlich die oberen Wasserschichten und von dort eventuell die Atmosphäre erreichen. Kalte Quellen und damit verbundene Gasemissionen kommen im gesamten Schwarzen Meer sehr häufig vor. Jedoch haben frühere Studien gezeigt, dass

Gasblasen, die in Wassertiefen unterhalb von 100 m aus dem Meeresboden austreten, vollständig in der Wassersäule gelöst werden. Im Fall, dass Blasen innerhalb der Gashydrat-Stabilitätszone (GHSZ) austreten, bilden sich Gashydrathüllen auf der Blasenoberfläche, die das Auflösen der Blasen verlangsamen. Wenn die aufsteigenden Blasen jedoch die GHSZ verlassen, lösen sich zunächst die Gashydrathüllen und dann die Blasen auf. Hinweise auf Methantransport von kalten Quellen in der Tiefsee bis in die Atmosphäre, gab es bislang nur durch einige Studien an natürlichen Ölquellen im Golf von Mexico. Dort wurde gezeigt, dass Ölfilme auf der Blasenoberfläche ähnliche Effekte haben wie Gashydrathüllen. Obwohl vermutet wird, dass es im Schwarzen Meer große Ölvorkommen gibt, ist wenig über natürliche Ölaustritte bekannt. Durch die Analyse eines umfangreichen Datensatzes von *Advanced Synthetic Aperture Radar* Satellitenbildern im Rahmen dieser Arbeit, konnten jedoch eine Vielzahl natürlicher Ölquellen entdeckt werden. Diese Ölquellen emittieren sporadisch bis permanent Öl in die Hydrosphäre, das schließlich die Wasseroberfläche erreicht. Für zwei Ölquellen konnte mittels der verfügbaren Satellitendaten eine Minimumabschätzung von Ölaustrittsraten vorgenommen werden. Ausschließlich von diesen zwei Quellen gelangen wenigstens 360.000 bis 1.810.000 l a^{-1} Öl an die Wasseroberfläche. Mittels Fächerlotkartierung wurde untersucht, ob der Öltransport durch die Wassersäule an Gasblasenaustritte gebunden ist. Letztere sind aufgrund von Impedanzunterschieden zwischen Wasser und Gas mit Echoloten sichtbar zu machen. Das eindruckvollste Ergebnis dieser Untersuchungen ist, dass an allen Ölquellen auch Gasblasenaustritte nachgewiesen werden konnten. Die hydroakustisch abgebildeten Blasenströme erreichten die durchmischte Schicht, d.h. ca. die obersten 50 m der Wassersäule, unabhängig von der Tiefe der Austrittsstelle. Aufgrund von visuellen Beobachtungen kann angenommen werden, dass ölige Gasblasen auch die Wasseroberfläche erreichen. Selbst wenn sich die Blasen vollständig in der durchmischten Schicht auflösen würden, könnte Methan von dort durch Diffusion in die Atmosphäre gelangen.

Neben der Beobachtung, dass Ölfilme auf der Oberfläche von Gasblasen deren Auflösung verlangsamen, entstand aufgrund des gemeinsamen Auftretens von Emissionen von Öl und thermogenem Gas die Idee, dass sich Gashydrathüllen der Gashydrat-Struktur II bilden könnten. Diese sind thermodynamisch deutlich stabiler als Struktur I Hydrate und könnten daher das Auflösen von Blasen weiter verzögern.

Der Einsatz des *autonomous underwater vehicle* (AUV) MARUM B-SEAL5000 und des ROV MARUM QUEST4000 ermöglichte die detaillierte Kartierung einer Ölquelle in ca. 1.020 m Wassertiefe. Die gewonnenen Daten zeigten eine sehr heterogene, kraterreiche Oberfläche des Meeresbodens. Die Entstehung dieser Strukturen wurde auf das häufige Loslösen und Auftreiben von Gashydraten, die sich nahe der Sedimentoberfläche bilden, zurückgeführt. Es konnte beobachtet werden, dass Gashydratpartikel die Wasseroberfläche erreichen.

Aufgrund der Ergebnisse dieser Arbeit wird vermutet, dass das Vorkommen von Ölquellen im Schwarzen Meer an die Migration von öl- und gasreichen Sedimenten gebunden ist. Starke und kontinuierliche Ölaustritte sind an Schlamm-Diapire gebunden, die fluidreiche Sedimente zum Meeresboden transportieren. An Quellen, die nur sporadisch Öl und Gas emittieren, werden Fluide entlang von Störungen oberhalb von Schlamm-Diapiren transportiert.

Die Hauptaussagen der vorliegenden Arbeit sind, dass Gasblasenemissionen deutlich mehr Methan in die Wassersäule transportieren als Flüsse gelösten Methans. Dies ist in erster Linie dadurch bedingt, dass gelöstes Methan durch biogeochemische Prozesse nahe der Grenzschicht zwischen Meeresboden und Wassersäule umgesetzt wird. Der Transport

von gasförmigen Kohlenwasserstoffen von kalten Quellen in der Tiefsee in die Atmosphäre spielt nur dort eine Rolle, wo neben Methan auch höhere Kohlenwasserstoffe austreten. Frühere Studien belegen das Blasen, die ausschließlich Methan enthalten, vollständig in der Wassersäule gelöst werden bevor sie die Atmosphäre erreichen. Im Rahmen dieser Arbeit wurde gezeigt, dass Gasblasen durch Ölhüllen und/oder Struktur II Gashydrathüllen aus großer Tiefe die Wasseroberfläche erreichen können. Da öl- und gasemittierende kalte Quellen scheinbar das größte Potential aufweisen atmosphärische Methankonzentrationen zu beeinflussen, wird angeregt, diese in Zukunft verstärkt zu erforschen. Die Erforschung und Beobachtung von kombinierten Öl- und Gasaustritten ist durch die hier vorgestellten Methoden auch großräumig sehr effizient möglich.

Thesis outline

The present work consists of eight chapters. The first chapter provides a detailed introduction to cold seeps and related chemical, biogeochemical and biological processes. The introduction closes with a brief review of the relevance of cold seepage in past and future climate change. Chapter 2 details the initial questions that stimulated this work. Chapter 3 introduces techniques commonly used to detect and characterize cold seeps. These comprise optical, hydroacoustic and satellite techniques. The fourth chapter constitutes a brief introduction into the study areas which have been investigated in this study – the Makran accretionary prism offshore Pakistan and the Black Sea. Chapters 5 through 7 represent the main scientific work of the thesis as manuscripts that are, or are to be submitted for publication. Chapter 5 presents a methane budget for an entire seep offshore Pakistan. Chapter 6 details oil seepage at two seeps in the Black Sea, including estimations of emission rates and seepage persistency. The seventh chapter provides an inventory of oil seeps in the Black Sea and discusses geologic processes triggering seepage and controlling seep distributions, and their potential impact on water column and atmospheric methane inventories. The last chapter presents the main conclusions and implications of the present work and provides an outlook for further studies.

Chapter 5: Methane budget of a cold seep (*Flare II*) associated with an incipient headwall, offshore Pakistan.

Jan-Hendrik Körber, Heiko Sahling, Gerhard Bohrmann
To be submitted to Marine Geology

The high-frequency (675 kHz) forward looking sonar of the ROV QUEST4000 was used to map the 'Flare II' seep (1025 m depthl) offshore Pakistan. The sonar allowed identifying the area influence by seepage activity due to distinct backscatter patterns in the sonar records, probably originating from the presence of authigenic and biogenic carbonates and. Subsequent video-mosaicking of parts of the seep area allowed estimating the total extent of certain chemosynthetic communities. These communities are related to distinct fluxes of dissolved methane which are available from literature. Extrapolation of these fluxes to the seep area inhabited by chemosynthetic communities provides methane turnover rates for the entire seep. Comparison of these to previously published bubble gas fluxes indicated that bubble emission are tow orders of magnitude larger than the volume of methane consumed by chemosynthetic communities. Sidescan sonar and seafloor investigation by ROV allow relating fluid flow to a major slope failure.

Chapter 6: Natural oil seepage at Kobuleti Ridge, eastern Black Sea

Jan-Hendrik Körber, Heiko Sahling, Thomas Pape, Christian dos Santos Ferreira, Ian MacDonald, Gerhard Bohrmann
Submitted to Marine and Petroleum Geology

In this chapter *Advanced Synthetic Aperture Radar* satellite images were used to identify two sites of prolific oil seepage in the eastern Black Sea offshore Georgia. Satellite images allowed determining rather persistent oil seepage since 2003. A minimum order of magnitude estimate yielded oil emission rates from $36*10^4$ to $181*10^4$ l yr^{-1}. Hydroacoustic water column investigations evidenced that gas bubbles rose more than 1,000 m to depth of ca. 50 m. Bubbles have visually been observed to surface above the seeps. High-resolution mapping of one site using the AUV B-SEAL5000 revealed a crater-rich morphology. The

Rafting of shallow gas hydrate deposits was proposed to shape the seabed morphology and to provide an additional mechanism to transport hydrocarbons to the sea surface.

Chapter 7: Oil seeps in the Black Sea: Hydroacoustic, geological, and satellite based investigations.

Jan-Hendrik Körber, Heiko Sahling, Christian dos Santos Ferreira, Paul Wintersteller, Ian MacDonald, Gerhard Bohrmann

To be submitted to Marine and Petroleum Geology

Advanced Synthetic Aperture Radar satellite imagery was used to investigate the entire Black Sea for occurrences of oil seepage. Despite the good spatial and temporal coverage of the entire Black Sea, identified oil seeps were located exclusively in the eastern Black Sea, with 11 seepage areas offshore Georgia and one offshore Turkey. Image analysis evidenced that the newly identified sites show much lower seepage rates and less persistent seepage than the previously investigated sites. Hydroacoustic investigations at all except one site, confirm findings of the previous study (Chapter 6) that gas bubbles released within the oil seepage areas reach shallow waters despite several hundreds of meters rise. The formation of the oil seeps and their exclusive occurrence in the eastern Black Sea is discussed with respect to the regional geology. Seepage of thermogenic hydrocarbons is proposed to be a potential contributor to local atmospheric methane budgets.

Chapter 1

Introduction

1.1 From quaint discoveries to an own research discipline

Fluid emissions from geological sources have been recognized for thousands of years. Early observations include freshwater discharge in shallow marine environments, observations of oil floating on the sea surface and tar accumulations on beaches of the Dead Sea or in the Santa Barbara Channel, California (Judd and Hovland, 2007). It was only in the second half of the 20th century that the first sub-circular morphological structures were discovered on the seabed whose genesis was linked to fluid emissions from underlying sediments (King and MacLean, 1970). These structures were named pockmarks. After these initial discoveries on the Scotian Shelf, pockmarks have been found to be widespread features, virtually occurring globally along continental margins (Judd and Hovland, 2007). Evidence that pockmarks are often related to migration and expulsion of hydrocarbon fluids, e.g. methane, sparked the interest of scientist and petroleum industry to unravel the geologic processes that lead to pockmark formation. Soon it became evident that fluid flow from geosphere to hydro- or atmosphere, called *seepage*, does not only impact the physical environment of the seafloor but also the local geochemical and biological environments (Levin, 2005; Milkov et al., 2004).

As research advanced, more morphological features or feature types related to seepage were identified and commonly denoted as *cold seeps*. These cold seeps include submarine mud volcanoes (Kopf, 2002; Krastel et al., 2003; Milkov, 2000), carbonate mounds (Foubert et al., 2008; Hovland et al., 2005; Plaza-Faverola et al., 2011), and gas hydrate mounds (Hester and Brewer, 2009; Hovland and Svensen, 2006; MacDonald et al., 2005). Also, fluid emission sites which do not exhibit specific morphology (Dimitrov, 2002; Hovland, 2002; Naudts et al., 2006) have been identified. Cold seep research from the last four decades indicates that the most common fluid expelled from the seafloor to the water column is methane, either in the dissolved phase or as free gas (Heeschen et al., 2005; Hovland et al., 1993; Sommer et al., 2006). Since methane is a powerful greenhouse gas (Lelieveld et al., 1998), the potential impact of marine emissions on global atmospheric budgets and climate has been questioned (Etiope, 2009; Etiope and Klusman, 2002; Judd, 2004; Judd et al., 2002; Kvenvolden and Rogers, 2005). Despite the growing evidence that geologic sources (marine and terrestrial) emit significant amounts of greenhouse gases, they are still not considered in the actual report of the *Intergovernmental Panel on Climate Change* (IPCC) (IPCC, 2007). Still, the current version (2007) does acknowledge current research on this topic and the potential relevance of geologic methane sources (IPCC, 2007).

The following paragraphs give a general overview on marine cold seeps that emit hydrocarbon gases and/ or oil, as well as origin and fate of seeping fluids and related geological and biological processes.

1.2 Origin of hydrocarbon fluids

This work deals with the detection, monitoring and quantification of hydrocarbons emitted at cold seeps. The fluids released at the studied sites consist mainly of methane and crude oil. Methane is by far the most common gas in shallow marine sediments (Judd et al., 2002). Global occurrences have been reported from shallow to deep water environments (Fleischer et al., 2001; Judd and Hovland, 2007). The generation of methane (CH_4) from organic matter follows two major processes which are microbial and thermocatalytic methanogenesis

(Schoell, 1988; Whiticar, 1999). Methane generated by the former process is also referred to as biogenic methane while methane originating from thermocatalytic processes is commonly denoted as thermogenic methane (Floodgate and Judd, 1992). Biogenic methane constitutes the major volume of the shallow gas accumulations within the upper 1,000 m of the sediment column (Floodgate and Judd, 1992). Biogenic gas is formed by microbial degradation of organic matter following three main pathways (Whiticar, 1999) (equations 1-3). These are the hydrogenotrophic pathway, i.e. carbonate reduction with hydrogen:

$$CO_2+8H^++8e^- \rightarrow CH_4+2H_2O \qquad \text{(eq. 1)},$$

the acetotrophic pathway:

$$CH_3COOH \rightarrow CH_4+ CO_2 \qquad \text{(eq. 2)},$$

and the methylotrophic pathway:

$$CH_3\text{-}A+H_2O \rightarrow CH_4+CO_2+AH \qquad \text{(eq. 3)}.$$

In the marine environment, the former two reactions (eqs. 1 and 2) are the most important ones. Yet, in water column and sediments which contain sufficient dissolved sulfate, sulfate reducing bacteria utilize carbon and hydrogen on the expense of methanogenesis (Whiticar, 1999). In sediments that are depleted in sulfate, organic matter is efficiently transferred to methane.

The second important process to degrade organic carbon and to generate hydrocarbons is the thermocatalytic pathway. At temperatures between approximately 60 and 200°C, organic matter is cracked and hydrocarbons are formed (Hunt, 1979) (Fig. 1). At temperatures exceeding 200°C, cracking of previously formed hydrocarbon gases and reservoir oil produce mainly methane (Tissot and Welte, 1984). The type of generated hydrocarbons depends on the source material, e.g. organic carbon from higher plants, lower plants or microbes (Floodgate and Judd, 1992). At low temperatures or burial depth, oil generation starts. Oil consists essentially of C_{15+} hydrocarbons. As temperature increases, gas formation becomes more dominant. First condensate (C_8-C_{15}), and then wet gas (C_2-C_7) is produced. Formation of dry gas (CH_4) dominates the thermogenic hydrocarbon generation within the highest temperature field at greatest burial depth (Floodgate and Judd, 1992).

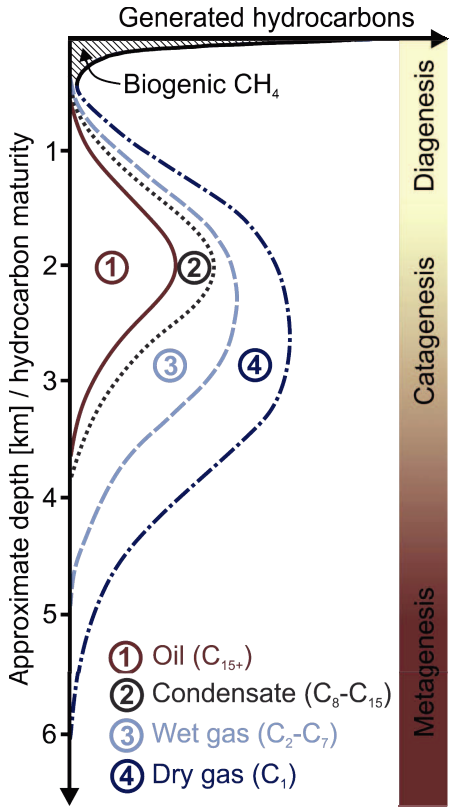

Fig. 1. Illustration of depth dependent generation of hydrocarbons. The depth in which different hydrocarbons are formed depends on local geothermal gradients (adapted from Floodgate and Judd, 1992).

To elucidate whether methane seeping from the seafloor (or terrestrial seeps) is of biogenic or thermogenic origin or a mixture of both, two chemical methods have been established. The analysis of the molecular ratio of C_1 (methane) to C_{2+} hydrocarbons is commonly employed as the first approach. Ratios greater than 1,000 are usually indicative for biogenic sources, since methane is the predominant gas generated in this phase. Lower ratios indicate contributions from thermogenic sources (Claypool and Kvenvolden, 1983). Combining C_1/C_{2+} ratios with data on the stable carbon isotope composition of methane ($\delta^{13}C$-CH_4) allows further specifying the hydrocarbon origin (Bernard et al., 1978) (Fig. 2a)

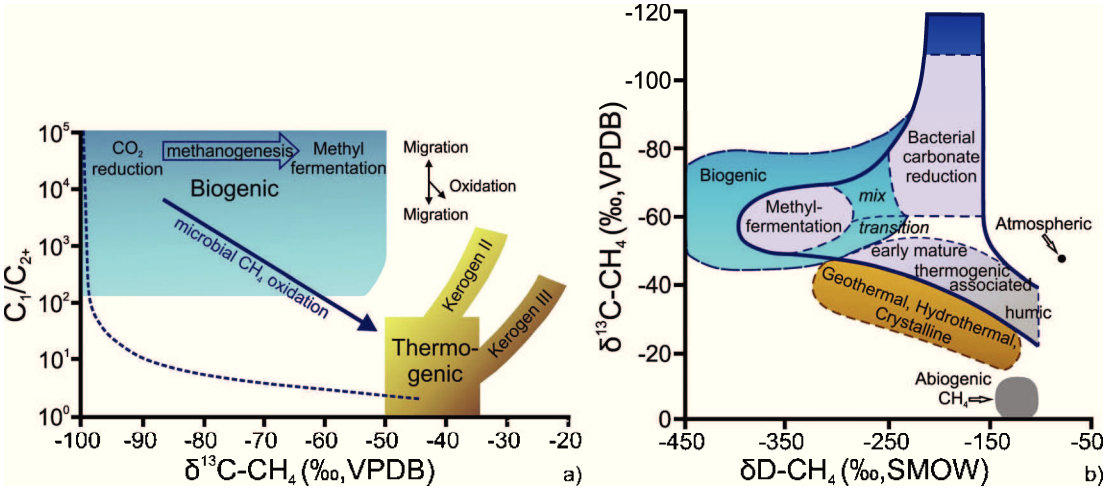

Fig. 2. a) Diagram showing the relation between stable isotope and molecular composition for methane of different origins. b) Graph illustrating the differentiation between biogenic and thermogenic methane based on $\delta^{13}C$-CH_4 and δD-CH_4 information (modified from Whiticar, 1999).

While $\delta^{13}C\text{-}CH_4$ values smaller than -50 ‰ Vienna-Pee Dee Belemnite Standard (V-PDB) are indicative of biogenic methane, greater values hint to thermogenic methane formation (Rice and Claypool, 1981; Whiticar, 1999). This is due to the preferred utilization of the lighter ^{12}C-isotope by microbes. This leads to an enrichment of the heavier ^{13}C-isotope in older sediments that are prone to thermocatalytic hydrocarbon generation. Source material and maturity level of the hydrocarbons further affects the $\delta^{13}C\text{-}CH_4$, with $\delta^{13}C\text{-}CH_4$ values increasing with hydrocarbon maturity (Whiticar, 1999). Hydrogen stable isotope compositions $\delta D\text{-}CH_4$ are indicative of the pathway of biogenic methane formation and can be employed together with $\delta^{13}C\text{-}CH_4$ to further elucidate the origin of methane (Fig. 2b) (Whiticar, 1999). $\delta D\text{-}CH_4$ values -150 to -250 ‰ Standard Mean Ocean Water (SMOW) are indicative of bacterial carbonate reduction. Methane generated via methyl fermentation is characterized by values -250 to -400 ‰ (Whiticar, 1999). Mixing of biogenic and thermogenic methane due to fluid migration from thermogenic through biogenic accumulations might produce a mixed signal, hampering the identification of the hydrocarbon origin (Pape et al., 2010) (Fig. 2b). It has also been proposed that microbial degradation of thermogenic hydrocarbons might alter the $\delta^{13}C\text{-}CH_4$ signature of biogenic gas (Blinova et al., 2003; Stadnitskaia et al., 2008).

Probably the most important biochemical process occurring in shallow anoxic sediments is the anaerobic oxidation of methane (AOM) (Barnes and Goldberg, 1976; Iversen and Jørgensen, 1985). In the course of AOM, consortia of methanotrophic archea and sulfate reducing bacteria oxidize methane with sulfate to hydrogen sulfide, water and carbonate (eq. 4) (Barnes and Goldberg, 1976; Boetius et al., 2000a):

$$CH_4+SO_4^{2-} \rightarrow HCO^{-3}+HS^{-}+H_20 \qquad \text{(eq. 4).}$$

During this process, the lighter ^{12}C isotope is preferably utilized, which causes an enrichment in ^{13}C in the remaining carbon pool (Whiticar, 1999). Furthermore, the proceeding microbial consumption of CH_4 might decrease the fraction of methane compared to higher hydrocarbons, leading to C_1/C_{2+} ratios that mimic those of thermogenic methane (Whiticar, 1999).

Though gas seeps account for most cold seep sites discovered so far, also sites of combined oil and gas seepage have been reported to be widespread phenomena (Kvenvolden and Cooper, 2003; Wilson et al., 1974). Intrinsically, areas of oil seepage are concentrated in oil provinces, yet oil seepage is not necessarily indicative for economic hydrocarbon accumulations (Macgregor, 1993; Thrasher et al., 1996). There is evidence from prolific oil seepage regions, as the Gulf of Mexico or the Santa Barbara Channel off California, that oil and gas seepage co-occur (De Beukelaer et al., 2003; Leifer et al., 2000). Along with the seeping oil, which is formed by thermocatalytic degradation of organic matter below the zone of predominantly biogenic hydrocarbon gas formation, thermogenic gases are emitted at these sites (Kinnaman et al., 2010; Sassen et al., 2001a). Due to migration from greater depths through the zone of microbial methanogenesis, the seeping gas might constitute isotopic compositions of methane that can be assigned to mixed sources, rather than to exclusively thermogenic sources.

1.3 Hydrocarbon migration

Cold seeps are only the seafloor expression of, and indication for, fluid migration from deeper sedimentary units to the seafloor. The physical, geochemical, and biological characteristics and spatial extent of seeps depend largely on the type of fluids and fluid flow rates they are associated with. For the present work, only hydrocarbon seeps are of concern.

Therefore, seepage of other than hydrocarbon gases or freshwater is not considered. Most important for the here considered seep systems is discharge of biogenic and thermogenic methane and oil.

With respect to thermogenic hydrocarbon migration, two types of migration may be distinguished. These are primary and secondary migration. The former describes the release of petroleum compounds from the source organic matter to the source rock and their movement within the source rock (Tissot and Welte, 1984). Secondary migration occurs when petroleum/ hydrocarbons migrate from source rocks to reservoir rocks where they may form large accumulations (Selley, 1998; Tissot and Welte, 1984). The process of oil and gas migration from reservoir rocks to adjacent lithological units is referred to as *leakage* (Thrasher et al., 1996). When these hydrocarbons are eventually released from the geosphere to hydro- or atmosphere, *seepage* occurs (Clarke and Cleverly, 1991). Within this work, only migration mechanisms leading to seepage are of relevance.

With respect to fluid migration from reservoirs towards seeps, two major physical transport mechanisms can be distinguished. These are fluid advection and diffusion. Advection describes fluid movement following either a pressure gradient, i.e. fluids migrate from high to lower pressure, or fluids move buoyancy-driven (Clennell et al., 2000). That is, a fluid with lower density than the surrounding medium experiences an upward directed force (Brown, 1990). Advective transport of hydrocarbons occurs in two different ways. Firstly, hydrocarbon gases might be dissolved in pore-water and be advected with it. Secondly, gas or oil can be advected as gas bubbles, oily gas bubbles, or gassy oil droplets through fractures, along faults or through pore space (Etiope and Martinelli, 2002). Generally, bubble or droplet movement along faults and through fractures is the fastest mechanism for oil and gas migration. The larger the bubbles or gassy droplets are the faster they rise. However, bubble and droplet size is determined by the width of the migration pathway (Etiope and Martinelli, 2002). Especially for oil migration, formation of gassy droplets or oily bubbles is important, since buoyancy of pure oil is rather low. Clarke and Cleverly (1991) suggested that oil leakage, sufficient enough to trigger seepage, only occurs if oil droplets contain sufficient amounts of gas. During advection, hydro- and lithostatic pressure decreases, which causes the expansion of gas entrained in oil droplets or gas bubbles and accelerates the migration (Clarke and Cleverly, 1991; Leifer and Boles, 2005). In high pressure regimes in which gas migration occurs, gas bubbles might displace all pore-water and flow as connected stream (Etiope and Martinelli, 2002). Given migration pathways with widths of at least 1 mm, gas bubbles or droplets might be advected with velocities between 0.001 to 20 cm s^{-1} (Etiope and Martinelli, 2002). If the overpressure of advecting pore-fluids exceeds the lithostatic pressure of the overburden, fluids might cause sediment fracturing (*hydrofracturing*), creating new migration pathways.

A special form of fluid advection is the upward movement of low density or overpressured sediments, which is commonly termed mud diapirism (Judd and Hovland, 2007; Kopf, 2002). The surface expression of mud diapirism are mud volcanoes which might expel fluids and fluidized sediments (Kopf, 2002). Fluid transport through mud diapirs occurs with the mud as single-phase flow (Brown, 1990; Kopf, 2002). In contrast, if fluid migration is decoupled from sediment migration but fluidizes the adjacent sediments, a mud diatreme is formed (Kopf, 2002). The plastic movement of muddy sediments (shale) is triggered by undercompaction or overpressurization. Undercompacted sediments contain too high volumes of pore-water with respect to their burial depth and overlaying sediment burden. Undercompacted lithological units originate in environments of high sedimentation rates where compaction of sediments is in disequilibrium with burial rate (Bjørlykke and Høeg, 1997). Undercompacted

lithological units have usually a lower density compared to overlaying units and therefore experience a buoyant uplift. Given pre-existing migration pathways, as faults, these sediments may intrude shallower units. Sediment movement might also be induced by pore-overpressure. Overpressure might form when pore-fluids, migrating along vertical pressure gradients, can not pass an impermeable layer (Mello et al., 1994), due to an increase in horizontal stress induced by tectonic compression, or because of an increase in pore-fluid volume (Osborne and Swarbrick, 1997). The latter might originate from clay mineral dewatering (Osborne and Swarbrick, 1997), hydrocarbon maturation (Hunt et al., 1994) or lateral inflow of fluids (Brown, 1990). It has also been proposed that gas hydrate decomposition might increase pore-fluid volumes, and create overpressure (Martin et al., 1996).

The second major process transporting hydrocarbon fluids is diffusion. Diffusion is much slower than advection (Clennell et al., 2000). Diffusion is movement of molecules along a concentration gradient and occurs without actual fluid movement (Etiope and Martinelli, 2002). Diffusion rates are proportional to concentration gradients (Judd and Hovland, 2007). Diffusion is only relevant in capillaries and fine porous media and is inefficient to displace large volumes of hydrocarbons (Clennell et al., 2000; Etiope and Martinelli, 2002).

The most common geologic settings favoring hydrocarbon migration which is eventually leading to seepage are sketched in Fig. 3. Schemes a) and b) depict seepage that is initiated by diapiric activity. In the first case, hydrocarbons are transported towards the seafloor by a mud diapir/ diatreme that pierces the seafloor and forms mud volcanoes. In the second scenario, a salt diapir deforms the overlaying sediments and induces diapiric faulting which acts as fluid migration pathway. Similar faulting may also be created by a mud diapir. Schemes c) to f) illustrate typical settings in which fluid migration is onset by tectonic faulting in either compressional or extensional regimes or by outcropping source units or aquifers through which hydrocarbons migrate. The last scheme illustrates the formation of oil impregnations in shallow sediments which are not accompanied by active seepage. These occur if a reservoir, sourcing seepage, is exhausted. Generally, the models in Fig. 3 apply also for gas migration from deeper sources. Seepage fed by shallow gas accumulations might be controlled by processes affecting only the surface sediments and seafloor morphology. Seeps are often located along the crest of ridges or upper parts of slopes (Naudts et al., 2006; Torres et al., 2009) or the headwalls of slumps (Parsons et al., 2005; Yun et al., 1999). An explanation for these occurrences might be that upslope sediments experience a gravity-driven extension while downslope sediments are compressed (Bjørlykke and Høeg, 1997). Due to the lower vertical stress, fluids can more easily breach the seafloor in upslope sediments (Judd and Hovland, 2007). Due to the weaker near-surface sediments, seepage can be induced by smaller gas accumulations since less overpressure is required to break these (Judd and Hovland, 2007). Consequently, such seeps will release less gas during an activity period. However, intervals of gas release might be more frequent than at seeps that are sourced from shallow reservoirs (Judd and Hovland, 2007).

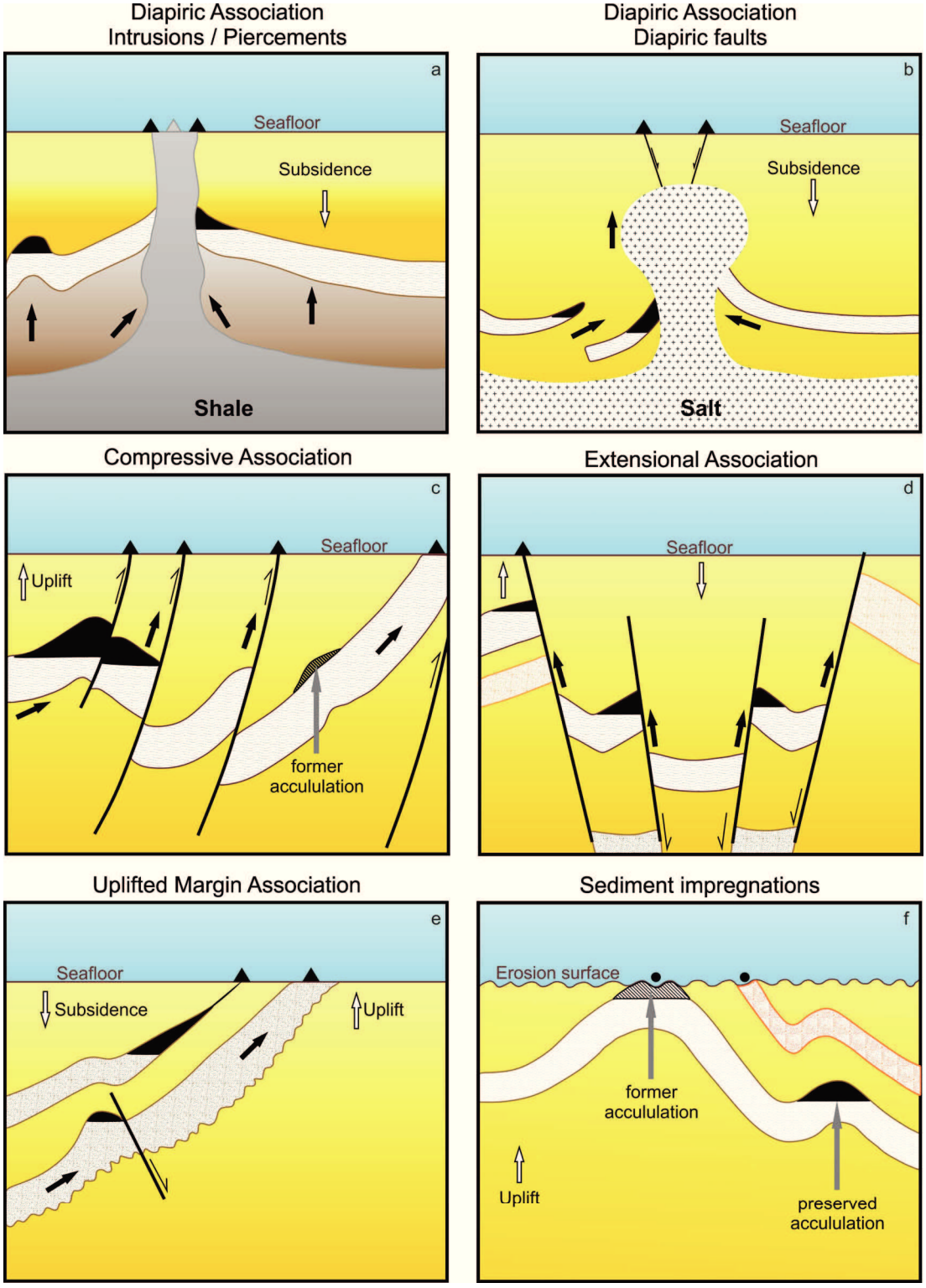

Fig. 3. General oil seep associations illustrating oil migration from reservoirs and source rocks towards the seabed. Black triangles denote active seeps, black dots oil impregnations. Black arrows indicate direction of fluid flow (modified from Macgregor, 1993).

1.4 Gas hydrates

Under certain physical and geochemical conditions, hydrocarbon gases might form ice-like structures within the sediments, so called gas hydrates. Gas hydrates form at temperatures usually below 25°C and pressures above 60 bar (Sloan, 2003) (Fig. 4). Gas hydrates incorporate large amounts of gas in their lattice. When decomposed under atmospheric pressure, one volume unit of hydrate might yield up to 164 volumes of gas and 0.8 volumes of water (Kvenvolden, 1993). During recent years, gas hydrates have got in the focus of research for three main reasons. Firstly, hydrates have been identified as a potential energy source, since vast amounts of carbon are thought to be stored in gas hydrate deposits worldwide (Boswell, 2009; Boswell and Collett, 2011; Lorenson et al., 2011). Estimates of total hydrate-bound carbon range from conservative 4-1000 (Burwicz et al., 2011) to optimistic 74,000 Gt (Klauda and Sandler, 2005), the latter value being probably too optimistic (Archer, 2007). Archer (2007) suggests an average of 500 to 3,000 Gt of hydrate-bound carbon as a sensible mean value. Secondly, gas hydrates have been identified to bear a large geohazard risk in case they decompose. Since most gas hydrate deposits occur in shallow marine sediments long continental slopes (Kvenvolden, 1993), their decomposition might cause slope instabilities and trigger e.g. tsunamis (Maslin et al., 2010, 2004). Geologic history provides evidence for such events (Mienert et al., 2005; Rothwell et al., 1998). Thirdly, research is conducted to investigate whether gas hydrates provide potential to store atmospheric CO_2 to mediate global warming (Brewer et al., 1999; Zhang and Lee, 2008).

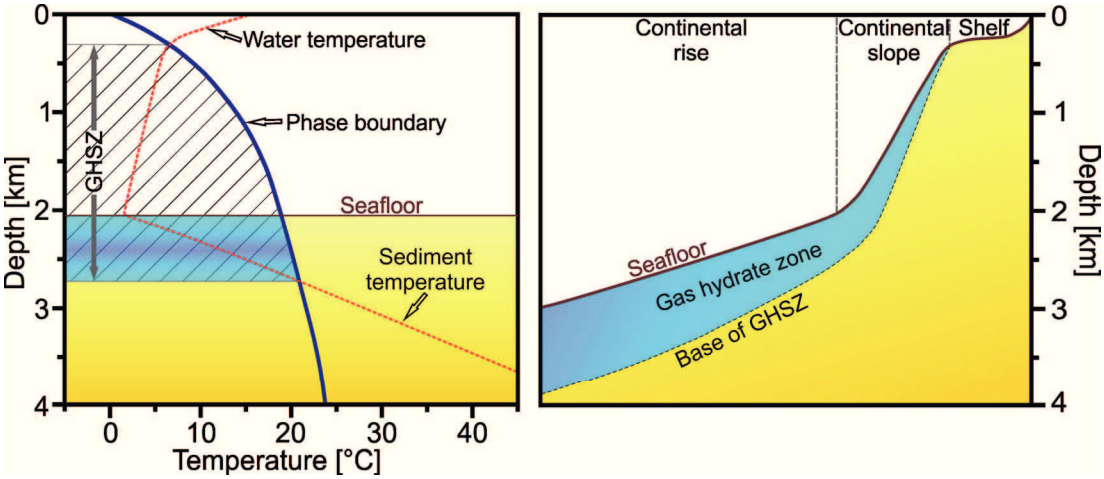

Fig. 4. Left side: Gas hydrate stability diagram showing the stability field for methane hydrate which depends on temperature (red dashed line) and pressure (water depth). Right side: Theoretical thickness of the gas hydrate zone in sediments based on a geothermal gradient of 28°C. GHSZ = Gas hydrate stability zone; (adapted from Bohrmann and Torres, 2006).

Gas hydrates may form three different structures; structure I, II and H (sI, sII and H) depending on the guest molecules (gases) they incorporate (Sloan, 2003) (Fig. 5). Hydrate structures I and II are the most common ones in the natural environment (Sloan, 2003) and therefore structure H is not considered here. Structure I hydrate enclathrates hydrocarbons smaller than propane (C_3H_8) and gases of comparable molecular size like CO_2 or H_2S (Bohrmann and Torres, 2006). Hydrate of structure II forms, in the presence of larger molecules as propane, iso-butane or similar-sized non-hydrocarbon gases, e.g. argon and nitrogen (Bohrmann and Torres, 2006). In both, sI and sII hydrate, the crystal structure

consists of water molecules pentagonally bond by hydrogen, forming a 12 faced cavity (5^{12}). This cavity enclathrates molecules smaller than propane. The 5^{12} cavities are joined either on the hydrogen-bound-vertices (sI) or at the faces (sII) (Sloan, 2003). Since neither of these connections allows the formation of crystal units without non-occupied space, hexagonal-faced cavities are incorporated. In case of sI hydrate, two ($5^{12}6^2$) and in case of sII hydrate, four ($5^{12}6^4$) of these cavities are needed, resulting in crystal units of $2*5^{12}+6*5^{12}6^2$ (sI) and $16*5^{12}+8*5^{12}6^2$ (sII) crystals (Sloan, 2003). Generally, formation of sII hydrates is expected to be related to thermogenic hydrocarbon sources since these usually include propane and iso-butane (Chapman et al., 2004; Sassen et al., 2001a).

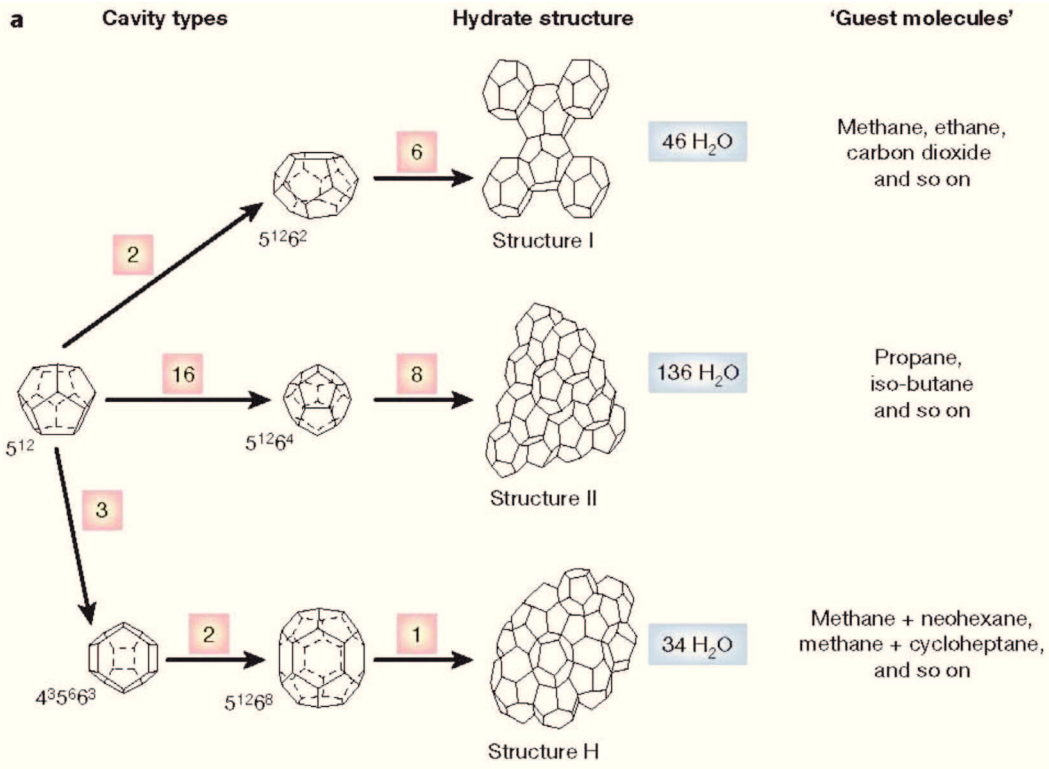

b

Hydrate crystal structure	I		II		H		
Cavity	Small	Large	Small	Large	Small	Medium	Large
Description	5^{12}	$5^{12}6^2$	5^{12}	$5^{12}6^4$	5^{12}	$4^3 5^6 6^3$	$5^{12}6^8$
Number of cavities per unit cell	2	6	16	8	3	2	1
Average cavity radius (Å)	3.95	4.33	3.91	4.73	3.91†	4.06†	5.71†
Coordination number*	20	24	20	28	20	20	36
Number of waters per unit cell	46		136		34		

*Number of oxygens at the periphery of each cavity.
†Estimates of structure H cavities from geometric models.

Fig. 5. Scheme of the three hydrate structures. $5^{12}6^4$describes a water cage of 12 pentagonal and four hexagonal faces. Numbers in boxes denote the numbers of cage types, e.g. sI hydrate forms from two 5^{12}, six $5^{12}6^4$ cages and 56 water molecules (from Sloan, 2003).

Gas hydrates form only if the gas content in sediments exceeds solubility in pore-water, and when enough water is available for hydrate formation (Bohrmann and Torres, 2006).

Structure II hydrates are thermodynamically more stable than sI hydrates (Kvenvolden, 1993). Therefore, gas hydrates forming from thermogenic hydrocarbon fluids occur in shallower depth than those formed from biogenic hydrocarbons. Comparison of the stability fields of sI and sII gas hydrates, e.g. for the Gulf of Mexico (Klapp et al., 2010a) or the Sea of Marmara (Bourry et al., 2009), shows that sII gas hydrates could occur in 200 to 450 m shallower water depth than sI hydrate. Yet, the inclusion of CO_2 or H_2S in sI hydrate extents also the stability field of sI hydrate (Bohrmann and Torres, 2006). Hydrate precipitates in varying sizes and shapes. Depending on flux rates, persistency, and available pore space, the precipitates range from small flakes to decimeter-sized accretions (Brooks et al., 1986). Larger deposits of gas hydrate only form when the flux of guest molecules from below is high (Torres et al., 2004) and compensates for hydrate dissociation. The latter might be caused by gas diffusion from the hydrate to methane-undersaturated pore-water or water column (Egorov et al., 1999; Paull et al., 1995) or by increase of temperature. At areas of high fluid flow, hydrate might form mounds on the seafloor that contain cubic meters of massive hydrate. Such hydrate mounds have been documented e.g. off Angola (Serié et al., 2012), off California (Paull et al., 2008), in the North Sea (Hovland and Svensen, 2006), off Vancouver Island (Chapman et al., 2004; Hester and Brewer, 2009) and in the Gulf of Mexico (MacDonald et al., 1994). Occasionally, hydrates might even breach the seafloor and expose hydrates to the water column (Hester and Brewer, 2009; MacDonald et al., 1994; Olu-Le Roy et al., 2007; Sassen et al., 2001a). Outcropping gas hydrates are often observed at sites of oil-gas seepage (Hester and Brewer, 2009; MacDonald et al., 1994), and it has been postulated that oil films on the hydrate impedes hydrate dissolution when hydrates are in contact with sea water. It has been proposed that buoyancy-driven detachment from the seafloor of such massive gas hydrate deposits shapes the local seafloor morphology (Pape et al., 2011; Suess et al., 2001), influences seepage activity and intensity (MacDonald et al., 1994) and provides a mechanism to transport methane trough the water column to the atmosphere (Suess et al., 2001).

1.5 Fate of hydrocarbons in the water column

Once hydrocarbons reach the seafloor, whether in the dissolved phase or as free gas and oil, they will be released to the hydrosphere. In case gas is dissolved in pore water which is seeping from the seabed, it will mix with the ambient seawater. In case of intensive fluxes, bottom water might be significantly enriched in methane (Linke et al., 2010; Mau et al., 2006). However, water enriched with methane will mix with the surrounding water body (Mau et al., 2006) or, in case of sufficiently high methane concentrations, e.g. >20 nmol L^{-1} be oxidized aerobically by microbes (Kessler et al., 2011; Valentine et al., 2001). Therefore, it is assumed that dissolved methane remains in or is consumed in the water column and does not reach the atmosphere.

Only few studies assessed the relative importance of dissolved versus bubble fluxes of hydrocarbons at cold seeps (e.g. Naudts et al., 2010; Sauter et al., 2006). The available data show that bubble fluxes inject much more methane into the water column during periods of active venting than dissolved fluxes do. Yet, it is widely accepted that gas bubbles released from seeps in deep water (>100 mbsl) do not reach the sea surface and thus do not directly contribute to atmospheric methane (McGinnis et al., 2006; Schmale et al., 2005). This is due to rapid bubble dissolution which is caused by the steep concentration gradient between the gases within bubbles (mainly methane) and the water column (Leifer and Judd, 2002; Rehder et al., 2009). Conversely, other gases, as nitrogen or oxygen, are more abundant in the water column than in seep bubbles and might therefore inflow the bubble (Leifer and

Judd, 2002). The rate of gas outflow to the water column and gas inflow from the water column as well as bubble growth due to loss of hydrostatic pressure during bubble rise are processes that control whether seep bubbles reach the water-atmosphere interface or not (Leifer and Judd, 2002) (Fig. 6). These processes also control the amount of methane being released to the atmosphere in case bubbles reach the sea surface.

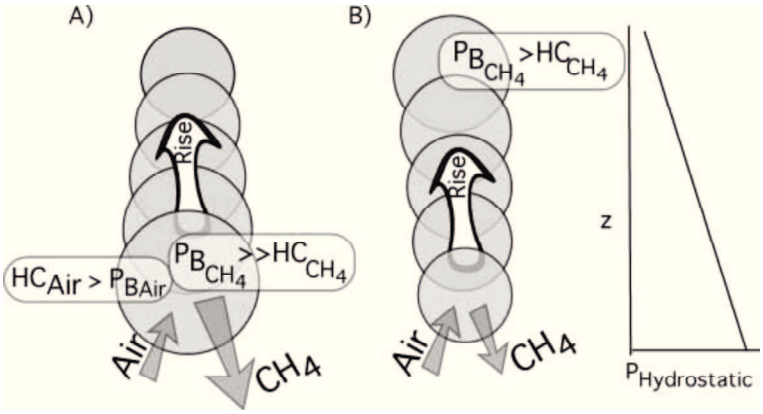

Fig. 6. Model of bubble growth and shrinkage during ascent. In A) gas outflow is greater than inflow and bubble shrinkage is not compensated by expansion due to loss of hydrostatic pressure. In B) in- and outflow of gas is equal but the bubble grows due to loss of hydrostatic pressure (from Leifer and Judd, 2002).

Despite the great number of studies showing that seep bubbles released in deep waters do not reach the sea surface (e.g. Greinert et al., 2006; Leifer and Judd, 2002; Merewether et al., 1985; Römer et al., *submitted;* Schmale et al., 2005), few studies evidenced that bubbles released in several hundreds of meters of depths might reach the sea surface (Cranston et al., 1994; De Beukelaer et al., 2003; Solomon et al., 2009). Several possible mechanisms enhancing bubble lifetime have been proposed in literature. These comprise gas hydrate shell formation around bubbles (Rehder et al., 2009, 2002), oil coatings around bubbles (MacDonald et al., 2002), upwelling flows generated by rising bubbles (Leifer et al., 2000; Leifer and Patro, 2002; Sauter et al., 2006) and enrichment of dissolved methane in water surrounding bubble plumes (MacDonald et al., 2002). These processes are detailed in the following paragraph.

Gas hydrate shelled bubbles: There is evidence from field studies as well as modeling that gas bubble dissolution is impeded within the gas hydrate stability zone (GHSZ) due to formation of hydrate shells on the bubble surface (Greinert et al., 2006; McGinnis et al., 2006; Merewether et al., 1985; Rehder et al., 2009, 2002). However, this shell will rapidly decompose upon reaching the upper boundary of the GHSZ. Rehder et al. (2009) showed that gas hydrate formation on bubble surfaces immobilizes these, which has a negative effect on the bubble rise velocity (Leifer and Patro, 2002). After hydrate shell formation, the gas exchange between bubble and water column is no longer controlled by differences in the chemical potential of free gas and gas dissolved in the sea water, but by the potential difference between hydrate and dissolved gas phase (Rehder et al., 2009). Methane hydrate has a lower chemical potential than gaseous methane, which results in a lower concentration gradient between bubble and water column. This causes slower bubble dissolution (Rehder et al., 2009). Also, the bubble-gas composition affects the bubble dissolution. Admixtures of gases other than methane, e.g. other hydrocarbon gases or CO_2, N, or O_2, attenuate the concentration gradients between gas bubble and water column, as well as the gas in- and

outflows, and thus bubble dissolution. If the bubble forming gas contains C_{2+} hydrocarbons, i.e. thermogenic gas, gas hydrate shells of sII hydrate can form. Since these are thermodynamically more stable than sI hydrate shells, they decompose in significantly shallower depth.

Oil coated bubbles: Oil coatings surrounding gas bubbles were shown to have dissolution hampering effects comparable to hydrate shells (MacDonald et al., 2002; Solomon et al., 2009). In contrast to gas hydrate shells, oil coatings do not decompose during bubble rise and thus provide a mechanism to transport bubble gas to the sea surface (De Beukelaer et al., 2003; Solomon et al., 2009). While the gas is released to the atmosphere, the oil remains on the sea surface where it might be observed visually or, in case sufficiently large oil slicks form, by air- and spaceborne remote sensing techniques (Hu et al., 2009; MacDonald et al., 1993). It was previously proposed that pure oil droplets would not be buoyant enough to be advected within the sediments and water column but need gas as a carrier (Clarke and Cleverly, 1991). Therefore, signatures of oil seepage on the sea surface might be taken as indicator for combined oil and gas transport through the sediments and from the seep to the water-atmosphere interface. Still, the gas originally contained in the bubbles might be exchanged by e.g. oxygen or nitrogen during ascent. Thus, bubbles might contain only small amounts of methane upon reaching surface waters (Hu et al., 2012).

Formation of plumes of dissolved gas: It was shown for deep water (Solomon et al., 2009) and shallow water (Clark et al., 2000; Mau et al., 2010) seep areas that plumes of dissolved methane might be produced by partly dissolving gas bubbles. In turn, the gas concentration gradient between bubbles rising within such plume is lower than that for bubbles rising through sea water with background dissolved methane concentration. This enhances their lifetime (Clark et al., 2003; MacDonald et al., 2002)

Upwelling: At sites of vigorous bubble emission, rising bubbles exert a drag on the surrounding water column, initiating an upwelling flow (Leifer and Patro, 2002). In this case, gas bubbles are injected into an upward moving water mass, which increases their rise velocities significantly. For instance, Clark et al. (2003) obtained upwelling velocities for shallow water seeps at Coal Oil Point off California that ranged between 15 and 40 cm s^{-1}, depending on vent size. MacDonald et al. (2002) reported upwelling flows of 10 cm s^{-1} for a deep water seep in the northern Gulf of Mexico. Bubbles rising in an upwelling flow have higher net rise velocities than bubble rising in steady water masses. Therefore, they have better chances to reach shallow waters or the sea surface (MacDonald et al., 2002).

1.6 Tectonic settings and global distribution of marine cold seeps

Marine cold seeps occur virtually globally along continental margins (Fig. 7). Prerequisites for cold seep formations are sufficient deposition of organic matter, allowing the generation of biogenic or thermogenic hydrocarbons, and tectonic or seismic activity or shallow sediment dynamics that provide pathways for hydrocarbon migration (Judd and Hovland, 2007). Generally, these prerequisites are met along continental margins and large intercontinental basins like the Black Sea or Caspian Sea. Cold seeps have been discovered in the full spectrum of continental margin and tectonic settings, as active margins, passive margins or transform plate-boundaries (Judd and Hovland, 2007; Suess, 2010).

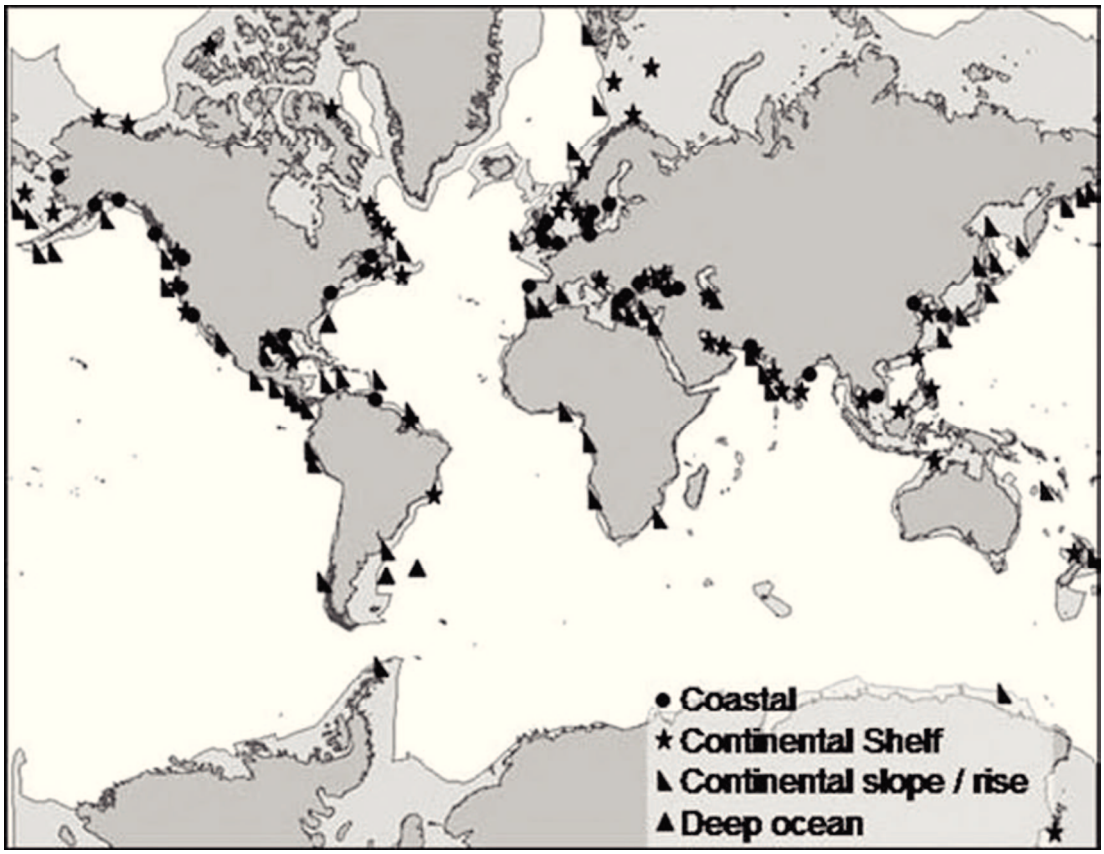

Fig. 7. Map showing the global distribution of cold seeps (from Judd, 2003).

At active margins, an oceanic plate is subducted either under a continental plate or under another oceanic plate. Active margins can be further distinguished in accretionary and erosive margins. At accretionary margins, sediments deposited on the subducting plate are partly (~20 %, von Huene and Scholl, 1991) scraped off by the overriding plate and accreted to it. This process is progressively extending the overriding plate and moving the subduction front seawards. The accreted sediments are faulted and folded, forming sequences of thrust slices (von Huene and Scholl, 1991; White, 1982). The subducted marine sediments are subject to pressure- and temperature-driven dewatering. Pore fluids expelled from these sediments migrate upward along the décollement zone towards the accretionary wedge (Talukder, 2012). Where thrust faults reach the décollement, fluids might migrate upward (Suess, 2010). These overpressured fluids might initiate diapirism, foster hydrocarbon migration from shallower accumulations, or transport dissolved gases towards the seafloor (Grando and McClay, 2007).

At erosive margins, sediments formerly accreted to the overriding plate (frontal erosion), or basal rock of the core of the overriding plate (basal erosion), are eroded by subduction of the oceanic plate (von Huene and Scholl, 1991). Therefore, the sediments being subducted are a mixture of oceanic sediments and continental crust. Parts of the oceanic sediments might be underthrusted or underplated at the base of the overriding plate (von Huene and Scholl, 1991). However, fluid migration generally follows the same mechanisms as described for accretionary prisms. Yet, Ranero et al. (2008) suggest that fluids originating from sediment dewatering might rather migrate through fractures in the overriding plate than along the décollement to the deformation front.

Passive margins are characterized by a smooth transition between continental and oceanic crust without active plate boundaries. The eastern Atlantic represents such passive margin. The upslope areas of passive margins represent extensional regimes, while the down slope areas are compressional regimes (Gay et al., 2007). A schematic model for seepage processes at passive margins was presented by Gay et al. (2007) (Fig. 8).

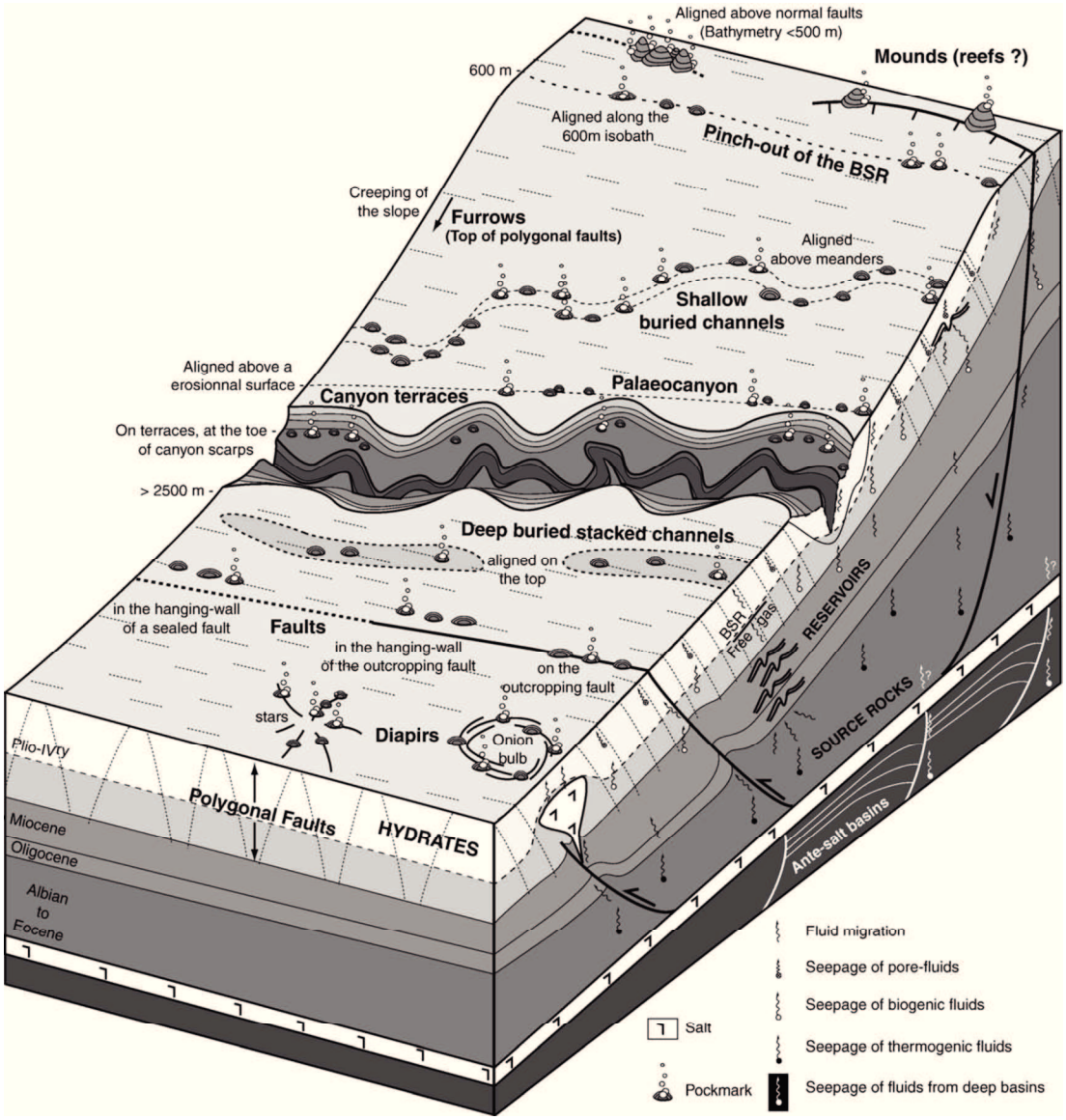

Fig. 8. Schematic model illustrating geologic processes and related cold seep features and processes at passive continental margins (from Gay et al., 2007).

At the landward section of passive margins, extensional faults might serve as preferred fluid migration pathways. At the seaward site of a passive margin, the compressional regime might induce salt or shale diapirism and create compressional faults which provide pathways for fluid migration (Andresen and Huuse, 2011; Gay et al., 2007; Serié et al., 2012). Surface expressions of fluid flow are very similar at passive and active margins, and they comprise a broad range of morphological features. These are pockmarks (Andresen and Huuse, 2011; Sahling et al., 2008a; Ussler III et al., 2003), hydrate mounds (Paull et al., 2008; Serié et al., 2012), carbonate pavements and chimneys (Dupré et al., 2010; Holland et al., 2006;

Peckmann et al., 2001; Vaughn Barrie et al., 2011) or mud volcanoes (Feseker et al., 2010; Grando and McClay, 2007). Cold seeps discharging non-oil hydrocarbons have been discovered and investigated globally along active erosive margins, e.g. at the Hikurangi (Klaucke et al., 2010; Naudts et al., 2010) and Costa Rica Margin (Bohrmann et al., 2002; Klaucke et al., 2008; Sahling et al., 2008b), at accretionary margins, e.g. the Makran Margin (Ding et al., 2010; Römer et al., *submitted;* von Rad et al., 2000; Wiedicke et al., 2001), as well as along passive margins, for instance at Blake Ridge off Carolina (Paull et al., 1995; Van Dover et al., 2003), in the Gulf of Mexico (Brüning et al., 2010; Heeschen et al., 2007; MacDonald et al., 2003),in the North Sea off Norway (Hovland and Thomsen, 1989; Schneider von Deimling et al., 2011), in the North Atlantic off Svalbard (Hustoft et al., 2009; Westbrook et al., 2009) and off India (Dandapath et al., 2010). Seepage along transform plate boundaries have been discovered in the Sea of Marmara (Géli et al., 2008) and offshore California (Canet et al., 2010; Hornafius et al., 1999; Orange et al., 1999a).

Oil seepage occurs only in places where great amounts of organic matter were buried through geologic history, burial rates were high enough to impede microbial degradation of organic matter, and enough time was given for thermocatalytic hydrocarbon generation. Therefore, oil seepage occurs predominantly along passive margins and in sedimentary basins (Wilson et al., 1974) (Fig. 9).

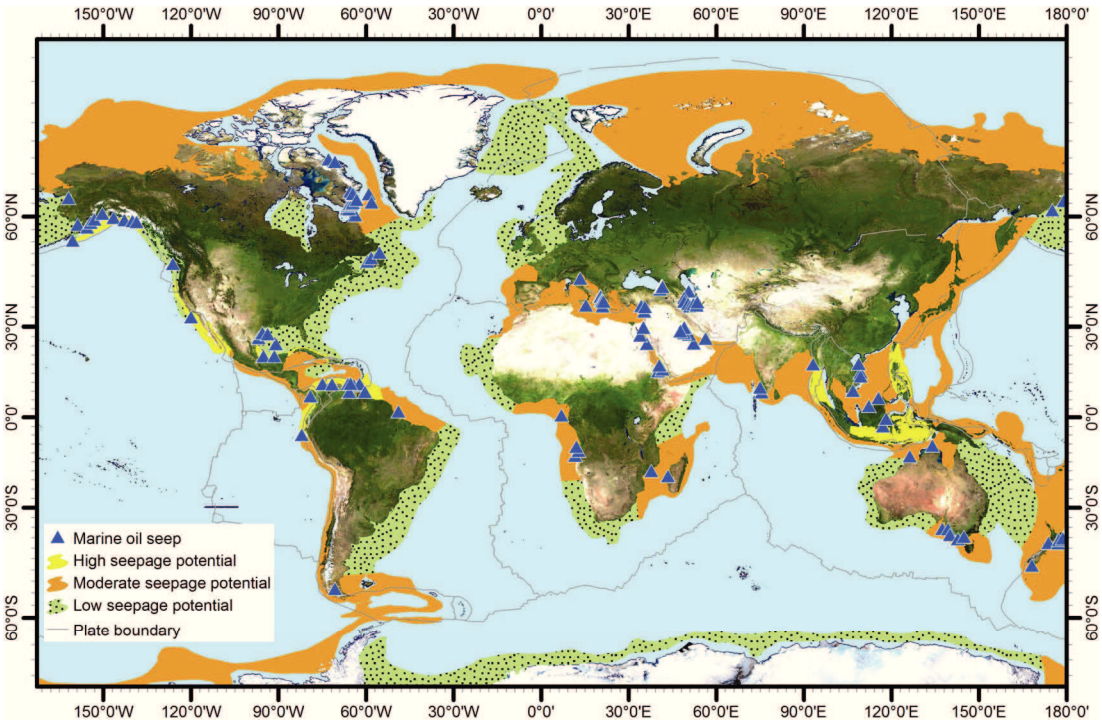

Fig. 9. Map showing the global distribution of oil seeps and potential oil seepage regions (compiled from Jauer and Budkewitsch, 2010; Levy and Ehrhardt, 1981; Logan et al., 2010; Page et al., 1997; Palacas et al., 1986; Traynor and Sladen, 1997; Udachin et al., 2007; Wilson et al., 1974)

Oil seepage was reported mostly for passive margins, e.g. off eastern Canada (Jauer and Budkewitsch, 2010), off Angola, in the Gulf of Mexico (Beisl et al., 2004; Brüning et al., 2010; De Beukelaer et al., 2003; Garcia-Pineda et al., 2010; Hu et al., 2009; Kornacki et al., 1994; MacDonald et al., 1993; Pellon de Miranda et al., 2004; Whelan et al., 2005), and off Vietnam (Traynor and Sladen, 1997). However, oil seeps have also been discovered along

active margins, e.g. off Alaska (Page et al., 1997) and offshore Vancouver Island (Hester and Brewer, 2009).

Seepage of oil and gas is often associated with deltas or fans of major rivers which deposit large amounts of terrigenous, organic matter rich sediments on shelfs and continental slopes. Prolific examples of such systems are the Nile fan off Egypt where gas seeps, seepage associated carbonate crusts and mud volcanoes have been described (Bayon et al., 2009a; Dupré et al., 2010; Feseker et al., 2010) or the Congo River fan (Andresen and Huuse, 2011; Olu et al., 2009; Sahling et al., 2008a). Thousands of gas seeps have been discovered on the Dnepr paleo-delta in the north-western Black Sea (Naudts et al., 2006). One of the world's most prolific oil and gas seepage regions is located in the northern Gulf of Mexico off Louisiana. It is associated with salt tectonic-driven deformation of sediments of the Mississippi fan (Kennicutt II et al., 1988; MacDonald and Peccini, 2009; Sassen et al., 2001a).

Academic research often focuses on the detection and investigation of gas seepage and associated gas hydrate occurrences. This is because of research interests in understanding gas hydrate dynamics in relation to climate change, or in exploration of the potential of hydrates as future energy source. Knowing the provinces that are prone to hydrate formation and seepage, new seep and hydrate bearing sites are continuously being discovered. Oil seepage is less intensively studied, which might be due to the generally lower abundance of oil seeps. As indicated in Fig. 9, which is based on the first approach by Wilson (1974) to identify potential oil seepage provinces and give an overview of known marine oil seeps, oil seepage is expectedly more widespread than currently known. It is striking that the number of known active oil seepage areas has not dramatically increased since the initial study by Wilson. However, with the advancement of air- and spaceborne remote sensing techniques, numerous new seeps have been discovered within known seepage areas. The most striking example might be the Gulf of Mexico. While Wilson (1974) indicated 72 seeps for the entire Gulf of Mexico, at present about 530 oil emitting seeps are known, of which approximately 400 are located in the northern Gulf of Mexico and 130 in the southern Gulf of Mexico (Garcia-Pineda, 2009).

1.7 Geochemical and biological processes at cold seeps

Irrespectively, if cold seeps discharge biogenic or thermogenic hydrocarbons, they represent unique systems of faunal and microbial activity that actively influence the seafloor morphology and geochemical cycles. These processes are generalized and summarized in Fig. 10. Probably the most important process occurring in shallow sediments where methane is migrating towards the sediment surface is AOM (see section 1.2, eq. 4). In the course of AOM, methane and sulfate are converted into hydrogen sulfide, water and carbonate (Barnes and Goldberg, 1976). The sulfate consumed in this process is percolating from the seawater into the sediments.

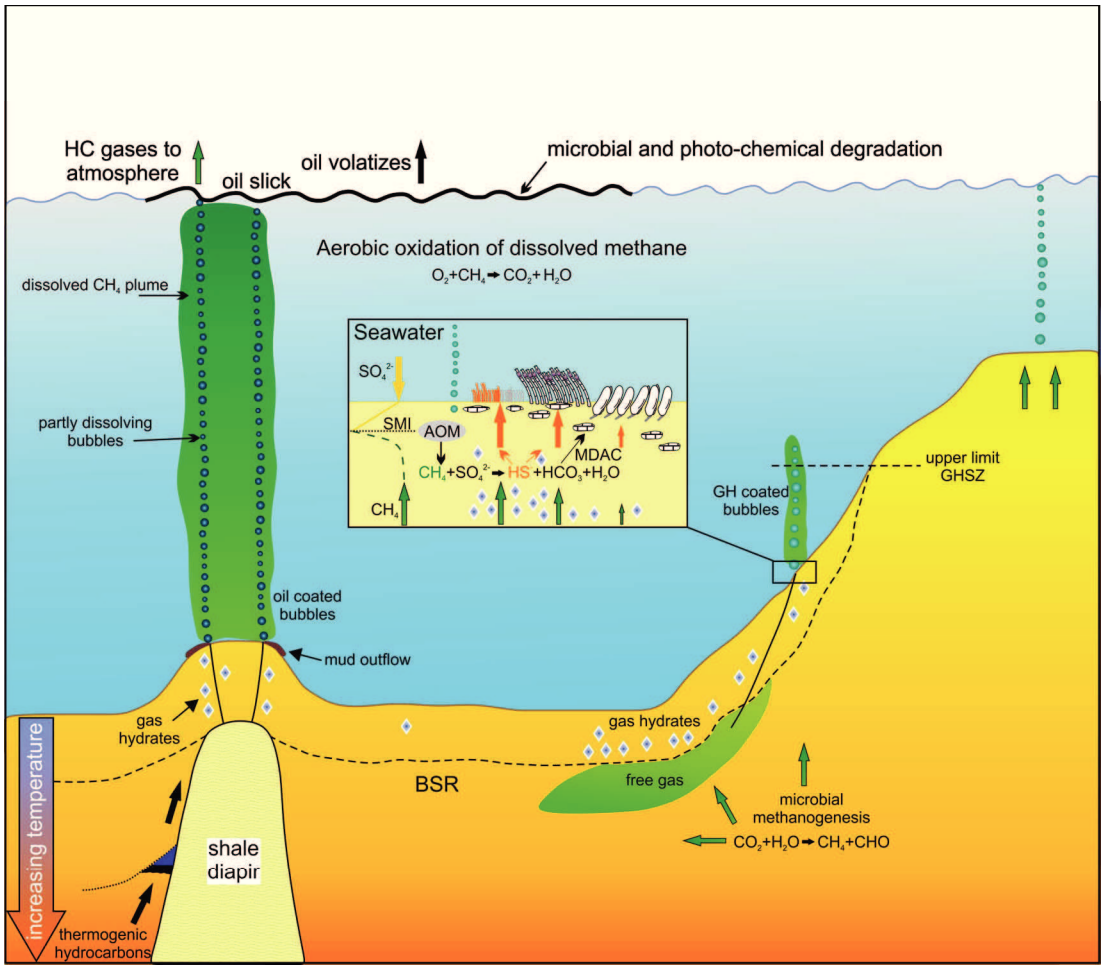

Fig. 10. Illustration of geological, geochemical and biological processes at cold seeps (compiled from Bohrmann and Torres, 2006; Dubilier et al., 2008; Luyendyk et al., 2005; Sibuet and Vangriesheim, 2009; Suess, 2010; Whelan et al., 2005). Abbreviations: AOM = Anaerobic oxidation of methane, BSR = Bottom simulating reflector, GH = Gas hydrate, GHSZ = Gas hydrate stability zone, HC = Hydrocarbon, MDAC = Methane derived authigenic carbonate, SMI = Sulfate-methane interface.

Sulfate concentration gradients in the sediment column have been established as robust proxy for methane fluxes from below. The higher the methane flux, the shallower the depth in which sulfate is entirely consumed by AOM (Borowski et al., 1996) (Fig.11).

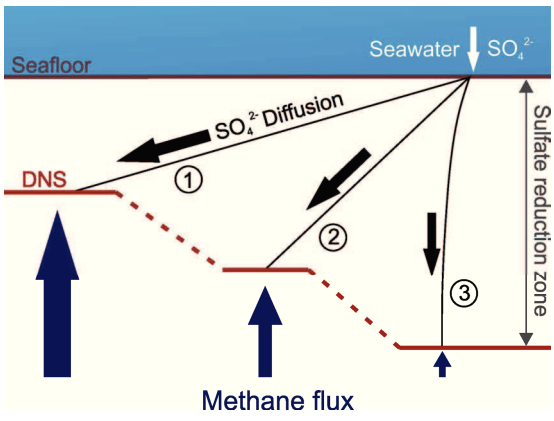

Fig. 11. Scheme showing the dependency of sulfate gradient on upward methane fluxes. Large blue arrows indicate high flux and a methane flux driven consumption of sulfate (1 and 2). At high methane fluxes the depth of no sulfate (DNS) shifts closer to the sediment surface. Profile 3 represents low methane flux and sulfate reduction by in-situ organic matter (modified from Borowski et al., 1996).

This depth of no sulfate is commonly denoted as sulfate-methane interface (SMI) (Borowski et al., 1999). It is thought that AOM consumes the vast majority of methane that is migrating towards the sediment-water interface (Barnes and Goldberg, 1976; Sommer et al., 2006). Vital communities of higher organisms as clams, mussels, and tubeworms are often found at cold seep sites within oxygenated waters (Levin, 2005; Sibuet and Olu, 1998). It was shown that these organisms live in symbiosis with either sulfur oxidizing microbes that utilize AOM-derived sulfide as energy source or methane oxidizing bacteria using methane which is not consumed within the sediments (Dubilier et al., 2008). Sahling et al. (2002) demonstrated that a correlation exists between rates of fluid flow, i.e. sulfide flux, and faunal and microbial communities populating cold seeps. It was shown that often concentric formations of different microbial and faunal species occur around sites of sporadic gas bubble emissions, which correspond to flux gradients, from the inner habitats (highest flux) towards outer habitats (lowest flux). Where methane and sulfate fluxes are at highest, dense mats of thiotrophic bacteria may be found, being surrounded by tubeworms and clams (Fischer et al., 2012; Sahling et al., 2002). Fischer and co-worker (2012) evidenced that clams populating the outer, low-flux areas of active vent sites actively shape their geochemical environment by pumping seawater and therewith sulfate into the sediments to enhance sulfide production.

Observations suggesting that chemosynthetic communities consume almost all dissolved methane and sulfide in surface near sediments, lead to the creation of the term benthic filter (Sommer et al., 2006). However, there is evidence that gas bubbles efficiently bypass this filter without being altered by AOM (Naudts et al., 2010; Sommer et al., 2006). In case methane flux and therewith AOM is sustained on long time scales (hundreds to thousands of years) (Luff et al., 2004), massive methane derived authigenic carbonates (MDAC; Fig. 10) form in the surface near sediments and on the sediment surface. These carbonates might form crusts , mounds (Dupré et al., 2010; Foubert et al., 2008), or chimneys (Vaughn Barrie et al., 2011). These carbonates may serve organism as substrate to settle and therefore influence the lifecycle of a cold seep and change its biological composition. Also, these seep carbonates provide valuable information on the seep and fluid flow history (Han et al., 2004) and the age of the system (Bayon et al., 2009a). The fact that certain cold seep organisms are obviously related to a narrow range of methane and sulfide fluxes allows using them as proxies to determine fluxes of these compounds.

1.8 Cold seeps and global climate (change)

The global climate and carbon cycle are closely interrelated as climate conditions might alter organic carbon production, deposition and decomposition. In turn, carbon release from deposits, e.g. as greenhouse gases like CO_2 or CH_4, impacts the climate. With the recognition that currently observed climate change is strongly affected by human activity (Barnett et al., 2001; Rosenzweig et al., 2008), efforts are made to determine the sources of atmospheric gases which, due to their radioactive forcing, significantly control the climate (Denman and al., 2007). The most relevant and abundant greenhouse gases are water vapor, CO_2 (~380 ppm) and by CH_4 (1,750 ppb) (Forster et al., 2007). The current concentrations of the latter two are higher than ever since the last 650 kyrs (Le Treut et al., 2007). Though the CH_4 concentration is lower than the CO_2 concentration, its radiative forcing potential is about 35 times higher (Lelieveld et al., 1998). In the global budget presented by the IPCC in 2007, various natural and anthropogenic sources sum up to an annual global methane emission to the atmosphere of about 582 Tg. These emissions are

almost balanced by a global sink of 581 Tg yr^{-1} (Denman and al., 2007). These estimates are slightly lower compared to the previous report (Kvenvolden and Rogers, 2005). As illustrated in Fig. 12, anthropogenic sources constitute about 60 % of the global CH_4 budget while only 40 % are of natural origin.

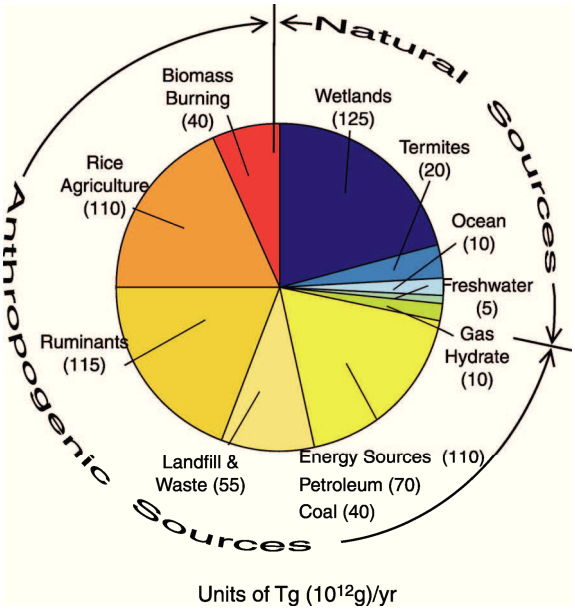

Fig. 12. Diagram showing the different natural and anthropogenic contributions to the global atmospheric methane budget (from Kvenvolden and Rogers, 2005).

The IPCC suggests that about 20 % of the anthropogenic contribution to the CH_4 budget originates from production and consumption of fossil fuels (Denman and al., 2007). The origin of methane may be assessed by mixing models which consider the $\delta^{13}C$-signatures of different sources (Etiope et al., 2008). The methane release from fossil fuel utilization is estimated based on the amount of fossil, non-radiocarbon methane. However, the current budget does not consider that also natural sources as terrestrial and marine seeps and mud volcanoes emit fossil methane, though this is acknowledged in the latest IPCC report (Denman and al., 2007). Numerous studies aimed to quantify the contribution of natural sources to the global atmospheric methane budget (Etiope et al., 2008; Hovland et al., 1993; Judd, 2003; Kvenvolden and Rogers, 2005). Uncertainties originate form sparse measurements of methane fluxes, especially from marine sources. Further, assessment of natural fluxes is complicated by uncertainties in occurrences of seeps and the fate of methane released from marine sources.

Kvenvolden and Rogers (2005) estimated, based on available data on methane emission rates and global distribution of seeps and mud volcanoes that natural sources may constitute as much as 45 Tg of the total 110 Tg of fossil methane in the global budget. This corresponds to 41 % of the fossil methane in the atmosphere which is to date solely assigned to fossil fuel utilization. In a more recent study, Etiope and co-workers (2008) reassessed data on natural methane emissions and estimate that geologic sources annually emit 53 ± 11 Tg methane to the atmosphere (Fig 13). They also suggest that 30 % of the atmospheric methane originates from fossil hydrocarbon sources which is about 10 % more compared to the latest IPCC budget (Denman and al., 2007).

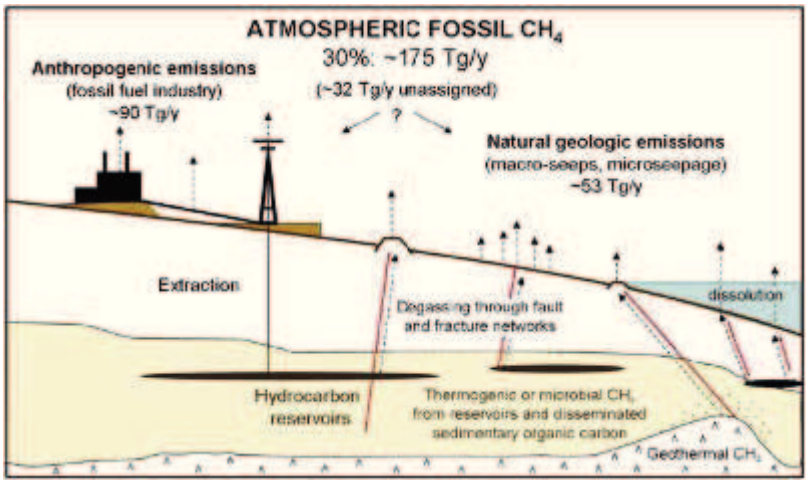

Fig. 13. Anthropogenic and geologic sources to the atmospheric pool of fossil methane (from Etiope et al., 2008).

While fluxes from terrestrial sources are relatively easy to measure (Etiope et al., 2007), assessment of marine gas emissions is complicated. Long-term monitoring data of gas bubble emissions is only available for one shallow-water site within the Coal Oil Point seep area offshore California (Clark et al., 2003). Other flux measurements are sparse and restricted to spatially and temporally discrete measurements (Leifer and MacDonald, 2003; Römer et al., *submitted;* Sahling et al., 2009; Sauter et al., 2006). Judd et al. (2002) used published data on fluxes from marine seeps, seep and gas hydrate distributions and considerations affecting hydrocarbon migration and emission to estimate that 7 to 20 Tg yr^{-1} of methane are released from continental margins to the atmosphere, with a similar amount remaining in the water column. These values correspond to 13 to 39 % of the total geologic methane sources identified by Etiope and co-workers (2008) and 1 to 4 % of the total global methane budget as mentioned in the latest IPCC report (Denman and al., 2007). Therewith, geologic methane sources might be as significant as the second largest natural source (termites) which is considered in the IPCC report (Denman and al., 2007) (Fig. 12).

With the growing evidence for significant contributions of geologic methane sources it may be questioned how changing climate and geologic hydrocarbon sources might interact. In paleoclimatology, it has been suggested that major greenhouse periods in earth's history, for instance the Paleocene-Eocene thermal maximum, may have been strongly influenced by massive methane release from dissociating gas hydrates (Dickens et al., 1995). In this scenario, initial warming induced by volcanic activity or orbital forcing (Dickens et al., 1995; Nisbet, 1990) induced warming of bottom-water masses which triggered gas hydrate decomposition. The subsequent release of a fraction of the liberated gas to the atmosphere enhanced global warming (Dickens, 1999). Though this theory has been challenged (Dickens, 2011; McInerney and Wing, 2011 and references therein), it seems obvious that gas hydrates and free gas below represent an important factor in future and past climate change scenarios (Archer et al., 2009). Various feedback mechanisms related to gas hydrate formation and decomposition and natural seepage have been proposed (Judd et al., 2002) (Fig. 14).

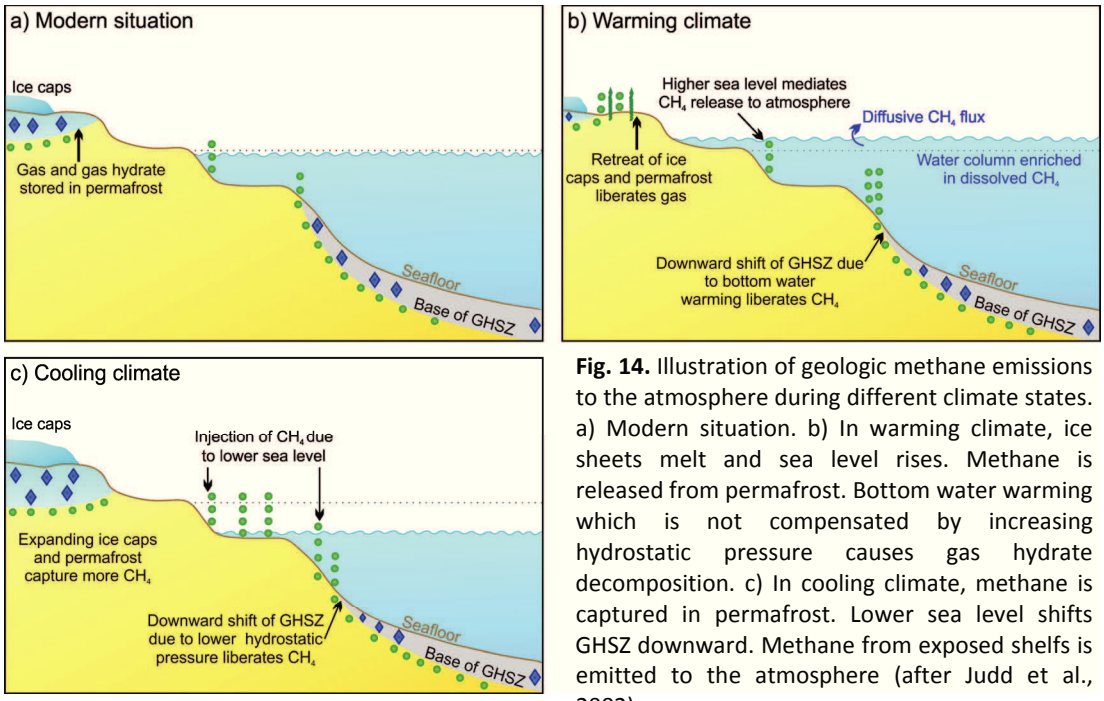

Fig. 14. Illustration of geologic methane emissions to the atmosphere during different climate states. a) Modern situation. b) In warming climate, ice sheets melt and sea level rises. Methane is released from permafrost. Bottom water warming which is not compensated by increasing hydrostatic pressure causes gas hydrate decomposition. c) In cooling climate, methane is captured in permafrost. Lower sea level shifts GHSZ downward. Methane from exposed shelfs is emitted to the atmosphere (after Judd et al., 2002).

In cooling climates, the advancement of permafrost might trap methane in soils and gas hydrates. Conversely, lower sea level in glacial periods shifts the upper boundary of the GHSZ down and causes gas hydrate dissociation. Also, seep areas in shallow shelf regions may be exposed to the atmosphere and inject methane straight to the atmosphere. These effects would induce climate warming (Judd et al., 2002). In warming climate, methane would be released from melting permafrost and bottom-water warming might destabilize gas hydrates. Yet, higher sea levels might buffer some of the enhanced methane emissions from the seafloor (Judd et al., 2002) (Fig. 14b). Evidence for these feedback mechanisms are given in recent literature. Luyendyk et al. (2005) showed that shallow seep areas offshore California have been exposed to the atmosphere during the Last Glacial Maximum and may have emitted significant volumes of hydrocarbons to the atmosphere. Discoveries of large paleo-pockmarks off New Zealand have been attributed to repetitive catastrophic gas releases due to gas hydrate decomposition during periods of lower sea levels (Davy et al., 2010). The occurrence of gas seepage offshore Svalbard was recently explained by warming of bottom waters during the last 30 yrs and subsequent downward shift of the GHSZ (Westbrook et al., 2009). In subarctic regions it was shown that melting of terrestrial and marine permafrost liberates methane to the atmosphere in magnitudes equal to the atmospheric contribution from all marine seeps (Shakhova et al., 2010).

These results show that important correlations between natural methane seepage and natural and anthropogenic climate change exist. However, especially better understanding of the significance of marine seepage and the fate of methane released to the hydrosphere, as well as a better understanding of the sensitivity of gas hydrates to climate change is needed to predict magnitudes of feedback mechanisms in future changing climates.

Chapter 2

Motivation for and main objectives of the present work

The overarching aim of the present work was to contribute to a better understanding of the relevance of marine hydrocarbon seepage in global carbon cycles. Therefore, it was aimed to develop new methods and approaches that would allow determining critical factors as areal gas emission rates, seepage variability, and occurrence on local to global scales.

Seepage of hydrocarbon fluids, predominantly methane, has been identified as global phenomenon along continental margins and is though to emit significant volumes of hydrocarbons to the hydrosphere. The assessment of the impact and importance of marine hydrocarbon seeps on global atmospheric methane budgets has been subject to numerous studies. The main conclusion of these is that marine seepage emits significant volumes of methane to the atmosphere. Yet, all of these studies are based on mass-balance calculations and extrapolations of sparse flux measurements. However, a putative discrepancy between global and local studies exists. The latter indicate that a large portion of methane migrating towards the seabed is consumed by microbial and faunal communities and that bubble-gas released to the hydrosphere is largely dissolved in the water column, never reaching the atmosphere. The so far only evidence of deep-sea methane emissions reaching the atmosphere to some extent was found at oil seeps in the northern Gulf of Mexico. From these uncertainties in the determination of the importance of seepage on atmospheric methane concentrations the following questions arose, stimulating the present work:

1.) Can optical and geophysical mapping techniques provide means to assess spatial extents of seeps, seepage activity, and turnover rates of methane?

Methane is transported from sediments towards the seafloor and hydrosphere either dissolved in pore-water or as gas bubbles. While the latter occurs at distinct sites where bubbles are discharged from the seabed, dissolved methane transport occurs over larger areas. Contrasting to gas bubble emissions, dissolved gas emissions are not directly recognizable by geophysical or visual observations. While local gas bubble emission rates may be obtained by visual or geophysical quantification methods, dissolved fluxes are inferred from in- or ex-situ flux measurements, e.g. using benthic chambers or by pore-water analysis. However, these methods fail to elucidate the relevance of areal fluxes of dissolved gas versus local bubble emissions.

Numerous studies have highlighted the correlation between certain chemosynthetic communities and a narrow range of dissolved methane fluxes. These communities might thus provide a proxy for areal methane fluxes. One of the most crucial aspects in determining areal methane budgets, including discharge and turnover rates, is therefore the precise mapping of *active* seepage areas. To address this problem, the capabilities of combined ROV-based high-frequency sonar seafloor mapping and video-mosaicking were tested to provide detailed information on seepage areas and occurrences of distinct chemosynthetic communities. These data might serve as a base to extrapolate local dissolved and gaseous methane flux measurements and turnover rates to obtain methane budgets of entire seeps.

2.) How relevant is dissolved methane transport and turnover compared to local gas bubble emissions?

Dissolved gas fluxes occur over large areas, while bubble emissions represent localized gas discharge. There is evidence that most dissolved methane is consumed by biogeochemical processes, while gas bubbles bypass these. However, only areal budgets, including dissolved and bubble effluxes, and consumption rates allow drawing conclusions on the relative importance of these different processes. This question, in concert with the first question, is addressed in Chapter 5.

3.) Are remote sensing techniques, such as satellite imagery, capable of identifying new seepage areas, and distinct seeps?

One problem in determining the importance of marine seepage in global carbon cycles arises from uncertainties in the occurrence of seeps, both in location and number. Commonly, cold seeps that emit gas are only detected by hydroacoustic methods, because they do not produce signatures on the sea surface. These investigation methods are limited in spatial coverage and costly in both time and money. However, in case cold seeps emit oil, this might form oil slicks on the sea surface which may be imaged by various air- and spaceborne remote sensing sensors. Here, it was investigated whether new oil seepage areas and distinct seeps can be identified based on *synthetic aperture radar* satellite image analysis. It was tested whether the derived information provide an accurate base for more detailed investigations during subsequent research cruises.

4.) Do satellite images provide a tool for monitoring seepage activity on large scale with good temporal and spatial accuracy?

Probably one of the most uncertain factors in cold seep research is the knowledge in seepage variability that is how seepage activity and magnitude change over time. Data on seepage variability are sparse since obtaining these relied largely on reconnaissance surveys in the past. Thus, snapshots of seepage activity over only few hours to days are available, with a revisiting frequency of few years at the best. Also, such low temporal resolution monitoring is restricted to a small number of sites. Further on, intensively studied sites are usually prolific seeps and do not represent the full spectrum of seepage magnitude and activity. Again, for sites of oil seepage, satellite images available to academia might provide a tool for monitoring changes in activity patterns over much longer periods and larger areas. The capability of this method was tested on oil seeps in the Black Sea.

5.) Does a positive correlation exist between oil seepage and transfer of methane bubbles to the atmosphere?

As detailed in section 1.5, evidence exists that gas emissions from deep-water seeps do not provide a significant source for atmospheric methane. Few previous observations show however, that combined oil and gas seepage might enhance the bubble transport of methane to the water-atmosphere interface. In the present work, detailed hydroacoustic water column investigations in oil seepage areas in the Black Sea were conducted to elucidate whether a positive correlation exists between oil emissions and bubble-gas transport to the atmosphere.

6.) Is there a difference in hydrocarbon transport through the water column between seeps emitting biogenic and those emitting thermogenic hydrocarbons?

In case oil reaches the sea surface from a seep, hydrocarbons are transported to the atmosphere intrinsically. However, it might be questioned if other conditions being unique to seeps emitting thermogenic hydrocarbons, e.g. the formation of structure II gas hydrates, might have an impact on seepage processes and methane transport to the sea surface. This question is addressed in Chapters 6 and 7.

7.) Do deep-sea hydrocarbon seeps provide the potential to directly impact atmospheric methane budgets?

Based on the preceding questions, this work aimed to provide new insights into the relevance of deep-sea seepage in atmospheric hydrocarbon budgets. Therefore, the potential of different sensors and methods to detect seeps and quantify emissions was tested. Combinations of satellite imagery, optical mapping, and hydroacoustic techniques are promoted for attaining reliable estimates of hydrocarbon fluxes from cold seeps on global scales.

Chapter 3

Methods and techniques for cold seep detection and mapping

The detection of marine seeps is challenging. Though it is generally known which regions are prone to seepage, so far the detection of hydrocarbon seeps is limited to hydroacoustic and visual ship-based investigation techniques. Hydroacoustic methods comprise low frequency techniques as multi-channel seismics (about 10-100 Hz), single- or multibeam sediment profiler (approximately 2.5-7 kHz), and high frequency techniques as sidescan sonar (up to few hundreds of kHz) (Lurton, 2010). Depending on the operation frequency, these techniques image sediment properties from the surface down to few kilometers sediment depth. The lower the frequency, the deeper the acoustic sediment penetration is. While sediment profiler and seismic reflection techniques produce 2D vertical profiles of the sediments, sidescan sonar images the surface near sediments or seafloor horizontally in 2D. Yet, all techniques image sedimentary units due to density and/ or seafloor rugosity changes. These influence the sound impedance and amount of energy reflected to the transducer (Lurton, 2010).

Seismics and sub-bottom profiler may image gas charged sediments as acoustic blank zones, i.e. none or very few of the energy transmitted from the sound source is reflected by the sediments. Also, these tools can image zones of weak reflectance and sediments without clear stratification which are characteristic of mud or salt diapirs (Bouriak et al., 2000; Serié et al., 2012). In case fluid emissions have shaped positive or negative seafloor morphology, these features will be imaged in a horizontal cross-section as well and might be immediately linked to seepage (Hustoft et al., 2009; Krastel et al., 2003; Serié et al., 2012). In areas where the physical and geochemical properties of the sediments allow the formation of gas hydrates, a so-called bottom-simulating reflector (BSR) is often imaged in seismic data (Riedel and Rohr, 2012; Shipley et al., 1979; Zillmer et al., 2005). The BSR represents the lower boundary of the GHSZ and marks the transition from the gas hydrate to free gas zone. In deformed sediments, the BSR may be easily identified as a reflector with inverse polarity that parallels the seafloor and crosscuts sedimentary units.

Techniques that are able to image the sediment column might provide direct evidence for the presence of free gas, gas hydrates, and fluid migration pathways. However, they are not able to detect active fluid seepage or seepage influenced seafloor. High frequency tools, as sidescan sonars which penetrate the upper few decimeters of the sediment at the most, might be used to indirectly identify seep areas since the sediment properties at cold seeps usually differ from the non-seep areas (Fig. 15).

Seep related features like shallow gas hydrate deposits, chemosynthetic communities. or precipitation of authigenic carbonates produce higher backscatter due to increased surface rugosity or hardiness of the sediments (Johnson et al., 2003; Klaucke et al., 2006; Sahling et al., 2008a). Mud volcanoes may be characterized by either high or low backscatter, depending on the viscosity of the expelled material. Low viscosity mud produces low backscatter (Sahling et al., 2009) while more viscous and brecciated mud produces higher backscatter (Ivanov et al., 1996; Limonov et al., 1997). Furthermore, unprocessed side-scan data allows imaging gas bubble emissions to the water column, as these produce a high backscatter signal in the nadir of the sonar where normally no data is obtained due to the incidence angle of the acoustic beam (Dupré et al., 2010; Klaucke et al., 2006).

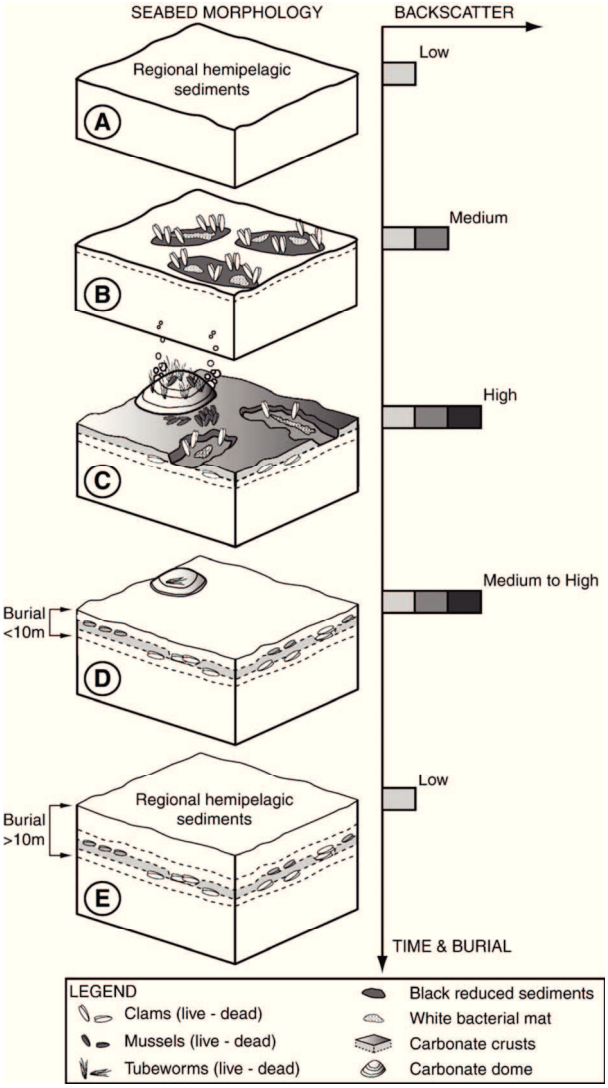

Fig. 15: Schematic illustration of the effects of seepage related features on the acoustic backscatter signal (from Gay et al., 2007).

Bathymetric data is obtained by using multibeam echosounders (MBES) which operate in a range from few tens of kHz to few hundreds of kHz. MBES are usually mounted on the hull of research vessels but increasingly they are deployed on remotely operated vehicles (ROV) (Hovland et al., 2010; Hovland and Svensen, 2006) and autonomous underwater vehicles (AUV) (Roberts et al., 2010; Römer et al., *in press*) to obtain higher resolution data. Besides providing information on the seabed relief, the amplitude information of the acoustic signal reflected back to the receiver can be processed to obtain information on the seafloor surface rugosity or sediment properties (Orange et al., 2002). However, resolution of these data is usually not comparable to those obtained by side-scan sonars.

For imaging active gas emissions from seep sites, single-beam echosounders have been traditionally used, for instance the Atlas PARASOUND or Kongsberg EK60 (Nikolovska et al., 2008; Westbrook et al., 2009). These echosounders are able to image free gas in the water column due to the large impedance contrast between gas and water (Nikolovska et al., 2008; Schneider von Deimling et al., 2007). The limitation of these echosounders is their beam width of approx. 4°-7°. The narrow beam angles hinder tracing gas bubble plumes in their full heights in case they experience significant current-induced horizontal deflections. This problem may be overcome by using the water column data recorded by MBES (Nikolovska et al., 2008). Since MBES can operate with opening angles of up to 150°, the

chance to image a gas bubble plume in full height despite possible deflections is greatly enhanced (Fig. 16). Recent advancements in water column data recording, storage, and processing might make MBES systems first choice tools for flare imaging in future. Gas flares are imaged in 'slices' by MBES, with one ping representing one slice (Fig. 16). Thus, the resolution of a flare being imaged depends on the ping rate and the speed of the vessel. The higher the ping rate and the slower the vessel moves, the more pings image one flare. New acquisition software, e.g. for the Kongsberg EM122 12 kHz echosounder, allow recording the water column data and bathymetry data separately or in combined files. Files containing water column data may be further processed, for instance using the Fledermaus Midwater Tool (© QPS). This tool allows replaying the water column data and to extract features of special interest. The flare highlighted in Fig. 16a) might be 'cropped' from the other data and exported to Fledermaus (© QPS) for 3D display. By this method, heights and deflections of flares can be assessed with high accuracy. For better visualization, the flare data may also be edited further, e.g. to delete soundings which do not represent the flare, using Fledermaus DMagic (© QPS). A drawback of the method is that 3D display of flares that show significant deflection requires lot of computer resources. This is because of the large amount of soundings representing such flares (Fig. 16b).

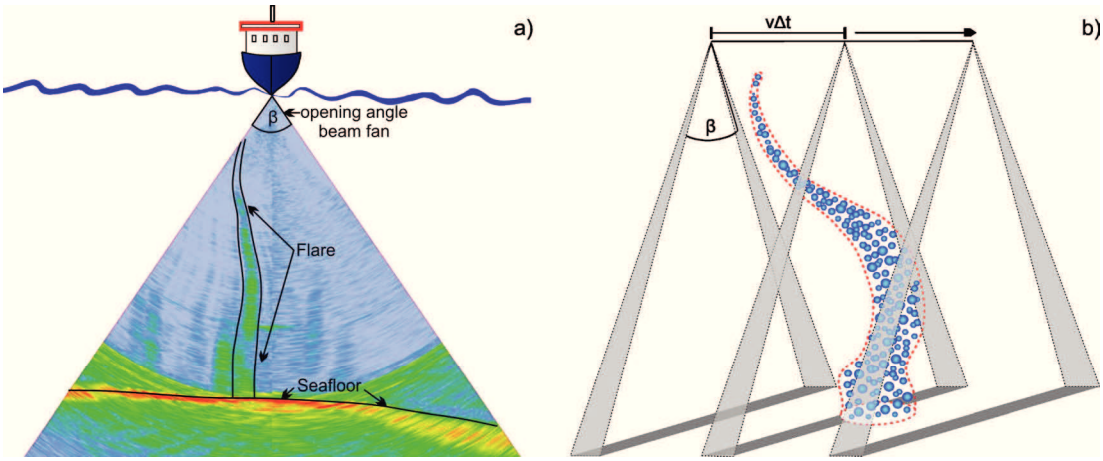

Fig. 16. a) Illustration of a fan-view of MBES data. The strong red reflector marks the seafloor, the data above represents the water column. Free gas causes acoustic anomalies in the records due to the impedance contrast between water and gas. b) Scheme of flare imaging by MBES each triangle represents one ping. The number of pings by which a flare is imaged depends on the ship speed (v) and the ping rate. The chance to image the entire flare height increases with the opening angle of the beam-fan (ß) (after Bohrmann et al., 2007).

Employing MBES systems for imaging the water column parallel to obtaining bathymetry and seabed amplitude maps provides a major improvement in seep detection and imaging. Yet, the areas which can be mapped are still limited, considering how much time is usually available for such investigations during multi-task scientific research cruises. Furthermore, detection of fluid emission sites depends on the activity patters of fluid emission (Greinert et al., 2006). During dormant periods, it is likely that a seep site which does not exhibit significant relief will not be identified. Also, monitoring data on seepage activity is sparse and limited to re-visiting of seep areas (Schneider von Deimling et al., 2011) or deployments of remotely controlled or autonomous observatories (Clark et al., 2003).

At sites where gas and oil seepage co-occurs, seep detection and monitoring is facilitated by a variety of space- and airborne remote sensing techniques which are able to detect oil

films on the water surface. Depending on the sensor, oil is visible due to its impact on sea surface roughness, thermal properties or emissivity of electromagnetic radiation (Fingas and Brown, 1997). Sensors used for oil detection on the sea surface comprise infrared, ultraviolet, laser fluorescence, Side-Looking Aperture Radar (SLAR), Synthetic Aperture Radar (SAR), optical sensors as MODIS or Landsat (Hu et al., 2009), multispectral sensors as QUICKBIRD or hyperspectral sensors (Wettle et al., 2009). Limiting factors of these remote sensing approaches are that most sensors provide only information on the presence of oil but not its quantity. Also, interpretation of data from these sensors bears the potential of false positive detection. That is, surface patterns might be identified as oil but are actually other surface films such as algae or patterns produced by wind, rain cells, input of fresh water or upwelling of colder water masses (Alpers and Espedal, 2004; Melsheimer et al., 2001; Solberg et al., 2007). Infrared sensors provide limited information on the thickness of oil slicks. While thick slicks (~50-150 µm) appear as warm areas, thin slicks (10-50µm) appear cold compared to the surrounding oil-free water (Elliott et al., 1986; Fingas and Brown, 1997; Salisbury et al., 1993). For assessing relative differences in slick thicknesses, radiometers can be employed. These measure the microwave radiation which is emitted from the sea surface. Oily water emits more radiation than non-oily water, and thicker slicks emit more than thin slicks (Fingas and Brown, 1997). The only techniques that, so far, allow unambiguously distinguishing between oil and other surfactants are fluorescence sensors. UV-light is electronically exciting petroleum compounds and these excitations are emitted as fluorescence emissions (Brown and Fingas, 2003; Fingas and Brown, 1997). A combination of UV-light and infrared sensors might therefore provide most reliable information on oil slick presence and thickness (Fingas and Brown, 1997). Yet, these kinds of sensors are, so far, only used on airborne vehicles, which makes their employment costly and provide only limited spatial and temporal coverage. For oil spill or oil slick detection, SAR satellite images are used most commonly (Garcia-Pineda et al., 2009; Solberg and Brekke, 2008; Topouzelis, 2008). SAR sensors emit microwaves and record the backscatter signal from the earth surface (ESA, 2007). Surfactants like oil dampen capillary waves on the sea surface (Brekke and Solberg, 2005; Solberg et al., 2007), which produces lower backscatter towards the emitting sensor (Fig. 17).

This low backscatter can be identified as dark area on processed images. A drawback of sea surface imaging with SAR is that oil slick-like features might be produced by rain cells (Melsheimer et al., 2001), wind patterns (Alpers et al., 1998), biogenic films or fresh water input (Alpers and Espedal, 2004) (Fig. 18). Despite these limitations, SAR imagery allows identifying natural oil seeps in areas which are not characterized by large scale upwelling of water masses, high abundance of sea ice and where wind speeds are not generally above 12 ms^{-1}. Since oil slicks originating from natural seeps can be expected to have rather fixed source points, which are the surfacing locations of the oil, repeated observations of oil slicks in the same spatial location are indicative for natural seepage. Analysis of multi-temporal SAR datasets and identification of oil slick origins on the sea surface have been successfully used to identify oil seeps in previous studies (Garcia-Pineda et al., 2010; Pellon de Miranda et al., 2004).

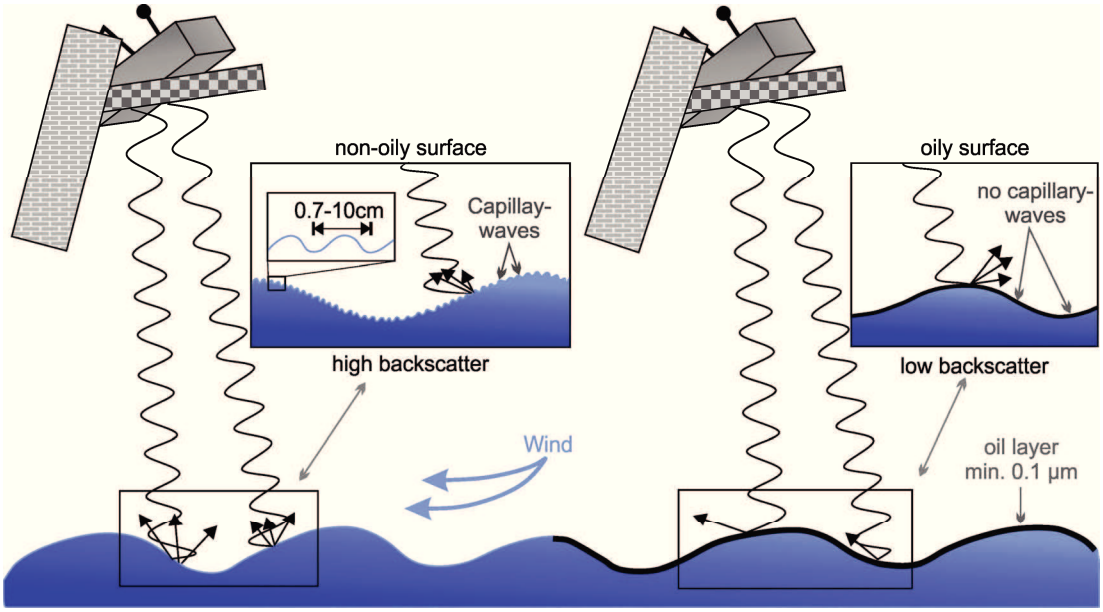

Fig. 17. Illustration of the effect of oily water on the backscatter signal in SAR satellite images. Oil dampens capillary surface waves, which results in less diffuse backscatter. More of the emitted microwaves are reflected away from the sensor from oily water, causing low backscatter (inspired by Garcia-Pineda et al., 2009).

In the present thesis, Advanced Synthetic Aperture Radar (ASAR) images acquired by the Environmental Satellite (ENVISAT) were used to identify natural oil seeps in the Black Sea. Image analysis, especially in the coastal areas, was complicated by frequent occurrences of look-alike surface patterns probably originating from wind shading effects of the Caucasus or Pontic Mountains, riverine input of fresh water, and phytoplankton blooms (Fig. 18). Despite this, natural seeps were identified due to the availability of a large data set providing high spatial and temporal coverage. The processed images were selected from the European Space Agency's (ESA) online archive EO-LISA and rolling archives based on pre-evaluation of low-resolution preview images. Due to the large file sizes of the high-resolution images (up to 2 GB), all images were reprojected and converted from N1 to 8 bit GeoTIFF format for further evaluation in a geographic information system (GIS). Each image was visually analyzed and potential oil slick origins were marked in image specific point shapefiles. Subsequent overlaying of all shape files allowed identifying cluster of oil slick origins. For each cluster, the spatial mean center was computed which is expected to correspond the best to the oil emitting seep on the seafloor (Fig. 19). The major advantages of (A)SAR in oil slick detection and seep identification is the high spatial and temporal coverage. Images have resolutions of up to 30 m and, depending on the latitude, the same areas might be covered approximately every five days. Thus, the technique allows investigating large areas. The chances to identify seeps characterized by intermittent activity patterns are by far more likely than by ship-based methods. An impressive example of SAR-based vs. ship-based oil seep detection in the Gulf of Mexico is shown in Fig. 20. Also, SAR imagery provides a convenient method for oil seepage monitoring over long time scales. The formation derived from the satellite image analysis may then serve as base for detailed hydroacoustic and seafloor investigations during subsequent research cruises.

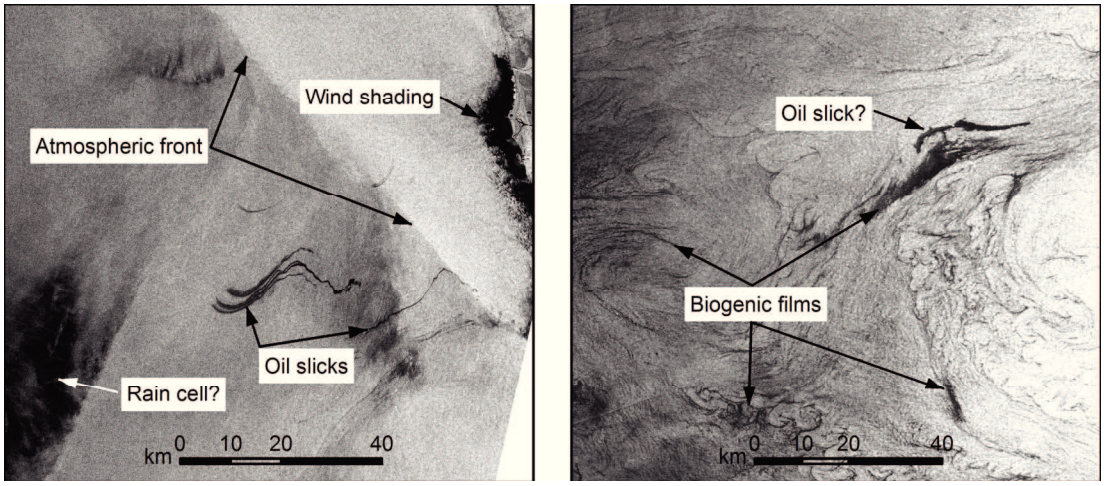

Fig. 18. Subsets of Advance Synthetic Aperture Radar images that show a variety of low backscatter (dark) patterns. Images provided by ESA.

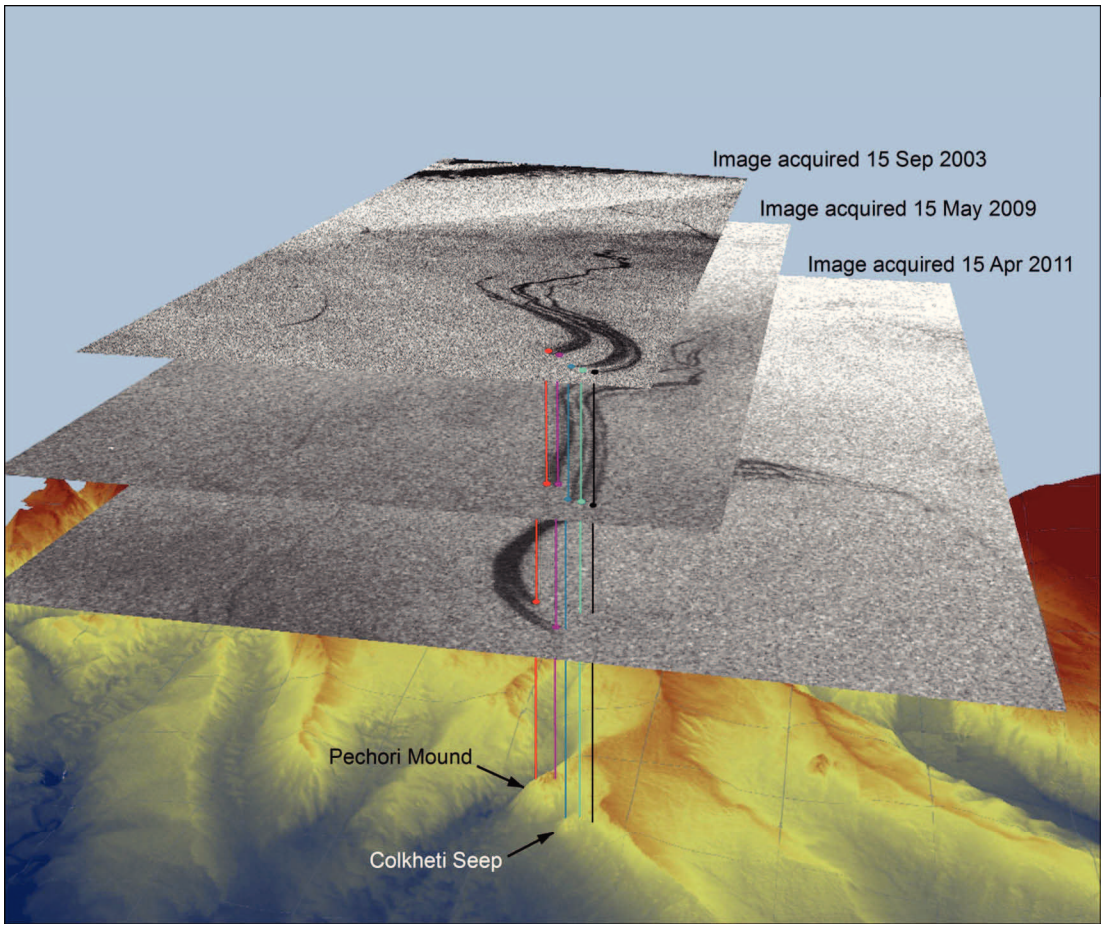

Fig. 19. Illustration of seep identification by ASAR satellite image analysis. Origins of surface oil slicks are identified in individual images. Oil seeps are located on the seafloor below locations of recurrent slick origins within radii of a few hundreds of meters.

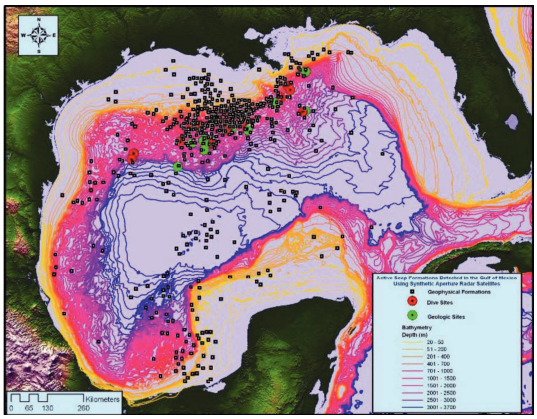

Fig. 20. Map showing oil seep identified on SAR satellite images (black dots) and seeps discovered by ship-based investigations (red and green circles) in the Gulf of Mexico (from Garcia-Pineda, 2009).

Satellite imagery proved to be a cost-efficient tool to investigate and monitor large areas with respect to oil seepage. On the contrary, much smaller scale investigations of actual seep sites on the seabed are commonly conducted using camera systems that are deployed by ROV or camera-sled systems and towed few meters above the seafloor. Both allow the production of video or still image footage covering a limited seafloor area. Visual evaluation of the video or image material in combination with the spatial information from the underwater navigation allows producing schematic maps of seafloor morphology, sediment properties and microbial or faunal communities (Bohrmann et al., 2002; Sahling et al., 2008b). However, these techniques are rather general descriptions of the seafloor environment and contain uncertainties in spatial location and extent of mapped features. Techniques which aim to overcome these limitations are video- or photo-mosaicking. Mosaics are produced by combining still images or converting video footage to a continuous still image, by identifying common points in consecutive images or video frames, and applying distortion and illumination corrections. By using dive- or tow-track information and parameters such as altitude, pitch and roll of the camera carrying vessel, reliably scaled image-maps of the seafloor can be produced (Gracias and Santos-Victor, 2000; Jerosch et al., 2006; Kourogi et al., 1999; Marks et al., 1995; Nicosevici et al., 2009; Singh et al., 2004). These maps allow delineating certain seafloor features in correct spatial extent and relation to each other. This information may then be correlated to local sediment samples or geochemical data as well as bathymetry and amplitude maps (Jerosch et al., 2007; Naudts et al., 2010; Olu-Le Roy et al., 2007; Orange et al., 2002). In the present work the software ADELIE, an extension for ArcGIS 9.2 (© ESRI) developed by the IFREMER, France, was used to produce mosaics from video footage covering a cold seep structure at the Makran accretionary margin, offshore Pakistan. Additionally, a 675 kHz sonar mounted on the ROV was used to image the surface properties of the seep structure. Combining this multi-sensor data in the GIS allowed the detailed characterization of an entire seep, comprising chemosynthetic communities and morphology. The array of different remote sensing and GIS techniques applied in the present work demonstrates how cold seep detection, monitoring, mapping and quantification of fluxes may be accomplished in a cost- and time-efficient manner.

Chapter 4

The study areas

4.1 The Makran accretionary margin

The Makran continental margin is considered as one of the largest accretionary systems. At present, it extents over about 500 km from north to south of which about 150 km are submarine (Fig. 21). The Makran spans about 800 km from west to east. Towards the west the Makran accretionary systems is bordered by the Minab strike-slip fault and to the east by the Ornach-Nal strike-slip fault. Due to on-going subduction of the Arabian and Omara plates under the Eurasian plate, a massive accretionary system forms since the Eocene (Byrne et al., 1992). About 4 km of the up to 7 km thick sediment pile deposited on the Arabian plate are scraped off, and accreted to the overriding Eurasian plate. The remaining sedimentary load of the oceanic plate is underthrust and partly underplated to the continental plate, which causes a rapid uplift of the overriding plate (Platt et al., 1985). The accreted sediments form thrust slices which are folded and partly faulted (White, 1982). These thrust slices form a succession of accretionary ridges with a subduction parallel strike (Kukowski et al., 2001).

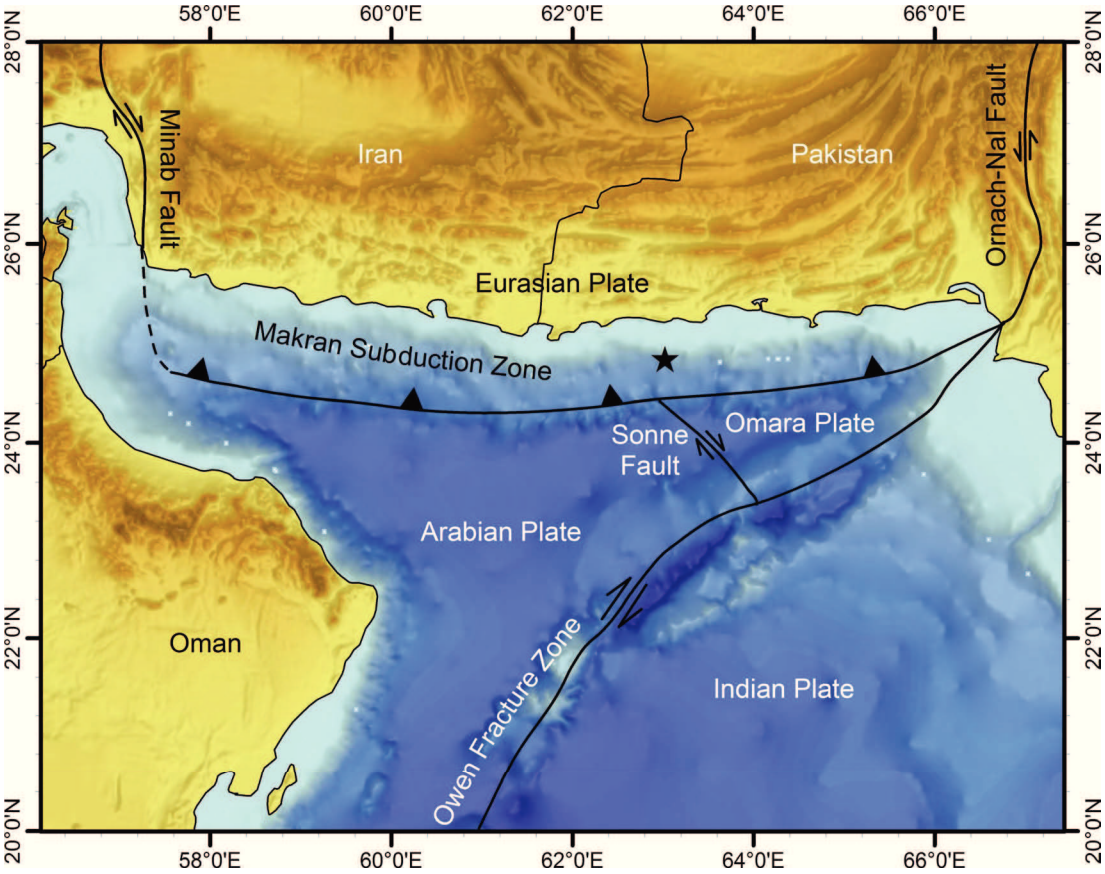

Fig. 21. Overview of the Makran accretionary complex. The black star indicates the location of the study area. Map adapted from Kukowski et al. (2001).

While the younger ridges raise several hundreds of meters above the abyssal pain, the older ridges are uplifted and the synclines separating the ridges are filled with terrigenous

sediments. This causes a shallowing of the seafloor morphology towards the coast (Fruehn et al., 1997; Kukowski et al., 2001). The underplating of subducted sediments towards the hinterland of the accretionary prism and the associated rapid uplift causes extensional faulting in the upslope area of the prism (Platt et al., 1985). It was proposed that the rapid uplift of the underplated sediments fosters diapirism of undercompacted shale sediments (Delisle et al., 2002). These shale diapirs are bound to the thrust plains or extensional faults (Delisle et al., 2002; Grando and McClay, 2007) and source mud volcanoes along the on- and offshore parts of the Makran margin (Delisle et al., 2002; Grando and McClay, 2007). From widespread occurrences of distinct BSRs along the submarine part of the Makran, the presence of large amounts of gas hydrates and underlying free gas was inferred (Minshull and White, 1989; Sain et al., 2000). The relatively sparse observation of cold seeps and seep related features on the seafloor within the GHSZ, and more widespread observation of seeps above the upper boundary of the GHSZ during initial investigations, led to the assumption that gas hydrates act as an efficient 'cap rock' for migrating hydrocarbons (Delisle and Berner, 2002). Yet, numerous new gas emitting seeps and associated faunal and microbial communities have been detected by hydroacoustic means during subsequent cruises (Bohrmann et al., 2008; Römer et al., *submitted*). It was shown that the distribution of these non-mud volcano cold seeps is associated with buried anticlinal structures originating from folded thrust slices (Ding et al., 2010). Ding et al. (2010) propose that these anticlines serve as structural traps for biogenic and thermogenic hydrocarbons. They argue that due to a normal pressure regime in the investigated area, seepage sourced from these structural traps is probably buoyancy driven and not induced by tectonic overpressuring as was previously proposed for the mud volcano feeding diapirs (Delisle et al., 2002). Though the new seep discoveries indicate that presence of gas hydrates controls the overall distribution of seeps less than initially anticipated, presence of gas hydrates in shallow sediments of seeps within the GHSZ has been evidenced (Bohrmann et al., 2008). One characteristic oceanographic feature of the Makran accretionary prism is a distinct oxygen-minimum zone (OMZ) which expands between 100 and 1,000 mbsl (Wyrtki, 1973). The OMZ has a significant impact on the distribution of chemosynthetic communities. While seeps are inhabited with faunal communities as vesicomyid clams or ampharetid polychaetes and microbial mats outside the OMZ (Fischer et al., 2012; von Rad et al., 2000), only microbial mats have been observed within the OMZ (Fischer et al., 2012; von Rad et al., 2000). The detailed geologic and biological characterization and an areal methane budget of one seep site which is located just below the OMZ, is presented in Chapter 5.

4.2 The Black Sea

Geologically, the recent Black Sea appears as large intra-continental basin (e.g. Nikishin et al., 2003) with a maximum depth of 2,206 mbsl (Ross et al., 1974). In the sub-seafloor, the Andrusov and Achangelsky Ridges form the Mid-Black Sea-High that separates the western and eastern basins (Fig. 22) (Zonenshain and Pichon, 1986). These basins developed from a back arc basin when the Neo-Tethys was closed by subduction under the Eurasian plate (Görür, 1988; Zonenshain and Pichon, 1986). The opening of both basins occurred simultaneously either in Late Cretaceous or Early Paleocene (Edwards et al., 2009; Meredith and Egan, 2002; Nikishin et al., 2003). Latest in Eocene, the extensional regime of the

evolving basins changed to a compressional due to the subduction of the African and Arabian plates under the Eurasian plate (Nikishin et al., 2003).

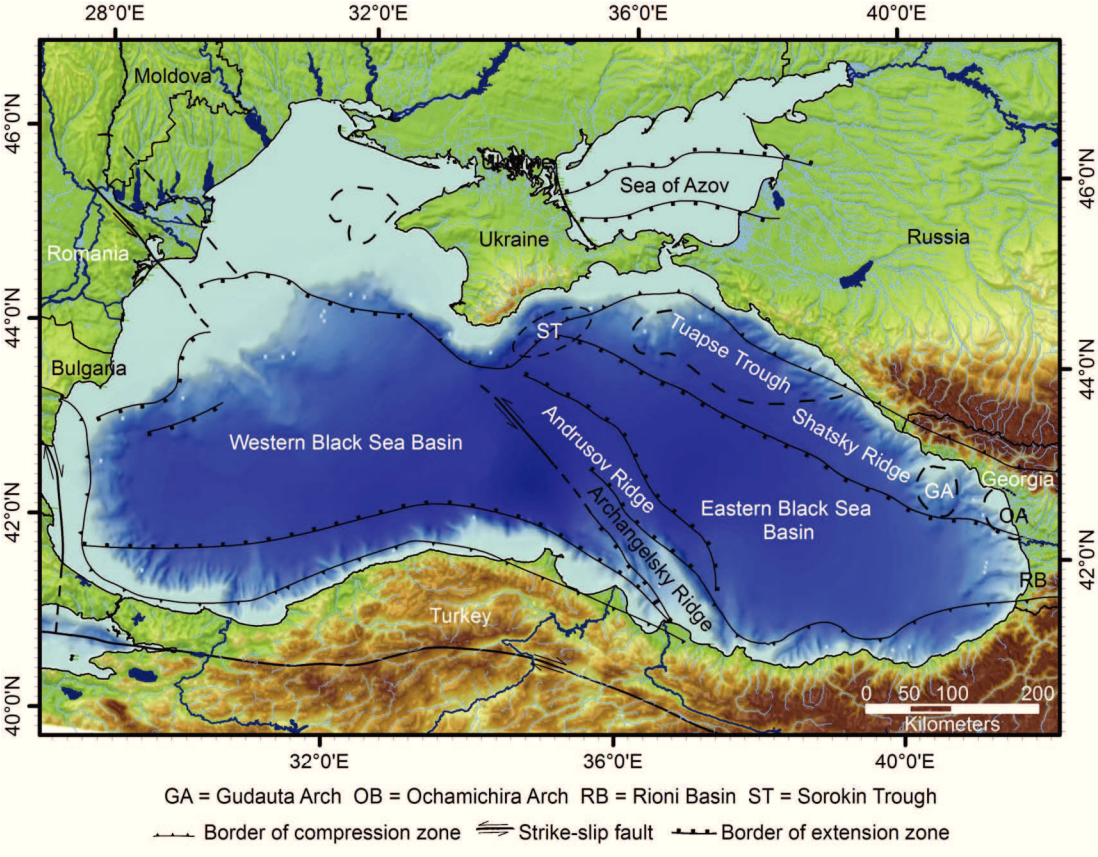

Fig. 22. Overview map of the Black Sea with major geologic features. Adapted from Robinson et al. (1996).

The central Black Sea sediments show mostly uniform parallel bedding of sedimentary horizons that only thin towards the margins and slopes of the separating Mid-Black Sea-High. Characteristic for both basins are thin syn-rift sediments that are overlain by thick post-rift sediment sequences, which are dominated by massive Quaternary sediments. During Oligocene to Miocene, the organic-rich Maikopian formation was deposited which is, due to high sedimentation rate and rapid subsidence, undercompacted (Robinson et al., 1997). The Maikopian formation has been identified as major hydrocarbon source rock (Robinson et al., 1997). The top of these shale deposits lays in depth between 6 km in the central Black Sea and less than 1 km on the Western Shelf and at the Eastern margin, e.g. on the Shatsky Ridge (Tugolesov et al., 1985). Corresponding to the burial depth, the thickness of these deposits varies from 2.3 km at the margins to 5 km in the central Black Sea (Tugolesov and Meisner, 2002). Undercompaction and hydrocarbon maturation create a significant overpressure within the Maikop formation, which is thought to induce mud volcanism that has been observed in the northern and central Black Sea (Ivanov et al., 1996; Krastel et al., 2003; Scott et al., 2009). In the north-western, northern and eastern Black Sea, buried anticlines have been interpreted at shale diapirs originating from the Maikopian formation (Tugolesov et al., 1985). Mud volcanism and formation of large mound structures throughout

the Black Sea have been suggested to relate to these diapirs (Akhmetzhanov et al., 2007; Ivanov et al., 1996; Wagner-Friedrichs et al., 2008).

During Quaternary times, deposition of chemical sediments and oil shales was followed by turbiditic terrigenous sediments (Degens and Stoffers, 1980). Sequences of carbonate and organic material rich sediments in the early Quaternary sequences evidence frequent changes of oxic and anoxic stages in the Black Sea. The thick recent sediments are characteristic of the entire Black Sea. The sedimentary units of the upper most six meters have been traced throughout the basin and described by Ross et al. (1970). Wide shelf areas have developed only in the north-western and northern parts of the Black Sea where large rivers as Danube, Dniester or Dnieper deposited huge amounts of terrigenous sediments. The organic-rich material in the fan deposits is thought to be the source of biogenic methane seepage (Limonov et al., 1997) which has been widely observed on the shallow shelf (Dimitrov, 2002; Naudts et al., 2006).

Seeps discovered in the Black Sea represent different morphologies ranging from different shaped mud volcanoes (Bohrmann et al., 2003; Krastel et al., 2003), pockmarks (Çifçi et al., 2003; Naudts et al., 2006), and gas emission sites without significant seabed morphology (Naudts et al., 2006). Further morphologies include gentle elevations formed by shallow gas hydrate deposits (Römer et al., *in press*) or roughed seabed morphology with decimeter-sized escarpments formed by gas hydrate rafting (Pape et al., 2011). The widespread occurrence of gas hydrates in sediments below 720 m water depth has been inferred from seismic reflection profiles (Lüdmann et al., 2004; Minshull and Keddie, 2010; Popescu et al., 2007, 2006; Zillmer et al., 2005) and evidenced by direct sampling (Bohrmann et al., 2003; Mazzini et al., 2004; Pape et al., 2011, 2010; Römer et al., *in press;* Sahling et al., 2009). Due to the more frequent occurrence of gas seepage above the upper boundary of the GHSZ of sI hydrate, it was suggested that gas hydrates may act as cap for upward migrating free gas, impeding seepage (Naudts et al., 2006; Popescu et al., 2007). Thus, seepage within the GHSZ would only occur if local heat flow anomalies shift the GHSZ upwards (Poort et al., 2007; Römer et al., *in press*). Seeps located above the GHSZ on the slope of the north-western Black Sea are related to lithological units, as proposed by Naudts and co-workers (2006). They suggest that free gas might accumulate under impermeable layers as fine-grained sediments or methane derived authigenic carbonates. Where these lithological traps are weakened, e.g. by slope failures, gas may breach the seafloor (Naudts et al., 2006).

Though seepage of both biogenic and thermogenic hydrocarbons has been frequently documented in the Black Sea, reports on oil seepage are sparse. Only one oil seep offshore Turkey was mentioned in recent literature (Kruglyakova et al., 2004; Robinson et al., 1996). Presence of oil impregnated sediments have been reported for four sites in the eastern Black Sea, namely the Pechori, Iberia and Petroleum Mound and the Colkheti Seep (Akhmetzhanov et al., 2007; Reitz et al., 2011). Within this work, numerous new oil seeps were identified and described (Chapters 6 and 7)

.

Chapter 5

1. Manuscript

Methane budget of a cold seep (Flare II) associated with an incipient headwall, offshore Pakistan

Jan-Hendrik Körber, Heiko Sahling, Gerhard Bohrmann

MARUM – Center for Marine Environmental Sciences and Department of Geosciences, University of Bremen, Klagenfurter Strasse, 28359 Bremen, Germany

to be submitted to *Marine Geology*

5.1 Abstract

A cold seep at the Makran accretionary prism offshore Pakistan was investigated by geophysical and optical techniques during R/V METEOR cruise M74/3 in 2007. The seep comprises an area of ~3,600 m² of which 1,440 m^2 are active. The seep is located in about 1,025 m water depth on the crest of a ridge of the continental slope just below the lower limit of the oxygen minimum zone. Systematic video surveys were conducted with the remotely operated vehicle (ROV) MARUM QUEST4000 for the construction of video-mosaics. The 675 kHz horizontally looking sonar of the ROV was used to map the seep area. By combining the backscatter information from the ROV's sonar and 30 kHz deep-towed sidescan sonar, with video-mosaics and seafloor images, a comprehensive description of the geological situation and distinct chemosynthetic communities is provided. Based on the interpretation of the hydroacoustic data, the formation of the seep is liked to a slope failure of the eastern ridge flank. The seep itself is proposed to represent the surface expression of an incipient headwall. The chemosynthetic communities optically mapped at the seep are used as proxies for distinct methane turnover rates. This allows providing an areal budget of dissolved methane fluxes. In combination with previously obtained data on gas bubble emissions from the same site, a methane budget for the entire seep is provided. This provides new insights on the importance of free gas ebullition vs. dissolved gas fluxes and consumption of methane by anaerobic oxidation (AOM). Within the seep area, ca. $1.14*10^4$ mol yr^{-1} of methane are removed by AOM and associated chemosynthetic communities, whereas $560*10^4$ mol yr^{-1} are injected into the water column as bubbles. This is only the second areal methane budget, comprising dissolved and bubble emissions, and turnover rates, for a cold seep. We promote the combination of local gas flux determinations in combination with video and acoustic mapping as potential tool to access large scale areal gas fluxes at cold seep structures.

Keywords

Video-mosaicking; acoustic backscatter; methane budget; cold seep; slump

5.2 Introduction

Cold seeps occur in a variety of geologic and oceanographic settings such as active continental margins (Bohrmann et al., 2002; Sahling et al., 2008b; Torres et al., 2009) and passive margins (Dupré et al., 2007; MacDonald et al., 2003; Sahling et al., 2008a; Serié et al., 2012) from shallow water (Eichhubl et al., 2000; Hovland, 2002; Schneider von Deimling et al., 2011) to deep water environments (Bohrmann et al., 2003; MacDonald et al., 2002; Olu-Le Roy et al., 2007). The widespread occurrence of cold seeps and the fact that seeps discharge predominantly methane (Mau et al., 2006; Pape et al., 2010; Römer et al., *submitted;* Torres et al., 2002) supports the assumption that cold seeps significantly contribute to water column and, possibly, atmospheric methane inventories (Judd, 2003; Kessler et al., 2006b; Kvenvolden and Rogers, 2005).

At cold seeps methane is transported towards the seabed and hydrosphere either dissolved in pore-water by advection or diffusion, or as free gas via bubbles (Leifer and MacDonald, 2003; Mau et al., 2006; Sahling et al., 2009; Sommer et al., 2009). Active gas bubble emissions might be identified and quantified by hydroacoustic techniques (Greinert et al., 2006; Nikolovska et al., 2008; Römer et al., *in press*). Assessment of dissolved methane fluxes relies on punctual seabed measurements using benthic chambers (Lichtschlag et al., 2010; Linke et al., 2005) or ex-situ pore-water analysis (Borowski et al., 1996). These measurements, however, do not allow determining areal dissolved fluxes. These challenges in assessing areal fluxes of dissolved and gaseous methane, and their relative importance for local water column methane concentrations, make available data on methane budgets for entire seep structures scarce.

To provide methane budgets for entire seeps, three parameters have to be known. These are the spatial extent of active fluid flow, and flux rates of dissolved and gaseous methane. Seafloor expressions of cold seeps, such as mud volcanoes, pockmarks, and various morphological types of authigenic carbonates might be detected by sidescan sonar or multibeam echosounders (Dupré et al., 2010; Klaucke et al., 2010, 2006; Orange et al., 2002). These data provide first information on the maximum seafloor area which is altered by seepage. Yet, areas of *active* fluid flow are usually much smaller. Indicators for persistent seepage are occurrences of chemotrophic microbial or faunal communities (chemosynthetic communities). These communities directly or indirectly utilize methane as energy source. The probably most important microbial process at cold seeps is the anaerobic oxidation of methane (AOM). In the process of AOM sulfate reducing bacteria and methane oxidizing archea generate hydrogen sulfide and bicarbonate (Barnes and Goldberg, 1976; Boetius et al., 2000a). The sulfide might serve as energy source for thiotrophic bacteria, for instance *Beggiatoa* spp. (Joye et al., 2004), or faunal species living in chemosymbiosis with such bacteria, e.g. vesicomyid clams or bathymodiolus mussels, and others (Dubilier et al., 2008; Duperron et al., 2008; Hovland and Thomsen, 1989; Krylova and Sahling, 2010; Levin, 2005; Sibuet and Olu, 1998). The close correlation of distinct chemosynthetic species with certain sulfide fluxes, maintained by AOM, was previously shown (e.g. Levin et al., 2003; Sahling et al., 2002). Observations indicating that AOM and associated chemosynthetic communities consume major volumes of dissolved methane in surface-near sediments, led to the term benthic filter (Niemann et al., 2006; Sommer et al., 2006). In contrast, gas bubbles may bypass this filter without consumption by microbial activity (Sahling et al., 2009; Sauter et al., 2006). Mapping of the areal coverage of chemosynthetic communities thus provides a proxy for the assessment of areal dissolved methane fluxes (Jerosch et al., 2007; Mau et al., 2006). Volumes of gaseous methane emission to the water column might be obtained from

hydroacoustic detection of emission sites, and subsequent optical measurements of number and size of emitted bubbles (Leifer and MacDonald, 2003; Sahling et al., 2009).

In this study we used a high-frequency sonar (675 kHz), mounted on a remotely operated vehicle (ROV), to map the spatial extent of a cold seep named *Flare II,* in 1,025 m water depth. Sediment sampling and visual seafloor observations confirm that distinct backscatter patterns in the sonar records are predominantly caused by massive AOM-derived carbonates. Subsequent production of video-mosaics allowed detailing compositions and distributions of chemosynthetic communities within the seep area. Previous studies showed that these communities are associated with distinct AOM-rates (Fischer et al., 2012) which allows using them as proxy for areal fluxes, and turnover of dissolved methane. Combining our results with high-resolution quantification of gas bubble discharge at Flare II by Römer et al. (*submitted*), allows us to present a methane budget for the entire seep. The results indicate that bubble emissions were the overwhelming methane source to the water column at the time of investigation, whereas dissolved fluxes did not contribute to the water column methane inventory.

Based on seafloor mapping by sidescan sonar and multibeam echosounder, we link the genesis of Flare II and the observed fluid flow to the failure of the ridge-slope just below the seep. While previously reported seeps that are linked to slumps and host chemosynthetic communities, are usually aligned with slump scars (e.g. Naehr et al., 2000), Flare II locates above the slump headwall. The seep is suggested to represent the origin of further slope failures.

5.3 Study Area and Geological Setting

The Makran accretionary prism is one of the world's largest accretionary complexes. It forms where the Arabian plate is subducted under the Eurasian plate and extents approximately 800 km from East to West and about 500 km from South to North (Fig. 23). The major part of the system lays presently subaerial on the Pakistani and Iranian parts of the Eurasian plate (e.g.White and Klitgord, 1976). The actual deformation front is located about 150 km offshore Pakistan where it forms the youngest of a series of seven successively older and higher plate-boundary parallel ridges (Kukowski et al., 2000). The Arabian plate is subducted by 3-5 cm yr^{-1} (McKenzie and Sclater, 1971; Minster and Jordan, 1978). The up to 7 km thick marine sediments (White, 1982) are partly subducted and partly folded and faulted forming imbricated thrust slices (Schlüter et al., 2002). Seismic reflection profiles indicate the presence of a bottom simulating reflector (BSR), marking the base of the gas hydrate stability zone (GHSZ), extending over water from 3,000 m to 1,350 m (Ding et al., 2010; Fruehn et al., 1997; Grevemeyer et al., 2000; Kukowski et al., 2001; Minshull and White, 1989; White, 1982).

The Makran continental margin is one of the most productive marine environments (Boetius et al., 2000b). High production rates of biogenic material enhance the sedimentation of organic carbon-rich material that is converted to hydrocarbons by biogenic or thermogenic processes (von Rad et al., 1996). Between ca. 100 and 1,100 m below sea level (mbsl) an oxygen minimum zone (OMZ) creates a metazoan life-hostile environment (Helly and Levin, 2004; Schmaljohann et al., 2001; von Rad et al., 1995).

First investigations of the Makran accretionary prism reported seeps and pockmark like features, assemblages of seep related biota and emissions of free gas in depth between 350 and 840 m as well as in water depth between 2,100 and 2,500 m (von Rad et al., 1996).

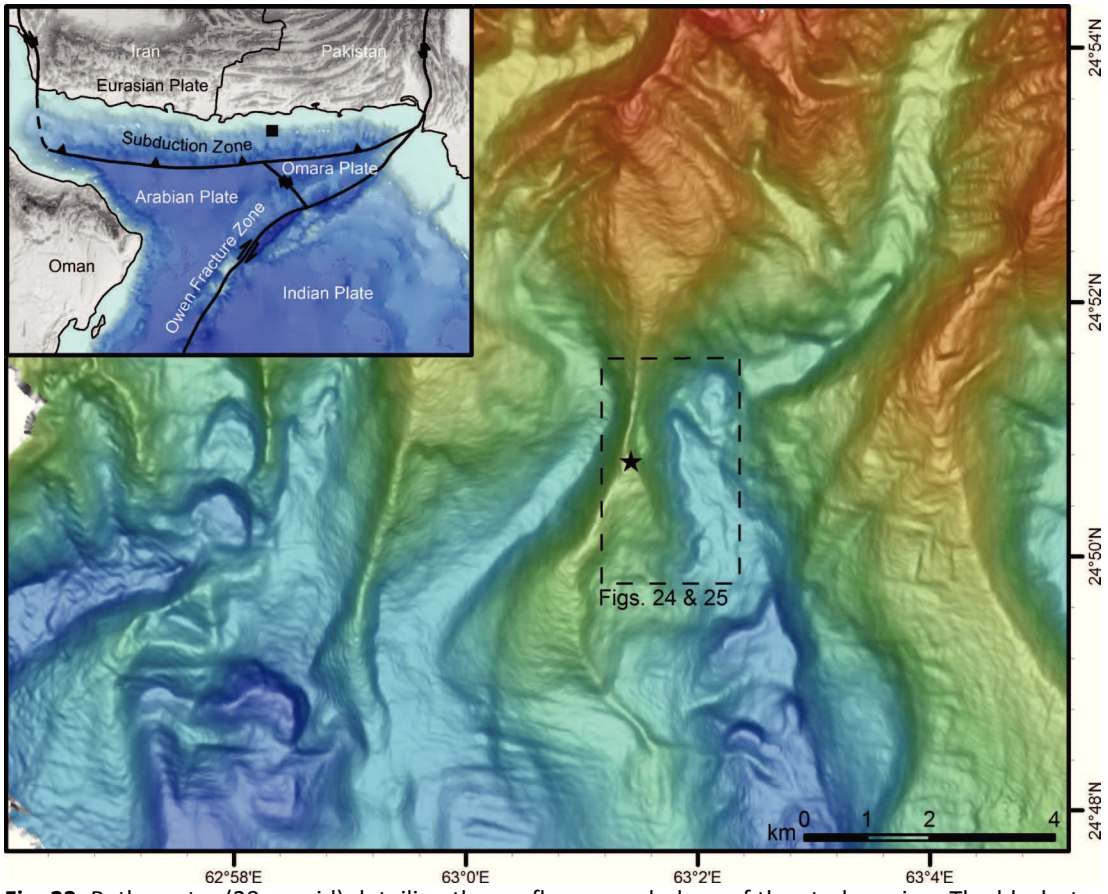

Fig. 23. Bathymetry (20 m grid) detailing the seafloor morphology of the study region. The black star denotes the location of Flare II. The insert shows the main geologic structures of the Makran accretionary margin and Arabian Sea (after Kukowski et al., 2001). The black square indicates the location of the study region. Bathymetry and topography in the insert: GEBCO 1min.

Within the OMZ large crusts of authigenic carbonates were found (von Rad et al., 1996). Generally sparse observations on seepage were first attributed to the presence of massive gas hydrate deposits which would efficiently trap free gas below (Delisle and Berner, 2002). More recent studies found numerous new seepage areas along the accretionary ridges, indicating that seepage occurs in all water depth within and above the GHSZ (Bohrmann et al., 2008; Römer et al., *submitted*). Based on deep-towed side scan sonar (Bohrmann et al., 2008) and single-beam echosounder surveys (Römer et al., *submitted*) 15 seep sites have been identified by bubble-induced acoustic anomalies in the water column and/ or backscatter anomalies in the side scan records. All of these seeps are associated to the accretionary ridges. However, most of them are located at the most shallow ridge (Bohrmann et al., 2008).

A recent study by Ding et al. (2010) presented a model explaining the observed fluid seepage. Based on seismic reflection data Ding et al. (2010) propose that seepage is related to buried anticlinal structures that act as traps for migrating fluids. In contrast to former studies (e.g Schlüter et al., 2002) they state that fluid migration is trigged by buoyancy of hydrocarbon-rich fluids rather than tectonically driven dewatering. Fluids migrate preferably along normal faults above the anticlines (Ding et al., 2010) and not, as considered earlier, along thrust faults (Schlüter et al., 2002).

5.4 Material and Methods

During cruises M72/2 and 72/3 (2007) with the German R/V METEOR parts of the Makran continental margin offshore Pakistan were investigated. Bathymetric data was obtained with the Kongsberg EM120 (12 kHz) echosounder. The data covering the study area was post-processed using MBSystem (http://www.mbari.org/data/mbsystem; GNU General Public License), and gridded to 20 m. Additionally, the study area was mapped with the TOBI deep-towed sidescan sonar (~30kHz) (Murton, 1992) which was towed at speeds around 2.5 knots and a transect line spacing of 5.5 km.

The Flare II seep was investigated during five dives with the ROV MARUM QUEST4000 (GeoB12313, 12315, 12328, 12333, and 12343) subsequent to the acoustic surveys. During all dives video and still images were acquired providing 4.4 km of along-track video footage. During dives GeoB12315 and GeoB12328 systematic video surveys were conducted to produce visual maps of the seep area. The survey was started in the northern part of the seep area. The transect lines crossed the northwest – southeast trending seep structure perpendicular with line spacing of 7.5 to 10 m. Transect lengths were about 20 m. Average flight height of the ROV was around 1 m during dive GeoB12315 and about 1.5 m during dive GeoB12328, resulting in a wider video footprint. The video data used for the latter creation of video-mosaics was recorded with a Deepsea Power and Light Seacam6500 mounted on the ROV. The camera has a low light sensitive 1/3 inch CCD sensor and records a PAL signal with an image resolution of 752 * 582 pixels. All videos were recorded in Sony HDCAM format on standard 60 min MiniDV tapes. Records of the ROV's horizontally looking 675 kHz sonar (HLS) (Kongsberg 1071) were recorded for latter evaluation of their capability to image the seafloor.

From all acquired video material, about 575 m were used for the creation of mosaics. Detailed analysis of the video data and post processing of video-mosaics was done using the ADELIE software package developed by the IFREMER Brest, France. The final mosaics and sonar records were georeferenced in ArcEditor (© ESRI) using the ROV's smoothed dive-track as spatial reference. For positioning of the ROV the ultra-short-baseline (USBL) positioning system POSIDONIA (IXSEA) was used. The positioning accuracy varied between 2 and 15 m with an average of ±5 m. For creating the best possible overlay of all HLS images small deviations from the ROV track were accepted within the positioning uncertainty of ±5 m. Combination of all data in a GIS allowed determining the extent of the seep structure, distinct chemosynthetic communities, and assessing the correlation of backscatter patterns, biologic communities and seafloor morphology.

Sediments of the Flare II area were sampled using a gravity corer (GC) with a 6 m core barrel and PVC liner. Seven cores (GeoB 12314-1, 12316-1, 12316-2, 12316-3, 12316-4, 12316-5, and 12342-2) were recovered from the northern part of the Flare II seep area to correlate sediment properties and backscatter signal within the seep area.

5.5 Results

5.5.1 Geological characteristics of Flare II

The area around Flare II was mapped by TOBI sidescan sonar but the sidescan information about the seep itself is limited due to the steep morphology, and the fact that the area is located in the outermost part of the sonar beam (Fig. 24). Flare II is located just below the sharp crest of a north – south trending ridge which is bordered by canyons to the west and east (Figs. 23 and 25). The general trend of the ridge is seen in the side scan sonar data as lowest backscatter on the western flank which is facing away from the tow-fish

and intermediate backscatter representing the eastern and south-dipping ridge flanks (Fig. 24).

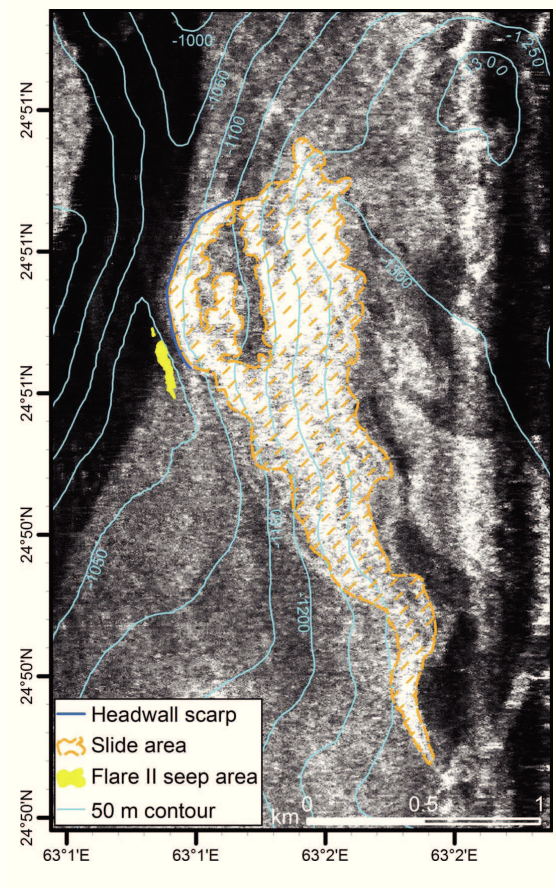

Fig. 24. 30 kHz TOBI sidescan sonar record indicating a slump of the ridge flank east of Flare II.

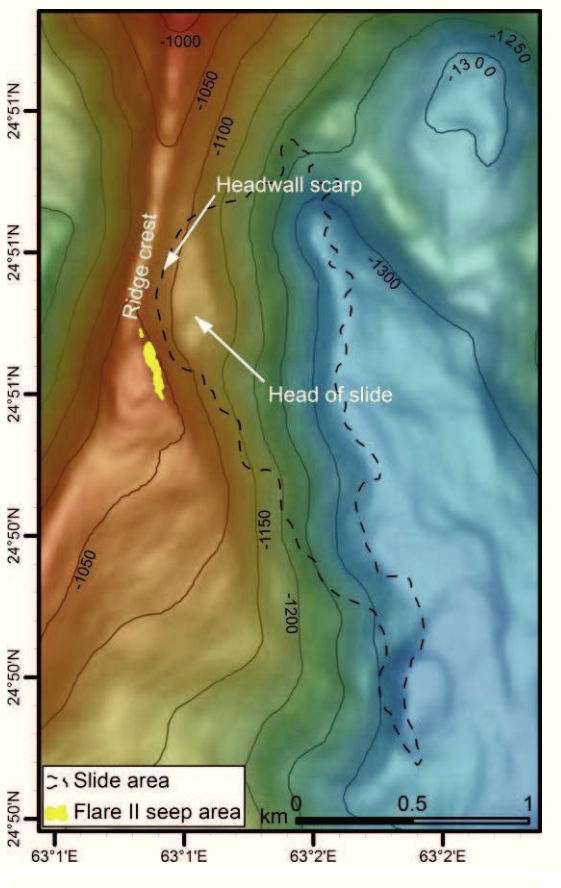

Fig. 25. Detailed bathymetry of study area. The yellow area denotes extent of Flare II. The bathymetry shows the head of a major slump. The dashed line indicates the slump area as identified in sidescan sonar records. The figure covers the same area as Fig. 24.

East of the Flare II, the ridge's flank is characterized by an arcuate area of distinctly higher backscatter. This area might originate from more indurate or roughed sediments, which were exposed after a slope failure. The bathymetry shows a plateau below the interpreted headwall (Fig. 25). Below this plateau the contours widen fan-like towards the slope toe. Detailed seafloor investigations by ROV revealed the presence of an approximately ridge-parallel trending depression along the central area of the seep. This depression was mapped based on video data and the ROV's sonar records (Fig. 26). Gas bubble emissions detected by ROV (Römer et al., *submitted*) were aligned along this depression (Fig. 26).

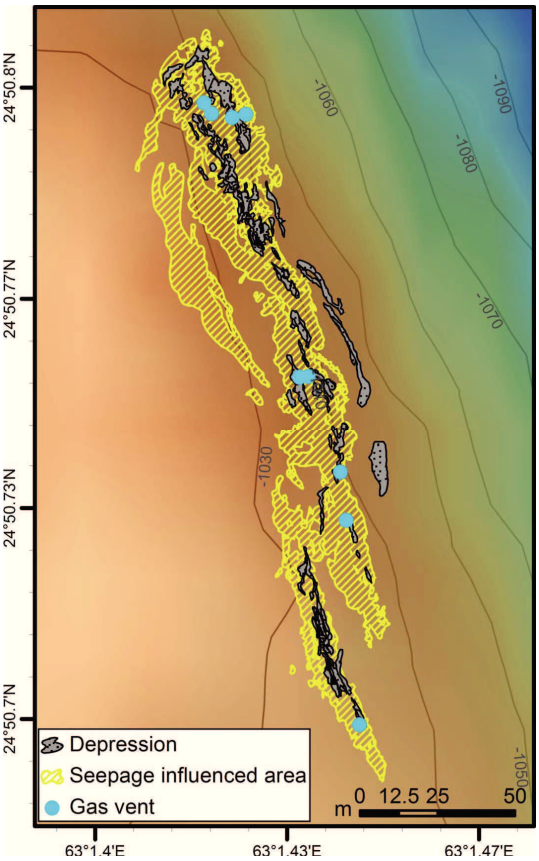

Fig. 26. Illustration of the depression (gray areas) which trends North – South through the seep area (yellow-striped area). Turquoise dots indicate sites of gas bubble ebullition.

5.5.2 Mapping of the seep extent and chemosynthetic communities

The horizontally looking sonar (HLS) showed areas of distinctively higher backscatter which matched the extent of the seep area identified by evaluation of video footage recorded during the five ROV-dives. The extent of seep-influenced seafloor, that is seafloor covered by living chemosynthetic communities or biogenic or authigenic carbonates, derived from the video data is shown in relation to the sonar records in Fig. 27. The HLS records cover an area of 16,046 m^2. Outside this area no indications of past or present seepage were found. To determine the maximum extent of the actual seep, all areas of high backscatter were manually outlined on the individual images. Subsequently, the areas were merged yielding a high backscatter area of 3,597 m^2. The maximum north – south extent of this area is about 270 m, the maximum width ca. 41 m (Figs. 26 and 27).

The central depression trending through the seep area (Fig. 26) was identified as low backscatter on some of the sonar records. The low backscatter was caused by the shallow incidence angle of the sonar. Due to this, no acoustic signal reached seabed within the depression and consequently no signal was scattered back. Sonar records recorded from different positions imaged seafloor of the depression, and revealed backscatter strength comparable to the surrounding seafloor. This indicates that the acoustic response is mainly caused by harder surface sediments like carbonates or shells of bivalves.

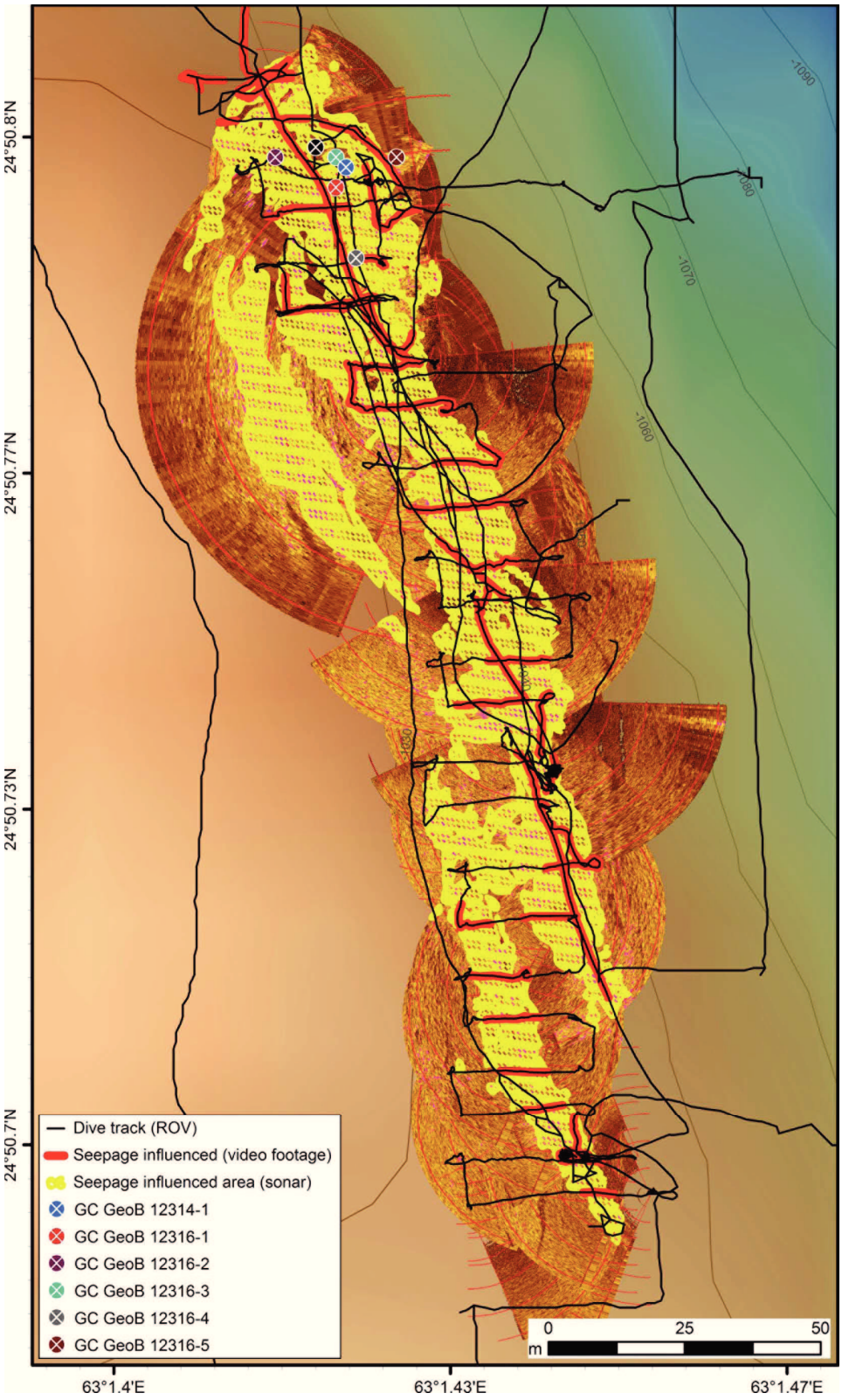

Fig. 27. Overlay of 42 horizontally-looking sonar images. Increased backscatter indicating seepage is marked by the yellow striped area. Red lines indicate seafloor areas showing signs of seepage (chemosynthetic communities, carbonates, etc.) in video footage. Locations of sediments sampling are indicted.

Preliminary investigation of the video material showed that the area inhabited by living chemosynthetic organisms (and thus area of *active* seepage) covered only a part of the seepage influenced area. To estimate how much of the entire seep area is actually covered by living organisms, 25 video-mosaics were created. The quality of the mosaics was sufficient to map the distribution and composition of chemosynthetic communities, and to estimate the extent of the active seepage area. The mosaics cover an area of 675 m^2 of which 270 m^2 were populated with chemosynthetic communities (Table 1), corresponding to 40 % of the total mosaic coverage (Table 2).

Table 1. Specifics of the 25 video-mosaics. Total area covered by individual mosaics, distinct habitats, and total area of each habitat type is indicated.

Mosaic	Area mosaic [m²]	Area habitat class [m²] H1 Microbial mat	H2 Transition	H3 Tubeworms	H4 Clams	∑
1	7.58	0.38	0.52	1.28	0.63	2.81
2	49.02	1.05	3.09	3.28	3.92	11.35
3	48.04	3.61	2.26	8.89	2.58	17.34
4	39.31	0.91	3.34	3.36	4.38	11.99
5	28.66	0.87	3.75	3.04	6.12	13.77
6	56.11	2.15	7.41	10.90	8.43	28.89
7	1.38	0.07	0.61	0.13	0.07	0.88
8	15.31	0.78	4.39	2.20	0.28	7.66
9	18.92	1.88	3.46	2.47	3.29	11.10
10	23.59	0.54	2.71	2.09	5.71	11.04
11	19.40	0.00	0.79	2.30	0.00	3.09
12	52.76	0.71	4.83	4.23	8.81	18.58
13	23.80	0.33	4.51	3.41	3.58	11.83
14	30.42	6.30	7.42	2.40	6.45	22.57
15	50.33	1.97	5.80	3.40	8.80	19.98
16	22.55	0.11	1.62	3.75	7.56	13.05
17	2.77	0.03	0.12	0.14	0.15	0.45
18	44.21	0.89	2.40	5.15	5.72	14.16
19	3.44	0.00	0.13	0.39	0.51	1.04
20	31.31	0.27	5.91	5.76	6.82	18.75
21	6.77	0.20	0.45	0.36	0.50	1.51
22	26.87	0.15	1.41	3.39	2.45	7.41
23	22.55	0.26	2.05	2.16	3.17	7.64
24	8.75	0.32	0.30	0.87	2.07	3.56
25	23.05	1.21	1.75	4.05	2.25	9.26
∑	674.50	25.01	72.38	78.04	94.27	269.70

Table 2. Areal methane (CH_4) turnover rates per habitat class and for the area of active seepage. Relative habitat coverage for the active seepage area is given in square meter and percent. The methane turnover rates are derived from sulfate fluxes modeled by Fischer et al. (2012).

Habitat	Proportion of entire seep area [m^2]	Proportion of entire seep area [%]	Areal CH_4 turnover [mol yr^{-1}]	CH_4 turnover rate [mol m^2 yr^{-1}]
H1	133	3.71	1197.0	9
H2	386	10.73	3358.2	8.7
H3	416	11.57	3494.4	8.4
H4	503	13.98	3319.8	6.6
∑	1438	39.99	11369.4	

The mosaics in combination with high resolution still images and ancillary video material allowed identifying characteristic zonation patterns of different habitat classes previously described by Fischer et al. (2012). Class one is dominated by bacterial mats which appear as whitish to orange colored, fluffy patches on the images (Fig. 28a and b).

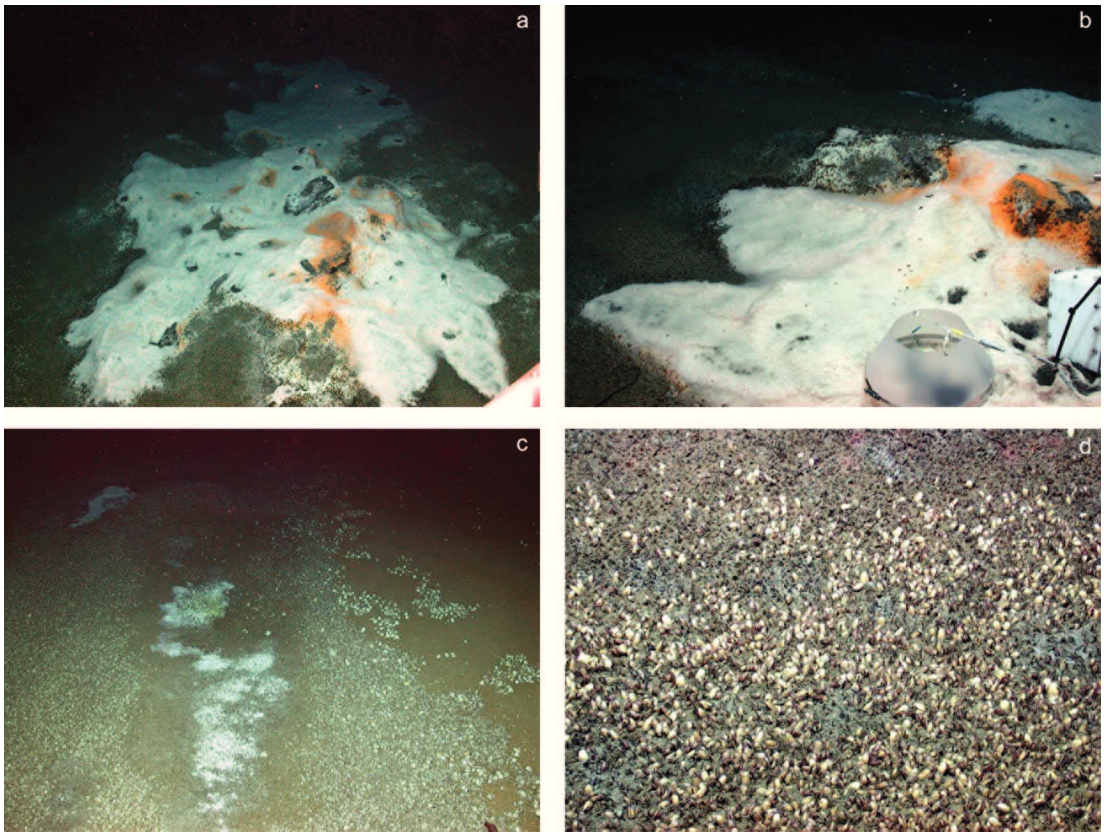

Fig. 28. Images illustrating the appearance of chemosynthetic communities at Flare II a) large patch of *Beggiatoa*. b) Detail of a) Filamentous bacterial mats. Gas bubbles are indicated by black arrows. c) Typical zonation of three main habitat types with bacterial mats being surrounded by tubeworms and clams. d) Transition from clam to tubeworm dominated habitat.

The second class consists mainly of ampharetid tubeworms (Fig. 28c). The third class comprises mostly clams and some ampharetid tubeworms characterized by a greenish-white speckled appearance on the mosaics (Figs. 28d and 29a). Additionally, we introduced a fourth class representing areas were distinguishing between tubeworms and or bacteria was not unambiguously possible. The different habitats were arranged concentrically. Habitat type one was surrounded by two and three (Fig. 28c). Using the video-mosaics and image material, the areas of active seepage were outlined manually. Figure 30a shows an example mosaic covering approximately 30 m^2. The different habitat types are outlined (Fig. 30b) and shown as colored patches (Fig. 30c) to visualize the concentric formation of the habitats and their relative proportions.

The spatial extent of the different habitats is not uniform and continuous but occurs in distinct patches of varying size and densities of the different organisms. The seep separates into two areas with few meters in between that do not show any signs of active or ceased seepage (Figs. 26 and 27). In general the densities of the communities seem to decrease towards the south. Coincident with the higher densities of chemosynthetic communities, emissions of gas bubbles cluster in the northern and middle part of the seep (Fig. 26). Gas vents are usually surrounded by mats of filamentous bacteria. In the central depression the habitat succession is less distinct than along the margins. Here only small patches of bacterial mats and some tubeworms were mapped. Within the depression large carbonate crusts and blocks (Fig. 29b) were observed and sampled by ROV (T. Himmler pers. Comm.).

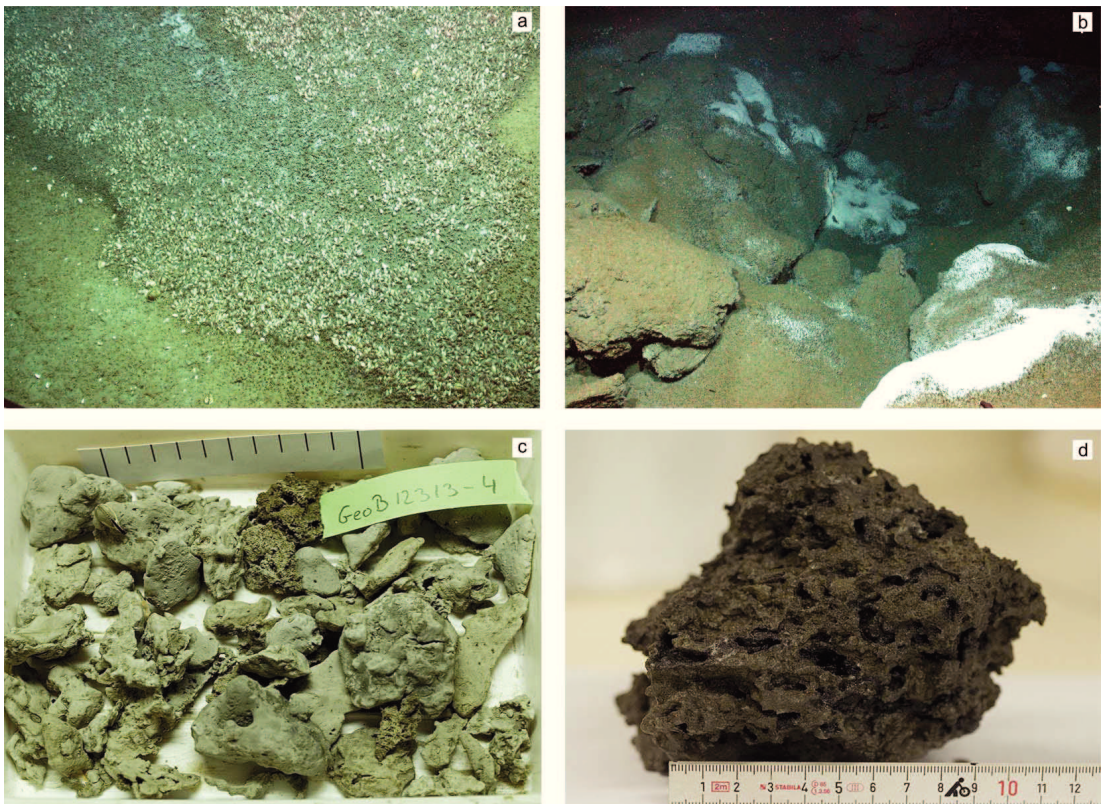

Fig. 29. Seafloor and sediments sample photographs. a) Borders between bacterial mat, tubeworm and clam dominated habitat and the seafloor void of chemosynthetic communities. b) Depression in the northern part of the seep area. Microbial mats and tubeworms indicate elevated gas fluxes within the depression. c) Small carbonates retrieved by gravity coring in the seep area. d) Carbonate found on top of a gravity core at the Flare II. All images © MARUM.

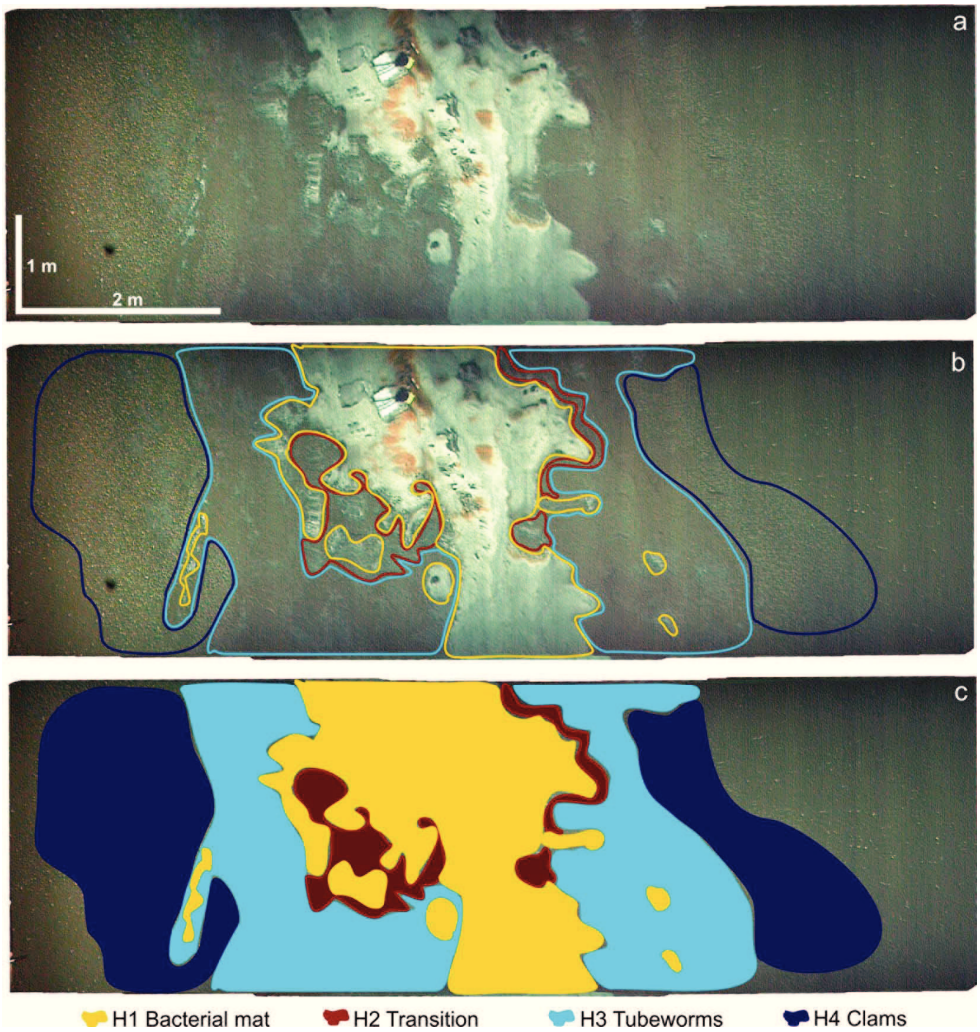

Fig. 30 Example of a video-mosaic covering ca. 30 m^2 used to map chemosynthetic communities. a) The mosaic illustrates the concentric zonation of different habitats. b) Habitat types outlined in different colors. c) Habitat classes shown as colored patches for easier recognition of the zonation pattern and proportions of different habitats.

5.5.3 Sediment sampling

The penetration of the three of the seven GCs (GeoB 12314-1, 12316-1, and 12316-5; Fig. 27) was blocked by massive carbonates. Core GeoB 12342-2 yielded only 40 cm sediments. These contained moussy to soupy clay and centimeter-sized gas hydrate and carbonate pieces. Thus, it might be that core penetration was blocked by either carbonates or gas hydrates in deeper sediments. The three other cores (Fig. 31) contained large, up to 10 cm wide, carbonates in a silty-clayey matrix. Sediment texture was moussy to soupy, suggesting decomposition of gas hydrates during recovery. From depth below ca. 60 m all three cores contained centimeter-sized gas hydrate pieces. Cores GeoB 12316-3 and 12316-4 contained also more than 10 cm wide, platy gas hydrates with bubble fabric below ca. 12 cm depth.

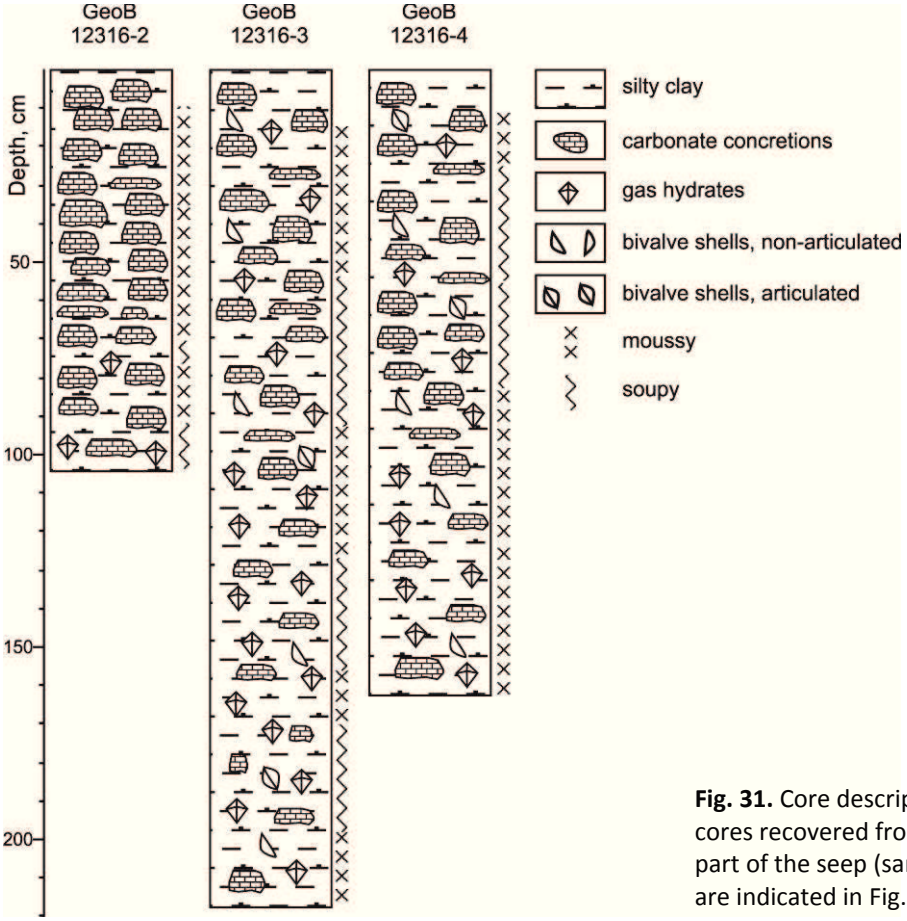

Fig. 31. Core descriptions of gravity cores recovered from the northern part of the seep (sampling locations are indicated in Fig. 27).

5.6 Discussion

5.6.1 Geologic situation at Flare II

We propose that the backscatter anomaly in the sidescan sonar data east of the Flare II seep is caused by a slope failure which exposed harder sediments on the ridges flank. The arcuate high backscatter area below the ridge's crest is suggested to mark the headwall of the slump (Fig. 24). The elongated low backscatter area at the slide toe may originate from the low inclination of the canyon floor and thus be rather a morphological effect than an indication of softer or undisturbed sediments. This is suggested because usually sediment erosion occurs within a channel which creates high backscatter. The bathymetry further details the geologic situation around Flare II. Just below the headwall of the slide a plateau-like feature is visible in the bathymetry (Fig. 25) which we interpret as the head of the slide. The fan-like widening of the bathymetry below the head of the slide could thus represent the main slide-mass. The area of intermediate backscatter which partly correlates with the head of the slide, might originate from relatively undisturbed sediments, which moved as a block. In this geologic scenario, we interpret the Flare II seepage area as a crown crack (Hampton et al., 1996) or an incipient headwall (e.g. Tréhu et al., 1999). This interpretation is supported by the linear shape of the seep with its central depression that trend parallel to the ridge's crest and the presumed headwall. The seep might represent the location for the next slumping event to originate from.

Our interpretation, that seepage could be related to slope failure in general is supported by previous observations in various regions (Eichhubl et al., 2000; Naehr et al., 2000; Orange et al., 1999b). Seepage supporting chemosynthetic communities, which is related to an incipient headwall *above* the main scar of a slide, was to our knowledge not reported so far. However, for instance Dimitrov and Woodside (2003) report on pockmarks that developed above a headwall, paralleling shape of the rupture surface of a slide in the Mediterranean Sea. Seep communities in the Monterey Bay, California, are closely related to fluid emissions along the head scarp of slides (Naehr et al., 2000; Orange et al., 1999b).

Submarine landslides or debris flows are features which are known to occur preferably at continental slopes and submarine canyon flanks, especially in environments with high sedimentation and fluid flow rates (e.g. Bünz et al., 2005; Hampton et al., 1996; Mulder and Cochonat, 1996; Orange and Breen, 1992; Tréhu et al., 1999). Driving forces for slope failures are slope oversteepening (Hampton et al., 1996), gas hydrate dissociation (Carpenter, 1981; Maslin et al., 1998; Paull et al., 1996), fluid flow, e.g. pore pressure (Li and Clark, 1991; Orange and Breen, 1992), and earthquakes (Hampton et al., 1996). All of these processes might play a role at the Flare II seep. However, due to the very steep declivity of the ridges flank and the apparent fluid flow we suggest that slope failure was mainly controlled by morphology and fluid migration.

Whether pre-existing faults originating, e.g. from slow sediment creeping, served as preferred pathways for migrating fluids which eventually triggered the slope failure, or if enhanced fluid migration only set in after the slumping occurred, cannot be resolved with our data. However, it was previously suggested that the pore pressure regime at the Makran margin is normal, and fluid migration rather buoyancy driven than by pore overpressure (Ding et al., 2010). Therefore, we favor the interpretation that slope failure induced the observed seepage. The fact that seepage occurs focused along the narrow depression within the seep area as evidenced by bubble emissions (Römer et al., *submitted*) (Fig. 26) and enhanced flux of dissolved methane as indicated by the abundances of chemosynthetic communities, evidences the interrelation of fluid flow and the slope failure.

5.6.2 Identification of areas of active seepage

Combining the data from the ROV's high-frequency horizontally-looking sonar and video data, the Flare II seep was mapped. We assume that the high backscatter patterns in the HLS records originate from higher rugosity of the seafloor and occurrence of biogenic and authigenic carbonates within the seepage area. The dependency of the backscatter of the acoustic signal on morphological and biological features has also successfully been used in other studies (e.g. Durand et al., 2002; Jones et al., 2010; Orange et al., 2002, 1999b; Sahling et al., 2008b; Taylor et al., 2008). The assumption that massive carbonates may cause the high backscatter is supported by sediment sampling that revealed the presence of massive carbonates and gas hydrates within the central area of the seeps. We suggest that the effect of gas hydrates which constitute a porous bubble fabric on the backscatter intensity is minor compared to the denser and harder carbonates.

The discrepancy between the high backscatter extent in the sonar records and the area covered by chemosynthetic communities implies that the backscatter strength is predominantly controlled by sediment properties. The more widespread occurrence of authigenic carbonates might be explained in two ways. Long term seepage (hundreds to thousands of years) of dissolved or gaseous methane is known to support the formation of large carbonate accretions (Bayon et al., 2009a; Luff et al., 2004). It has been suggested that such carbonate crusts would grow laterally from the initial site of highest fluid fluxes

towards the surrounding area. The lateral growth might be induced by increasing impermeability of sediments due to carbonate precipitation, and subsequent channeling of fluids towards the margins of carbonate formations (Dupré et al., 2010). In this scenario, gas bubble emissions and aggregations of chemosynthetic communities would be expected to be found along the margins of the high backscatter area we mapped. Instead, chemosynthetic communities and gas emissions were found in close vicinity to a depression in the central part of the elongated seep. This suggests that fluid flow rates are highest in the central part of the seep. We therefore propose, that fluid flow in the marginal areas of the seep is too low or unstable to support the development of chemosynthetic communities. Similar interpretations on distributions of carbonates and chemosynthetic communities were previously suggested for, e.g., seeps associated with headwall scarps (Faure et al., 2006; Orange et al., 1999b) or for seeps associated with outcropping faults (Dupré et al., 2010; MacDonald et al., 1989; Sibuet et al., 1988). Low or intermittent methane flux would still allow for the formation of AOM-derived carbonates, the presence of which is inferred from the sonar records. We can exclude that seafloor morphology influenced the strength of the backscatter in the outer parts of the seep since visual investigations confirm that the seafloor is very smooth in this area. The lack of observations of carbonate crusts being exposed on the seabed at the marginal seep areas, suggests that carbonate formation does not occur just below or at the seafloor surface but in some decimeters of depth. This would be consistent with low methane flux rates (Borowski et al., 1996) and it might be assumed that all dissolved methane is consumed by AOM. Within the central depression centimeter to decimeter-sized carbonates were found within the uppermost 2 m (Fig. 31). On the seafloor, outcrops of carbonates have been observed and sampled during ROV dives. Both observations imply flux rates are higher in this area. Further, precipitation of AOM-derived carbonates, and thus fluid seepage, must be active since at least a few hundreds to thousands of years at this site.

Fischer et al. (2012) demonstrated that fluid flow decreases from central bacterial mat habitats towards outer clams habitats. This is consistent with the observation that gas bubble emissions are usually surrounded by microbial mats (Fischer et al., 2012; Römer et al., *submitted*) (Fig. 28b). Correspondingly, no gas emissions have been observed along the margins of the seep area while they occurred within or close to the central depression. Also, mostly microbial mats and tubeworms have been observed while clams were absent around bubble emission sites. Changes in gas flux intensity or a general decrease of methane supply towards the margins of the seep area is indicated by shells of dead clams. Aggregations of non-articulated clams have been found in some distance to living communities. We speculate that only the slump weakened the carbonate cemented areas and fostered fluid flow that is strong enough to fuel chemosynthetic communities, and discharge free gas.

5.6.3 Methane flux quantification

The detailed mapping of chemosynthetic communities allows obtaining an areal budget of methane turnover based on fluxes previously determined by Fischer et al. (2012). These are compared to the methane discharge by gas bubbles provided by Römer et al. (*submitted*) to assess the relative importance of dissolved and gaseous methane fluxes. As detailed in section 5.6.2 we assume that methane fluxes outside the chemosynthetic communities are very low and completely consumed by AOM. Therefore, only the area covered with chemosynthetic communities might potentially discharge dissolved methane to the water column.

Fischer et al. (2012) obtained sulfate fluxes from pore-water modeling. Furthermore the model indicates an advective rather than diffusive flow. Though no direct methane flux measurements are available for the Flare II seep area, we assume that the sulfate fluxes mimic methane fluxes. It was shown that that linear sulfate gradients and a complete consumption of sulfate in the sulfate-methane-transition zone (SMT) are a robust proxy for upward methane fluxes (Borowski et al., 1996). Since the ratio sulfate reduction and methane oxidation mediated by AOM is 1 (Boetius et al., 2000a; Reeburgh, 1976), sulfate fluxes correspond to methane fluxes (Borowski et al., 1996). The modeled data by Fischer et al. (2012), indicate that within all chemosynthetic habitats, methane is completely consumed by AOM and associated chemosynthetic communities. Therefore, no dissolved methane is exported to the water column. Extrapolating areal methane fluxes thus provides a methane turnover rate for the Flare II seep. For the bacterial mat habitat a sulfate, i.e. methane flux of 9 mol m^{-1} yr^{-1} was assumed, for the polychaetes habitat a flux of 8.4 mol m^{-2} yr^{-1}, and for the clam habitat a flux of 6.6 mol m^{-2} yr^{-1} (Fischer et al., 2012). For the fourth habitat class introduced in this study, the mean flux of the bacterial mat and polychaetes habitat is applied (8.7 m^{-2} yr^{-1}). The areal fluxes for the mapped chemosynthetic communities are detailed in Table 2. The total areal methane turnover at Flare II sums up to $1.14*10^4$ mol yr^{-1}. Compared to the complete consumption of dissolved methane, Römer et al. (*submitted*) obtained a gas bubble discharge from the same area that amounts to $5.6\pm3.36*10^6$ mol yr^{-1} which is two orders of magnitude larger that the turnover rate. This highlights the importance of methane transport by bubbles for the water column methane budget.

5.6.4 Relevance of processes observed at Flare II compared to other sites

This study presents, to the best of our knowledge, the first methane budget, comprising areal estimates of dissolved methane turnover and gaseous emissions, for a non-mud volcano type seep. The only comparable methane budget that might be compiled from literature is available for the Håkon Mosby Mud Volcano (HMMV). In the following we compare the areal extent of the Flare II and relative fluxes to data published on other cold seeps to elucidate how representative the Flare II might be.

5.6.5 Areal extent of the seep and chemosynthetic communities

Numerous studies investigated non-mud volcano type cold seeps, as pockmarks (Ondréas et al., 2005; Sahling et al., 2008a) or large seafloor pavements of AOM-derived carbonates (Bayon et al., 2009b; Dupré et al., 2010). These studies indicate that cold seeps, and seafloor which is influenced by seepage processes, might span over several hundreds of meters. For many of these seeps, different chemosynthetic communities, occurring in various densities, have been reported (MacDonald et al., 2003; Olu-Le Roy et al., 2007, 1996; Sahling et al., 2002). Detailed area estimates of these communities are, however, sparse. A detailed study on the REGAB pockmark by Olu- Le Roy et al. (2007) determined the area of the entire structure to be ca. 80,000 m^2. Detailed video-mosaicking of a ca. 12,000 m^2 area suggests that about 34 % of the entire structure is covered by chemosynthetic communities. This proportion of seep area featuring chemosynthetic communities equals the one observed at Flare II. Mean sizes of distinct patches of chemosynthetic organisms ranged from 3 to 550 m^2 at the REGAB site which is significantly larger than at the Flare II. Here, patch-sizes varied between 0.4 and 11 m^2. Cluster of clams, comparable to those observed at the Flare II, have been mapped by Van Dover et al. (2003) within a seep site of ca. 2,000 m^2 on Blake Ridge, offshore South Carolina. Further area

estimations of cold seep structures have been obtained for submarine mud volcanoes. However, it should be considered that mud volcanoes emit fluids and fluidized sediments and usually form larger mound structures which are not necessarily equal to the area of active seepage. Detailed mapping of the HMMV yielded a size of about 0.75 km^2 for the entire structure. Of this area about 86 % are inhabited by chemosynthetic organisms in varying densities (Jerosch et al., 2007). Mau et al. (2006) extrapolated visual seafloor observations of chemosynthetic communities to total areas of a number of mud mounds offshore Costa Rica. These estimates yielded active seepage areas from 500 to 20,000 m^2. The mapped aggregations of bacterial mats and clams ranged between 0.2 and 3.2 m^2 which is comparable to our observations.

Theses comparisons indicate that the Flare II seep is in the range of the smaller structures, for which area estimates are available. The patch-sizes of chemosynthetic organisms are in good agreement with those observed at many other sites (MacDonald et al., 1990; Mau et al., 2006; Sahling et al., 2002; Van Dover et al., 2003). The latter might indicate that communities generally settle around distinct gas migration pathways, where flux rates decrease with distance from a central conduit. Thus, extent of chemosynthetic communities could be controlled rather by the number of gas conduits than magnitude of areal dissolved fluxes of methane.

5.6.6 Methane emissions and turnover rates and geological controls of fluid flow

The only areal methane budget comprising dissolved and gaseous effluxes and turnover rates was so far available for the HMMV (Felden et al., 2010; Jerosch et al., 2007; Niemann et al., 2006; Sauter et al., 2006). The annual methane turnover by AOM and aerobic oxidation of methane for the 0.75 km^2 large structure was estimated to be about $3.76*10^6$ mol yr^{-1} (5.01 mol m^2 yr^{-1}) (Felden et al., 2010). About $13.54*10^6$ mol yr^{-1} (ca. 18.1 mol m^2 yr^{-1}) of dissolved methane is emitted to the water column (Felden et al., 2010). The bubble discharge from HMMV was estimated to 8-$35*10^6$ mol yr^{-1} (Sauter et al., 2006). The methane turnover rates and bubble emissions are therewith in the same range as at the Flare II. The higher total turnover of methane is explained by the larger area of the active seep site. The discrepancy of dissolved methane effluxes, which are virtually absent at Flare II, but are comparable to bubble emissions at the HMMV, implies that dissolved methane fluxes are much higher at the HMMV.

Local dissolved and bubble effluxes of methane have been presented by Torres et al. (2002) for Hydrate Ridge offshore Oregon. Benthic barrel measurements at bacterial mats yielded dissolved effluxes of 11 to 37 mol m^2 yr^{-1}. At clam fields, effluxes of ca. 0.16 mol m^2 yr^{-1} were obtained (Torres et al., 2002). Methane turnover by AOM in bacterial mat habitats amounts to 0.37 to 73 mol m^2 yr^{-1}, and within clam dominated habitats to 5.8 to 37 mol m^2 yr^{-1} (Treude et al., 2003). Quantification of gas bubble emissions within an 80 m^2 large area yielded $21.9*10^6$ mol yr^{-1}. The turnover rates determined for the Flare II seep area (Fischer et al., 2012) fall within the broad range of rates obtained for the Hydrate Ridge communities. That also much higher turnover rates were measured at Hydrate Ridge might be explained by higher dissolved methane fluxes which are also expressed in the high effluxes. It can be assumed that the efficiency of AOM and associated chemosynthetic communities increases with increasing fluxes, given a sufficient sulfate supply from the sea water (Nauhaus et al., 2002).

For a number of other sites dissolved methane turnover rates and emissions are available. For instance a recent study at the Dvurechenskii Mud Volcano in the Black Sea by Lichtschlag et al. (2010), suggests a dissolved methane discharge from the entire mud

volcano in the order of $1.3*10^7$ mol yr^{-1} (ca. 17.24 mol m^2 yr^{-1}). Turnover rates varied between ca. 26 and 37 mol m^2 yr^{-1} which is about four times higher than at Flare II. For the Captain Arutyunov Mud Volcano in the Gulf of Cadiz, Sommer at al. (2009) provided an areal budget of dissolved methane emissions, based on visual mapping and benthic chamber flux measurements. For the ca. 0.081 km^2 large seepage area they extrapolated an efflux of $0.006*10^6$ mol yr^{-1} (0.07 mol m^2 yr^{-1}). However, no turnover and bubble fluxes are available for this site.

Local bubble emissions at deep-water seeps have been quantified for instance at the Vodianitskii Mud Volcano in the Black Sea to be in the order of $0.9 \pm 0.5*10^6$ mol yr^{-1} (Sahling et al., 2009). In the Gulf of Mexico, bubble fluxes from two distinct seeps (GC185 and G234) were estimated to inject 60.75 mmol s^{-1} ($1.916*10^6$ mol yr^{-1}) and 1.64 mmol s^{-1} ($0.052*10^6$ mol yr^{-1}), respectively, to the water column (Leifer and MacDonald, 2003). Along the Makran accretionary margin, Römer et al. (*submitted*) quantified bubble-gas emissions for two further seep areas. These amount to $0.13 \pm 0.06 *10^6$ mol yr^{-1} (*Flare 1*) and $5.26 \pm 3 *10^6$ mol yr^{-1} (*Flare 5*). The comparison of the Flare II methane budget with fluxes obtained at other sites illustrates that volumes of bubble-gas emitted from the relatively small area of the Flare II, are among the largest ones reported in literature. The turnover rates of dissolved methane are in the lower range of values available in recent literature.

The virtual lack of any discharge of dissolved methane within the Flare II area is a rather unique observation. This indicates that dissolved methane fluxes at the Flare II are low compared to other sites and, compared to bubble-gas transport, insignificant.

It might be speculated that massive carbonates and carbonate cemented sediments down to sediment depth of at least 2 m impede pore-water and free gas advection. Only where sediments are weakened by fracturing, i.e. along faults created by the slope failure, migration of free gas through open conduits is greatly enhanced. This assumption is in agreement with the observation that most intensive fluid emission occurred along the elongated depression at the Flare II. We suggest that pore pressure in sediments along the margins of the depression are reduced by the extensional stress induced by the slump, and therefore allow for higher dissolved methane flow rates than outside the seep area. Local fractures or capillaries provide pathways for bubble emission. This scenario is in agreement with the concentric formation of chemosynthetic habitats around gas vents as well as the generally depression-parallel, elongated orientation of the habitats. This assumption is further supported by fluid flow modeling by Fischer et al. (2012), who obtained advection rates of >1 cm yr^{-1} within the outer clam habitats to 11 cm yr^{-1} in bacterial mat habitats near gas vents.

Though this interpretation of geological controls of fluid emission and the good correlation between variations in fluid flow rates and distinct chemosynthetic communities is consistent, we acknowledge that this model explains only a ‘snap-shot’ of the Flare II. Gaseous as well as dissolved fluxes of methane are highly variable on spatial and temporal scales and might thus change in their relative importance. Especially regarding emissions of gas bubbles it is known that ebullitions vary over time and spatial distribution as well as intensity (Heeschen et al., 2003; Leifer and MacDonald, 2003; Linke et al., 2010; Naudts et al., 2010; Nikolovska et al., 2008; Sauter et al., 2006; Torres et al., 2002). However, the dense abundances of vital chemosynthetic communities indicate that active seepage of at least dissolved methane is rather persistent at Flare II.

5.7 Conclusion

Here we presented new data on areal methane emissions and geological processes driving fluid flow at the Flare II seep. Previous studies investigated the geologic evolution of the Makran accretionary margin and large scale processes that control fluid migration. However, little is known about non-mud volcano cold seep formation, persistency of seepage, and contributions of methane seeps on local water column methane inventories. We provide evidence that dissolved methane is entirely consumed by biogeochemical processes and does not contribute to the hydrosphere's methane budget. Based on geophysical and optical mapping we estimate that about $1.14*10^4$ mol yr^{-1} of dissolved methane are consumed by AOM within the Flare II area. In comparison to this turnover Römer et al. (*in press; submitted*) showed that about $556*10^4$ mol yr^{-1} methane are discharged to the hydrosphere by bubbles. The here presented high-resolution sonar and optical mapping showed that mere geophysical seep-mapping significantly overestimates the area of active seepage. Therefore, using only this approach will overestimate any areal turnover and discharge rates of dissolved methane. We promote optical mapping to better constrain the area of active seepage, i.e. the area that features distinct chemosynthetic communities.

Our data indicates that fluid flow at Flare II is generally controlled by a major slump which created migration pathways. The interpretation of the seep structure as incipient headwall indicates where the next slope failure will originate from. However, the development of chemosynthetic communities shows that the system is stable in its current configuration since probably tens of years.

This study emphasizes the importance of assessing methane budgets for entire seeps to better constrain the relative importance of dissolved and bubble gas fluxes. Only such budgets provide reliable estimates of deep-sea seepage contributions to water column or atmospheric methane inventories. Our results, in combination with findings by Römer et al. (*submitted*) suggest that deep-water seeps off Pakistan do not transfer any methane to the atmosphere.

5.8 Acknowledgements

We thank captain and crew of R/V METEOR (cruise M74/3) for their support at sea. We are grateful to the team of the ROV MARUM QUEST4000 for enabling the acquisition of the video data and seafloor images this work is based on. We are indebted to Markus Brüning for processing the sidescan data and Christian dos Santos Ferreira and Marten Schmager for processing the bathymetry data. This work was funded through DFG-Research Center/ Cluster of Excellence „The Ocean in the Earth System".

Chapter 6

2. Manuscript

Natural oil seepage at Kobuleti Ridge, eastern Black Sea

Jan-Hendrik Körber[a*], Heiko Sahling[a], Thomas Pape[a], Christian dos Santos Ferreira[a], Ian MacDonald[b], Gerhard Bohrmann[a]

[a]MARUM - Center for Marine Environmental Sciences and Department of Geosciences, University of Bremen, Klagenfurter Strasse, 28359 Bremen, Germany

[b]Florida State University, Department of Oceanography, 117N Woodward Avenue, P.O. Box 3064320, Tallahassee, Florida32306-4320, USA

submitted to *Marine and Petroleum Geology*

6.1 Abstract

Analysis of Advanced Synthetic Aperture Radar satellite images in combination with water column and seafloor investigations documented oil seepage from Pechori Mound and Colkheti Seep in 1,000 – 1,200 m water depth at the northern Kobuleti Ridge in the eastern Black Sea offshore Georgia. Hydroacoustic imaging of the water column using multibeam echosounder evidenced numerous gas emissions from both features. Gas bubbles rose as high as 45 m below sea level. It is proposed that oil coatings around gas bubbles hamper their dissolution allowing them to reach the sea surface, where widespread oil slicks are formed. Slow bubble rise velocities (14 cm s^{-1}) of bubbles with diameters of 5.3 ± 1.5 mm (n=101) derived from video data obtained with remotely operated vehicle MARUM QUEST4000, corroborate the assumption that bubbles are contaminated with oil. High resolution seafloor mapping by autonomous underwater vehicle MARUM B-SEAL5000 at one site revealed a crater-strewn morphology whose formation is explained by frequent rafting of shallow gas hydrate deposits. Satellite imaging of oil slicks on the sea surface above both sites indicates that oil seepage is rather persistent since 2003. An order-of-magnitude estimation of minimum oil seepage rates ranges from ~40 to 200 liters per hour from both sites. This is the first comprehensive description of oil seepage in the Black Sea.

Keywords

Seepage; oil; gas; oil slick; hydrocarbon; Black Sea; remote sensing

6.2 Introduction

Natural seepage of methane and gas hydrate dissociation have been identified as major sources sustaining the Black Sea's high content of dissolved methane (Kessler et al., 2006a; Schmale et al., 2011). Seepage has previously been reported for various locations around the Black Sea basin ranging from the shallow shelf areas (Çifçi et al., 2003; Dimitrov, 2002; Naudts et al., 2006) to the deep sea (Bohrmann et al., 2003; Krastel et al., 2003; Nikolovska et al., 2008; Sahling et al., 2009). Three types of submarine cold seeps may be distinguished in the Black Sea depending on their seafloor expression and the water depth in which they occur.

One type is found in shallow waters on the shelf and upper continental slope above the gas hydrate stability zone (GHSZ) where temperature and/or pressure conditions are unfavorable for the formation of gas hydrates. The upper stability limit of pure methane hydrates lies at ca. 700 m below sea level (bsl) (Bohrmann et al., 2003; Sahling et al., 2009). This seepage type is dominated by emissions of biogenic methane with thousands of gas vents occurring at the Dnepr and Danube paleo-deltas offshore Ukraine and Romania (Michaelis et al., 2002; Naudts et al., 2006; Schmale et al., 2010) as well as at the shelf and upper slope offshore Bulgaria (Dimitrov, 2002), Turkey (Çifçi et al., 2003; Ergün et al., 2002), and Georgia (Egorov et al., 2003). A second seep type may be distinguished by the fact that gas bubbles are emitted from the seafloor within the GHSZ. These seeps may be considered as 'gas-driven' systems where a part of the bubbles rising through the sediments is sequestered as gas hydrate at shallow sediment depths while the remaining fraction is emitted to the water column. Though it is generally considered that gas hydrate formation in the continental margin slope sediments impedes seepage, these particular sites are pathways for gaseous methane through the sediments into the water column (Naudts et al., 2006; Römer et al., *in press*). Only few sites emitting bubbles within the GHSZ have been described so far, e.g. the Batumi Seep area offshore Georgia (Klaucke et al., 2006; Nikolovska et al., 2008; Pape et al., 2011, 2010) and the Kerch Flare area offshore eastern Ukraine (Römer et al., *in press*). However, in the maps by Naudts et al. (2006) and Popescu et al. (2006) additional sites are indicated at the Dnepr and Danube paleo-deltas suggesting that this seep type is more common than anticipated so far. Gases fuelling these seeps are predominantly biogenic low molecular weight hydrocarbons (LMWH), mainly methane (Mazzini et al., 2004; Pape et al., 2010; Römer et al., *in press*). A third seep type is represented by seeps with considerable seafloor morphology such as mounds or submarine mud volcanoes. For simplicity, we use the expression 'mud volcano' for all positive seafloor features formed by extrusion of fluid-rich material which is transported upwards from deeper sedimentary units. In the Black Sea, mud volcanoes described so far are exclusively located within the GHSZ (Akhmetzhanov et al., 2007; Bahr et al., 2009; Bohrmann et al., 2003; Ivanov et al., 1996; Krastel et al., 2003; Mazzini et al., 2008; Meisner et al., 1996). Presence of gas hydrates and gas bubble emissions has previously been reported for Black Sea mud volcanoes (Bohrmann et al., 2003; Greinert et al., 2006; Ivanov et al., 1996; Klapp et al., 2010b), which legitimates to consider them as seeps.

Though the Black Sea, especially the eastern part, is known to bear potential for oil generation (Robinson et al., 1996), few is known about oil seepage from the seafloor and oil occurrence in shallow sediments which is common in other hydrocarbon provinces, e.g. the Gulf of Mexico (Brooks et al., 1984; MacDonald et al., 1993). Several mud volcanoes show evidence for admixtures of thermogenic hydrocarbons to the predominant biogenic LMWH (Blinova et al., 2003; Kruglyakova et al., 2004; Stadnitskaia et al., 2008) but no oil seepage has been evidenced so far. Kruglyakova et al. (2004) mention an oil seep off Rize, Turkey,

where oil reaches the sea surface but no images or data are given to illustrate this. In this study, we comprehensively describe oil seepage at Kobuleti Ridge offshore Georgia, as novel seepage type in the Black Sea. The two seep structures Pechori Mound and Colkheti Seep have been discovered, along with other structures showing oil impregnated sediments, during the Training-Trough-Research (TTR) cruise 15 with R/V LOGACHEV (Akhmetzhanov et al., 2007). The microstructure of gas hydrates (Klapp et al., 2010b) as well as the geochemistry of oil impregnated sediments (Reitz et al., 2011) sampled at both seeps have been described previously.

There is evidence that gas emissions from all seep types contribute to the high water column methane concentrations (Kessler et al., 2006a). Yet, previous studies indicate that no free gas emitted from depths below about 100 m reaches the water-atmosphere interface due to bubble dissolution (Greinert et al., 2006; McGinnis et al., 2006). Bubbles reaching the sea surface from hundreds of meters depth have, so far, only been reported for sites of combined oil and gas seepage in the Gulf of Mexico (De Beukelaer et al., 2003; MacDonald et al., 2002) and one gas seep in the Sea of Okhotsk (Cranston et al., 1994). It was proposed that oil coatings around gas bubbles hamper their dissolution, allowing them to reach the sea surface (De Beukelaer et al., 2003; Leifer and MacDonald, 2003). A study by Solomon et al. (2009) highlighted the contribution of oil-coated bubbles to elevated dissolved methane concentrations in near-surface waters which might be a significant source of atmospheric methane. However, a follow-up study at the same sites could not confirm the previously suggested magnitude of sea-air methane flux (Hu et al., 2012). When oil-coated bubbles reach the sea surface, the oil forms widespread slicks (De Beukelaer et al., 2003). These are visible on *Synthetic Aperture Radar* (SAR) satellite images (De Beukelaer et al., 2003; Garcia-Pineda, 2009; Leifer and MacDonald, 2003) and allow pinpointing the source on the seafloor with good accuracy (Garcia-Pineda et al., 2010).

In this study satellite and hydroacoustic investigations in combination with visual seafloor inspections were performed to characterize the two oil seeps Pechori Mound and Colkheti Seep. In the following we describe the seeps and related seepage processes that allow oily bubbles to reach the sea surface from depth >1,000 m. Due to their unique characteristics, we discuss the oil seeps as novel seepage type that was not described in the Black Sea so far.

6.3 Study area and geological settings

The Black Sea is an intercontinental basin (Fig. 32) characterized by a well stratified water mass with an oxygenated uppermost layer and an O_2/H_2S transition around 200 mbsl (Murray et al., 1989). A permanent pycnocline is developed between 100 and 200 mbsl (Murray et al., 1991), impeding ventilation of the deeper water mass. Due to its stable stratification and negligible exchange of water masses through the Bosporus, the Black Sea became the largest surface reservoir of dissolved methane (Kessler et al., 2006b; Reeburgh et al., 1991).

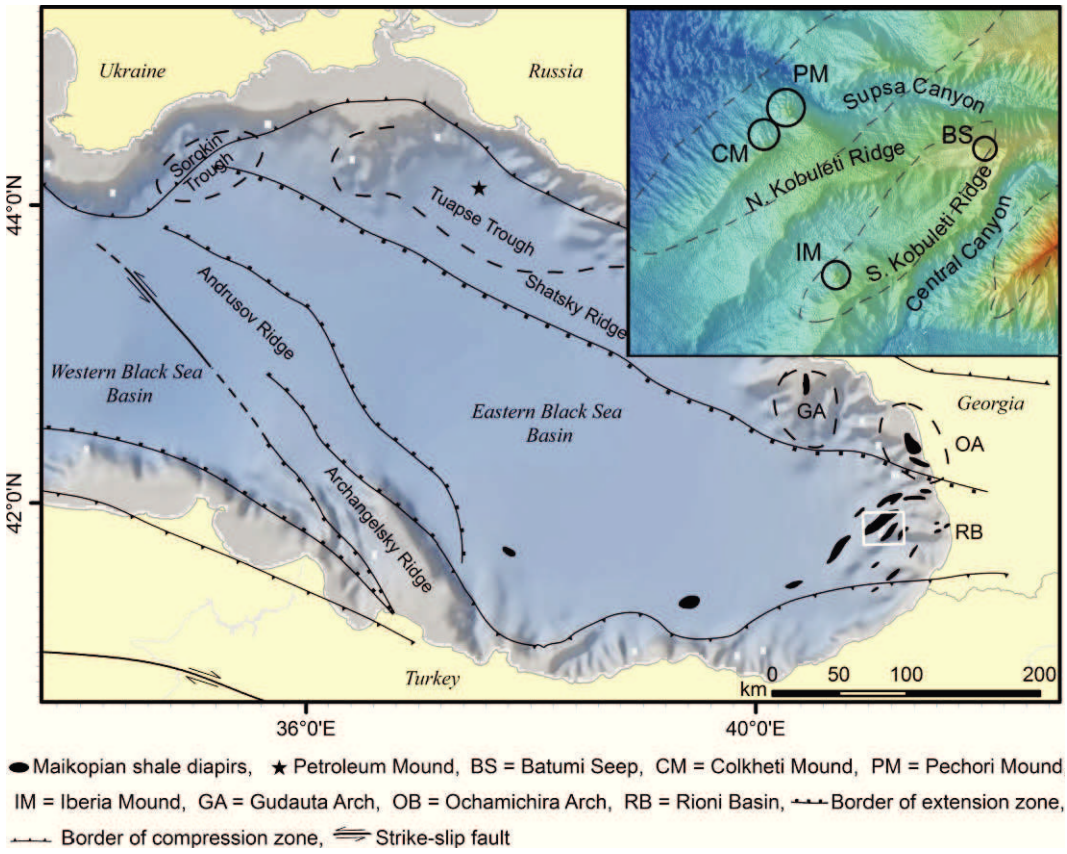

Fig. 32. Main geological structures of the Black Sea (after Robinson et al., 1996). Location of the study region in the eastern Black Sea (insert) is indicated by the white box. Locations of Maikopian shale diapirs are adapted from Tugolesov et al. (1985). Dashed lines in the insert indicate locations of Maikopian shale diapirs. Bathymetry of main map: GEBCO 1 min; bathymetry of inset: multibeam echosounder data acquired as part of this study.

The recent Black Sea has a maximum depth of 2,206 m (Ross et al., 1974). In the sub-seafloor the Andrusov and Achangelsky Ridges form the Mid-Black Sea-High that separates a western and eastern basin (Fig. 32). These basins developed from a back-arc basin when the Neo-Tethys was closed by subduction under the Eurasian plate (Görür, 1988; Zonenshain and Pichon, 1986) in Late Cretaceous or Early Palaeocene (Meredith and Egan, 2002; Nikishin et al., 2003). Latest in Eocene the extensional regime of the evolving basins changed to a compressional one due to the subduction of the African and Arabian plates under the Eurasian plate (Meredith and Egan, 2002; Nikishin et al., 2003).

With respect to hydrocarbon maturation special attention has been drawn to the Oligocene-Miocene Maikopian formation which is known to bear great hydrocarbon potential in the eastern Black Sea off- and onshore region (Robinson et al., 1997). The study area is located in the offshore part of the Rioni Basin (Fig. 32), which has formed between the Greater Caucasus Thrust Belt in the north and the Adjara-Trialet-Fold Belt in the south (Banks et al., 1997). While there is a wealth of literature on the regional geology of the eastern Black Sea in Russian language (e.g. Tugolesov et al., 1985, 1983), only summarizing aspects have been available to us through personal communication with Leonid Meisner and colleagues from the Marine Geology and Hydrocarbon Potential Department “SSC Yuzhmorgeologiya” in Gelendzhik, Russia. Based on deep seismic reflection profiles Tugolesov et al. (1985) interpreted anticlinal folds in the offshore part of the

Rioni Basin as caused by Maikopian shale diapirs (Fig. 32). The interplay between diapiric uplift and erosion has probably shaped the canyon-ridge systems at the continental slope as shown in Figure 32 (inset). Kobuleti Ridge is a complex ridge structure bordered by the Supsa Canyon to the north and the Central Canyon to the south (Klaucke et al., 2006).

Four hydrocarbon seeps have been described at Kobuleti Ridge (Fig. 32): at Batumi Seep vigorous bubble streams of mainly biogenic methane are emitted through gas hydrate deposits in shallow sediments (Nikolovska et al., 2008; Pape et al., 2011, 2010). Batumi Seep does not show a markedly positive seafloor morphology which contrasts the protruding structures of Pechori Mound, Colkheti Seep, and Iberia Mound (Fig. 32). Oil-stained sediments were recovered from the latter three structures in 2005 (Akhmetzhanov et al., 2007). Geochemical studies at Pechori Mound revealed pore fluids containing thermogenic hydrocarbons that are altered by mineral/water reactions at elevated temperatures of 60 to 110 °C (Reitz et al., 2011). Based on the presence of the biomarker oleanane, Reitz et al. (2011) suggest that the hydrocarbon source rocks belong to the Maikopian Formation.

6.4 Material and methods

Stimulated by preliminary results on oil seepage at Kobuleti Ridge obtained during research cruises with R/V PROFESSOR LOGATCHEV (TTR15, 2005) (Akhmetzhanov et al., 2007) and R/V METEOR (M72/3, 2007) (Bohrmann et al., 2007) the study area was investigated with respect to oil seepage by ASAR satellite imagery. During following research cruises with R/V MARIA S. MERIAN (MSM 15/2, 2010) et al., 2011a) and R/V METEOR (M84/2, 2011) (Bohrmann et al., 2011b), existing data sets have been complemented by detailed seafloor and water column investigations.

6.4.1 Sea surface investigations by satellite imagery

Advanced Synthetic Aperture Radar (ASAR) images acquired by the *Environmental Satellite* (ENVISAT) operated by the *European Space Agency* (ESA) were used to detect sites of natural oil seepage in the eastern Black Sea. The ASAR is an active sensor that emits microwaves and records their backscatter signal from the earth surface (ESA, 2007). Following Bragg's law, smoother surfaces scatter more radiation away from the sensor than rougher surfaces. Oil is imaged by the sensor because it dampens capillary waves at sub-centimeter to 10 cm wavelengths (Espedal and Johannessen, 2000). These are waves controlled by surface tension that promote along the water-atmosphere interface. Due to higher surface tension oily water surfaces are smoother (darker areas in processed images) compared to the surrounding oil free areas (Espedal and Johannessen, 2000). Boundary conditions for oil detection using ASAR are minimum slick thicknesses of ~0.1 µm (Garcia-Pineda et al., 2009) and wind velocities between 3.5 and 15 ms^{-1} (Solberg et al., 2007).

A set of 42 ENVISAT ASAR *Image Mode Precision* (IMP) images, 4 *Image Mode Medium Resolution* (IMM) and 9 *Wide Swath Mode* (WSM) were available in this study. 26 of these images were suitable for detection of natural oil slicks. The remaining images showed widespread surface patterns like rain cells and biogenic films restricting oil slick identification.

All images have been visually analyzed for natural oil slicks. Therefore, the images have been converted from N1 to 8-bit geoTiff format and loaded into a geographic information system (GIS) (ArcInfo, © ESRI). Oil slick origins (OSO) which are the surfacing locations of the slick-forming oil (Garcia-Pineda et al., 2010) have been identified and marked for each slick in individual images. Clusters of OSOs have been identified by combining information

on OSO locations from all images. The geometric mean centers of the clusters were considered as location of natural oil vents at the seafloor.

6.4.2 Water column and seafloor investigations by hydroacoustic techniques

During three cruises (2007, 2010, and 2011) extensive hydroacoustic surveys were conducted in the study area. Acoustic water column data acquired with the 18 kHz frequency of the Atlas PARASOUND single beam echosounder are available from all cruises. In 2011 bathymetry and water column data was recorded with the Kongsberg EM122 multibeam echosounder. The EM122 is a 12 kHz swath system that allows recording and displaying water column data in addition to bathymetry data. For imaging seepage activity, dedicated surveys were conducted with settings optimized for the detection of so-called gas flares (acoustic anomalies caused by uprising gas bubbles): Ping mode was set to shallow for all water depths, the beam fan was set to an opening angle of 70°, and ship speed was around 5 knots. Flares were extracted from the water column data using the Fledermaus Midwater tool (© QPS). These data were loaded in Fledermaus (© QPS) allowing the 3D investigation of flare heights and deflections in the water column.

In 2010 the autonomous underwater vehicle (AUV) MARUM B-SEAL5000 was used to map Colkheti Seep using a Reson SeaBat 7125 multibeam echosounder which operates with a 400 kHz frequency and 512 beams (Römer et al., *in press*). During the survey the AUV flew about 40 m above the seafloor. The bathymetry data obtained using the ships multibeam system was gridded to 5-10 m resolution depending on coverage and data quality. The AUV data yielded a 0.5 m grid. Both datasets have been post-processed using MB System (http://www.mbari.org/data/mbsystem; GNU General Public License). For the ships multibeam echosounder dataset the backscatter data was processed using MB System. These data are corrected for differences in backscatter intensity that are due to beam angle and seafloor morphology.

6.4.3 Seafloor observations and sampling

In 2007 the remotely operated vehicle (ROV) MARUM QUEST4000 was deployed for one dive (dive no. 155) at Colkheti Seep. During nine hours of bottom time the ROV's horizontally looking obstacle avoidance sonar (Kongsberg MS1000, 675 kHz) was used to detect gas emissions from the seafloor (Nikolovska et al., 2008). One emission site was sampled for gas chemical analysis using a gas bubble sampler (Pape et al., 2010). Continuous video footage was recorded on standard Sony miniDV tapes with two PAL video cameras. On demand, high resolution video was recorded with an InsitePacific ZEUSPLUS HD-TV camera. Still images were acquired with a 3.34 megapixel InsitePacific SCORPIO camera. Additionally, video footage and sampling from TV-guided-grab surveys conducted at Pechori Mound and Colkheti Seep in 2005 (Akhmetzhanov et al., 2007) were available. Individual bubble rise velocities and sizes were obtained from the ROV video data using a method previously described in Sahling et al. (2009). Bubble volumes have been calculated assuming that bubbles are rotation ellipsoids with the measured minor axis being the rotation axis.

6.5 Results

6.5.1 Oil slicks

6.5.1.1 ASAR images of oil slicks

ASAR images show evidence for oil slicks that originate from Pechori Mound and Colkheti Seep as is illustrated in Fig. 33. An overview on the specifics of 26 ASAR images showing oil slicks and information on the total oil covered sea surface area is given in Table 3. Except for one image, which only covers Pechori Mound (18 February 2004), and one image that covers only Colkheti Seep (30 September 2007) both seep sites are covered. At least one image is available that covers both sites for each year under investigation (2003 to 2011). All images indicate active seepage from Pechori Mound in terms of distinct oil slicks. For the adjacent Colkheti Seep only one image (acquired on 13 April 2005) does not reveal the presence of an oil slick.

Table 3. Overview of ASAR images used in the study. Date of acquisition and total oil-covered area originating from Colkheti and Pechori Mound shown. Values are rounded to full km².

Date of image acquisition	Pechori Mound covered	Colkheti Seep covered	Slick-covered area [km²]	Image type[a]
15-Sep-03	yes	yes	48	IMP
5-Nov-03	yes	yes	32	IMP
29-Dec-03	yes	yes	27	IMP
18-Feb-04	yes	no	14	IMP
2-Jun-04	yes	yes	19	IMP
28-Mar-05	yes	yes	15	IMP
13-Apr-05	yes	yes[c]	2	IMP
31-Jul-06	yes	yes	*	IMP
7-Feb-07	yes	yes	23	IMP
01-Aug-07	yes	yes	98	IMP
30-Sep-07	no	yes	3	IMP
20-Nov-07	yes	yes	3	IMP
8-Apr-08	yes	yes	35	IMP
20-Nov-08	yes	yes	12	IMP
14-May-09	yes	yes	46	IMP
11-Jan-10	yes	yes	12	IMP
22-Mar-10	yes	yes	12	IMP
24-May-10	yes	yes	6	WSM
16-Jun-10	yes	yes	34	IMP
13-Sep-10	yes	yes	201	WSM
18-Oct-10	yes	yes	119	WSM
6-Apr-11	yes	yes	79	WSM
6-May-11	yes	yes	65	WSM
3-Sep-11	yes	yes	61	WSM
5-Sep-11	yes	yes	28	WSM
19-Sep-11	yes	yes	160	WSM

[a] IMP= Image Mode Precision, WSM=Wide Swath Mode
[b] Areal extent uncertain due to non-slick surfactants merging with slicks
[c] No oil slick above Colkheti Seep

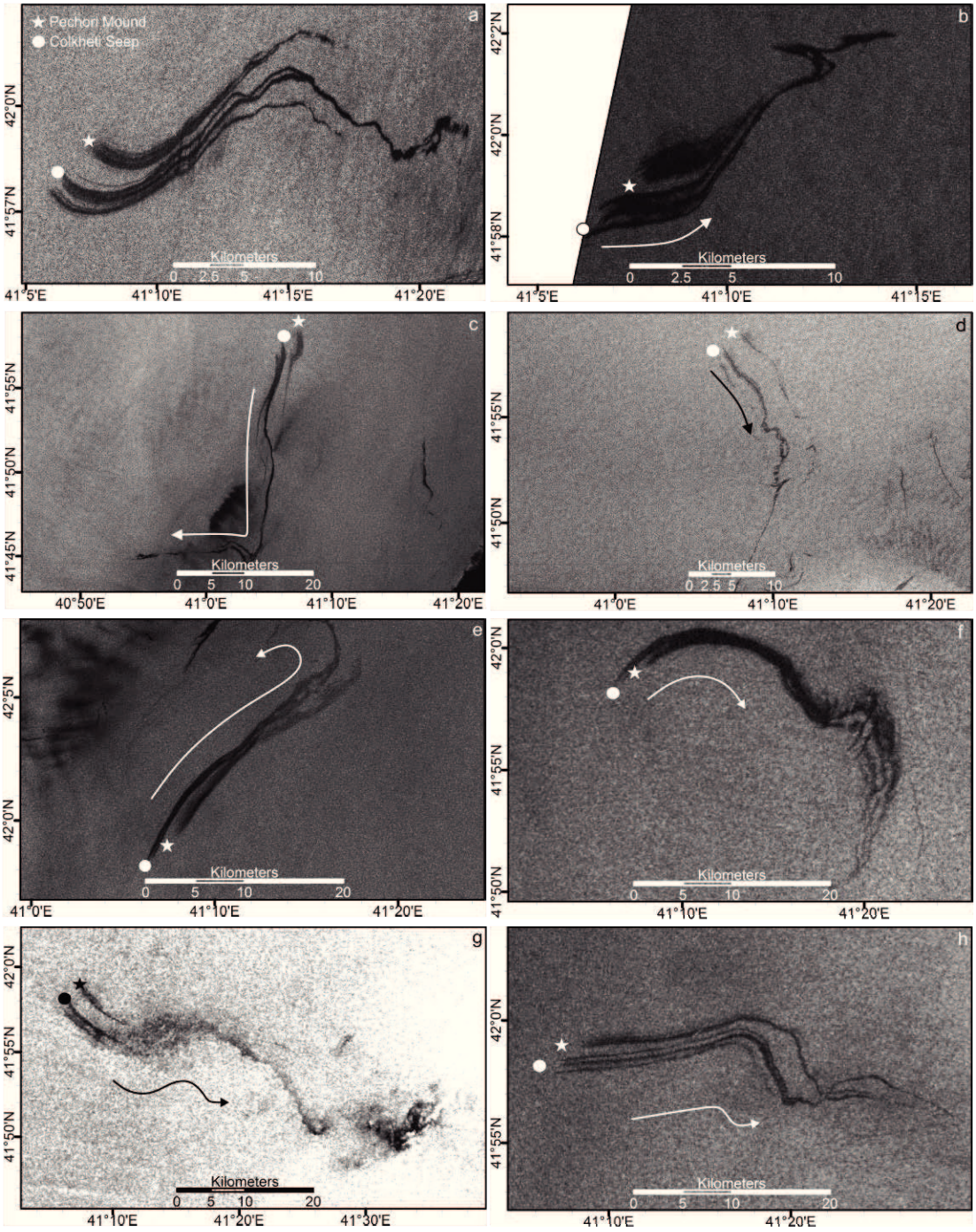

Fig. 33. Subsets of ASAR IMP (a, b, c, d, e) and ASAR WSM (f, g, h) images showing oil slicks on the sea surface related to natural seepage at Colkheti Seep and Pechori Mound. Arrows indicate drift direction of the slicks. Images were acquired on a) 15 September 2003, b) 07 February 2007, c) 08 April 2008, d) 29 December 2003, e) 14 September 2009, f) 06 April 2011, g) 13 September 2010, and h) 14 May 2011. Note different scales. All images provided by ESA.

Though many individual slicks originating from Colkheti Seep and Pechori Mound coalesce when being drifted away from their origin, it is evident that slicks forming above Colkheti Mound are in general longer and cover larger areas than those above Pechori Mound (see e.g., Figs. 33a, 33b, 33d and 33h). The total sea surface area covered by oil varies from approx. 2 to 201 km². Maximum slick length might exceed 65 km. Oil slick orientations depend on wind and ocean current directions. The slick in Fig. 33c for instance seems to mimic an anti-cyclonic pattern, forming a spiraling, curved, elongated shape. Slicks in Fig. 33e were deflected to the south from their origin while the trailing end is drifted to the west. Outlines of slicks derived from some images illustrate different deflections from their origin and spatial extents (Fig. 34).

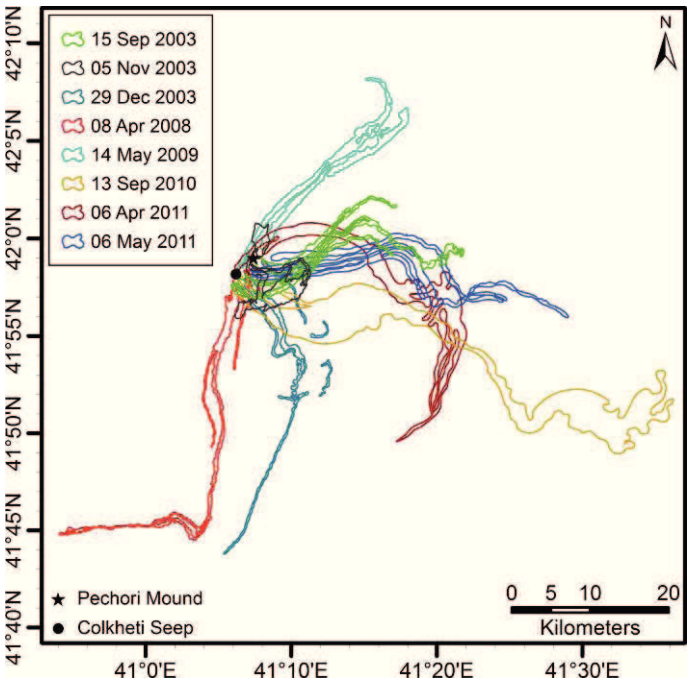

Fig. 34. Outlines of oil slicks detected above Colkheti and Pechori Mound between 2003 and 2011, illustrating different wind induced deflections and spreading of oil on the sea surface.

6.5.1.2 Visual observations of oil slicks

During the expedition in 2010 oily bubbles or oil droplets have been visually observed to reach the surface above Colkheti Mound (Fig. 35a). Single bubbles surfaced in a distance of few meters from each other, immediately forming thin silvery sheens (Fig. 35b) to thick red-brownish layers of oil (Fig. 35a). Widespread oil slicks have been visible from the vessel (Fig. 35c). These visual observations correlate well with information on oil slick locations and extents derived from an ASAR image acquired on the previous day (Fig. 35d). The image shows almost uniform low backscatter in the study area which corresponds to low wind speeds (< 3 ms^{-1}) and calm sea during the previous days. The oil slicks appear as dark roundish patches due to a lack of wind drift and water currents (Fig. 35d). The total sea surface coverage of both patches was 5.5 km².

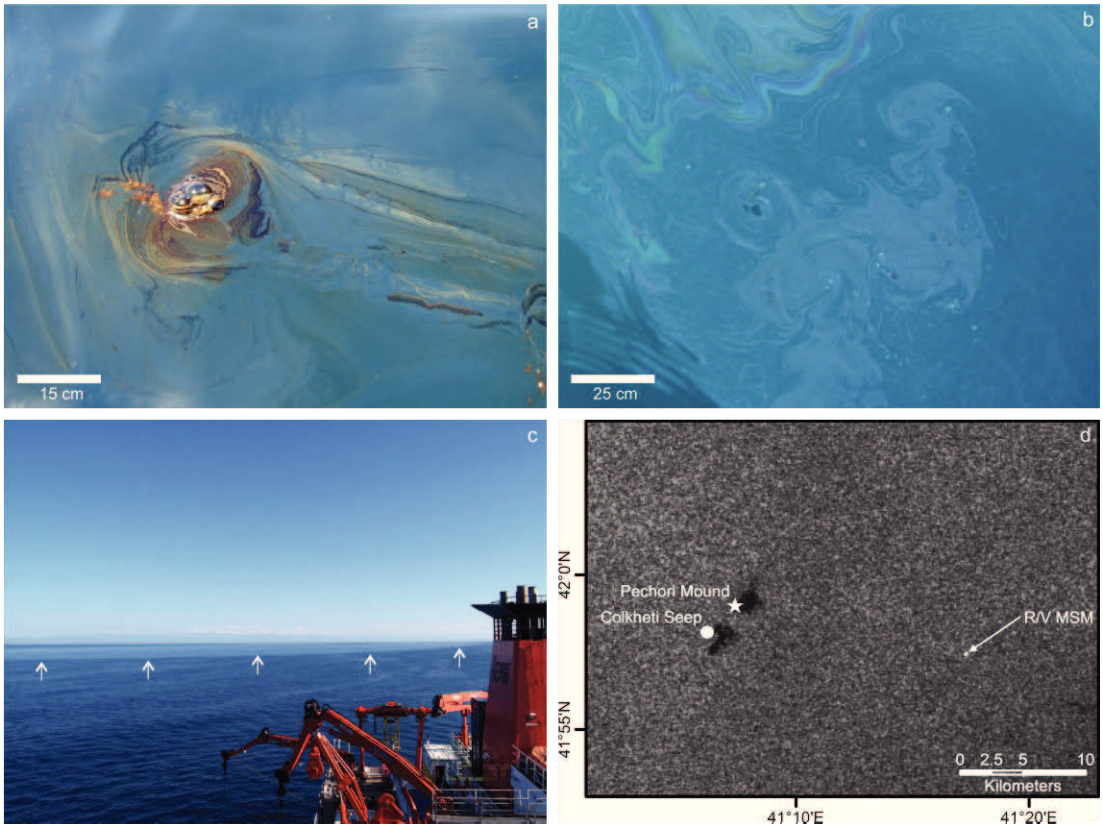

Fig. 35. Visual evidence for oil seepage at Colkheti Seep. a) & b) Bubbles surfacing above Colkheti Mound, forming oil layers on the sea surface. c) Photograph taken from *R/V Maria S. Merian* on 25 May 2010 facing to the east. Arrows indicate the boundary of oily (above) and non-oily water surface (width of the vessel is about 20 m). d) Subset of ASAR image acquired on 24 May 2010 showing oil slicks above Colkheti Seep and Pechori Mound (image provided by ESA).

6.5.2 Bathymetry, seafloor backscatter, and visual seafloor observations

Pechori Mound and Colkheti Seep are positive seafloor structures that protrude the northern slope of Kobuleti Ridge (Fig. 36). All OSOs identified in the area were found close to these mounds (black stars in Fig. 36), indicating that these are the sites of oil seepage as detailed in section *6.5.3*. In general, there is evidence for sediment erosion of the slope of Kobuleti Ridge including Pechori Mound and Colkheti Seep. The bathymetric map shows numerous gullies at the north-western slope as well as on the northern slope that is part of the Supsa Canyon. Sediment erosion is further indicated by characteristic backscatter patterns in the backscatter image derived from the multibeam echosounder data (Fig. 37). Smooth and soft sediments prevail at Kobuleti Ridge causing low backscatter. In contrast, the gully-bases and the seafloor in Supsa Canyon are characterized by high backscatter, suggesting that recent sediment erosion exposed harder material.

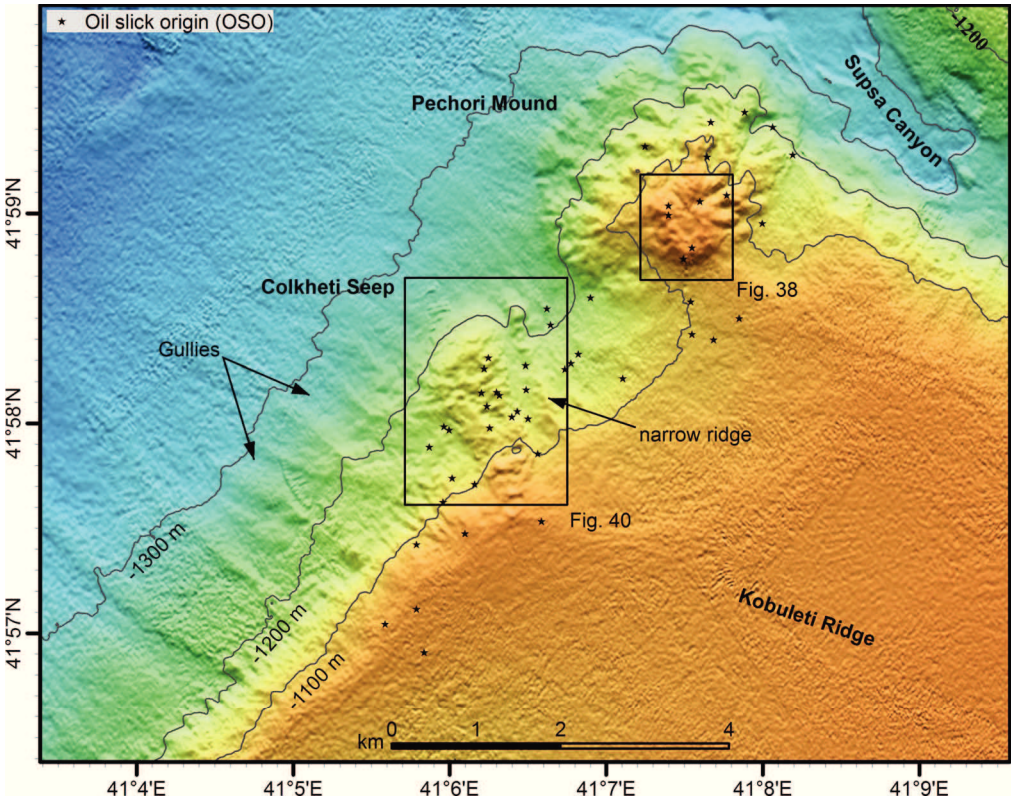

Fig. 36. Swath bathymetry of the study region.

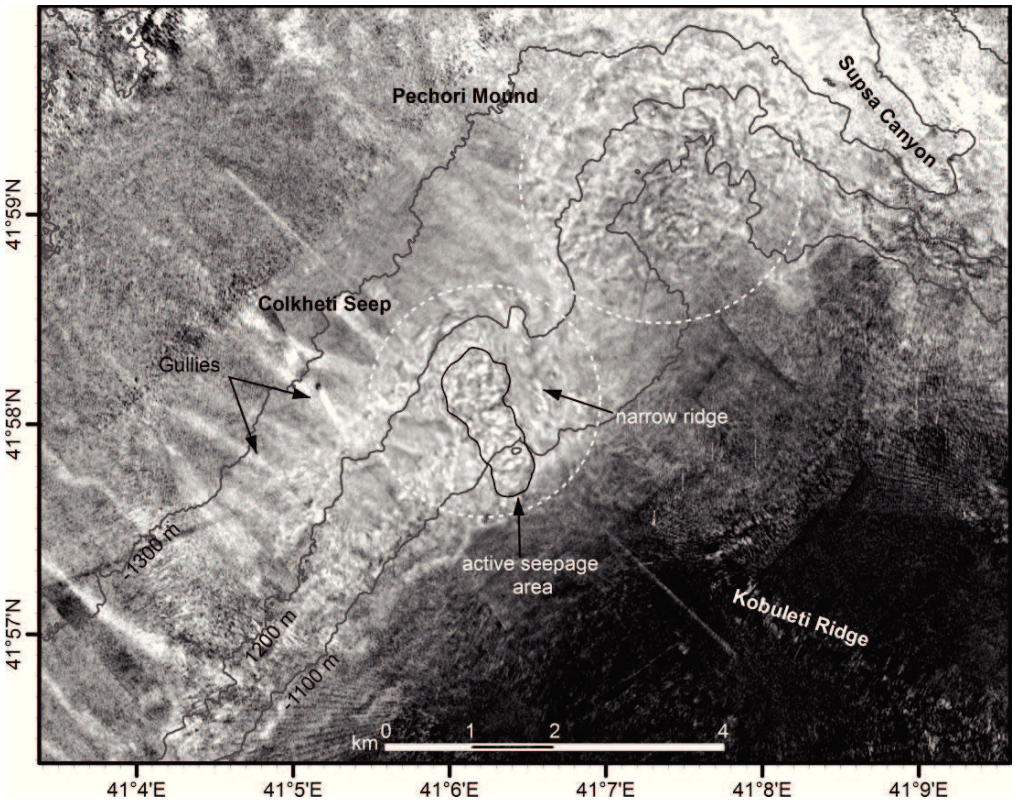

Fig. 37. Backscatter map of the study region. Dark colors indicate low backscatter, light colors high backscatter. The map extent equals Fig. 36.

6.5.2.1 Pechori Mound

Pechori Mound is a cone-shaped sub-circular structure with a basal diameter of about 3.4 km and an elevation of approximately 250 m above the slope toe of the Kobuleti Ridge's flank (Fig. 36). The circular summit is formed by a 400/500 m (N-S/W-E) wide rim surrounding an 8-10 m deep depression (Fig. 38). From its centre an elevation rises to approximately the depth level of the rim. Towards the SE the mound has a steep slope that foots on the flank of the NW Kobuleti ridge. The Pechori Mound's flanks are cut by deeply incised gullies that are most pronounced on the northern and eastern flanks indicating erosive processes.

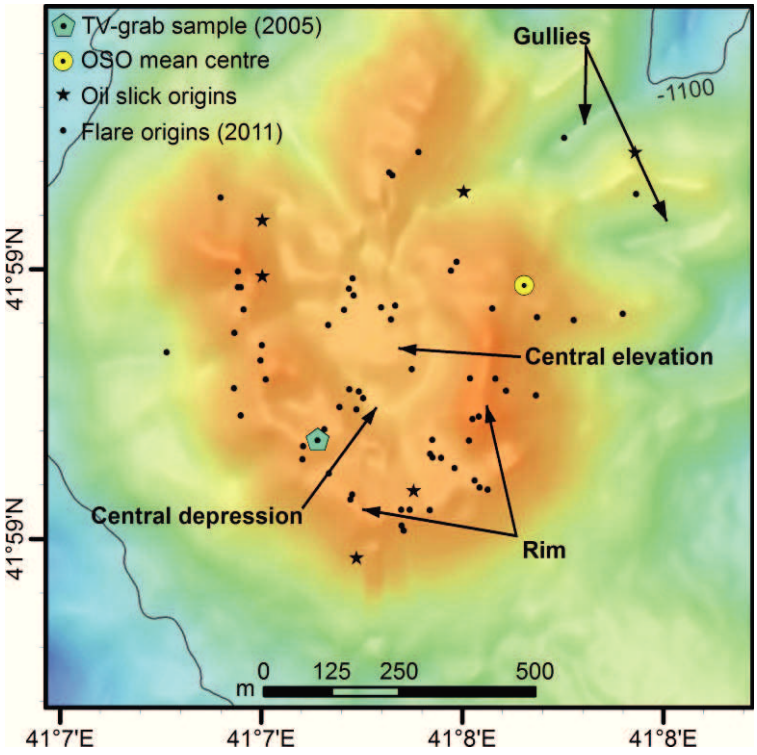

Fig. 38. Swath bathymetry of the Pechori Mound's summit area. Centers of gas emissions (flares) derived from multibeam echosounder data shown by black dots. Black stars denote oil slick origins (OSOs) on the sea surface. The yellow dot indicates the mean geometric centre of all mapped OSOs.

This is further confirmed by a TV-grab survey (TTR-15, BS358GR) revealing steep morphology with exposed bedding structures (Fig. 39a). Furthermore, clusters of holes were observed that probably originate from bubble emissions. A surface sample of bulk sediments retrieved by the TV-grab was heavily contaminated with oil (Fig. 39b; see Fig. 38 for sampling location).

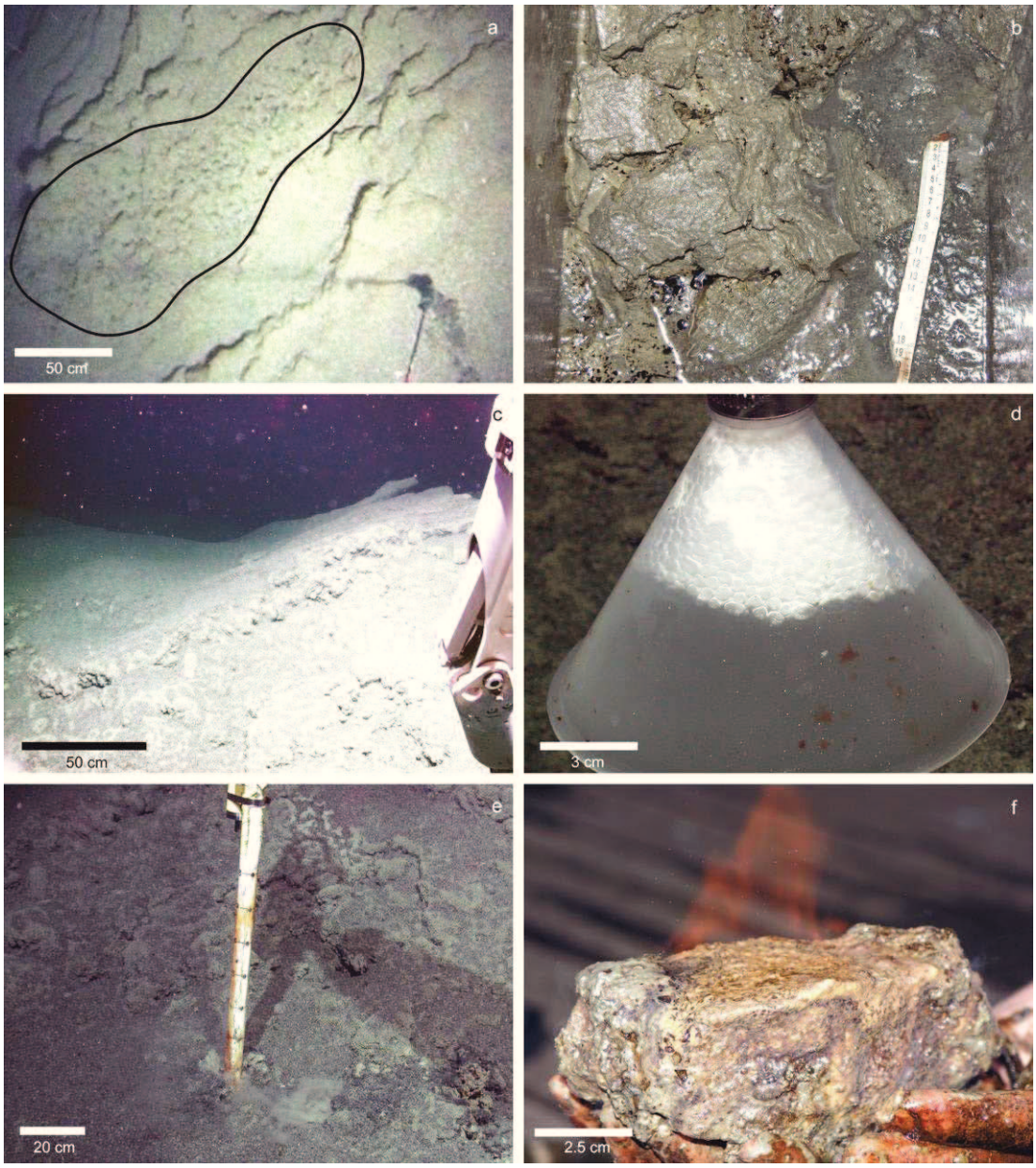

Fig. 39. Seafloor images of Colkheti Seep. a) Video frame grab taken during a TV-grab survey (TTR-15, BS358GR) at Pechori Mound showing bubble holes (outlined) and bedding structure. b) Photo of oil stained sediments retrieved by TV-grab (TTR-15, BS358GR) at Pechori Mound. c) Photo taken by ROV showing the rough flank of a crater-like depression and seafloor morphology close to a bubble emission site at Colkheti Seep (ROV QUEST manipulator seen on the right). d) Gas bubbles caught in a gas bubble sampler funnel at Colkheti Seep. Bubbles instantly formed gas hydrate shells; brownish oil stains on the funnel. e) Photo taken by ROV showing oil stained temperature-lance after deployment in a bubble vent. f) Massive oil stained gas hydrate retrieved by TV-grab (TTR-15, BS380GR) at Colkheti Mound. (ROV seafloor images © MARUM-University of Bremen).

6.5.2.2 Colkheti Seep

Colkheti Seep is a complex seafloor structure that is morphologically composed of an elongated mound rising about 140 m from the seafloor down-slope Kobuleti Ridge and a narrow parallel ridge NE of the mound (Fig. 40). The mound spans over 1.38 km² with a maximum NW-SE extent of 1.95 km and a maximum width in NE-SW direction of 1.06 km. The structure has steep flanks towards southwest and northeast and a shallower slope towards northwest. To the south the seep structure merges with the Kobuleti Ridge.

The AUV-based bathymetry shows remarkable morphology at the summit of the mound. The crater-like structures are up to 14 m deep and 160 m long. Some craters seem to coalesce others appear to have formed on top of small mounds (Fig. 41). Some of the craters flanks are rather smooth while others show a more stepped morphology from their base to the rims. We relate the formation of the crater-like structures to recent fluid emissions. Therefore, the area were these craters occur is marked as active seepage area in Fig. 40. The backscatter map shows numerous sub-circular high backscatter patches within this area which contrasts the surrounding backscatter pattern (Fig. 37). In absence of an apparent correlation between the crater-rich morphology and the distribution of high backscatter patches we attribute these to hard materials as gas hydrates or authigenic carbonates. A TV-grab sample (TTR-15, BS380Gr) confirmed the occurrence of massive gas hydrate chunks in the sediments just below the seafloor (Fig. 39f; see Fig. 40 for location). The pieces were up to 10 cm thick and oil-stained. Authigenic carbonates were only found as mm-thin sub-horizontal layers between the hydrates.

Visual investigations by ROV revealed that smooth sediments change with fragmented material that is exposed at the seafloor within the crater dominated area. Pronounced small escarpments exposing chaotic sediment textures were interpreted as the crater flanks (Fig. 39c). During the dive one site was found within a crater where continuous bubble streams (about 150 bubbles min^{-1}) were observed for approximately two hours. Whether the bubbles were oil or gas hydrate coated could not be assessed visually. However, bubbles caught in a gas bubble sampler immediately formed gas hydrate (Fig. 39d). From the video material bubble rise velocities of about 14 ± 1 cm s^{-1} (n=101) have been obtained. The mean equivalent spherical bubble diameter calculated was 5.3 ± 1.5 mm (n=101) with a corresponding bubble volume of 116 ± 114 mm³. From oil impregnated sediments sporadic emanation of oil droplets was observed. These droplets were larger than the bubbles, rose much slower, and showed significant wobbling during ascent. Sampling tools deployed at the bubble sites became oil stained (Fig. 39e).

Towards the southwest of the main seep an approx. 750 m long and 100 m wide chain of craters seems to continue, paralleling the mid slope of Kobuleti ridge (Fig. 40). To the northeast a narrow ridge parallels Colkheti Seep. It is separated from the main structure by an approximately 170 m wide gully (Fig. 40). The ridge originates as narrow spur from the crest of Kobuleti Ridge and widens to its north-western termination as cone like elevation with a maximum width of 270 m.

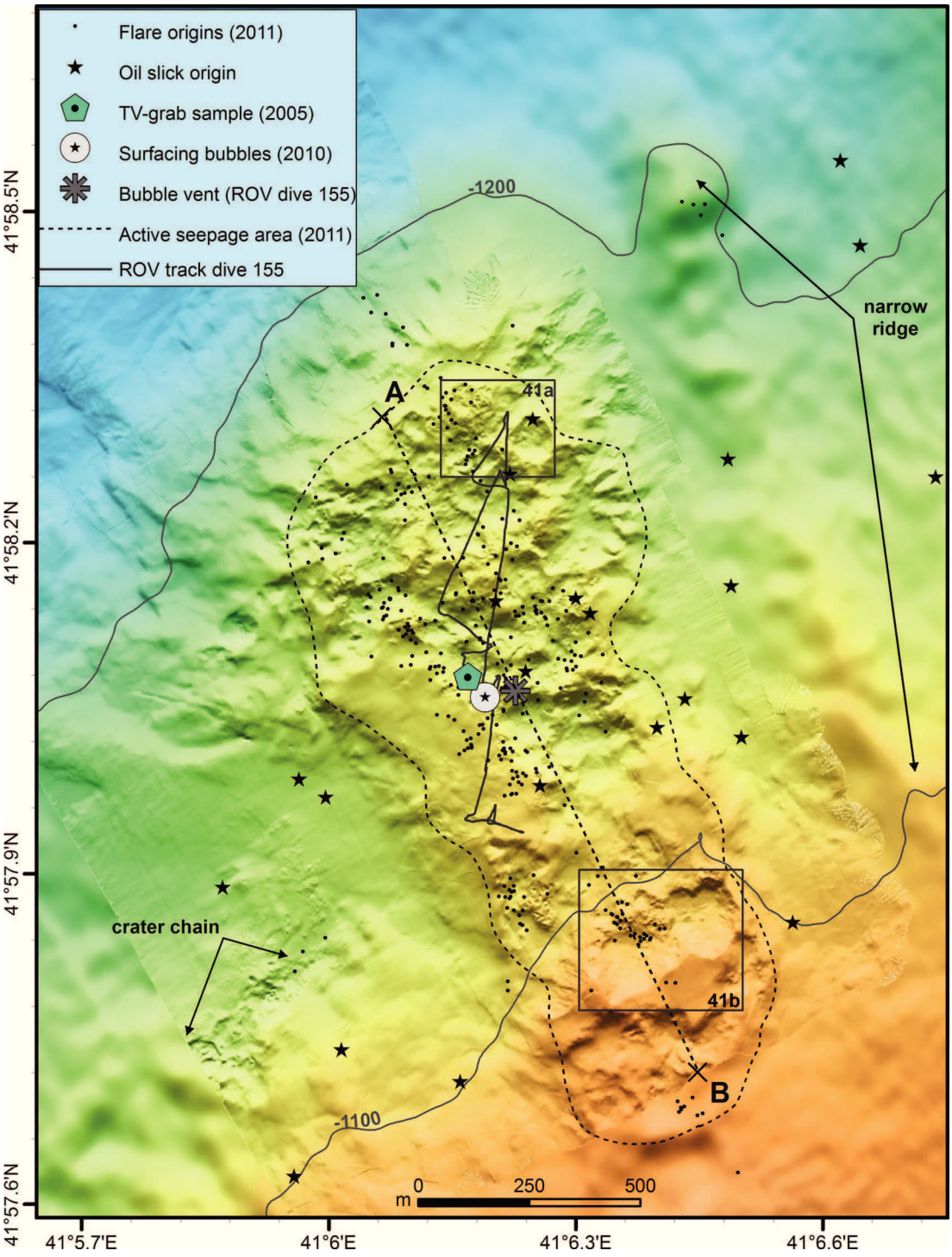

Fig. 40. Swath bathymetry of Colkheti Seep combining AUV-based and ship-based multi beam echosounder data. Centers of gas emissions (flares) derived from MBES, bubble emission observed by ROV (2007), surfacing location of oily bubbles (2011), TV-grab sampling location (2005) and oil slick origins on the sea surface (black stars) are indicated. Line A-B indicates location of profile in Fig. 41c.

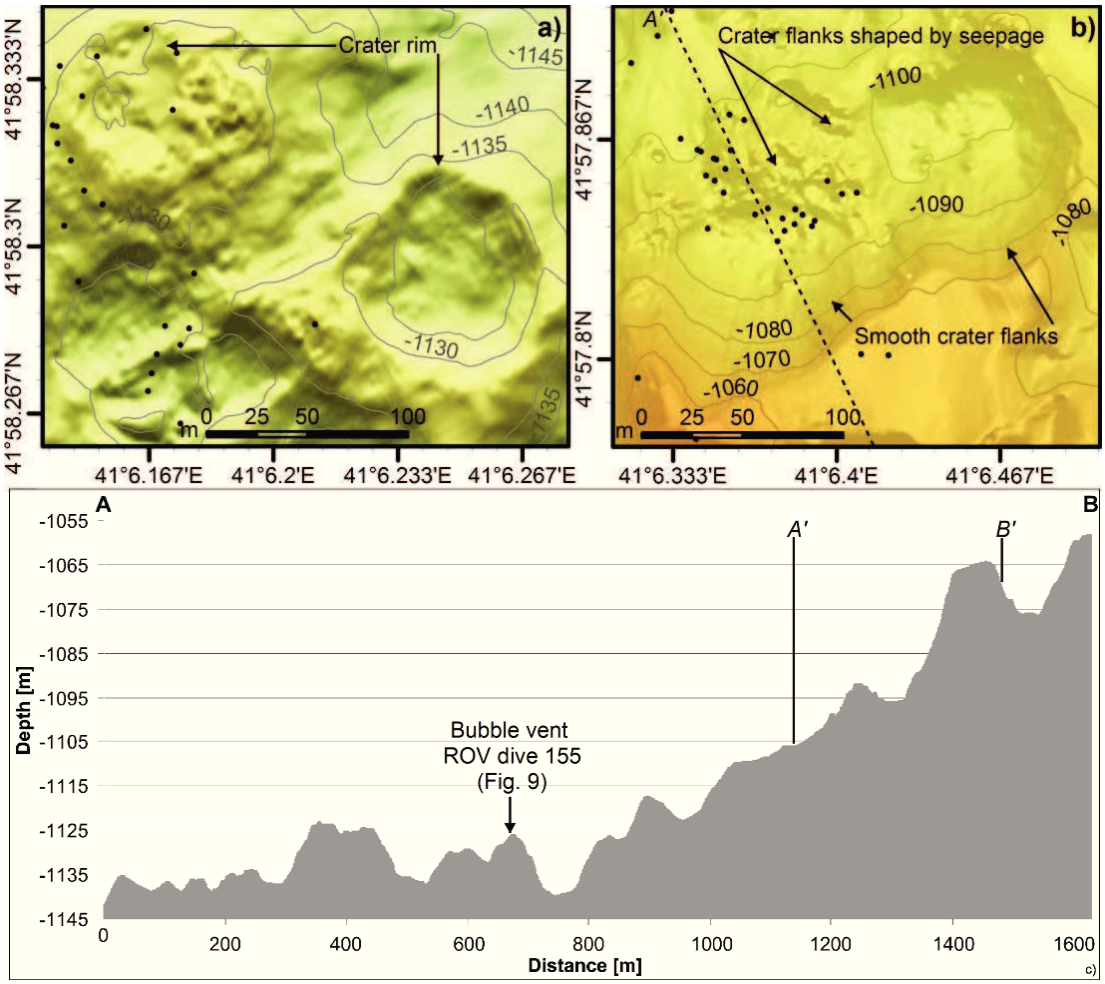

Fig. 41. Images illustrating small-scale morphology at Colkheti Seep (see Fig. 40 for location). a) Zoom-in of two circular crater structures that top mounded bathymetry. Stepped morphology of the crater/mound flanks probably shaped by seepage. Gas emissions (2011) indicated by black dots. b) Zoom-in of two coalescing craters with smooth southern flanks and roughed topography to the north that coincides with gas emissions (black dots). c) NW-SE profile through the area of active seepage (see Fig. 40); part of the profile crossing b) indicated as *A'-B'*.

6.5.3 Gas bubble streams in the water column

Surveys with the PARASOUND echosounder during three cruises in 2007, 2010, and 2011 evidenced gas bubble emissions from Pechori Mound and Colkheti Seep. In 2011 multibeam echosounder data was used to locate gas emissions at the seafloor with high spatial resolution and to assess flare heights and horizontal deflections. For illustration, Figure 42 shows a 3D representation of only one flare at Pechori Mound. The central seafloor coordinates of such flare were derived for all flares that were observed repeatedly at Pechori Mound and Colkheti Seep and plotted on top of the bathymetry. The distribution of flare origins at Pechori Mound (Fig. 38) shows that bubble emissions are constrained to the summit area (approx. 0.16 km²). In contrast, bubble emissions are more numerous and widespread (approx. 1.3 km²) at Colkheti Seep (Fig. 40). Most of the bubble emissions at Colkheti Seep were observed within the crater-rich area at the summit confirming that this is the seepage influenced area. Additionally, bubbles were emitted at the crater chain to the SW and the cone-shaped end of the narrow ridge to the NE (Fig. 40).

Flares originating from Pechori Mound and Colkheti Seep imaged in 2011 were traced throughout the water column up to 45 mbsl before the signal was lost from the multibeam echosounder swath due to strong horizontal deflections of the flares. Flares from both seeps showed similar deflection patterns and maximum heights, though the top of Colkheti Mound lays approx. 100 m deeper. For most flares, strongest deflections were measured above 400 mbsl as illustrated in Fig. 42. The height of this particular flare is 967 m with a peak at 55 mbsl. Between ~1,000 and 600 mbsl the flare shows only minor deflections, while being deflected about 50 m between 600 and 300 mbsl. Between 200 and 50 mbsl the deflection increases to a total of 150 m. For the highest flares the overall deflection ranged between 150 m and 200 m. These flares reached water depth between 45 and 100 mbsl before becoming indistinguishable form ambient noise or being lost from the multibeam echosounder swath.

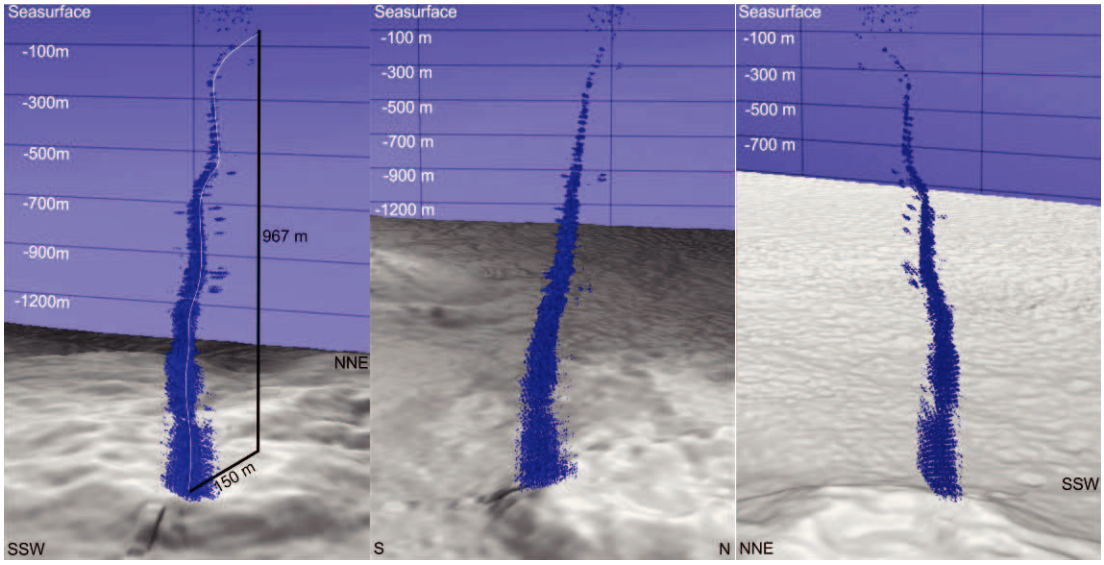

Fig. 42. 3D views from different directions on an individual flare indicative for uprising gas bubbles at Pechori Mound, illustrating current induced deflection and rising heights.

6.6 Discussion

The present study provides the first comprehensive description of oil seepage in the Black Sea. ASAR satellite imagery and visual observations evidenced surfacing oil above two positive relief structures. Seafloor investigations and sampling showed oil impregnations and gas hydrates in surface near sediments. In the following paragraphs we discuss possible relations of Pechori Mound and Colkheti Seep to subsurface structures and the origin of oil. Second, the possibility that frequent gas hydrate rafting shapes the crater-rich morphology of Colkheti Seep is discussed. Since, at no other seeps in the deep Black Sea gas bubbles have been observed that reach as shallow water depths (45 mbsl) as at Pechori Mound and Colkheti Seep, the effect of oil coatings on bubble lifetimes is discussed. Finally, a minimum estimate of oil seepage rates is presented in order to elucidate the significance of this novel seepage type in the Black Sea.

6.6.1 Subsurface structures at Pechori Mound and Colkheti Seep and the origin of oil

Pechori Mound and Colkheti Seep are amongst the largest seep structures protruding the seafloor of the Black Sea. Putatively, both sites are formed by uprising high viscosity material. Therefore, we consider them as mud volcano-like seeps. Yet, due to the unique observation of oil seepage at these two sites and the lack of mud breccia in recovered sediments, differences must exist compared to the mud volcanoes described in the Sorokin Trough (Bohrmann et al., 2003; Krastel et al., 2003; Sahling et al., 2009) or central western basin (Ivanov et al., 1996).

Mud volcanoes are surface expressions of sediment and fluid transport from depth (Brown, 1990). Mud or shale diapirs originate from overpressured, undercompacted deposits and intrude the overlying sediments (Kopf, 2002). As the fluid-rich material rises within the sediment column, contained gases expand and foster the buoyancy driven sediment migration. In case a diapir remains in the subsurface, mud volcanoes would form by mud migration trough diapiric faults or faults induced by hydrofracturing (Brown, 1990). Alternatively, mud volcanoes can be the surface expression of a diapir that pierces the seafloor. These features may be called diatremes for distinction (Kopf, 2002). This geologic configuration has been identified to be one of the basic mechanisms triggering oil seepage (Macgregor, 1993). Within a diapir fluid and sediment migration occurs mostly as single-phase flow (Kopf, 2002). In a diatreme buoyant rise of fluids might causes fluidization of the sediments within its host environment and produce less viscous material (Kopf, 2002). Such low viscosity sediments may ascent to the seafloor and form a mud volcano (Kopf, 2002).

Formation of mud volcanoes throughout the Black Sea has been linked to diapirism originating from the hydrocarbon-rich Maikopian shale formation (Ivanov et al., 1996; Krastel et al., 2003; Tugolesov et al., 1985). The top of the Maikopian formation lies about 6 km below seafloor (kmbsf) in the central Black Sea and 1 kmbsf at the basins margins (Tugolesov et al., 1985, 1983). The Maikopian formation is overpressured, possibly due to undercompaction and hydrocarbon maturation (Scott et al., 2009). Still, Scott et al. (2009) conclude from seismic investigations in the eastern basin and Mid-Black Sea-High that the overpressure is too weak to induce fracturing of the overburden. They suggest that mud volcanism is therefore controlled by tectonic compression that locally weakens the overlying sediments. Tugolesov et al. (1985) inferred anticlinal structures in the subsurface from seismic reflection profiles and interpreted these as Maikopian shale diapirs. The locations of these structures generally match mud volcanoes investigated in the Black Sea (Bohrmann et al., 2003; Ivanov et al., 1996; Krastel et al., 2003) (Fig. 32). Mud volcanoes in the Sorokin Trough locate either on the margins of the diapirs or on their apices (Krastel et al., 2003). Pechori Mound and Colkheti Seep are also underlain by one of the anticlinal structures mapped by Tugolesov et al. (1985). Both structures are located above the centre of the diapir (Fig. 32).

Morphologically mud volcanoes in the Black Sea comprise flat-topped shallow structures, cone-shaped structures and irregular collapse structures (Ivanov et al., 1996; Krastel et al., 2003). The general structure is related to the viscosity of the expelled materials which depends on their fluid content. Large cone shaped structures like the Kasakov mud volcano in the Sorokin Trough (Krastel et al., 2003) which raise 100-200 m above the seafloor should consist of relatively viscous material to be stable. We assume that these structures represent outcropping diapirs, since theses shales have presumably higher viscosity than mud originating from fluidization of less compacted, shallower sediments. Oil seepage should be associated with such mud volcanoes in the first place. Flat-topped mud volcanoes like the Dvurechenskii mud volcano (DMV) (Bohrmann et al., 2003; Sahling et al., 2009) would be

sourced by low viscosity material transported trough faults originating above diapirs as was inferred from seismic profiles (Krastel et al., 2003). This assumption is supported by the different backscatter characteristics of these mud volcanoes. The uniform, patchily distributed high backscatter at Pechori Mound and Colkheti Seep suggests that uniform material is exposed at the seafloor (Fig. 37). In contrast, pie-shaped mud volcanoes in the central western basin and the Sorokin Trough produce low backscatter indicating highly fluid mud (Krastel et al., 2003). Alternatively, they may be composed of several generations of mud flows interplaying with seepage-related collapse structures as interpreted based on backscatter images (Ivanov et al., 1996; Sahling et al., 2009).

As further evidence that Pechori Mound and Colkheti Seep represent parts of an outcropping diapir, we refer to a seismic reflection profile acquired during cruise TTR-15 (Akhmetzhanov et al., 2007). Due to weak signal penetration and poor resolution, only fragments of the anticline along with onlapping weak reflections of stratified sediments at its sides were imaged. The seismic profile shows vertically acoustic transparent zones below Pechori Mound, which might be explained by the presence of gas saturated sediments. However, the seismic record also legitimates the interpretation that these acoustically transparent zones are caused by homogenous, fluid-rich material of a diapir that pierces the seafloor (Akhmetzhanov et al., 2007). More precisely, we suggest that Pechori Mound and Colkheti Seep formed due to retrograde erosion of Kobuleti Ridge which exposed the older and indurated sediments of the diapir that intruded the overburden sediments. As evidence for this assumption we refer to the erosion patterns of Kobuleti Ridge and the two seeps. Gullies cutting in the north-western flank of Kobuleti Ridge and the Supsa Canyon to the northeast clearly indicate sediment erosion (Fig. 36). This is supported by the backscatter data which suggests the presence of harder material within the canyon and the gullies by higher backscatter in these areas (Fig. 37). Erosion has probably removed some of the sediments into which the uprising mud had intruded. Pechori Mound is more exposed to sediment erosion on its western, northern and especially eastern side which faces the Supsa Canyon, and is therefore the larger structure. Ongoing erosion may expose more of the diapir at Colkheti Seep that is currently covered by the slope sediment.

The assumption that Pechori Mound and Colkheti Seep represent parts of outcropping diapirs, is supported by pore water analysis suggesting Maikopian aged sediments (Reitz et al., 2011). Onboard interpretation of sediments from Pechori Mound and Colkheti Seep revealed the presence of regular deep Black Sea sediments of Unit 1 and 2 above sediments probably originating from the Maikopian formation (Akhmetzhanov et al., 2007). The presence of Unit 1 and 2 shows that Pechori Mound and Colkheti Seep have received a drape of sediments through the last few thousand years. This indicates how long these structures exist at least in their current configuration.

The fact that no oil seepage or oil impregnated sediments have been observed at mud volcanoes in the Sorokin Trough or central western basin might be explained by the fluid origin, depth of the putative Maikopian source rocks and local variations in heat flux and corresponding maturity levels of hydrocarbons. Detailed geochemical studies on pore fluids derived from mud volcano sediments in the Sorokin Trough revealed varying mixtures of microbially altered thermogenic hydrocarbons and secondary methane derived from biodegradation of petroleum (Stadnitskaia et al., 2008). Besides these processes blurring the chemical signature of the original fluids, Stadnitskaia et al. (2008) suggest that these originate from thermal cracking of oil. They propose that the fluid source might be the lower part of the Maikopian formation or even deeper. This implies that fluids migrating within diapirs or diatremes originate at depth below the oil window and that therefore no oil

seepage is observed. However, the Maikopian formation is thought to have thicknesses of up to 6 km in the Sorokin Trough (Tugolesov et al., 1985) and therewith hydrocarbons generated within this unit might have different maturity levels. In fact, Stadnitskaia et al. (2007) refer to a study on rock clasts from Maikopian aged mud breccia by Kozlova (2003) that indicates that only a quarter of the analyzed clasts originate from the upper end of the oil window, whereas the remaining are immature. This implies that mud expelled at many mud volcanoes, at least in the Sorokin Trough, originates from depth above the oil window which may explain why no oil is transported to the seafloor by fluidized sediments. The source depth of the thermogenic hydrocarbons seeping at Pechori Mound and Colkheti Seep is thought to be between 1.2 and 2.2 km (Reitz et al., 2011) which is much shallower compared to the mud volcanoes in the Sorokin Trough (Stadnitskaia et al., 2008). We therefore conclude that the observed oil seepage at Pechori Mound and Colkheti Seep may be a result of outcropping diapirs that efficiently transport oil and gas from the source rock or a reservoir to the surface without significant mixing with shallower sediments or fluids, and without major microbial alteration. Also burial depth of the Maikopian formation and local geothermal gradients may favor oil generation in this region. It might further be speculated that seepage on the margin of the eastern Black Sea is favored by the general flattening, uplift and folding of the Maikopian formation (Meisner et al., 2009) which might promote hydrocarbon migration from the deeper basin towards the margins. There it may accumulate in structural traps as diapiric anticlines or find its way to the seabed through outcropping diapirs.

6.6.2 Hydrate rafting – a possible process shaping the seafloor morphology at Colkheti Seep

The AUV-based bathymetry obtained at Colkheti Seep revealed complex crater structures within the area of active seepage (Fig. 40). Several mechanisms have previously been proposed to create pockmarks or crater-like structures on the seafloor. Most of these are related to fluid expulsions of different magnitudes (Judd and Hovland, 2007). Alternatively, formation of massive gas hydrate deposits in shallow sediments and buoyancy driven detachment of these was proposed to shape heterogeneous seafloor morphology, e.g. at the nearby Batumi Seep area (Pape et al., 2011), at the Cascadia Margin (Suess et al., 2001) or at the slope of the northern Gulf of Mexico (MacDonald et al., 1994). We suggest that the latter is the major process that shaped the observed topography of Colkheti Seep for the following reasons. Decimeter-sized blocks of gas hydrates have been sampled from surface sediments at Colkheti Seep within the area of active seepage (Fig. 39f). The occurrence of shallow gas hydrate deposits requires intensive flux of methane and other C_{2+} gases from below. Such an intensive flux is indicated by the numerous gas emissions that were mapped using a multibeam echosounder in 2011 (Fig. 40). Furthermore, hydroacoustic investigations in 2007, 2010 and 2012 revealed gas emissions from Colkheti Seep and Pechori Mound and satellite imagery suggests rather persistent seepage since at least 2002. Such high seepage activity makes it unlikely that large free gas accumulations build up in greater depth, eventually leading to a violent outburst, which has been proposed as mechanism to form large pockmarks, e.g. off Norway (Hovland et al., 2005).

Persistent flux of gaseous hydrocarbons will consequently lead to the formation of gas hydrates in the shallow sediments. As hydrate deposits grow locally, free gas ascending in conduits might be trapped and subsequently be transferred to gas hydrate. In turn, hydrate aggregation might redirect migration of free gas laterally towards the edges of the deposits. When the buoyancy of the gas hydrate deposits exceeds the sediment burden, hydrates will eventually float up and create a depression. Assuming this to be a repetitive process, small

depressions might merge forming the large crater observed in the AUV-bathymetry. Indications for such processes are e.g. the rough topography of the northern flank of the crater shown in Fig. 41b that seems to consist of meter-sized depressions. MacDonald et al. (1994) found that formation and rafting or dissociation respectively, of surface hydrate deposits in the northern Gulf of Mexico occurs on timescales of about one year or less. This would be a sufficiently effective process to form the observed morphology at Colkheti Seep despite the high sedimentation rates of ~30 cm 1,000 yrs^{-1} (Ross et al., 1970). As gas hydrates retrieved from Colkheti Seep are often nerved by oil inclusions, sporadic hydrate rafting provides additional means to transport methane and oil to surface waters and sea surface.

6.6.3 Enhanced bubble lifetimes due to oil coatings

Our observations that gas bubbles reach water depth of about 45 mbsl from seeps located below 1,000 mbsl (Fig. 42) contrasts previous studies on gas emissions in the Black Sea, which show that bubbles dissolve entirely before reaching surface waters when being released below 90 mbsl (Schmale et al., 2005). We propose that the enhanced lifetime is mainly the result of oil coatings around the bubbles which impede dissolution. This mechanism was proposed earlier by De Beukelaer et al. (2003) who traced bubbles from hydrocarbon seeps in the Gulf of Mexico located 550 mbsl to near the sea surface by hydroacoustic techniques. Similar to our observations, De Beukelaer et al. (2003) observed oil slicks at the sea surface above these high-rising bubble streams, suggesting that oil is transported to the sea surface as coating around bubbles. For the same area, Leifer and MacDonald (2003) provide visual evidence for oily bubbles emitted at the seafloor. They found that oil-coated bubbles rise slower than their clean counterparts, which corresponds to our observations at Colkheti Seep. While clean bubbles of about 5.6 mm diameter should have rise velocities of 25 cm s^{-1} (Leifer and MacDonald, 2003), those emitted at Colkheti Seep rose with 14 cm s^{-1}.

A further mechanism that enhances bubble lifetime is the coating with gas hydrate (Rehder et al., 2009). Bubbles have been traced by echosounders to rise more than 1,000 m through the water column within the GHSZ, e.g. at mud volcanoes in the Sorokin Trough in the Black Sea (Greinert et al., 2006) or at the Makran continental margin (Römer et al., *submitted*). However, as soon as they reach the upper limit of the hydrate stability zone, they disappear from the echosounder records. This strongly suggests that they rapidly dissolve at that depth (Greinert et al., 2006; Römer et al., *submitted*). Hydrate coatings are likely to occur around bubbles emitted at Pechori Mound and Colkheti Seep as well, since hydrate was instantaneously formed when the bubbles were collected close to the seafloor (Fig. 39d). Gas composition analysis from free gas samples of Pechori Mound and Colkheti Seep reveals presence of higher hydrocarbons (Pape et al., personal comm.) which enable the formation of structure II hydrate around the oil-coated bubbles. While the upper stability limit for structure I hydrate locates in about 700 mbsl at typical Black Sea water column temperatures of 9 °C (Bohrmann et al., 2003) that of structure II locates in about 200 mbsl (Bourry et al., 2009). Consequently, hydrate formation is an additional mechanism that might allow bubbles to rise to water depth as shallow as about 200 mbsl. However, this mechanism alone can not explain the further rise of the bubbles to depths as shallow as 45 mbsl, as we observed. We therefore conclude that the enhanced lifetime of bubbles in our study area mainly results from oil coatings that impede bubble dissolution.

While we have, so far, discussed the effect of oil coatings on bubble dissolution, it may be questioned if these oil-coated bubbles are actually causing the observed oil slicks at the sea

surface or if the oil might be transported though the water column as single-phased oil droplets. As outlined in the following, oil drops would be transported horizontally too far away from their origin at the seafloor to cause the observed dense clustering of oil slick origins (Fig. 33, 34).

The horizontal current velocities may be calculated using the data on bubble rise velocity (14 cm s^{-1}) and the observed deflection (150 m) of the acoustically imaged flare (Fig. 42). In order to rise from 1,020 mbsl to 55 mbsl, a bubble with the rise velocity of 14 cm s^{-1} would need about 6,900 seconds (ca. 2 hours). Meanwhile, it is deflected horizontally about 150 m resulting in a horizontal velocity of 2 cm s^{-1}. This is a minimum estimation as most of the deflection is likely to occur within the near sea-surface current. However, our hydroacoustic tracing of bubbles ends 55 mbsl. Oil droplets rise much slower through the water column with typical values of about 0.01 ms^{-1} (MacDonald et al., 2002). Consequently, an oil droplet would reach the sea surface after 102,000 s (ca. 28 hours), being deflected by 2,040 m from the emission site. As this is a minimum estimate, the radius of oil slick origins around its source at the seafloor would likely be even larger if caused exclusively by oil droplets. In contrast, most oil slick origins show a much smaller offset from the seep sites. This suggests that oil is transported trough the water column as bubble coating.

6.6.4 Minimum estimation of oil seepage at Colkheti Seep and Pechori Mound

Based on slick areas and length a minimum order-of-magnitude estimation of oil spread on the sea surface and seepage rates might be done. Assuming that oil slicks have a uniform thickness of 0.1 µm, which corresponds to the detection limit of oil slicks by ASAR (Garcia-Pineda et al., 2009), 1 km² of oil slick contains 0.1 m³ of oil. The spreading of oil is affected by wind and sea surface currents. In absence of surface current and wind velocity data for the study area, a simplified oil drift calculation based on reasonable wind velocities was applied. It is assumed that oil drifts with 3 % of the prevailing wind velocity 15° towards right of the wind direction (Bern, 1993; Espedal and Wahl, 1999). As boundary conditions, the lower and upper wind velocities required for oil slick detection by ASAR (3 to 15 m s^{-1}; Solberg et al., 2007) were employed, yielding a minimum drift velocity of 0.09 m s^{-1} and a maximum drift velocity of 0.45 m s^{-1}. This range of drift speeds in combination with slick areas allows assessing minimum order-of-magnitude seepage rates.

A calculation is exemplified for the slicks in Fig. 33a which were imaged on 15 September 2003 (Table 3). The slicks above Colkheti Seep and Pechori Mound together cover a surface area of 44.7 km² which is approximately the average area of all slicks identified during 2003 and 2011 (Table 3). Of this area 31.3 % (~14 km²) can be assigned to slicks originating from Pechori Mound and 68.7 % (30.7 km²) to slicks above Colkheti Seep. Consequently, the Pechori Mound's slicks contain at least 1.4 m³ of oil and those above Colkheti Seep 3.1 m³. Slicks originate right above the seeps and form continuous streaks that indicate permanent oil seepage. Assuming the maximum and minimum oil drift (0.45 m s^{-1} and 0.09 m s^{-1}) 22 to 108 hours are needed to form the longest slicks. This yields maximum and minimum oil seepage rates of ~65 l h^{-1} and ~13 l h^{-1} for Pechori Mound and 142 l h^{-1} and 28 l h^{-1} for Colkheti Seep. Accordingly, the combined oil seepage rate of both seeps ranges between 41 l h^{-1} and 207 l h^{-1} or $36*10^4$ to $181*10^4$ l yr^{-1}.

For comparison, Hornafius et al. (1999) estimated a flux of $584*10^4$ l yr^{-1} from the prominent 18 km² large Coal Oil Point seep field in the Santa Barbara Channel, California. MacDonald et al. (1993) estimated oil seepage in the Gulf of Mexico off Louisiana to be in the order of $200*10^5$ l yr^{-1}. Kvenvolden and Cooper (2003) combined data from MacDonald et al. (1993) and Mitchell et al. (1999) to estimate an annual oil seepage rate of 73,000 t

(~62*10^6 l) for the northern Gulf of Mexico and 140,000 t (~119*10^6 l) for the entire Gulf of Mexico. These data indicate that Colkheti Seep and Pechori Mound release a significant amount of oil compared to the total release from the world's most prominent oil seepage areas.

In years for which ASAR images have been available in high temporal resolution, e.g. 2010 (Table 3), the extents of slick areas and periods of continuous seepage required to form these slicks suggest that seepage activity was rather persistent over month. Periods of quiescence of seepage at Colkheti Seep and Pechori Mound were probably in the order of hours to few days rather than weeks or month since oil slicks of the observed extents could probably not have formed otherwise. Nevertheless, the different extents of oil slicks during different month (Table 3) hint to fluctuations in seepage intensities. The here presented data revealed seepage activity at least for some month each year between September 2003 and 2011 (Table 3).

6.7 Conclusion

Satellite imagery was used to identify two distinct sites of oil seepage in the eastern Black Sea. Subsequent hydroacoustic investigations, including ship and autonomous underwater vehicle based multibeam echosounder seafloor and water column imaging, revealed combined oil and gas seepage from Pechori Mound and Colkheti Seep. Gas flares originating from these structures reached as far as 45 mbsl from depth >1,000 m and oily bubbles have visually been observed to surface above these sites. It was shown that oil coatings in combination with gas hydrate shells hamper dissolution of gas bubbles and foster their transport to the water-atmosphere interface. The available satellite data suggests that seepage at both mounds is active at least since 2003, being subject to phases of quiescence on the order of few days to weeks only. However, differences in oil covered areas above the sites hints to variations in seepage intensity.

Hydroacoustic and satellite data, seafloor investigations by remotely operated vehicle, and sediment sampling in combination with data from previous seismic and geochemical studies suggest that the so far unique observation of combined oil and gas seepage offshore Georgia is triggered by diapirs that locally intrude shallow sediments and enhance migration of thermogenic hydrocarbons probably originating from the Oligocene-Miocene Maikopian formation. It is proposed that Colkheti Seep and Pechori Mound represent a new seep type which is characterized by oil-impregnated sediments, oily gas hydrates and oil-coated bubbles that reach the sea surface, forming quasi-persistent oil slicks. However, detailed investigations of the fate of hydrocarbons emitted from these seeps during ascent of the oil-coated bubbles should be subject to further investigations.

Satellite imagery proved great capabilities to identify new seep sites and might also be used to investigate the occurrence of other oil seepage sites similar to those described here in future studies. This would allow elucidating the relevance of hydrocarbon transport through the hydrosphere at oil-gas seeps compared to known seep systems in the Black Sea. The minimum order-of-magnitude estimate of oil emissions from Pechori Mound and Colkheti Seep (360,000 to 1,810,000 l yr^{-1}) suggest a significant impact of oil on the Black Sea's ecosystem.

6.8 Acknowledgements

We are thankful to captains and crews of R/V PROFESSOR LOGATCHEV (TTR-15), R/V METEOR (cruises M72/3 and M84/2) and R/V MARIA S. MERIAN (cruise MSM 15/2) for their support at sea. We are grateful to the technical teams of the ROV MARUM QUEST4000 and AUV MARUM B-SEAL5000 for enabling the acquisition of high resolution data. We thank Oscar Garcia-Pineda (Florida State University, Tallahassee) for help with the satellite image analysis. All satellite images used in this study were provided by the European Space Agency within project C1.P7157. This study was funded through the DFG-Research Center/Excellence Cluster 'The Ocean in the Earth System'.

Chapter 7

3. Manuscript

Oil seeps in the Black Sea: Hydroacoustic, geological, and satellite based investigations

Jan-Hendrik Körber[a], Heiko Sahling[a], Christian dos Santos Ferreira[a], Paul Wintersteller[a], Ian MacDonald[b], Gerhard Bohrmann[a]

[a]MARUM - Center for Marine Environmental Sciences and Department of Geosciences, University of Bremen, Klagenfurter Strasse, 28359 Bremen, Germany

[b]Florida State University, Department of Oceanography, 117N Woodward Avenue, P.O. Box 3064320, Tallahassee, Florida 32306-4320, USA

to be submitted to *Marine and Petroleum Geology*

7.1 Abstract

Here, the first inventory and geologic interpretation of oil seeps in the entire Black Sea is presented. A set of 179 Advanced Synthetic Aperture Radar satellite images acquired between 2002 and 2011, covering the entire Black Sea, was analyzed to delineate oil slicks on the sea surface. Locations showing recurrent oil slicks were identified as sites of oil seepage. In total nine, previously unknown, sites of intermittent oil seepage were identified. All sites were located in the eastern Black Sea offshore Georgia in water depth of 300 to 1,150 m. Hydroacoustic water column and seafloor investigations offshore Georgia during R/V METEOR cruise M84/2 (2011) evidenced gas emissions from the anticipated oil seep sites. Gas bubbles were imaged by multibeam echosounders to reach depth as shallow as 20 m. On average gas bubbles were traced to depth of 50 m, irrespectively of the depth of the emission site. Our results support previous findings that combined oil and gas seepage provides a mechanism to transport hydrocarbons to shallow water and sea surface. The widespread occurrence of oil seepage in this part of the Black Sea is suggested to have a relevant impact on the local methane budget of the Black Sea. Possible controls for the concentration of oil seeps in the eastern Black Sea are discussed with respect to the regional geology.

Keywords: Oil seep; Black Sea; ASAR; hydroacoustic; cold seep, methane

7.2 Introduction

The Black Sea is the largest surface reservoir of dissolved methane with an estimated content of 96 Tg methane (Reeburgh et al., 1991). Methane concentrations increase from values close to atmospheric equilibrium in surface waters to concentrations of up to 13 µmol in depth below 500 m (Kessler et al., 2006a). Below water depth of ca. 150 m the Black Sea is anoxic (Özsoy and Ünlüata, 1997; Pape et al., 2008). Oxygen depletion is sustained by microbial methane oxidation and impeded ventilation of the water mass (Reeburgh et al., 1991). The latter is due to limited water mass exchange with the world ocean through the narrow Bosporus and the stable stratification of the water body. Due to the inflow of fresh water from large rivers, as for instance Danube, low salinities of about 17.9 ‰ prevail above the permanent pycnocline at about 150 m below sea level (mbsl) (Özsoy and Ünlüata, 1997). Below the pycnocline salinities increase to about 22.5 ‰ (Murray et al., 1991).

The high methane concentrations in the Black Sea are sourced by diffusive flux from the sediments, dissolving gas hydrates, and bubble emissions from cold seeps (Kessler et al., 2006a). The assumption that gas hydrates and methane seepage contribute a significant volume of methane to the Black Sea water body is supported by their frequent observation (Pape et al., 2008). Due to stable water temperatures of approximately 9°C through all water depth, pure methane hydrates are stable below a depth of ca. 700 m in the Black Sea (Bohrmann et al., 2003). Gas hydrates have been sampled at mud volcanoes (Bohrmann et al., 2003; Sahling et al., 2009) and non-mud volcano cold seeps (Pape et al., 2011, 2010; Römer et al., *in press*). Further on, widespread occurrence of gas hydrates has been inferred from seismic reflection profiles (Korsakov et al., 1989; Minshull and Keddie, 2010). Seepage of predominantly biogenic methane has been reported to occur in shallow water shelf areas, e.g. in the northwestern Black Sea (Naudts et al., 2006; Peckmann et al., 2001), offshore Bulgaria (Dimitrov, 2002), and offshore Turkey (Çifçi et al., 2003). Along the slopes of the Black Sea basin seepage just above and below the gas hydrate stability zone has been reported (Egorov et al., 2003; Naudts et al., 2006; Pape et al., 2010; Römer et al., *in press*). Gas seepage in the deep Black Sea was documented exclusively for mud volcanoes (Ivanov et al., 1996; Sahling et al., 2009).

Sampling of venting gas and gas hydrates suggests that cold seeps in the Black Sea discharge predominantly biogenic methane (Dimitrov, 2002; Pape et al., 2010; Sahling et al., 2009). Little evidence for emissions of thermogenic gases exists. These are related to mud volcanoes in the Sorokin Trough where admixtures of thermogenic methane and higher hydrocarbons were measured (Blinova et al., 2003; Stadnitskaia et al., 2008). The only cold seep not related to mud volcanism which shows traces of thermogenic gases is the Batumi seep offshore Georgia (Pape et al., 2011, 2010). Analogue to sparse observations on thermogenic gas seepage, little is known about oil seepage in the Black Sea. Despite the assumption that the Black Sea bears great potential for oil exploration (Robinson et al., 1996) so far only three oil seeps have been reported. One site is located northeast of the Turkish city of Rize (Robinson et al., 1996), two other sites have been recently described offshore Georgia (Körber et al., submitted).

To elucidate whether oil seeps are indeed an exceptional phenomenon in the Black Sea or if they are more widespread than previously anticipated we conducted the first comprehensive study on oil seepage. New oil seep sites were inferred from high spatial and temporal resolution satellite remote sensing. Seepage at these sites was confirmed by hydroacoustic investigations and sampling during research cruises. We present an inventory and detailed description of oil seeps in the Black Sea. Based on extensive hydroacoustic investigations, we propose that combined oil and gas seepage might represent a methane

source to shallow water and local atmospheric methane concentrations. The exclusive occurrence oil seepage in the eastern Black Sea is discussed regarding the unique geological situation in this part of the Black Sea.

7.3 Geological settings

The contemporary Black Sea is a single large depocenter, characterized by relatively homogenous seafloor morphology of the deep basin (Fig. 43). In the sub-seafloor the Black Sea is separated into an eastern and western basin. Both basins are separated by the Andrusov and Archangelsky Ridges that form the Mid-Black Sea-High (Rangin et al., 2002) which is buried under Mesozoic to Quaternary sediments (Edwards et al., 2009; Zonenshain and Pichon, 1986). It was proposed that both basins evolved from back-arc extension in Late Cretaceous or Early Paleocene (Edwards et al., 2009; Meredith and Egan, 2002). Since Eocene, a compressional tectonic regime prevails due to the subduction of the Arabian and African plates under the Eurasian plate (Robinson et al., 1996). While the western basin formed by N-SE rifting of the Moesian platform, forming the Western Pontides to the south, the eastern basin opened by rotational separation of the Shatsky Ridge from the Mid-Black Sea-High (Edwards et al., 2009; Robinson et al., 1996). During the ongoing compression of the Black Sea region, mountain ranges like the Crimean Mountains and the Greater Caucasus Truth belt formed. These are accompanied by several foredeeps and troughs as the Sorokin and Tuapse Trough in the Black Sea or the Indo-Kuban Trough onshore Russia (Meisner et al., 2009; Starostenko et al., 2004). In the south-eastern Black Sea region the Rioni basin formed as Neogene flexural basin between the Greater Caucasus and Achara Trialet thrust and fold belt by partial closure of the eastern basin (Banks et al., 1997). The Achara Trialet belt as southern margin of the Rioni basin trends W-E through Georgia and connects with the eastern Pontides and related geologic structures in Turkey by a southwest-bend offshore Georgia (Banks et al., 1997).

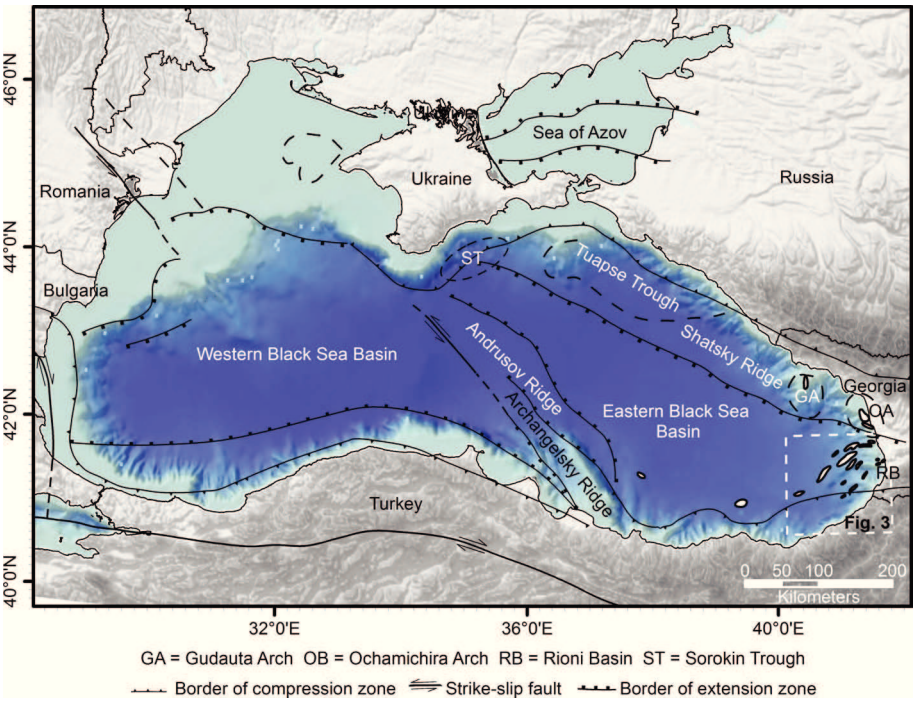

Fig. 43. Major geological features of the Black Sea. White polygons in the eastern basin indicate locations of diapiric anticlines (after Tugolesov et al., 1985). Bathymetry and topography: GEBCO 1 min.

Both Black Sea basins are filled with thick post-rift sediments of more than 10 km which are characterized by uniform parallel stratification that thins only updip the basins margins (Edwards et al., 2009; Zonenshain and Pichon, 1986). The shelf along most of the Black Sea is very narrow and connected by steep slopes to the deep Black Sea. Only in the north-western and northern Black Sea riverine sediment input from large river, e.g. Danube and Dnieper, and sediment-rich outflow from the Sea of Azov through the Straight of Kerch, build up large shelf areas (Fig. 43).

7.4 Material and Methods

7.4.1 Satellite imagery

A set of 179 *Advanced Synthetic Apertu re Radar* (ASAR) images acquired by the Environmental Satellite (ENVISAT) was analyzed in order to detect sites where natural oil seepage reaches the sea surface. Images were acquired between 2002 and 2011 and cover the entire Black Sea (Fig. 44). 117 Images of type Image Mode Precision (IMP) with a coverage of 100 x 100 km (30 m resolution), 8 Image Mode Medium Resolution (IMM) with a coverage of 150 x 150 km (100 m resolution), and 54 Wide Swath Mode (WSM) with 405 x 405 km coverage (100 m resolution) were obtained from the European Space Agency's (ESA) online archive EOLI, the Rolling Archives, and Webfile Server. ASAR images oil slicks on the sea surface as backscatter anomalies which originate form the effect of oil to dampen capillary surface waves (e.g. Garcia-Pineda et al., 2009). This makes oily water surfaces smoother compared to non-oily ones. Smoother areas appear darker on the processed images.

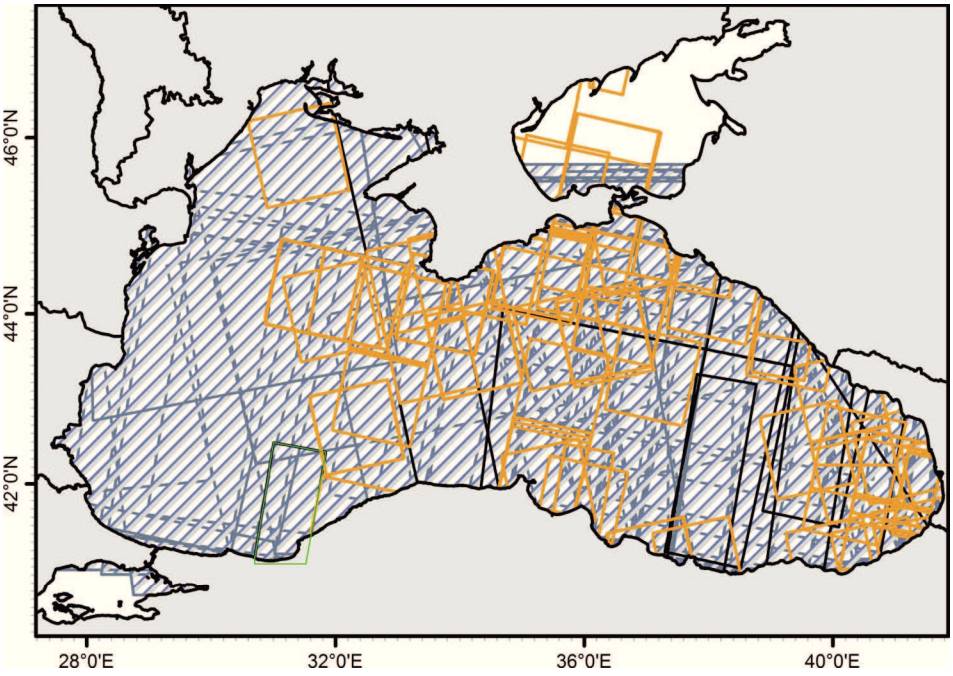

Fig. 44. Illustration of ASAR satellite image coverage and different cross-over path. Yellow rectangles indicate Image Mode Precision Images, blue rectangles with hatch fill Wide Swath Mode images and black rectangles Image Mode Medium resolution images.

All images have been converted to 8bit geoTiff images and imported to a geodatabase for further manual inspection in a geographic information system (GIS) (ArcInfo, © ESRI). The

origin of potential oil slicks (OSO; Garcia-Pineda et al., 2008) were identified in image-specific shapefiles. Subsequently, clusters of OSOs were identified by overlaying the image specific shapefiles. These clusters indicate that oil slicks originated at the same spatial location on multiple images, i.e. at different dates, suggesting a fixed point source of the oil. Calculated spatial mean centers of the OSO cluster were considered as central areas of oil emission.

7.4.2 Hydroacoustic and geological investigations

During research expedition M84/2 with German R/V METEOR in 2011 the Kongsberg EM122 multibeam echosounder was used to map the seafloor offshore Georgia where satellite image analysis indicated oil seepage. The EM122 is a 12 kHz swath echosounder with 288 beams, rated for all water depth. In addition to bathymetry, water column data was continuously recorded. The water column data allows detecting free gas bubbles in the water column, so called *flares*, which cause acoustic anomalies by impeding the sound propagation. For flare imaging, multibeam echosounder have the advantage over single-beam echosounder that they image flares along-track and across-track. This provides a three-dimensional image of rising gas bubbles. Flare images obtained from single-beam echosounders provide an one-dimensional cross-section of a flare along the ship track. Dedicated flare imaging surveys were conducted to assess spatial correlations of gas emissions from sediments to the water column and OSOs on the sea surface. During flare surveys ship speed was reduced to about 5 knots. The beam fan of the echosounder was reduced to 70° in order to minimize radial noise and facilitate flare detection compared to mapping with full swath. In shallow water depth around 300 m below sea level (mbsl) the beam fan was set to the maximum opening angle (150°) to image flares with a wider swath. Ping mode was set to shallow for all investigated areas (ca. 300 to 1,400 mbsl) providing maximum resolution water column data. The water column data was processed using the Fledermaus Midwater tool (© QPS). Soundings representing acoustic anomalies caused by flares were extracted and exported into Fledermaus (© QPS) for obtaining information on horizontal deflections and rising heights of individual flares. Additionally, water column data obtained by the Atlas PARASOUND single-beam echosounder was available for one of the potential oil seep sites (G1) from cruise MSM 15/2 (2010) with German R/V MARIA S. MERIAN (Bohrmann et al., 2011a). The primary high frequency (PHF; 18 kHz) of the system was used to detect free gas in the water column. Subbottom data recorded with the secondary low frequency (SLF; 4 kHz) of the PARASOUND system was recorded parallel to bathymetry and water column data in 2011 and evaluated for selected seepage areas. The bathymetry data were post-processed using MBSystem (http://www.mbari.org/data/mbsystem; GNU General Public License) and gridded to 20 m.

Gravity cores (GC) were obtained at three of the potential oil seep locations (Bohrmann et al., 2011b).

7.5 Results

7.5.1 Satellite imagery

Recurrent oil slicks on the sea surface at the same spatial locations are interpreted as indications of natural oil seepage. Oil seepage was inferred from satellite images at 11 locations offshore Georgia and one location offshore Turkey (Fig. 45). The two sites showing the largest and most persistent oil slicks correspond to the Pechori Mound and Colkheti Seep which were previously described in detail (Körber et al., submitted). The site off Turkey

might be identical to the *Rize oil seep* (Derman and Iztan, 1997; Kruglyakova et al., 2004; Robinson et al., 1996). The previously unknown sites were given the initial names G1 to G6 (with G2b, G5b, and G6b) following the order of field investigations.

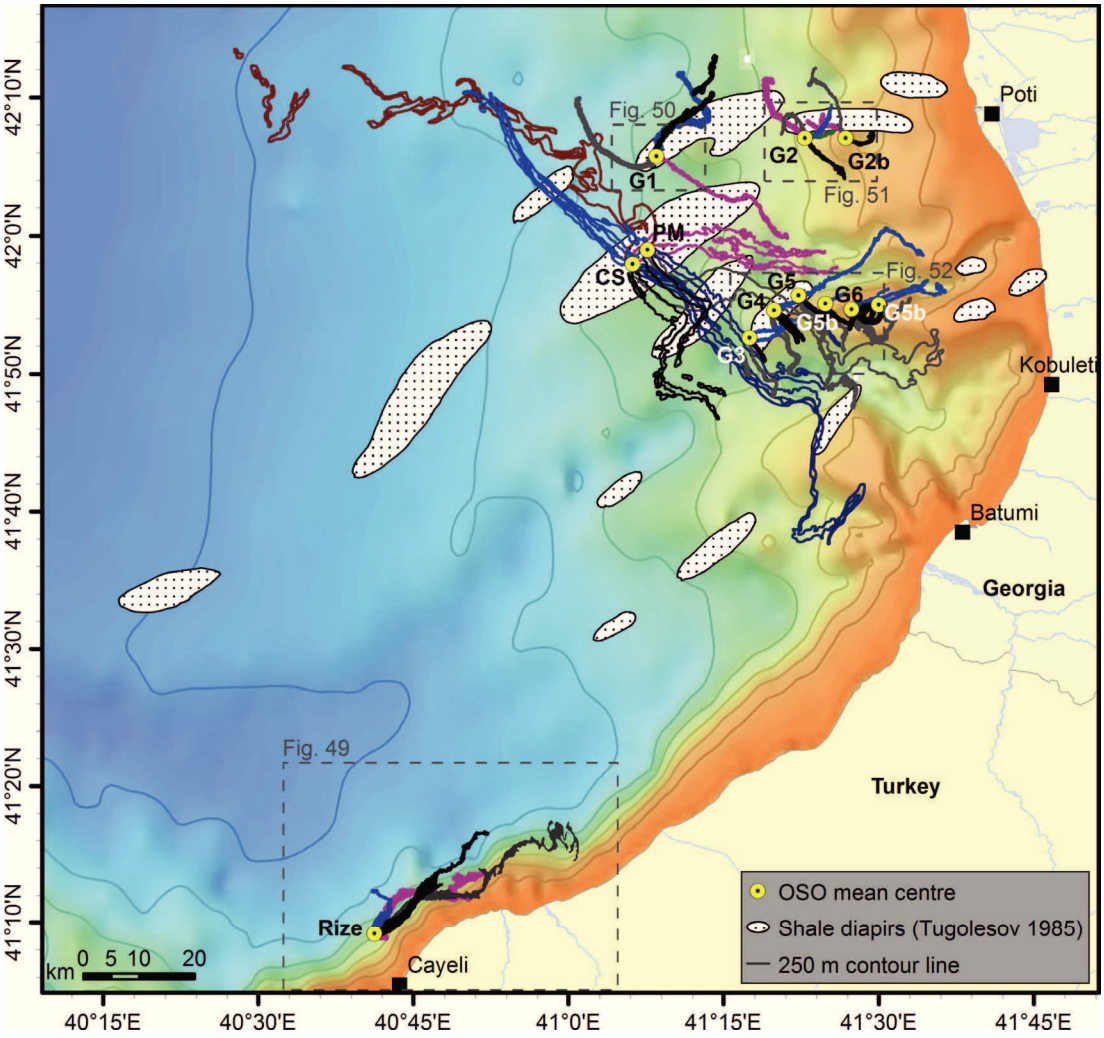

Fig. 45. Illustration of oil slicks identified on satellite images. Slicks are deflected towards different directions by prevailing winds and sea surface currents. Filled polygons are slicks from the newly identified seeps, empty polygons slicks originating from Pechori Mound and Colkheti Seep. Note the different extents of slicks above Pechori Mound (**PM**) and Colkheti Seep (**CS**) and other sites. Bathymetry: GEBCO 1 min.

Table 4 lists details of all identified oil seeps along with the sites for which previously evidence for oil seepage or oil in shallow sediments was given. Oil slicks mapped offshore Georgia show strong variations in size and temporal persistency (Figs. 46, 47, and 48). For the most persistent site (G1, Fig. 45) oil slicks have been mapped on 18 out of 26 images covering the site. On each image one slick with a single distinct origin can be identified (Figs. 46a-d). Five images did not allow distinguishing unambiguously between oil slicks and other surfactants. Three images did not show any slick.

Table 4. Overview of known oil seeps in the Black Sea.

Seep name	Latitude	Longitude	Depth [m]	Seepage[a]	Oil sampled[b]	Reference
G1	42°05.759'N	41°08.508'E	-1140	yes	yes	This study
G2	42°07.055'N	41°22.874'E	-706	yes	yes	This study
G2b	42°07.063'N	41°26.802'E	-436	yes	no	This study
G3	41°52.633'N	41°17.516'E	-913	yes	yes	This study
G4	41°54.619'N	41°19.905'E	-822	yes	no	This study
G5	41°55.689'N	41°22.275'E	-1015	yes	no	This study
G5b	41°55.103'N	41°24.858'E	-561	yes	no	This study
G6	41°54.677'N	41°27.386'E	-490	yes	no	This study
G6b	41°55.018'N	41°30.011'E	-308	yes	no	This study
Rize Seep	41°09.155'N	40°41.241'E	-1035	yes	yes	(Robinson et al., 1996)
Colkheti Seep	41°58.022'N	41°06.256'E	-1130	yes	yes	(Akhmetzhanov et al., 2007)
Iberia Mound	41°52.871'N	41°10.001'E	-1010	no	yes	(Akhmetzhanov et al., 2007)
Pechori Mound	41°58.955'N	41°07.522'E	-1030	yes	yes	(Akhmetzhanov et al., 2007)
Petroleum Mound	44°14.621'N	37°27.445'E	-1950	no	yes	(Akhmetzhanov et al., 2007)

[a] Indicates if oil seepage was inferred from satellite images within this or previous studies. [b] Indicates if oil was sampled within this or previous investigations. No sampling does not indicate that no oil is present in sediments.

For oil seep area G2 (Fig. 45) oil slicks have been identified on 16 out of 27 images, while nine images do not show any slick. For two images slick identification was uncertain. Slicks might consist of multiple bands, i.e. they have more than one distinct origin (Fig. 46e) or appear as slicks that have a single source (Figs. 46f-h). At least one image per year acquired between 2003 and 2011 shows oil slicks above site G2. Site G2b is located approximately 7 km east of G2. Images covering the site were available for the years 2003 to 2011. Only on images from the year 2005 no oil slicks were identified. Of the 27 images available, 11 indicated oil seepage, for two images distinguishing between slicks and other backscatter anomalies was not possible, and 14 images do not indicate oil slicks. All slicks identified appear to have one distinct origin (Figs. 46f and 46g). For the oil seepage areas G3 and G4 (Fig. 47) 25 images have been available. Six of these allowed identifying oil slicks, eight images did not show slicks, and for 11 images slick identification was ambiguous due to large scale surface patterns caused by wind or biogenic films. Available images were acquired in 2003, 2004, 2006-2008, 2010, and 2011. For site G5 and G5b 25 images acquired between 2003 and 2011 were available (Fig. 47). For site G5, 13 of these show oil slicks, three do not, and for nine images slick identification was uncertain. For the years 2006 to 2008 no slick was unambiguously identified at site G5. Site G5b showed seepage activity in the years 2003, 2004 and 2007. For oil seep sites G6 and G6b 24 images for the years 2003 to 2011 were available in this study. For site G6 no slick was identified on the images from the years 2008 and 2009. For the years 2006 and 2007 slick identification was hampered by the presence of non-oil slick surfactants. In total nine images allowed slick identification. The most eastward occurrence of oil slicks indicated seepage activity at site G6b at least during the years 2003, 2004, 2007 and 2011 (Fig. 47).

Outside Georgian waters one seep site was identified. It is located about 30 km northeast off the Turkish city of Rize (Figs. 48 and 49). 25 images covering the potential oil seepage area were available. Images were acquired between 2003 and 2006 and 2008 and 2011. For the images obtained in 2003 and 2006 the identification of slicks was not certain due to large

scale surface patterns in the region. However, 15 of the 25 images allowed identifying oil slicks and only three showed no evidence for oil seepage.

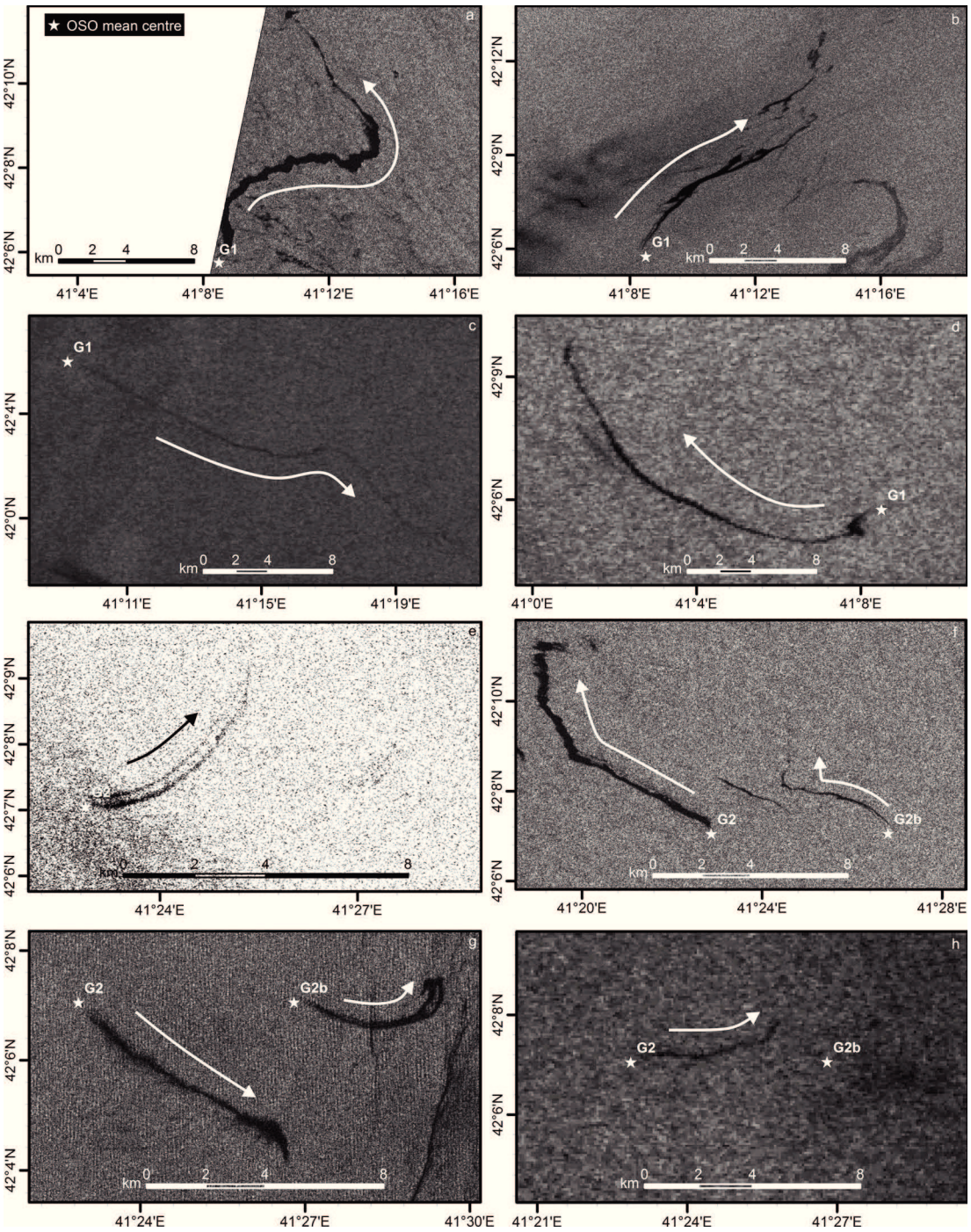

Fig. 46. Subsets of ASAR images showing distinct oil slicks originating above seep site G1 (a-d) and G2 and G2b (e-h). Arrows indicate the drift direction of the oil. Image were acquired on a) 01 August 2007, b) 14 May 2009, c) 15 June 2005, d) 20 January 2004, e) 15 August 2003, f) 01 August 2007, g) 16 June 201, and h) 15 June 2005. All images provided by ESA.

For all other regions of the Black Sea no clear evidence of oil seepage was found. Tough many satellite images, covering all areas of the Black Sea, show distinct oil slicks, these do

not re-occur in multiple images. Therefore these slicks where classified as oil spills, i.e. man-made oil pollution.

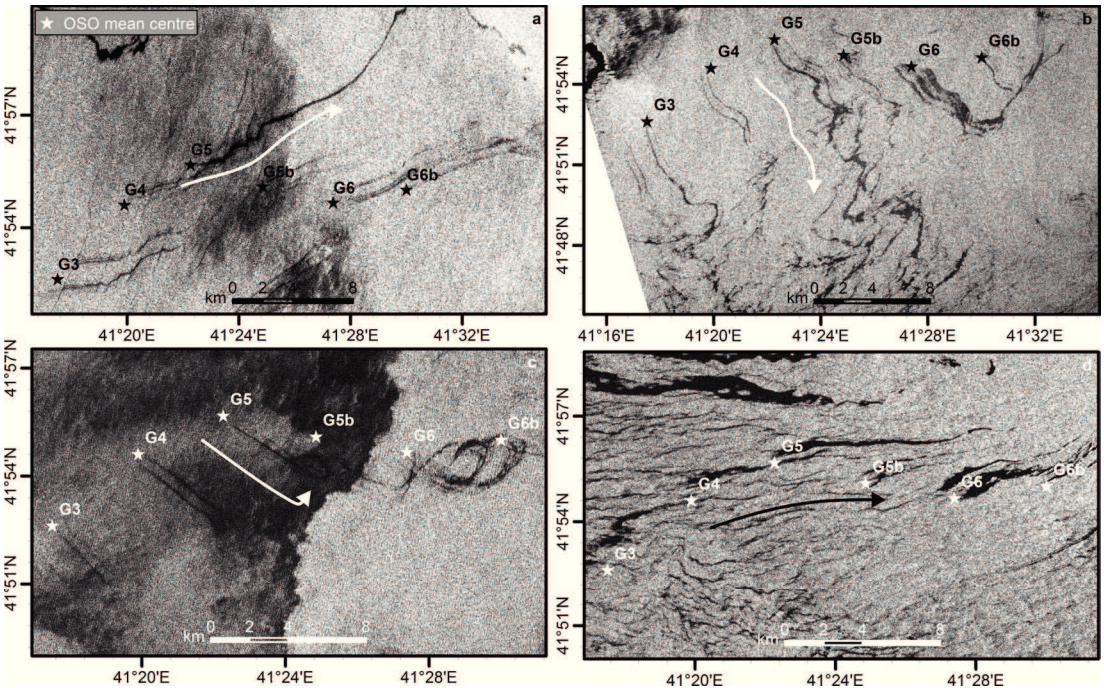

Fig. 47. Subsets of ASAR images showing distinct oil slicks originating above seep site G3 to G6b. Arrows indicate the drift direction of the oil. Images were acquired on a) 15 September 2003, b) 29 July 2004, c) 01 August 2007, d) 16 June 2010, and e) 26 April 2010. All images provided by ESA.

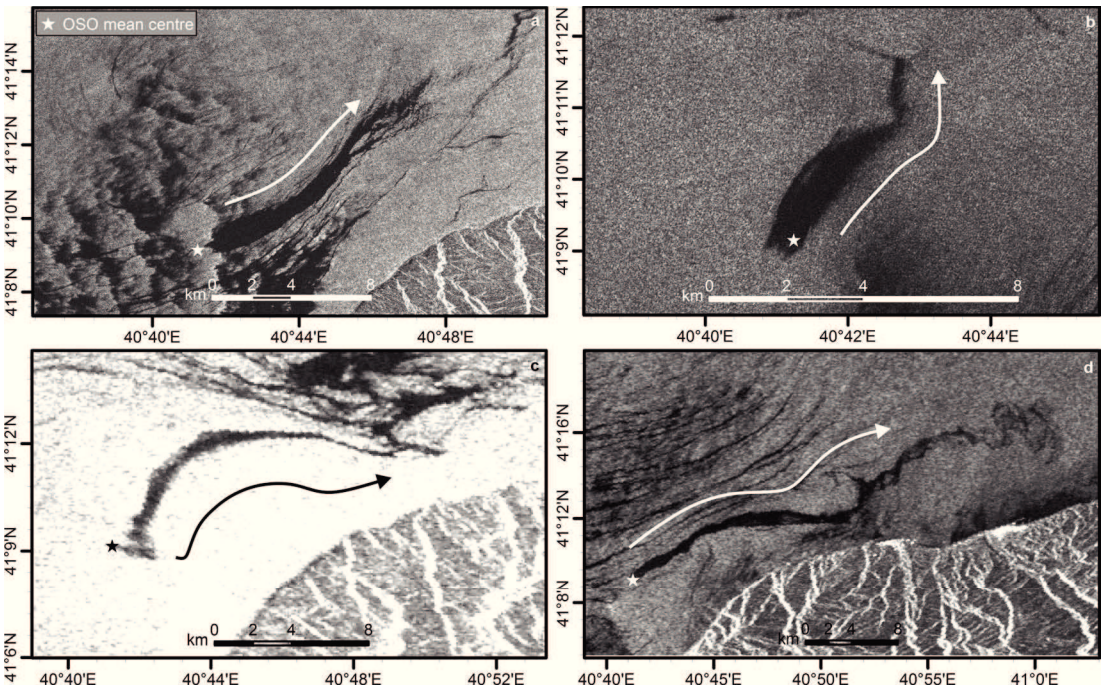

Fig. 48. Subsets of ASAR images showing distinct oil slicks offshore Cayeli. Arrows indicate the drift direction of the oil. Images were acquired on a) 26 April 2010, b) 26 May 2008, c) 05 June 2004, and d) 19 September 2011. All images provided by ESA.

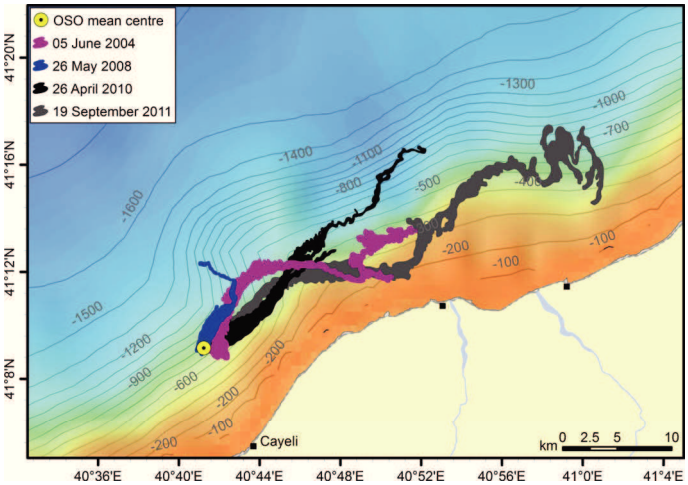

Fig. 49. Illustration of oil slicks above the *Rize* oil seep as identified on different satellite images. Colors denote date of acquisition. The seep is presumably identical with the one reported on previously by Robinson et al. (1996).

7.5.2 Acoustic water column imaging at seep sites

In 2010 active gas seepage at the G1 site was evidenced by acoustic anomalies in the 18 kHz records of the PARASOUND echosounder. The flare origins coincided with the OSO center identified from satellite images (Fig. 50). The maximum flare height identified was approximately 400 m with a flare peak at ca. 800 mbsl. In 2011 gas emissions at the same location were imaged with the EM122 multibeam echosounder. Imaged flares reached up to 220 mbsl, corresponding to a rising heights of 810 m.

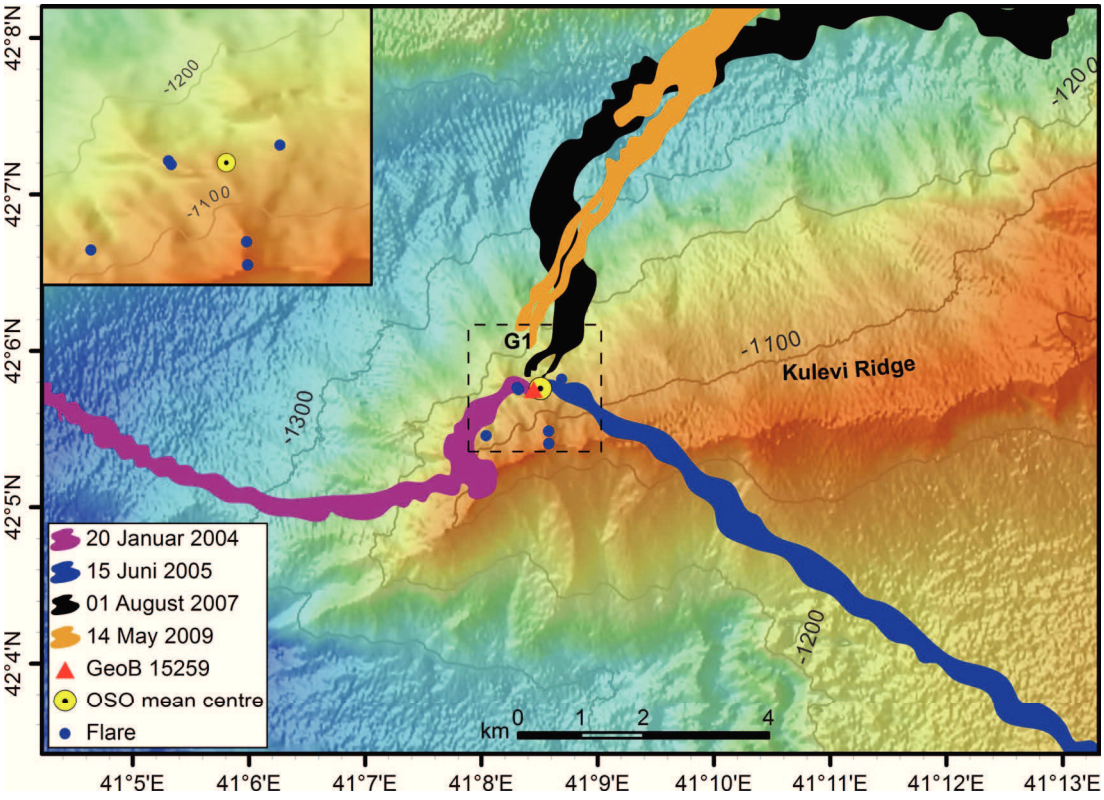

Fig. 50: Oil seep G1 on Kulevi Ridge. Polygons illustrate different extents and orientations of oil slicks as identified on different satellite images. Insert details the bathymetry of the active seepage area. Blue dots denote gas emissions mapped in 2011, red triangle indicates sediment sampling location.

The potential oil seep sites G2 to G6b were first investigated in 2011. At all sites gas emissions were evident in the hydroacoustic water column data (Figs. 51 and 52). The flare origins derived from 3D flare models correlate well with OSOs mapped on satellite images. However, gas emissions are more widespread than potential oil seep areas.

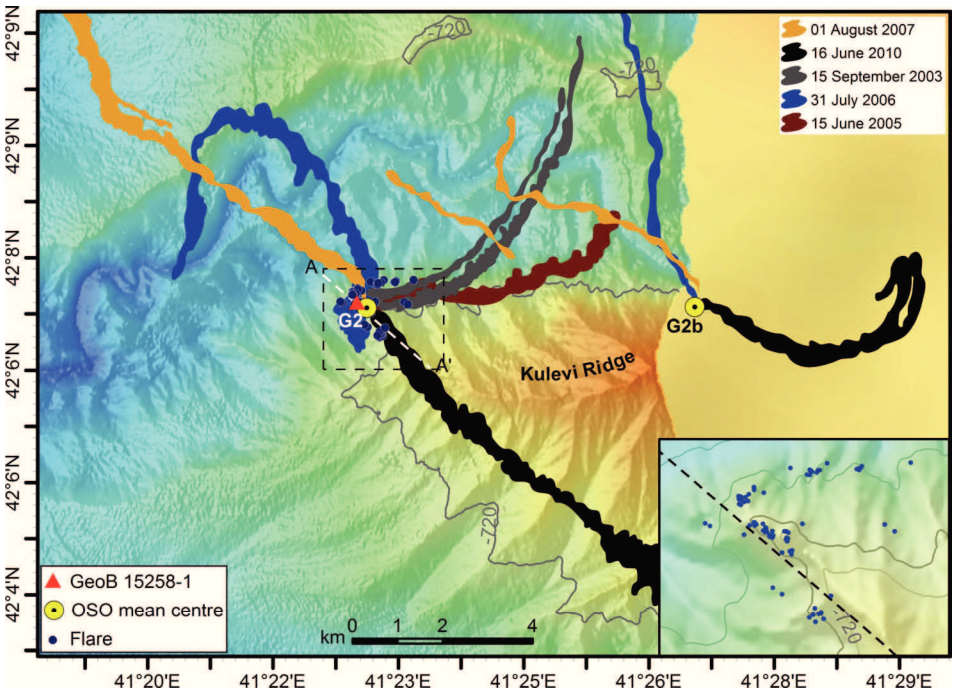

Fig. 51: Oil seeps G2 (west) and G2b (east) on Kulevi Ridge. Polygons illustrate different extents and orientations of oil slicks as identified on different satellite images. Insert details the bathymetry of the active seepage area. Blue dots denote gas emissions mapped in 2011. Sediment sampling location and Parasound sub-bottom profiler line (A-A') shown in Figure 55 are indicated.

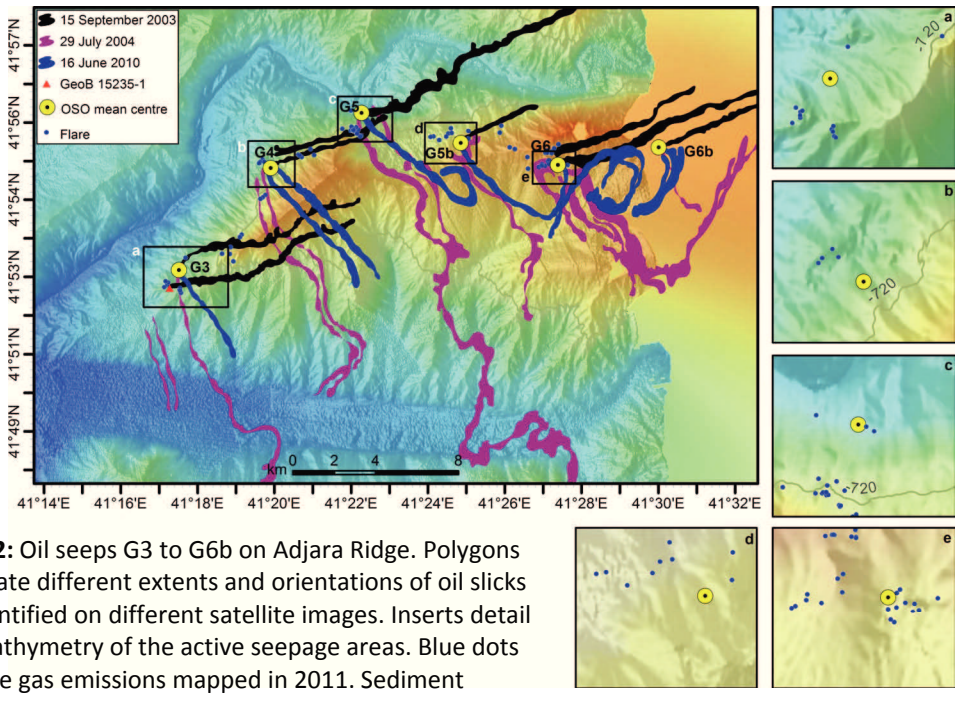

Fig. 52: Oil seeps G3 to G6b on Adjara Ridge. Polygons illustrate different extents and orientations of oil slicks as identified on different satellite images. Inserts detail the bathymetry of the active seepage areas. Blue dots denote gas emissions mapped in 2011. Sediment sampling location at G3 is indicated by the red triangle.

All gas flares identified from the multibeam echosounder data show significant horizontal deflections from their origin (Fig. 53). Despite dense flare imaging survey lines probably no flare was imaged in full heights (Fig. 53). The flares either bended out of the swath of the multibeam system or became indistinguishable from aeration noise under the vessel at shallower depth. At site G2 gas bubbles were imaged to depth between 40 and 140 mbsl. The flares originated in depth between 788 m and 622 m. At sites G3 to G5 imaged flares reached depth between 57 m and 80 m. The depth of gas emission sites ranged between 823 m and 655 m. Gas bubbles in the G6 area were observed to rise to depths of 20 m to 72 mbsl. The flares originated in depth between 872 m and 360 m. For none of the sites a correlation between the depths to which an individual flare was traced and its origin depth existed. For the easternmost site G6b off Georgia and the site off Turkey no water column data was available.

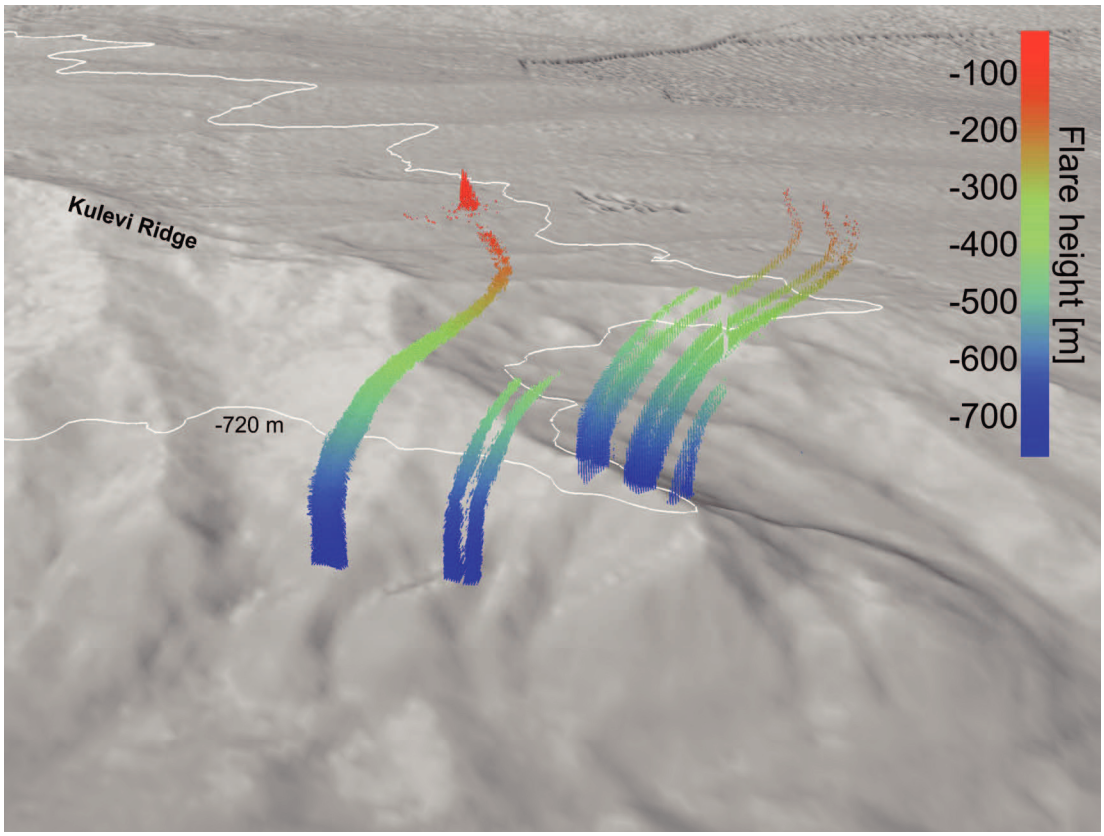

Fig. 53. 3-dimensional view of gas flares in the G2 oil seepage area on Kulevi Ridge. Total horizontal deflection of the highest flares is ca. 400 m. Shorter flares where not imaged in full heights by the multibeam echosounder swath. Contour represents the upper boundary of the gas hydrate stability zone of structure I hydrate.

Flares imaged in 2011 originated mostly from the flanks of the east-west trending ridges with only few exceptions of flares originating from crests (Figs. 50, 51, and 52). On the flanks, however, gas emissions seemed to be bound to the spurs and their flanks rather than the gullies. Imaged flares were concentrated on the northern slopes and in case of the G6 site on the southern slope. This corresponds to the locations of OSO centers. Additionally, the OSO center G6b is located on the southern flank of Adjara Ridge as well.

7.5.3 Seafloor mapping

The bathymetry data obtained offshore Georgia in 2010 and 2011 was combined with available data acquired during previous cruises. The new dataset details the morphologic characteristics of the east-west trending canyon-ridge system (Fig. 54) with Kulevi Ridge in the north, followed by the Northern Canyon, Poti Ridge, Supsa Canyon, Kobuleti Ridge, Central Canyon, Adjara Ridge, and Natanebi Canyon to south (Fig. 54).

Oil seep sites inferred from satellite imagery and gas emissions mapped in 2011 were located on the Kulevi and Adjara Ridge, respectively. Both ridges are characterized by sharp crests and slopes that are incised by gullies, forming sharp spurs. These spurs often separate in the lower part to two or more branches (Fig. 52, insert a). The crest of Kulevi Ridge is eroded by a southward meander of the canyon north of Kulevi Ridge at about 41°20'E. Seepage areas G2 and G3 are located on morphologic features that appear as fan-like widening spurs on the lower northern slopes of Kulevi and Adjara Ridge, respectively. In case of the G3 area a depression like feature might identified on the bathymetry (Fig. 52, insert a).

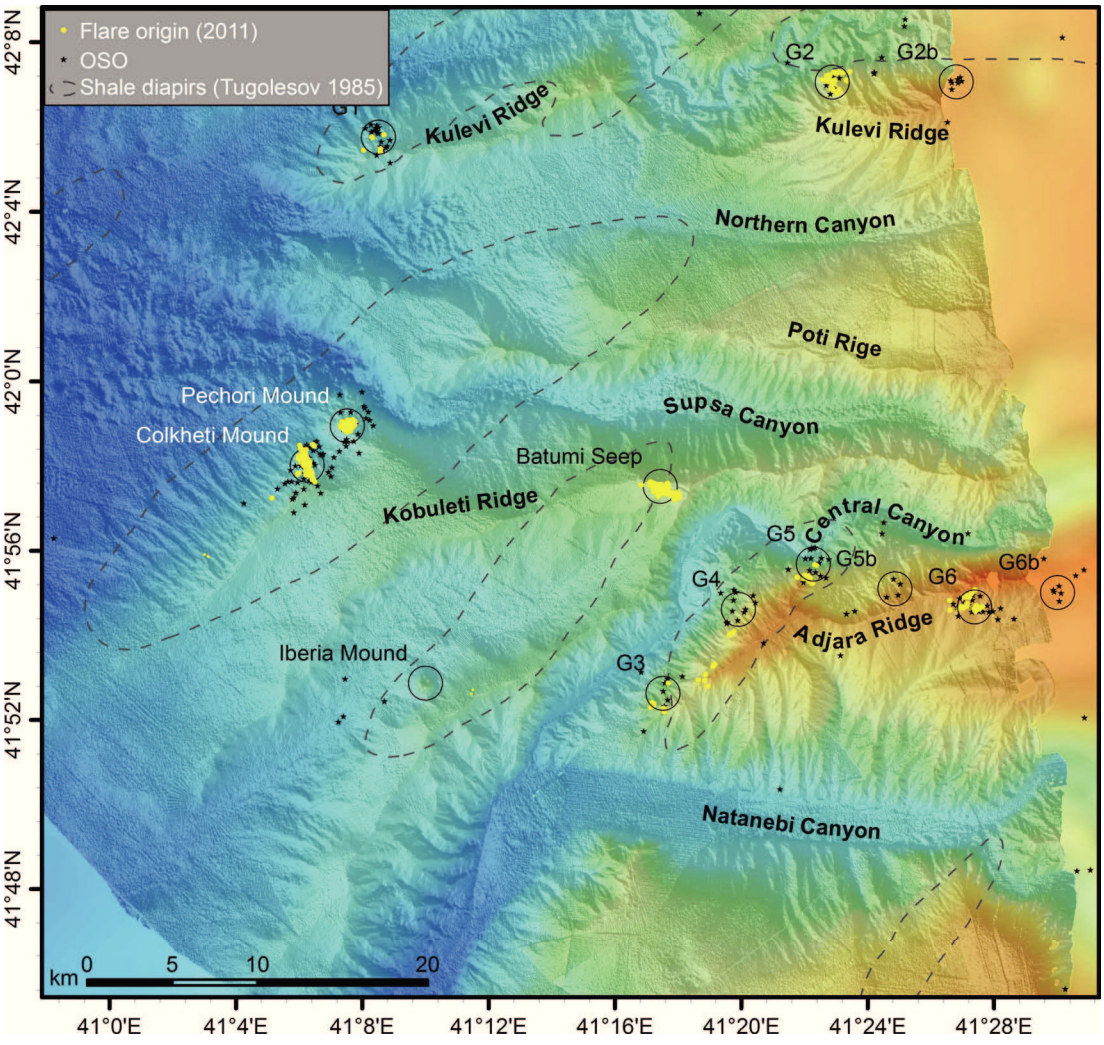

Fig. 54. 20 m gridded bathymetry overview of the canyon-ridge system offshore Georgia. Yellow dots indicate gas emission mapped by multibeam echosounder in 2011. Black stars denote individual oil slick origins identified on satellite images. The bathymetry data was acquired within this study in 2011. Background: GEBCO 1 min.

The ridge south of the Central Canyon and Natanebi Canyon respectively does not form a distinct crest but rather a plateau like top which gently fades towards the abyssal plain. The ridge is separated from Adjara Ridge by the Natanebi Canyon to the north and by the Central Canyon from the Kobuleti Ridge to the northwest. The Northern slope covered by the here presented data does show gully-spur structures as well, however these are less distinct in the eastern part where the ridge parallels Adjara Ridge (Fig. 54) Also, the slope shows shallower declivity compared to the other ridges. The slope towards the Central Canyon is steeper and shaped by deeper incised gullies.

The records of the 4 kHz PARASOUND sediment echosounder generally evidenced presence of gassy sediments in areas where gas emissions have been imaged, in case the seafloor morphology was not too steep. However, gas emissions in expected oil seep areas originated on the steep flanks of Kulevi and Adjara Ridge where the signal penetration was usually poor. Figure 55 illustrates the coincidence of gas emissions and acoustic blanking for the G2 oil seep area (see Fig. 51 for location).

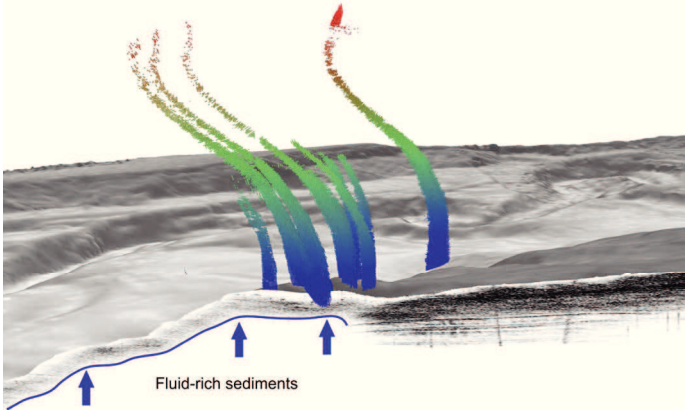

Fig. 55. Block image showing the bathymetry and sediment structure (4 kHz PARASOUND record) below gas emissions at site G2.

7.5.4 Sediment sampling

Three sediment cores were obtained from the potential oil seep sites G1 (GeoB 15259, 41°5.753'N, 41°8.449'E), G2 (GeoB 15258-1, 41°7.104'N, 41°22.753'E) and G3 (GeoB 15235-1, 41°57.277'N, 41°17.270'E) (see Figs. 50, 51, and 52 for locations). Core descriptions are detailed in Figure 56a. Core recovery at the G1 site was 270 cm. The uppermost 24 cm consisted of finely laminated coccolith ooze layers known as *Unit 1* with a transition to *Unit 2* sediments at 37 cm below seafloor (cmbsf). At 88 to 111 cmbsf the sediment sequence was interrupted by an unconformity and folded sediments suggesting a slumping event (Fig. 56b). Between 50 and 115 cmbsf, the sediments were disturbed by degassing cracks. From 116 to 222 cmbsf sediments consisted of *Unit 3*, fine-sandy clays and sparse calcareous microfossils. Black stained fault plains and cracks were identified between 173 and 222 cmbsf, followed by a 1 cm erosive unconformity and 18 cm of disturbed sediments hinting to another slumping event. At 252 cmbsf a sharp boundary separates a succession of well-cemented silty-sand and clay layers. The lower part of the core exuded a bituminous odor. Oil stained material was recovered in the core catcher.

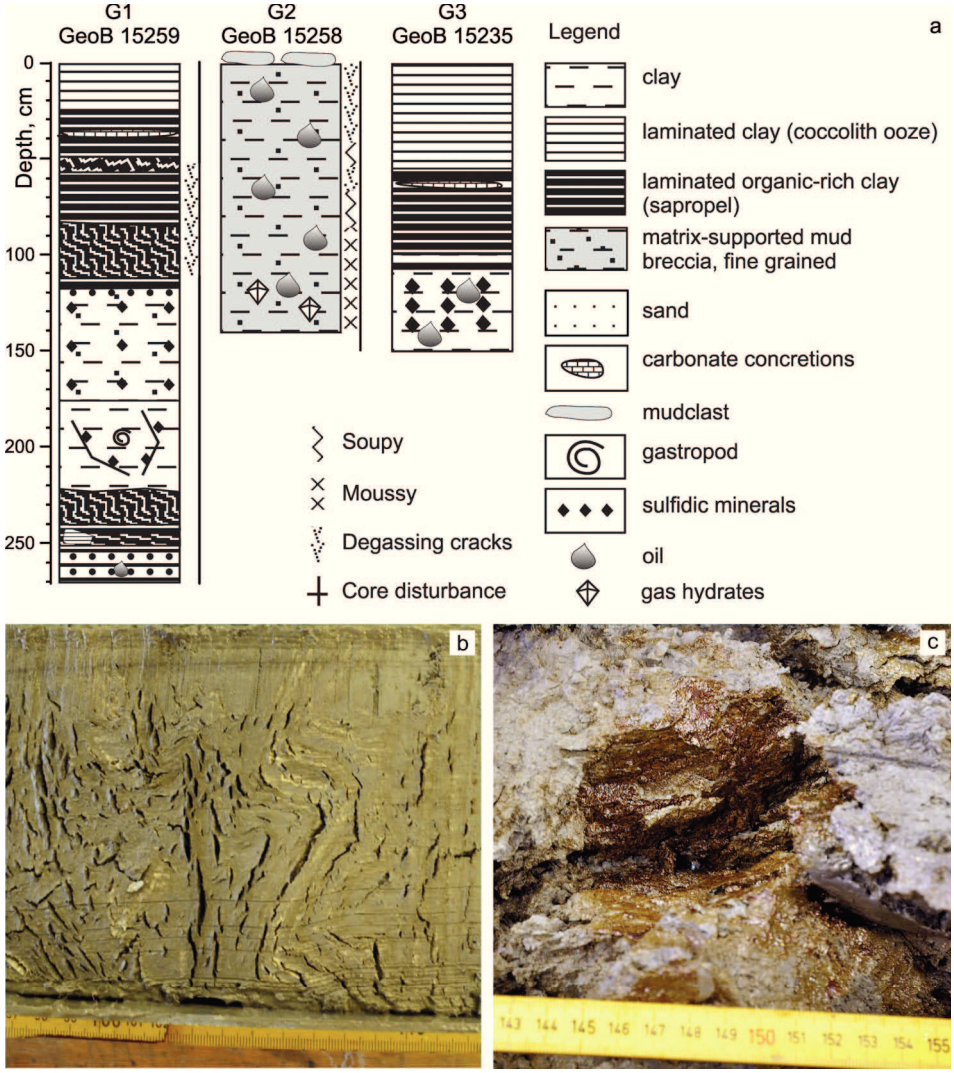

Fig. 56. Details of sediment sampling at oil seeps G1, G2, and G3 (see Figs. 50, 51, and 52 for sampling locations). a) Core descriptions, b) photo illustrating a folded unconformity indicating a slump, c) photo of oily sediments recovered at site G3.

The core retrieved from site G3 was 150 cm long. The upper 65 cm consisted of undisturbed Unit 1, followed by 42 cm of Unit 2. The Unit 2 sequence was possibly interrupted by two millimeter thick layers of darker Unit 3 material and a three centimeter thick Unit 3 mud layer below 100 cm sediment depth. Below 107 cmbsf the core consisted of Unit 3 sediments which exhibited oil-stained cracks above 111 cmbsf and were throughout oil-stained below (Fig. 56c).

At site G2 142 cm of oil stained clayey sediments were recovered (Fig. 57). Throughout the core sand-sized mud clasts were found. Sediments were disrupted by degassing cracks. From 40 to 54 cmbsf and 64 to 85 cmbsf the sediments structure was soupy and between 102 and 142 cmbsf moussy suggesting the presence of fine gas hydrate grains which decomposed during core recovery (Fig. 57). On the top of the liner two, two centimeters thick and five to eight centimeter wide mud clasts were recovered, probably marking the sediment surface.

Fig. 57. Photographs of sediment samples from oil seep G2 at Kulevi Ridge (see Fig. 51 for location). a) Two mud clasts recovered on top of the gravity core. b) Millimeter-sized gas hydrate grains were dispersed throughout the core. c) Oil stained, muddy sediments of upper half of the core.

7.6 Discussion

At the oil seep sites that were identified by ASAR satellite imagery and which have been investigated during subsequent research cruises, gas bubble emissions were detected by hydroacoustics. Good correlation existed between oil slicks on the sea surface, gas bubbles in the water column, and oil and gas hydrate containing sediments sampled at the seep sites. This suggests that oil and gas seepage are interrelated features.

7.6.1 Geological controls of oil seep occurrence

Our observations on the occurrence and distribution of oil seeps suggest that oil seepage is restricted to the eastern Black Sea. Previously known oil seeps are also located in the eastern Black Sea (Akhmetzhanov et al., 2007; Körber et al., submitted; Robinson et al., 1996) which supports our assumption. We propose that the exclusive occurrence of oil seepage in the eastern Black Sea is related to a unique interplay of the depth of hydrocarbon generation, compressional tectonics fostering diapiric sediment and fluid migration, and the relatively thin sedimentary overburden on the potential source rocks. These assumptions are based on previous studies that provide evidence for these physical constrains of oil seepage.

The oil potential of the Black Sea has previously been studied in great detail (e.g. Robinson et al., 1996) and oil exploration in the Black Sea region has a history of more than 150 years (Benton, 1997). Thus it might be assumed that the little evidence for marine oil seeps is due the restricted occurrence of such seeps. Some further oil seeps exist onshore along the Turkish Black Sea coast (Derman and Iztan, 1997). In the Rioni Basin, two oil fields have been discovered onshore, few kilometers from the Georgian coast, on the same latitude as the offshore oil seeps. These are the Supsa and Natanebi fields (Robinson et al.,

1997). All the previously known oil seeps in the Black Sea, as well as the mentioned onshore seeps and oil discoveries are sourced from the same lithological unit (Akhmetzhanov et al., 2007; Derman and Iztan, 1997; Reitz et al., 2011; Robinson et al., 1997, 1996). This unit is commonly referred to as Maikopian Formation. There is geochemical evidence that also thermogenic gases emitted at mud volcanoes in the Sorokin Trough (Blinova et al., 2003; Stadnitskaia et al., 2008) and at the Batumi Seep (Pape et al., 2010) originate from the Maikopian formation. We therefore suggest that the here described oil seeps are sourced from this unit as well. The Maikopian formation is an organic matter rich shale unit that occurs in the entire Black Sea and Caspian Sea region (Inan et al., 1997; Robinson et al., 1996). Commonly the Maikopian formation is thought to be of Oligocene to Lower Miocene age (Efendiyeva, 2004). However, Robinson et al. (1996) identified the highest hydrocarbon potential for shales of Upper Eocene age, and suggested these might still belong to the Maikopian formation.

If all thermogenic hydrocarbon seeps in the Black Sea and the surrounding regions are sourced by the Maikopian formation, but oil seepage occurs only along the margins of the eastern Black Sea this suggests differences in depth of fluid origin and migration. Previously, fluid migration at sites showing signs of thermogenic gas or oil emissions has been linked to diapiric structures in the sub-seafloor throughout the Black Sea (Akhmetzhanov et al., 2007; Ivanov et al., 1996; Krastel et al., 2003; Meisner et al., 2009; Wagner-Friedrichs et al., 2008). These diapirs have been suggested to affect the Maikopian formation and transport fluid-rich sediments towards the seabed. In case seepage is related to mud volcanism these diapirs, or feeder channels originating from diapirs, intrude shallow sediments and pierce the seafloor (Krastel et al., 2003; Wagner-Friedrichs, 2007). Seepage of biogenic and thermogenic hydrocarbons at the Batumi Seep was linked to fluid migration along faults above a deep-seated diapir (Wagner-Friedrichs, 2007). Only the Rize oil seep off Turkey is not sourced by a diapir but outcropping of the Maikopian Formation (Robinson et al., 1996).

We propose that oil seepage offshore Georgia is controlled by diapiric structures affecting the Maikopian formation. We base this assumption on the generally good correlation between the location of the here identified seeps and presence of diapiric structures that have been inferred from seismic reflection profiles by Tugolesov et al. (1985). Tugolesov et al. do not indicate the reference depth of the diapir outlines they indicate in their maps. Thus we do not know whether these structures intrude surface near sediments. However, the assumption that diapirism controls fluid migration is supported by seismic reflection profiles obtained during Training-Trough-research cruise 15 (TTR-15; Akhmetzhanov et al., 2007). Profiles crossing the seep sites G2 and G5 indicate the presence of sediments with weak acoustic reflection and without clear stratification just below the seafloor (Akhmetzhanov et al., 2007; Wagner-Friedrichs, 2007). These reflection patterns are indicative of fluid-rich sediments and might represent the diapirs themselves. Gas charged sediments below gas emissions at site G2 are also evident from sediment echosounder profiles recorded in 2011 (Fig. 55). The seismic profile crossing site G5 evidenced that on the northern flank of Adjara Ridge a large sediment block slid, exposing weak acoustic reflection sediments to the seafloor (Akhmetzhanov et al., 2007). This correlates well with the location of oil seep site G5 just above the slide-block. These data indicate that oil and gas seepage occurs predominantly where fluid migration is related to diapiric sediment movement rather than faults. The assumption that diapirism controls oil migration from the Maikopian source rock into shallower sediments is further supported by analogue observations made on the Kerch and Taman peninsulas. Here, oil accumulations were linked to stratigraphic traps above diapiric anticlines (Robinson et al., 1996).

If migration of thermogenic fluids, whether liquid or gaseous, from the Maikopian formation is generally controlled by diapirism, presence or absence of oil in seeping fluids must be controlled by the local depth of the oil window. Indeed, it was suggested that thermogenic gases emitted at some mud volcanoes in the Sorokin Trough might originate from thermocatalytic oil cracking, implying a source below the oil window (Stadnitskaia et al., 2008). This is in good agreement with the burial depth of the Maikopian formation in the deep Black Sea, where the top of this unit is expected at depth of ca. 5-6 km and the base at about 10 km (Tugolesov et al., 1985, 1983; Tugolesov and Meisner, 2002). Towards the basins margins the Maikopian formation thins and updips to depth of about one kilometer, with an approximate thickness of 2 km (Tugolesov et al., 1985). Assuming a normal geothermal gradient, the Maikopian formation would be well within the oil window (Tissot and Welte, 1984) in this region. Thus, the main factor restricting the occurrence of oil seepage might be the depth of oil generation. This assumption is supported by thermal modeling of hydrocarbon generation by Robinson et al. (1996) which shows that central parts of the Black Sea are producing gas while marginal areas are present-day oil kitchens.

We explain our observation that oil seepage occurs only offshore Georgia and eastern Turkey, but not in other parts along the Black Sea margins where the Maikopian formation should contain oil, with the tectonic regime. In the region where oil seepage is observed, diapiric sediment and fluid migration from the Maikopian formation might be enhanced by compressional stress related to the Achara Trialet fold belt. The strike of the diapiric anticlines offshore Georgia and Turkey as indicated by Tugolesov et al. (1985), generally aligns well with the trend of the major thrust (Banks et al., 1997). We propose that the thrusting of lithological units increases the overpressure of the Maikopian formation which originates from undercompaction and hydrocarbon generation (Scott et al., 2009). Where sediment burden above the Maikopian formation is weakened, e.g. by thrust or normal faults, diapirs might form and provide vertical migration pathways for oil and gas.

7.6.2 Geologic controls of seep morphology and seepage variability

We linked the observed oil seepage in the eastern Black Sea to the presence of diapirs that transport fluid-rich sediments close to the seafloor. This interpretation is consistent with the general location of seeps above or at the margins of the diapiric structures indicated by Tugolesov et al. (1985). Only at the G6 and G6b seeps no diapiric structure in the sub-seafloor was indicated by Tugolesov et al. (Fig. 54). The majority of the oil slicks identified on satellite images were located above the northern flanks of Kulevi and Achara Ridge. The hydroacoustic imaging of gas flares showed that most gas emissions originated from the walls of gullies which incise the canyon flanks. Beside this observation no distinct morphological seafloor features were identified that could be related to seepage. This contrasts previous observations on Kobuleti Ridge where oil seepage is related to distinct mound structures (Körber et al., submitted). Those seeps were suggested to represent outcropping diapirs (Wagner-Friedrichs, 2007) or to be a result of retrograde erosion of the ridge (Körber et al., submitted). The lack of such structures on Kulevi and Achara Ridge indicates that diapirs are buried under a thicker cover of younger sediments. Thus seepage might not primarily be controlled by migration of fluidized sediments to the seabed but rather by oil and gas migration through fractures and capillaries. The morphological characteristics of oil and gas seeps on Kulevi and Achara Ridge correspond to those observed on the northwestern slope of the Black Sea (Naudts et al., 2006). Naudts et al. (2006) explained the concentration of gas seeps along erosional ridges by gas driven uplift and fracturing of the sedimentary overburden. We interpret the concentration of oil and gas emissions on the

crests of ridges and gully walls as being mainly controlled by gravity driven weakening of the surface sediments. Due to downslope sediment movement, sediments around the crests experience extension while sediments in the gullies are compressed (Bjørlykke and Høeg, 1997). Therefore, pore pressure in sediments around the crests of spurs or ridges is lower which enhances fluid migration.

Generally combined oil and gas seepage offshore Georgia seems to occur only on the flanks of the east-west trending ridges, while gas seepage also occurs on the crests of the ridges (Fig. 54). We propose that this pattern is mainly controlled by the thickness of sediments covering the fluid carrying diapirs. On the ridges flanks the sediment burden might be thinner due to erosion. Lower lithostatic pressure compared to the ridges' crests might enhance the buoyancy driven migration of oil or oily gas bubbles through fractures. Gas, which has higher buoyancy compared to oil, might also migrate through thicker sediments towards the crests of ridges. This assumption is in agreement with previous interpretations, suggesting that sediment erosion around diapiric intrusions allows for rather persistent oil and gas seepage at the Colkheti Seep and Pechori Mound oil seeps (Körber et al., submitted). Gas seepage at the Batumi Seep on the crest of Kobuleti Ridge was suggested to be controlled by faults above a deep-seated diapir (Wagner-Friedrichs, 2007). Further support for our interpretation of seep distribution is provided by seismic reflection profiles obtained in 2005 (Akhmetzhanov et al., 2007; Wagner-Friedrichs, 2007). These indicate that surface sediments at seep sites G2 and G5 on the northern flanks of Kulevi and Achara Ridge are fluid-charged. On the southern flanks of these ridges, zones of acoustic blanking are onlapped by thick sequences of stratified sediments.

The assumption that gas and oil migrate through fractures and pore-space is supported by sediment cores from seep sites G1 and G3 which generally show stratified sediments with oil impregnations in the lower core sections. Samples from seep site G2, however, showed throughout moussy to soupy, oil stained clay and presence of large mud clasts. This indicates sediment transport processes which would be expected from a mud volcano like seep. It might be speculated that at this seep site a diatreme originating from the underlying diapir pierces the seafloor. The G3 site might be at an early stage of mound formation.

The analysis of satellite imagery showed that the oil seep sites G1 to G6b and the Rize seep have been intermittently active since at least 2003. These non-persistent seepage patterns contrast the rather persistent seepage observed at Colkheti Seep and Pechori Mound (Körber et al., submitted). Differences in seepage persistency might be directly linked to the different fluid migration mechanisms we proposed. While persistent oil and gas seepage is sustained by migration of fluidized sediments from the source unit to the seabed, intermittent seepage might be controlled by re-charging shallow hydrocarbon traps. Oily gas bubbles might migrate buoyancy driven along fractures or through pore space (Clarke and Cleverly, 1991). We assume that fluid migration through pore space does not allow for seepage that is intensive enough to produce the observed oil slicks on the sea surface. For fluid flow through fractures however, pore overpressure must be high enough to keep fractures open (Etiope and Martinelli, 2002). Accumulations of hydrocarbons in shallow traps might create overpressure that is high enough to breach the sediment burden or activate fractures. When the shallow oil and gas accumulations are exhausted and pressure decreases, fractures might close and cause seepage cessation. A re-charging of the shallow hydrocarbon reservoirs would allow for the observed intermittent seepage.

Alternative explanations for intermittent gas seepage comprise hydrostatic pressure variations induced by tides (Torres et al., 2002), atmospheric pressure changes (Emeis et al., 2004), and seismic activity (Manga et al., 2009). Due to the lack of tidal cycles in the

Black Sea, these can be ruled out as mechanism to control seepage. Also, we propose that changes in atmospheric pressure are unlikely to affect seepage in depth up to 1,150 mbsl. Seismic activity might have an impact on pore pressure and thus seepage activity. Yet, the seepage patterns which we inferred from the satellite data, suggest that periods of active seepage differ between the oil seep sites off Georgia. Therefore, we assume that they are not primarily controlled by seismic activity. However, we do not have data that would confirm or reject this assumption.

7.6.3 Hydrocarbon transport through the water column and possible relevance for atmospheric methane concentrations

Most of the detected gas flares reached water depth of ca. 50 m with their origin being located at 350 to 1,200 mbsl. Still, we assume that total flare heights was not imaged in most cases due to strong deflections (Fig. 53). These observations contrast those made at pure gas seeps in the Black Sea which indicate that gas bubbles dissolve entirely after some tens of meters rise or, in case seeps locate within the GHSZ, upon reaching the upper boundary of the structure I (sI) gas hydrate stability (Greinert et al., 2006; McGinnis et al., 2006; Schmale et al., 2005). However, our observations correspond well to previous observations of high rising gas bubbles at other oil seeps in the Black Sea (Körber et al., submitted) and Gulf of Mexico (De Beukelaer et al., 2003; Solomon et al., 2009). Körber et al. (submitted) postulated that a combination of oil coatings and structure II (sII) gas hydrate forming on bubble surfaces hamper bubble dissolution. The presence of oil coated bubbles was previously inferred from bubble rise velocities and observed flare deflections. It was concluded that pure oil droplets would rise too slow to produce the observed oil slicks (Körber et al., submitted). Following the general approach of MacDonald et al. (2002) and Körber et al. (submitted) we suggest that oil is transported to the sea surface as bubble shells at all oil seeps investigated in this study. To exemplify this, the highest flare in Fig. 53 rises about 750 m while being deflected by 400 m. Assuming a realistic range of bubble rise velocities of 14 to 27 cm s^{-1} which were previously measured at seeps in the Black Sea (Körber et al., submitted; Sahling et al., 2009), bubbles would need between 47 min and 89 min to rise 750 m. If the bubbles are deflected by 400 m during ascent, horizontal current velocities of 0.075 to 0.14 m s^{-1} are obtained based on the time a bubble would need to rise 750 m. Taking into account that pure oil droplets have a much lower buoyant rise velocity of about 0.01 m s^{-1} (MacDonald et al., 2002), it is evident that oil droplets would reach the sea surface with much greater offset from their emission site (5.6 -10.5 km) than we observed.

Further on, also the formation of sII gas hydrate shells must be considered at the oil seeps investigated in this study. Analysis of dissolved gas hydrates recovered from some of the seeps evidenced the presence of C_{2+} hydrocarbons which allow the formation of sII hydrate (T. Pape, pers. comm.).

Flares rising to depth of at least 50 mbsl are already within the mixed layer of the water column (Staneva et al., 2001). Here, the efflux of dissolved methane to the atmosphere can be expected to be faster than microbial methane oxidation (Rehder et al., 2009; Solomon et al., 2009; Valentine et al., 2001) in case the water column methane concentrations exceed atmospheric concentrations. This is the case in the Black Sea also in non-seepage areas (Reeburgh et al., 1991). It was shown that at shallow seep sites the surface water is enriched in dissolved methane and that methane diffusion to the atmosphere is up to five times higher compared to non-seep areas (Schmale et al., 2005). Based on observations at seeps emitting biogenic methane (Schmale et al., 2005) and modeling (McGinnis et al., 2006) is was previously proposed that deep water seeps do not affect shallow water and

local atmospheric methane concentrations. Analogue to findings by Körber et al. (submitted) and observations by Solomon et al. (2009) in the Gulf of Mexico, we postulate that the here described oil seepage might provide an so far neglected source of methane to shallow waters and atmosphere in the Black Sea region.

Previous modeling of massive methane release from mud volcanoes or decomposing gas hydrates suggested that even optimistic large quantities of methane being injected as free gas to the deep Black Sea or just above the GHSZ for sI gas hydrate would only have negligible effects on surface water concentrations of dissolved methane and the water-atmosphere flux (Schmale et al., 2011). However, the model considered only the release of pure methane from mud volcanoes and subsequent formation of sI hydrate shells around bubbles, neglecting the positive effect of sII hydrate shells on bubble lifetimes. The formation of the latter should be considered, since analysis of gases sampled at mud volcanoes indicated admixtures of C_{2+} hydrocarbons (e.g. Blinova et al., 2003). Also, in the modeling approach it is assumed that bubbles originating form violent outbursts would rapidly dissolve above the GHSZ (Schmale et al., 2011). Yet, it was shown that vigorous gas emissions might induce upwelling or create plumes of dissolved methane around the rising bubbles which allow bubbles to reach shallow waters from depth of several hundreds of meters (Solomon et al., 2009). Observations of oily bubbles reaching surface waters and sea surface (this study; Körber et al., submitted) from depth >1,000 m further advocate the suggestion that also local non-violent but rather persistent seepage in the Black Sea might transport bubble gas to surface waters and water-atmosphere interface in case seepage is sourced by thermogenic hydrocarbons.

Previous studies indicate that microbial degradation of methane in gas bubbles and methane entrained in bubble plumes is rather insignificant (MacDonald et al., 2002; Solomon et al., 2009). Therefore, it might be assumed that sites of combined oil and gas seepage or gas seepage induced upwelling, provide a notable source of methane to the mixed layer. From the mixed layer it might reach the atmosphere by diffusion or directly by bubbles reaching the sea surface. However, we acknowledge that a significant volume of methane contained in bubbles upon ebullition at the seafloor might be dissolved or stripped by other gases during ascent (Leifer and Judd, 2002). Dedicated water column gas sampling within the oil seepage areas is therefore needed to further confirm our suggestions.

7.7 Conclusion

Satellite images in high spatial and temporal resolution allowed identifying oil seeps in the Black Sea. The method provided high certainty that during the period of investigation (2002-2011) no further oil seepage occurred in the Black Sea and that all active oil seeps were located in the eastern Black Sea. Dedicated multibeam echosounder seafloor and water column investigations evidenced that oil transport to the sea surface is coupled to gas bubble emissions. The combination of oil and gas seepage allows gas bubbles to reach shallow waters and the water-atmosphere interface irrespectively of their origin depth.

In contrast to previously described oil seeps, the here identified sites do not show distinct seafloor morphology. All oil seepage areas offshore Georgia are related to the crests of spurs on the flanks of large canyon-ridge systems. Yet, sediment sampling suggested that shale diapirs intrude locally very shallow sediments, providing the main mechanism for fluid transport. We propose that the Eocene-Miocene Maikop Formation is the source for the seeping hydrocarbons. The magnitude of oil seepage is primarily controlled by the depth of diapirs and therewith the transport efficiency of fluids or fluidized sediments to the seabed. The exclusive occurrence of oil seepage in the eastern Black Sea is suggested to be

controlled by the compressional tectonic regime inducing the thrusting of the Adjara-Trialet fold belt, depth of hydrocarbon generation, and erosion of anticlines cored by diapirs.

Synthetic Aperture Radar satellite images proved to be a powerful tool to map oil seeps and monitor seepage activity over a large area. The frequent occurrence of oil seepage in the eastern Black Sea suggests that combined oil and gas seepage is a significant contributor to shallow water and possibly local atmospheric methane concentrations. Dedicated water column gas sampling in oil seepage areas are proposed to further elucidate the magnitude of methane reaching the sea surface near water. Assessment of typical oil-gas ratios in bubbles released at the seabed would allow using satellite imagery for estimating minimum order-of-magnitude gas release to the atmosphere based on mapped oil slick areas.

7.8 Acknowledgements

We are thankful to captain and crew of R/V METEOR cruise M84/2 for their support at sea. We thank André Bahr (Institute of Geosciences, University of Frankfurt, Main) for providing the core descriptions. Oscar Garcia-Pineda (Florida State University, Tallahassee) is thanked for the help with the satellite image analysis. All satellite images used in this study were provided by the European Space Agency within project C1.P7157. This study was funded through the DFG-Research Center/Excellence Cluster ‘The Ocean in the Earth System’.

Chapter 8

Conclusions and perspectives

8.1 Summary and conclusion

The three case studies which are main parts of this work are documenting seepage processes and hydrocarbon emissions from local to regional scales. The combination of different remote sensing techniques, ranging from optical seafloor mapping to satellite imagery, and the analysis of the obtained multi-sensor datasets in a GIS allowed identifying causalities between different phenomena. These are oil slicks and gas emissions, distinct seafloor morphology, and biological communities. The results provide new insights into hydrocarbon transport processes, e.g. relevance of dissolved versus bubble gas fluxes or emissions of oily versus non-oily gas bubbles in shallow water methane budgets. ASAR satellite images proved great potential to locate oil seeps, monitor their activity and emissions rates. Multibeam-echosounders showed advantage over traditionally employed single-beam systems in gas flare imaging, since their wide swath allows tracing also strongly deflected flares to shallow water. The combination of ROV-mounted sonar together with optical mapping of seep systems proved to be a potent method for assessing areal hydrocarbon fluxes and turnover rates which cannot be obtained by traditional sampling and geochemical methods alone.

The first case study at the Makran accretionary margin evidenced that seep areas identified solely based on hydroacoustic data, might overestimate the area of active seepage. High-frequency hydroacoustic techniques image predominantly shallow sediments and might provide information on sediment surfaces that are altered by seepage. For instance, methane derived authigenic carbonates produce distinct backscatter patterns in sonar records. However, where massive carbonates have formed, seepage is impeded. Areas of active methane seepage were identified and mapped with visual and optical techniques. The precise identification of active seepage areas, allowed calculating the methane budget for an entire seep. The detailed mapping of chemosynthetic communities that represent distinct dissolved methane fluxes, allowed assessing the total turnover rate of the seep, and relating this to the anticipated effluxes of gaseous and dissolved methane. At the seep studied, about $1.14*10^4$ mol yr^{-1} of dissolved methane are consumed by chemosynthetic communities, while about $556*10^4$ mol yr^{-1} are assumed to bypass this filter. The study emphasized that, though biogeochemical processes prevent significant volumes of dissolved methane from being released to the hydrosphere, much larger amounts of methane are emitted as gas bubbles from local vents. The combination of the employed mapping techniques provided a powerful tool to characterize the biological nature and methane budget of large seafloor areas and to relate these to geological processes. The latter were derived from ship-based hydroacoustic investigation methods, including for instance sidescan sonar and multibeam echosounder surveys. More routine employment of such combined survey and local sampling methods would provide a broader base on methane budgets of cold seeps, and help sharpening our understanding of the relevance of cold seeps in the global methane cycle and climate.

The importance of hydrocarbon transport to the hydrosphere by bubble ebullition was highlighted in the first case study. Yet, numerous previous studies showed that gas bubbles emitted from deep-sea seeps dissolve entirely in the water column and do not contribute to the atmospheric methane inventory. Bubbles discharged within the GHSZ will form hydrate shells, allowing them to rise to the upper limit of the GHSZ and only then dissolve. It was

previously suggested that formation of oil coatings around bubbles may prolong their lifetime and allow for methane transport from deep-water seeps to the atmosphere. Large scale studies were conducted on oil seeps in the Black Sea to elucidate whether these observations hold true also in this oil seepage region. Pre-dating this thesis, only one oil seep was known in the Black Sea. The analysis of a large ASAR satellite image dataset revealed the presence of numerous oil seeps, and allowed to assess the temporal variability of seepage, and differences in seepage magnitudes between different sites. Further on, it provided minimum order of magnitude estimations of oil flux to the sea surface. These suggested that the two most prolific oil seeps emit from $36*10^4$ to $181*10^4$ l yr^{-1} oil which corresponds to 0.3 to 1.5 % of the oil emitted by 530 seep in entire Gulf of Mexico. Multibeam echosounder water column investigations, conducted in the newly identified oil seepage areas, evidenced gas bubbles that rose up to 20 mbsl, though emission sites were located between 350 and 1,200 mbsl. The new geophysical data fortify the assumption that slick-forming oil is transported to the sea surface as coating around gas bubbles. The present study therewith corroborates previous findings, and suggests that the oil transport through the hydrosphere might be coupled to gas bubbles also in other oil seepage regions. Natural oil slicks might therefore serve as indicator for seeps that transfer methane to the atmosphere.

Based on detailed seafloor investigations by ROV and AUV it is suggested that frequent rafting of shallow gas hydrate deposits is shaping the seafloor morphology and provides means for hydrocarbon transport to surface waters. From there it might then contribute to atmospheric methane concentrations. Visual observations of millimeter-sized gas hydrates pieces, surfacing above one oil seep, confirm this assumption. Observations on seepage processes in the Black Sea with complementary geochemical data lead to the conclusion that the formation of structure II gas hydrate might form around oily gas bubbles that are emitted from these seeps. This would provide an additional mechanism to enhance bubble lifetime since the upper stability limit of structure II hydrate lays about 530 m higher compared to sI hydrate. This implies that seeps emitting thermogenic hydrocarbons have a much greater potential to transfer climate relevant methane from deep-sea sediments to the atmosphere.

The major findings of this work along with previous knowledge of hydrocarbon transport from the submarine geosphere to the atmosphere are summarized in Fig. 58. In addition to other investigations, the present work shows that bubble gas fluxes are more relevant than dissolved fluxes to methane budgets of the hydrosphere. Deep-sea seeps discharging thermogenic hydrocarbons have the greatest potential to contribute to atmospheric methane concentrations, since these sites might emit oil which, as coating around bubbles, hampers bubble dissolution. The presence of C_{2+} hydrocarbons might stimulate the formation of sII hydrate which further impedes gas bubble dissolution. Dislocation of gas hydrates from the seabed is another potential process transporting methane to the water-atmosphere interface.

Except the Gulf of Mexico, and now the Black Sea, no other deep-water oil seepage region was investigated with respect to emissions of methane and other hydrocarbon to shallow water and atmosphere. However, if the identified seepage processes are relevant in other oil seepage regions, these should be in the research focus when aiming to constrain quantitative and qualitative estimates of the impact of marine seeps on atmospheric hydrocarbon budgets and climate.

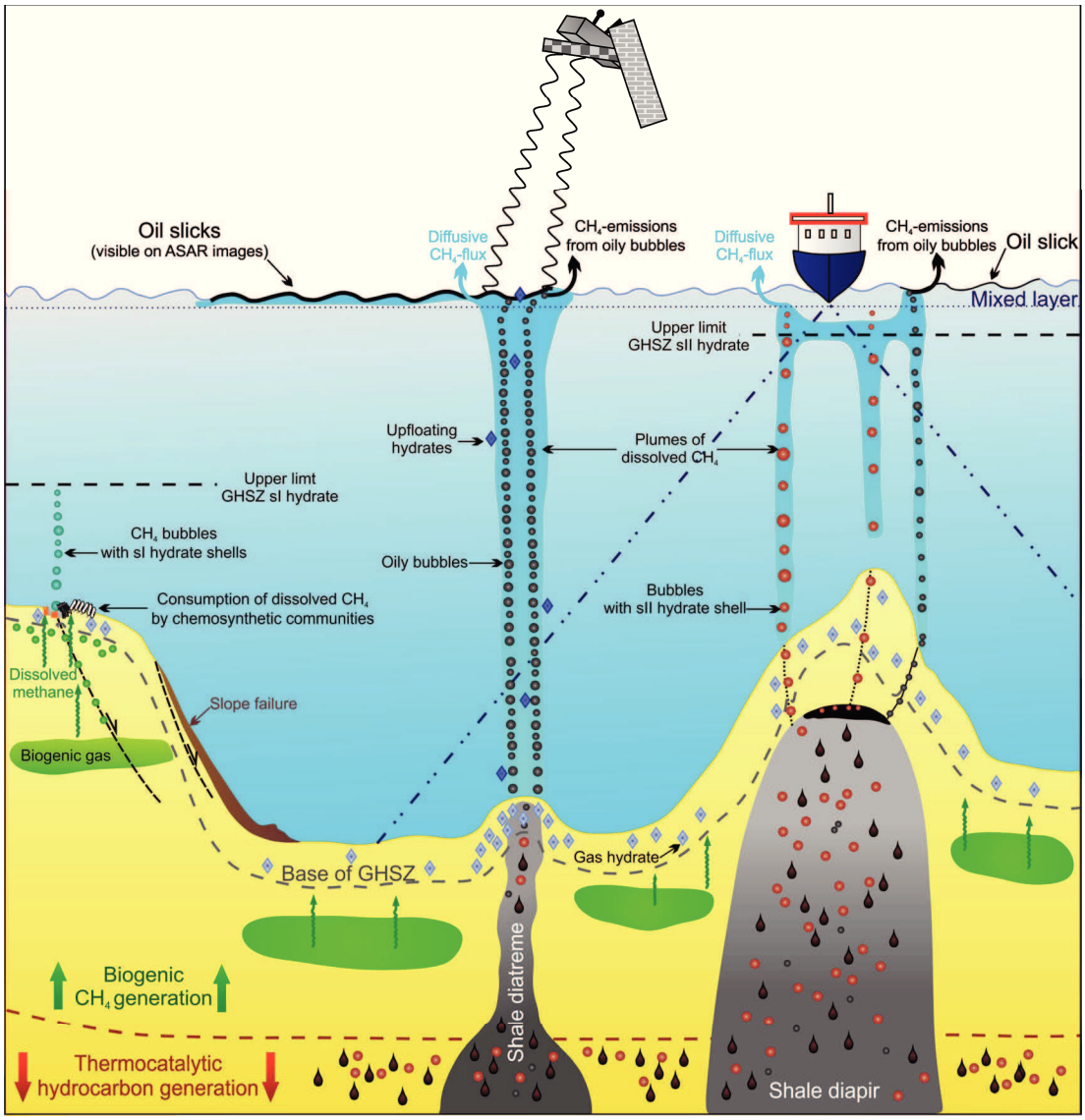

Fig. 58. Illustration of deep-sea seepage processes and associated hydrocarbon transfer through the hydrosphere to the atmosphere. The majority of dissolved methane migrating towards the seabed is consumed by chemosynthetic communities. Pure methane gas bubbles discharged to the water column dissolve before reaching the sea surface or mixed layer. At thermogenic hydrocarbon seeps, oil coatings or structure II hydrate shells impede bubble dissolution and might allow bubbles to reach the sea surface and inject the remaining methane to the atmosphere. These sites can be identified and monitored by satellite imagery. Hydrate rafting might also transport hydrocarbons towards the sea surface at sites of vigorous gas flux. Partial dissolution of high rising bubbles might create plumes of dissolved methane, which enhance bubble lifetime. From the mixed layer dissolved methane might diffuse to the atmosphere.

8.2 Outlook

The present work emphasized the potential of various ship and spaceborne remote sensing techniques in facilitating and improving the detection and investigation of cold seeps. Yet, the applied techniques bear potential for improvement or further development. Firstly, the production of seafloor images by video-mosaicking might be considered to be substituted by photo-mosaicking. Recording of continuous video-footage is on the one hand convenient because there is no risk to acquire images that do not overlap. On the other hand, production of mosaics from video is hampered when the seafloor is too homogenous. In this case no, control points defining common areas in consecutive video-frames are found, which creates distortions in the resulting image. These could be manually identified on photo-mosaics. Also, video-mosaicking requires a constant illumination of the seafloor. Standard spots on the ROV QUEST4000 failed to provide a homogenous and sufficiently bright illumination, causing further distortion problems on mosaics. For photo-mosaicking, a strong strobe, or better, two strobes mounted on the sites of the ROV would provide much better illumination of the seafloor.

ASAR satellite images proved great potential for investigating oil seepage processes. The estimation of flux rates, and especially the assessment of gas fluxes associated with oil fluxes, could be improved by local measurements of bubble oiliness. Assessment of oil-to-gas ratios upon bubble discharge from the seabed would allow establishing relations of bubble rise velocities versus size and oil content since the latter two parameters significantly affect the bubble rise velocity. In Chapter 6, horizontal current velocities in the water column have been obtained from measured bubble rise velocities and horizontal gas flare deflections in the water column. However, the measurement of bubble rise velocities required costly ROV investigations. If it was possible to directly measure water column currents during flare imaging surveys e.g. by hull-mounted Acoustic Doppler Current Profiler (ADCP), it might be feasible to estimate bubble rise velocities based on current velocities and flare deflections. These might then provide a proxy for the oil-to-gas ratio of rising bubbles. In combination with estimates on minimum oil emissions derived from satellite images, an estimate of associated gas release could be provided.

Dedicated water column gas sampling in oil seepage areas is needed to asses the fate of the gas which is contained in bubbles upon discharge at the seafloor. Only such measurements can, in last instance, confirm whether bubbles that reach the sea surface still contain methane or not. Furthermore, research is needed on sampling of gas hydrates that raft to the sea surface, as was observed in the Black Sea. It is proposed that these small chunks release by far more methane to the atmosphere when decomposing at the sea surface than oily gas bubbles do. However, evidence is needed for that the putative hydrates still contain gas and are not plain ice. Since chances to observe natural hydrate rafting are small, it might be appropriate to manually induce hydrate rafting, e.g. during a ROV dive, to enable collection of hydrate samples on the sea surface in gas tight containers for later chemical analysis.

On local scale, it would be interesting to combine satellite based monitoring of a single oil seep area with seafloor observatories. If, for instance, sensors measuring sediment pore pressure were installed at an oil seep, changes in oil seepage activity and magnitude could directly be linked to, e.g., seismic activity.

References

Akhmetzhanov, A.M., Ivanov, M.K., Kenyon, N.H., Mazzini, A., 2007. Deep-water cold seeps, sedimentary environments and ecosystems of the Black Sea and Tyrrehnian Seas and Gulf of Cadiz, IOC Technical Series. UNESCO.

Alpers, W., Espedal, H.A., 2004. Oil and surfactants, in: Jackson, C.R., Apel, J.R. (Eds.), Synthetic Aperture Radar Marine User's manual. U.S. Department of Commerce, National Oceanic and Atmospheric Administration, Washington D.C., pp. 263-275.

Alpers, W., Pahl, U., Gross, G., 1998. Katabatic wind fields in coastal areas studied by ERS-1 synthetic aperture radar imagery and numerical modeling. J. Geophys. Res. 103, 7875-7886.

Andresen, K.J., Huuse, M., 2011. 'Bulls-eye' pockmarks and polygonal faulting in the Lower Congo Basin: Relative timing and implications for fluid expulsion during shallow burial. Marine Geology 279, 111-127.

Archer, D., 2007. Methane hydrate stability and anthropogenic climate change. Biogeosciences 4, 521-544.

Archer, D., Buffett, B., Brovkin, V., 2009. Ocean methane hydrates as a slow tipping point in the global carbon cycle. Proceedings of the National Academy of Sciences 106, 20596-20601.

Bahr, A., Pape, T., Bohrmann, G., Mazzini, A., Haeckel, M., Reitz, A., Ivanov, M., 2009. Authigenic carbonate precipitates from the NE Black Sea: a mineralogical, geochemical, and lipid biomarker study. International Journal of Earth Sciences 98, 677-695.

Banks, C.J., Robinson, A.G., Williams, M.P., 1997. Structure and regional tectonics of the Achara-Trialet fold belt and the adjacent Rioni and Kartli foreland basins, in: Robinson, A.G. (Ed.), Regional Petroleum Geology of the Black Sea and Surrounding Region AAPG, pp. 19-38.

Barnes, R.O., Goldberg, E.D., 1976. Methane production and consumption in anoxic marine sediments. Geology 4, 297-300.

Barnett, T.P., Pierce, D.W., Schnur, R., 2001. Detection of Anthropogenic Climate Change in the World's Oceans. Science 292, 270-274.

Bayon, G., Henderson, G.M., Bohn, M., 2009a. U-Th stratigraphy of a cold seep carbonate crust. Chemical Geology 260, 47-56.

Bayon, G., Loncke, L., Dupré, S., Caprais, J.C., Ducassou, E., Duperron, S., Etoubleau, J., Foucher, J.P., Fouquet, Y., Gontharet, S., Henderson, G.M., Huguen, C., Klaucke, I., Mascle, J., Migeon, S., Olu-Le Roy, K., Ondréas, H., Pierre, C., Sibuet, M., Stadnitskaia, A., Woodside, J., 2009b. Multi-disciplinary investigation of fluid seepage on an unstable margin: The case of the Central Nile deep sea fan. Marine Geology 261, 92-104.

Beisl, C.H., Pedroso, E.C., Soler, L.S., Evsukoff, A.G., Miranda, F.P., Mendoza, A., Vera, A., Macedo, J.M., 2004. Use of genetic algorithm to identify the source point of seepage slick clusters interpreted from Radarsat-1 images in the Gulf of Mexico, Geoscience and Remote Sensing Symposium, 2004. IGARSS '04. Proceedings. 2004 IEEE International, pp. 4139-4142 vol.4136.

Benton, J., 1997. Exploration history of the Black Sea province, in: Robinson, A.G. (Ed.), Regional and petroleum geology of the Black Sea and surrounding region. AAPG, pp. 7-18.

Bern, T., 1993. Oil slick study, Norwegian Slick Study, Trondheim, Norway.

Bernard, B.B., Brooks, J.M., Sackett, W.M., 1978. Light Hydrocarbons in Recent Texas Continental Shelf and Slope Sediments. J. Geophys. Res. 83, 4053-4061.

Bjørlykke, K., Høeg, K., 1997. Effects of burial diagenesis on stresses, compaction and fluid flow in sedimentary basins. Marine and Petroleum Geology 14, 267-276.

Blinova, V.N., Ivanov, M.K., Bohrmann, G., 2003. Hydrocarbon gases in deposits from mud volcanoes in the Sorokin Trough, north-eastern Black Sea. Geo-Marine Letters 23, 250-257.

Boetius, A., Ravenschlag, K., Schubert, C.J., Rickert, D., Widdel, F., Gieseke, A., Amann, R., Jorgensen, B.B., Witte, U., Pfannkuche, O., 2000a. A marine microbial consortium apparently mediating anaerobic oxidation of methane. Nature 407, 623-626.

Boetius, A., Ferdelman, T., Lochte, K., 2000b. Bacterial activity in sediments of the deep Arabian Sea in relation to vertical flux. Deep Sea Research Part II: Topical Studies in Oceanography 47, 2835-2875.

Bohrmann, G., and cruise participants, 2008. Report and preliminary results of R/V Meteor Cruise M74/3, Fujairah - Male, 30 October - 28 November, 2007 Cold Seeps of the Makran Subduction Zone (Continental Margin off Pakistan), Berichte, Fachbereich Geowissenschaften, Universität Bremen, p. 161.

Bohrmann, G., Heeschen, K., Jung, C., Weinrebe, W., Baranov, B., Cailleau, B., Heath, R., Hühnerbach, V., Hort, M., Masson, D., Trummer, I., 2002. Widespread fluid expulsion along the seafloor of the Costa Rica convergent margin. Terra Nova 14, 69-79.

Bohrmann, G., Ivanov, M., Foucher, J.P., Spiess, V., Bialas, J., Greinert, J., Weinrebe, W., Abegg, F., Aloisi, G., Artemov, Y., Blinova, V., Drews, M., Heidersdorf, F., Krabbenhöft, A., Klaucke, I., Krastel, S., Leder, T., Polikarpov, I., Saburova, M., Schmale, O., Seifert, R., Volkonskaya, A., Zillmer, M., 2003. Mud volcanoes and gas hydrates in the Black Sea: new data from Dvurechenskii and Odessa mud volcanoes. Geo-Marine Letters 23, 239-249.

Bohrmann, G., Pape, T., and cruise participants, 2007. Report and preliminary results of R/V Meteor Cruise M72/3, Istanbul-Trabzon-Istanbul, 17 march - 23 April, 2007. Marine gas hydrates of the Eastern Black Sea., Berichte, Fachbereich Geowissenschaften. Universität Bremen, Bremen, p. 176.

Bohrmann, G., and cruise participants, 2011a. Report and preliminary results of RV MARIA S. MERIAN Cruise MSM15/2, Stanbul (Turkey) - Piraeus (Greece), 10 May - 2 June 2010. Origin and structure of methane, gas hydrates and fluid flows in the Black Sea., Berichte, Fachbereich Geowissenschaften, Universität Bremen, Bremen, p. 130.

Bohrmann, G., and cruise participants, 2011b. Report and preliminary results of RV METEOR Cruise M84/2, Istanbul - Istanbul, 26 February - 02 April, 2011. Origin and Distribution of Methane and Methane Hydrates in the Black Sea., Berichte, Fachbereich Geowissenschaften, Universität Bremen, Bremen, p. 164.

Bohrmann, G., Torres, M.E., 2006. Gas Hydrates in Marine Sediments. Marine Geochemistry, in: Schulz, H.D., Zabel, M. (Eds.). Springer Berlin Heidelberg, pp. 481-512.

Borowski, W.S., Paull, C.K., Ussler, W., 1999. Global and local variations of interstitial sulfate gradients in deep-water, continental margin sediments: Sensitivity to underlying methane and gas hydrates. Marine Geology 159, 131-154.

Borowski, W.S., Paull, C.K., Ussler, W., III, 1996. Marine pore-water sulfate profiles indicate in situ methane flux from underlying gas hydrate. Geology 24, 655-658.

Boswell, R., 2009. Is Gas Hydrate Energy Within Reach? Science 325, 957-958.

Boswell, R., Collett, T.S., 2011. Current perspectives on gas hydrate resources. Energy & Environmental Science 4, 1206-1215.

Bouriak, S., Vanneste, M., Saoutkine, A., 2000. Inferred gas hydrates and clay diapirs near the Storegga Slide on the southern edge of the Vøring Plateau, offshore Norway. Marine Geology 163, 125-148.

Bourry, C., Chazallon, B., Charlou, J.L., Pierre Donval, J., Ruffine, L., Henry, P., Geli, L., Çagatay, M.N., İnan, S., Moreau, M., 2009. Free gas and gas hydrates from the Sea of Marmara, Turkey: Chemical and structural characterization. Chemical Geology 264, 197-206.

Brekke, C., Solberg, A.H.S., 2005. Oil spill detection by satellite remote sensing. Remote Sensing of Environment 95, 1-13.

Brewer, P.G., Friederich, G., Peltzer, E.T., Orr Jr., F.M., 1999. Direct Experiments on the Ocean Disposal of Fossil Fuel CO2. Science 284, 943-945.

Brooks, J.M., Cox, H.B., Bryant, W.R., Kennicutt Ii, M.C., Mann, R.G., McDonald, T.J., 1986. Association of gas hydrates and oil seepage in the Gulf of Mexico. Organic Geochemistry 10, 221-234.

Brooks, J.M., Kennicut, M.C., Fay, R.R., McDonald, T.J., Sassen, R., 1984. Thermogenic Gas Hydrates in the Gulf of Mexico. Science 225, 409-411.

Brown, C.E., Fingas, M.F., 2003. Development of airborne oil thickness measurements. Marine Pollution Bulletin 47, 485-492.

Brown, K.M., 1990. The Nature and Hydrogeologic Significance of Mud Diapirs and Diatremes for Accretionary Systems. Journal of Geophysical Research 95, 8969-8982.

Brüning, M., Sahling, H., MacDonald, I.R., Ding, F., Bohrmann, G., 2010. Origin, distribution, and alteration of asphalts at Chapopote Knoll, Southern Gulf of Mexico. Marine and Petroleum Geology 27, 1093-1106.

Bünz, S., Mienert, J., Bryn, P., Berg, K., 2005. Fluid flow impact on slope failure from 3D seismic data: a case study in the Storegga Slide. Basin Research 17, 109-122.

Burwicz, E.B., Rüpke, L.H., Wallmann, K., 2011. Estimation of the global amount of submarine gas hydrates formed via microbial methane formation based on numerical reaction-transport modeling and a novel parameterization of Holocene sedimentation. Geochimica et Cosmochimica Acta 75, 4562-4576.

Byrne, D.E., Sykes, L.R., Davis, D.M., 1992. Great Thrust Earthquakes and Aseismic Slip Along the Plate Boundary of the Makran Subduction Zone. J. Geophys. Res. 97, 449-478.

Canet, C., Prol-Ledesma, R.M., Dando, P.R., Vázquez-Figueroa, V., Shumilin, E., Birosta, E., Sánchez, A., Robinson, C.J., Camprubí, A., Tauler, E., 2010. Discovery of massive seafloor gas seepage along the Wagner Fault, northern Gulf of California. Sedimentary Geology 228, 292-303.

Carpenter, G., 1981. Coincident sediment slump/clathrate complexes on the U.S. Atlantic continental slope. Geo-Marine Letters 1, 29-32.

Chapman, R., Pohlman, J., Coffin, R., Chanton, J., Lapham, L., 2004. Thermogenic gas hydrates in the northern Cascadia margin. Eos Trans. AGU 85.

Çifçi, G., Dondurur, D., Ergün, M., 2003. Deep and shallow structures of large pockmarks in the Turkish shelf, Eastern Black Sea. Geo-Marine Letters 23, 311-322.

Clark, J.F., Leifer, I., Washburn, L., Luyendyk, B.P., 2003. Compositional changes in natural gas bubble plumes: observations from the Coal Oil Point marine hydrocarbon seep field. Geo-Marine Letters 23, 187-193.

Clark, J.F., Washburn, L., Hornafius, J.S., Luyendyk, B.P., 2000. Dissolved hydrocarbon flux from natural marine seeps to the southern California Bight. J. Geophys. Res. 105.

Clarke, R.H., Cleverly, R.W., 1991. Petroleum seepage and post-accumulation migration. Geological Society, London, Special Publications 59, 265-271.

Claypool, G.E., Kvenvolden, K.A., 1983. Methane and other Hydrocarbon Gases in Marine Sediment. Annual Review of Earth and Planetary Sciences 11, 299-327.

Clennell, M.B., Judd, A.G., Hovland, M., 2000. Movement and accumulation of methane in marine sediments: relation to gas hydrate systems, in: Max, M.D. (Ed.), Natural Gas Hydrate in Oceanic and Permafrost Environments. Kluwer Academic Press, pp. 105-122.

Cranston, R.E., Ginsburg, G.D., Soloviev, V.A., Lorenson, T.D., 1994. Gas venting and hydrate deposits in the Okhotsk Sea. Bulletin of the Geological Society of Denmark 41, 80-85.

Dandapath, S., Chakraborty, B., Karisiddaiah, S.M., Menezes, A., Ranade, G., Fernandes, W., Naik, D.K., Prudhvi Raju, K.N., 2010. Morphology of pockmarks along the western continental margin of India: Employing multibeam bathymetry and backscatter data. Marine and Petroleum Geology 27, 2107-2117.

Davy, B., Pecher, I., Wood, R., Carter, L., Gohl, K., 2010. Gas escape features off New Zealand: Evidence of massive release of methane from hydrates. Geophys. Res. Lett. 37, L21309.

De Beukelaer, S.M., MacDonald, I.R., Guinnasso, N.L., Murray, J.A., 2003. Distinct side-scan sonar, RADARSAT SAR, and acoustic profiler signatures of gas and oil seeps on the Gulf of Mexico slope. Geo-Marine Letters 23, 177-186.

Degens, E.T., Stoffers, P., 1980. Environmental events recorded in Quaternary sediments of the Black Sea. Journal of the Geological Society 137, 131-138.

Delisle, G., Berner, U., 2002. Gas hydrates acting as cap rock to fluid discharge in the Makran accretionary prism?, in: Clift, P.D., Kroon, D., Gaedicke, C., Craig, J. (Eds.), The tectonic and climatic evolution of the arabian sea region. The Geological Society, London, pp. 137-146.

Delisle, G.D., von Rad, U.v.R., Andruleit, H.A., von Daniels, C.v.D., Tabrez, A.T., Inam, A.I., 2002. Active mud volcanoes on- and offshore eastern Makran, Pakistan. International Journal of Earth Sciences 91, 93-110.

Denman, K.L., al., e., 2007. Couplings between changes in the climate systems and biogeochemistry, in: Solomon, S., al., e. (Eds.), Climate 2007: The Physical Science Basis. Contribution of Working Group I to the Fourth Assessment Report of theIntergovernmental Panel on Climate Change. Cambridge University Press, pp. 499-587.

Derman, A.S., Iztan, Y.H., 1997. Results of geochemical analysis of seeps and potential source rocks from northern Turkey and the Turkish Black Sea, in: Robinson, A.G. (Ed.), Regional Petroleum Geology of the Black Sea and Surrounding Region AAPG, pp. 313-330.

Dickens, G.R., 1999. Carbon cycle: The blast in the past. Nature 401, 752-755.

Dickens, G.R., 2011. Down the Rabbit Hole: toward appropriate discussion of methane release from gas hydrate systems during the Paleocene-Eocene thermal maximum and other past hyperthermal events. Clim. Past 7, 831-846.

Dickens, G.R., O'Neil, J.R., Rea, D.K., Owen, R.M., 1995. Dissociation of Oceanic Methane Hydrate as a Cause of the Carbon Isotope Excursion at the End of the Paleocene. Paleoceanography 10, 965-971.

Dimitrov, L., 2002. Contribution to atmospheric methane by natural seepages on the Bulgarian continental shelf. Continental Shelf Research 22, 2429-2442.

Dimitrov, L., Woodside, J., 2003. Deep sea pockmark environments in the eastern Mediterranean. Marine Geology 195, 263-276.

Ding, F., Spiess, V., Fekete, N., Murton, B., Brüning, M., Bohrmann, G., 2010. Interaction between accretionary thrust faulting and slope sedimentation at the frontal Makran accretionary prism and its implications for hydrocarbon fluid seepage. J. Geophys. Res. 115, B08106.

Dubilier, N., Bergin, C., Lott, C., 2008. Symbiotic diversity in marine animals: the art of harnessing chemosynthesis. Nat Rev Micro 6, 725-740.

Duperron, S., Halary, S., Lorion, J., Sibuet, M., Gaill, F., 2008. Unexpected co-occurrence of six bacterial symbionts in the gills of the cold seep mussel Idas sp. (Bivalvia: Mytilidae). Environmental Microbiology 10, 433-445.

Dupré, S., Woodside, J., Foucher, J.-P., de Lange, G., Mascle, J., Boetius, A., Mastalerz, V., Stadnitskaia, A., Ondréas, H., Huguen, C., Harmégnies, F., Gontharet, S., Loncke, L., Deville, E., Niemann, H., Omoregie, E., Olu-Le Roy, K., Fiala-Medioni, A., Dählmann, A., Caprais, J.-C., Prinzhofer, A., Sibuet, M., Pierre, C., Damsté, J.S., 2007. Seafloor geological studies above active gas chimneys off Egypt (Central Nile Deep Sea Fan). Deep Sea Research Part I: Oceanographic Research Papers 54, 1146-1172.

Dupré, S., Woodside, J., Klaucke, I., Mascle, J., Foucher, J.-P., 2010. Widespread active seepage activity on the Nile Deep Sea Fan (offshore Egypt) revealed by high-definition geophysical imagery. Marine Geology 275, 1-19.

Durand, S., Le Bel, M., Juniper, K., Legendre, P., 2002. The use of video surveys, a Geographic Information System and sonar backscatter data to study faunal community dynamics at Juan de Fruca Ridge hydrothermal vents. Cah . Biol. Mar. 43 235-240.

Edwards, R.A., Scott, C.L., Shillington, D.J., Minshull, T.A., Brown, P.J., White, N.J., 2009. Wide-angle seismic data reveal sedimentary and crustal structure of the Eastern Black Sea. The Leading Edge 28, 1056-1065.

Efendiyeva, M.A., 2004. Anoxia in waters of the Maikop paleobasin (Tethys Ocean, Azeri sector), with implications for the modern Caspian Sea. Geo-Marine Letters 24, 177-181.

Egorov, A.V., Crane, K., Vogt, P.R., Rozhkov, A.N., Shirshov, P.P., 1999. Gas hydrates that outcrop on the sea floor: stability models. Geo-Marine Letters 19, 68-75.

Egorov, V., Polikarpov, G.G., Gulin, S.B., Artemov, Y.G., Stokozov, N.A., Kostova, S.K., 2003. Present-day views on the environment-forming and ecological role of the Black Sea methane gas seeps (in Russian). Marine Ecological Journal 2, 5-26

Eichhubl, P., Greene, H.G., Naehr, T., Maher, N., 2000. Structural control of fluid flow: offshore fluid seepage in the Santa Barbara Basin, California. Journal of Geochemical Exploration 69-70, 545-549.

Elliott, A.J., Hurford, N., Penn, C.J., 1986. Shear diffusion and the spreading of oil slicks. Marine Pollution Bulletin 17, 308-313.

Emeis, K.C., Brüchert, V., Currie, B., Endler, R., Ferdelman, T., Kiessling, A., Leipe, T., Noli-Peard, K., Struck, U., Vogt, T., 2004. Shallow gas in shelf sediments of the Namibian coastal upwelling ecosystem. Continental Shelf Research 24, 627-642.

Ergün, M., Dondurur, D., Çifçi, G., 2002. Acoustic evidence for shallow gas accumulations in the sediments of the Eastern Black Sea. Terra Nova 14, 313-320.

ESA, 2007. ASAR Product Handbook. European Space Agency.

Espedal, H.A., Johannessen, O.M., 2000. Detection of oil spills near offshore installations using synthetic aperture radar (SAR). International Journal of Remote Sensing 21, 2141-2144.

Espedal, H.A., Wahl, T., 1999. Satellite SAR oil spill detection using wind history information. International Journal of Remote Sensing 20, 49-65.

Etiope, G., 2009. Natural emissions of methane from geological seepage in Europe. Atmospheric Environment 43, 1430-1443.

Etiope, G., Klusman, R.W., 2002. Geologic emissions of methane to the atmosphere. Chemosphere 49, 777-789.

Etiope, G., Lassey, K.R., Klusman, R.W., Boschi, E., 2008. Reappraisal of the fossil methane budget and related emission from geologic sources. Geophys. Res. Lett. 35, L09307.

Etiope, G., Martinelli, G., 2002. Migration of carrier and trace gases in the geosphere: an overview. Physics of The Earth and Planetary Interiors 129, 185-204.

Etiope, G., Martinelli, G., Caracausi, A., Italiano, F., 2007. Methane seeps and mud volcanoes in Italy: Gas origin, fractionation and emission to the atmosphere. Geophys. Res. Lett. 34, L14303.

Faure, K., Greinert, J., Pecher, I.A., Graham, I.J., Massoth, G.J., de Ronde, C.E.J., Wright, I.C., Baker, E.T., Olson, E.J., 2006. Methane seepage and its relation to slumping and gas hydrate at the Hikurangi margin, New Zealand. New Zealand Journal of Geology and Geophysics 49, 503-516.

Felden, J., Wenzhöfer, F., Feseker, T., Boetius, A., 2010. Transport and consumption of oxygen and methane in different habitats of the Håkon Mosby Mud Volcano (HMMV). Limnology and Oceanography 55, 2366-2380.

Feseker, T., Brown, K., Blanchet, C., Scholz, F., Nuzzo, M., Reitz, A., Schmidt, M., Hensen, C., 2010. Active mud volcanoes on the upper slope of the western Nile deep-sea fan—first results from the P362/2 cruise of R/V Poseidon. Geo-Marine Letters 30, 169-186.

Fingas, M.F., Brown, C.E., 1997. Review of oil spill remote sensing. Spill Science & Technology Bulletin 4, 199-208.

Fischer, D., Sahling, H., Nöthen, K., Bohrmann, G., Zabel, M., Kasten, S., 2012. Interaction between hydrocarbon seepage, chemosynthetic communities, and bottom water redox at cold seeps of the Makran accretionary prism: insights from habitat-specific pore water sampling and modeling. Biogeosciences 9, 2013-2031.

Fleischer, Fleischer, P., Orsi, Orsi, T., Richardson, Richardson, M., Anderson, Anderson, A., 2001. Distribution of free gas in marine sediments: a global overview. Geo-Marine Letters 21, 103-122.

Floodgate, G.D., Judd, A.G., 1992. The origins of shallow gas. Continental Shelf Research 12, 1145-1156.

Forster, P., Ramaswamy, V., Artaxo, T. Berntsen, P., Betts, R., Fahey, D.W., Haywood, J., Lean, J., Lowe, D.C., Myhre, G., Nganga, J., Prinn, R., Raga, G., Schulz, M., Van Dorland, R., 2007. Changes in Atmospheric Constituents and in Radiative Forcing, in: Solomon, S., Qin, D., Manning, M.R., Chen, Z., Marquis, M., Averyt, K.B., Tignor, M., Miller, H.L. (Eds.), Climate Change 2007: The Physical Science Basis. Contribution of Working Group I to the Fourth Assessment Report of the intergovernmental Panel on Climate Change. Cambridge University Press Cambridge, United Kingdom and New York, NY, USA.

Foubert, A., Depreiter, D., Beck, T., Maignien, L., Pannemans, B., Frank, N., Blamart, D., Henriet, J.-P., 2008. Carbonate mounds in a mud volcano province off north-west Morocco: Key to processes and controls. Marine Geology 248, 74-96.

Fruehn, J., White, R.S., Minshull, T.A., 1997. Internal deformation and compaction of the Makran accretionary wedge. Terra Nova 9, 101-104.

Garcia-Pineda, O., 2009. Spatial and tempoal analysis of oil slicks in the Gulf of mexico based on remote sensing. Texas A & M University, Corpus-Christi, p. 155.

Garcia-Pineda, O., MacDonald, I., Zimmer, B., 2008. Synthetic Aperture Radar Image Processing using the Supervised Textural-Neural Network Classification Algorithm, Geoscience and Remote Sensing Symposium, 2008. IGARSS 2008. IEEE International, pp. 1265-1268.

Garcia-Pineda, O., MacDonald, I., Zimmer, B., Shedd, B., Roberts, H., 2010. Remote-sensing evaluation of geophysical anomaly sites in the outer continental slope, northern Gulf of Mexico. Deep Sea Research Part II: Topical Studies in Oceanography 57, 1859-1869.

Garcia-Pineda, O., Zimmer, B., Howard, M., Pichel, W., Li, X., MacDonald, I., 2009. Using SAR images to delineate ocean oil slicks with a texture-classifying neural network algorithm (TCNNA). Canadian Journal of Remote Sensing 35, 411-421.

Gay, A., Lopez, M., Berndt, C., Séranne, M., 2007. Geological controls on focused fluid flow associated with seafloor seeps in the Lower Congo Basin. Marine Geology 244, 68-92.

Géli, L., Henry, P., Zitter, T., Dupré, S., Tryon, M., Çağatay, M.N., de Lépinay, B.M., Le Pichon, X., Şengör, A.M.C., Görür, N., Natalin, B., Uçarkuş, G., Özeren, S., Volker, D., Gasperini, L., Burnard, P., Bourlange, S., the Marnaut Scientific, P., 2008. Gas emissions and active tectonics within the submerged section of the North Anatolian Fault zone in the Sea of Marmara. Earth and Planetary Science Letters 274, 34-39.

Görür, N., 1988. Timing of opening of the Black Sea basin. Tectonophysics 147, 247-262.

Gracias, N., Santos-Victor, J., 2000. Underwater Video Mosaics as Visual Navigation Maps. Computer Vision and Image Understanding 79, 66-91.

Grando, G., McClay, K., 2007. Morphotectonics domains and structural styles in the Makran accretionary prism, offshore Iran. Sedimentary Geology 196, 157-179.

Greinert, J., Artemov, Y., Egorov, V., De Batist, M., McGinnis, D., 2006. 1300-m-high rising bubbles from mud volcanoes at 2080 m in the Black Sea: Hydroacoustic characteristics and temporal variability. Earth and Planetary Science Letters 244, 1-15.

Grevemeyer, I., Rosenberger, A., Villinger, H., 2000. Natural gas hydrates on the continental slope off Pakistan: constraints from seismic techniques. Geophysical Journal International, Volume 140, Issue 2, pp. 295-310 140, 15.

Hampton, M.A., Lee, H.J., Locat, J., 1996. Submarine landslides. Rev. Geophys. 34, 33-59.

Han, X., Suess, E., Sahling, H., Wallmann, K., 2004. Fluid venting activity on the Costa Rica margin: new results from authigenic carbonates. International Journal of Earth Sciences 93, 596-611.

Heeschen, K.U., Collier, R.W., de Angelis, M.A., Suess, E., Rehder, G., Linke, P., Klinkhammer, G.P., 2005. Methane sources, distributions, and fluxes from cold vent sites at Hydrate Ridge, Cascadia Margin. Global Biogeochem. Cycles 19, GB2016.

Heeschen, K.U., Hohnberg, H.J., Haeckel, M., Abegg, F., Drews, M., Bohrmann, G., 2007. In situ hydrocarbon concentrations from pressurized cores in surface sediments, Northern Gulf of Mexico. Marine Chemistry 107, 498-515.

Heeschen, K.U., Tréhu, A.M., Collier, R.W., Suess, E., Rehder, G., 2003. Distribution and height of methane bubble plumes on the Cascadia Margin characterized by acoustic imaging. Geophys. Res. Lett. 30, 1643.

Helly, J.J., Levin, L.A., 2004. Global distribution of naturally occurring marine hypoxia on continental margins. Deep Sea Research Part I: Oceanographic Research Papers 51, 1159-1168.

Hester, K.C., Brewer, P.G., 2009. Clathrate Hydrates in Nature. Annual Review of Marine Science 1, 303-327.

Holland, C.W., Weber, T.C., Etiope, G., 2006. Acoustic scattering from mud volcanoes and carbonate mounds. The Journal of the Acoustical Society of America 120, 3553-3565.

Hornafius, J.S., Quigley, D., Luyendyk, B.P., 1999. The world's most spectacular marine hydrocarbon seeps (Coal Oil Point, Santa Barbara Channel, California): Quantification of emissions. Journal of Geophysical Research 104.

Hovland, M., 2002. On the self-sealing nature of marine seeps. Continental Shelf Research 22, 2387-2394.

Hovland, M., Heggland, R., De Vries, M.H., Tjelta, T.I., 2010. Unit-pockmarks and their potential significance for predicting fluid flow. Marine and Petroleum Geology 27, 1190-1199.

Hovland, M., Judd, A.G., Burke, R.A., 1993. Global flux of methane from shallow submarine sediments. Chemosphere 26, 559-578.

Hovland, M., Svensen, H., 2006. Submarine pingoes: Indicators of shallow gas hydrates in a pockmark at Nyegga, Norwegian Sea. Marine Geology 228, 15-23.

Hovland, M., Svensen, H., Forsberg, C.F., Johansen, H., Fichler, C., Fosså, J.H., Jonsson, R., Rueslåtten, H., 2005. Complex pockmarks with carbonate-ridges off mid-Norway: Products of sediment degassing. Marine Geology 218, 191-206.

Hovland, M., Thomsen, E., 1989. Hydrocarbon-based Communities in the North Sea. Sarsia 74, 13.

Hu, C., Li, X., Pichel, W.G., Muller-Karger, F.E., 2009. Detection of natural oil slicks in the NW Gulf of Mexico using MODIS imagery. Geophysical Research Letters 36, L01604.

Hu, L., Yvon-Lewis, S.A., Kessler, J.D., MacDonald, I.R., 2012. Methane fluxes to the atmosphere from deepwater hydrocarbon seeps in the northern Gulf of Mexico. Journal of Geophysical Research 117, C01009.

Hunt, J.M., 1979. Petroleum Geochemistry and Geology. Freemann and Company, San Francisco.

Hunt, J.M., Whelan, J.K., Eglinton, L.B., Cathles, L.M.I., 1994. Gas generation -- A major cause of deep Gulf Coast overpressures. Journal Name: Oil and Gas Journal; (United States); Journal Volume: 92:29, Medium: X; Size: Pages: 59-63.

Hustoft, S., Bünz, S., Mienert, J., Chand, S., 2009. Gas hydrate reservoir and active methane-venting province in sediments on < 20 Ma young oceanic crust in the Fram Strait, offshore NW-Svalbard. Earth and Planetary Science Letters 284, 12-24.

Inan, S., Namik Yalçin, M., Guliev, I.S., Kuliev, K., Akper Feizullayev, A., 1997. Deep petroleum occurrences in the Lower Kura Depression, South Caspian Basin, Azerbaijan: an organic geochemical and basin modeling study. Marine and Petroleum Geology 14, 731-762.

IPCC, 2007 Climate Change 2007, Cambridge, United Kingdom and New York, NY, USA.

Ivanov, M.K., Limonov, A.F., van Weering, T.C.E., 1996. Comparative characteristics of the Black Sea and Mediterranean Ridge mud volcanoes. Marine Geology 132, 253-271.

Iversen, N., Jørgensen, B.B., 1985. Anaerobic methane oxidation rates at the sulfate-methane transition in marine sediments from Kattegat and Skagerrak (Denmark). Limnology and Oceanography 30, 944-955.

Jauer, C.D., Budkewitsch, P., 2010. Old marine seismic and new satellite radar data: Petroleum exploration of north west Labrador Sea, Canada. Marine and Petroleum Geology 27, 1379-1394.

Jerosch, K., Schlüter, M., Foucher, J.-P., Allais, A.-G., Klages, M., Edy, C., 2007. Spatial distribution of mud flows, chemoautotrophic communities, and biogeochemical habitats at Håkon Mosby Mud Volcano. Marine Geology 243, 1-17.

Jerosch, K., Schlüter, M., Pesch, R., 2006. Spatial analysis of marine categorical information using indicator kriging applied to georeferenced video mosaics of the deep-sea Håkon Mosby Mud Volcano. Ecological Informatics 1, 391-406.

Johnson, J.E., Goldfinger, C., Suess, E., 2003. Geophysical constraints on the surface distribution of authigenic carbonates across the Hydrate Ridge region, Cascadia margin. Marine Geology 202, 79-120.

Jones, A.T., Greinert, J., Bowden, D.A., Klaucke, I., Petersen, C.J., Netzeband, G.L., Weinrebe, W., 2010. Acoustic and visual characterisation of methane-rich seabed seeps at Omakere Ridge on the Hikurangi Margin, New Zealand. Marine Geology 272, 154-169.

Joye, S.B., Boetius, A., Orcutt, B.N., Montoya, J.P., Schulz, H.N., Erickson, M.J., Lugo, S.K., 2004. The anaerobic oxidation of methane and sulfate reduction in sediments from Gulf of Mexico cold seeps. Chemical Geology 205, 219-238.

Judd, A.G., 2003. The global importance and context of methane escape from the seabed. Geo-Marine Letters 23, 147-154.

Judd, A.G., 2004. Natural seabed gas seeps as sources of atmospheric methane. Environmental Geology 46, 988-996.

Judd, A.G., Hovland, M., 2007. Seabed fluid flow - The impact on geology, biology, and the marine environment. Cambridge University Press.

Judd, A.G., Hovland, M., Dimitrov, L.I., Gil, S.G., Jukes, V., 2002. The geological methane budget at Continental Margins and its influence on climate change. Geofluids 2, 109-126.

Kennicutt II, M.C., Brooks, J.M., Bidigare, R.R., Denoux, G.J., 1988. Gulf of Mexico hydrocarbon seep communities--I. Regional distribution of hydrocarbon seepage and associated fauna. Deep Sea Research Part A. Oceanographic Research Papers 35, 1639-1651.

Kessler, J.D., Reeburgh, W.S., Southon, J., Seifert, R., Michaelis, W., Tyler, S.C., 2006a. Basin-wide estimates of the input of methane from seeps and clathrates to the Black Sea. Earth and Planetary Science Letters 243, 366-375.

Kessler, J.D., Reeburgh, W.S., Tyler, S.C., 2006b. Controls on methane concentration and stable isotope (δ^2H-CH_4 and δ^{13}C-CH_4) distributions in the water columns of the Black Sea and Cariaco Basin. Global Biogeochemical Cycles 20, GB4004.

Kessler, J.D., Valentine, D.L., Redmond, M.C., Du, M., Chan, E.W., Mendes, S.D., Quiroz, E.W., Villanueva, C.J., Shusta, S.S., Werra, L.M., Yvon-Lewis, S.A., Weber, T.C., 2011. A Persistent Oxygen Anomaly Reveals the Fate of Spilled Methane in the Deep Gulf of Mexico. Science 331, 312-315.

King, L.H., MacLean, B., 1970. Pockmarks on the Scotian Shelf. Geological Society of America (Bulletin) 81, 3141–3148.

Kinnaman, F., Kimball, J., Busso, L., Birgel, D., Ding, H., Hinrichs, K.-U., Valentine, D., 2010. Gas flux and carbonate occurrence at a shallow seep of thermogenic natural gas. Geo-Marine Letters 30, 355-365.

Klapp, S.A., Bohrmann, G., Kuhs, W.F., Mangir Murshed, M., Pape, T., Klein, H., Techmer, K.S., Heeschen, K.U., Abegg, F., 2010a. Microstructures of structure I and II gas hydrates from the Gulf of Mexico. Marine and Petroleum Geology 27, 116-125.

Klapp, S.A., Hemes, S., Klein, H., Bohrmann, G., MacDonald, I., Kuhs, W.F., 2010b. Grain size measurements of natural gas hydrates. Marine Geology 274, 85-94.

Klaucke, I., Masson, D.G., Petersen, C.J., Weinrebe, W., Ranero, C.R., 2008. Multifrequency geoacoustic imaging of fluid escape structures offshore Costa Rica: Implications for the quantification of seep processes. Geochem. Geophys. Geosyst. 9, Q04010.

Klaucke, I., Sahling, H., Weinrebe, W., Blinova, V., Bürk, D., Lursmanashvili, N., Bohrmann, G., 2006. Acoustic investigation of cold seeps offshore Georgia, eastern Black Sea. Marine Geology 231, 51-67.

Klaucke, I., Weinrebe, W., Petersen, C.J., Bowden, D., 2010. Temporal variability of gas seeps offshore New Zealand: Multi-frequency geoacoustic imaging of the Wairarapa area, Hikurangi margin. Marine Geology 272, 49-58.

Klauda, J.B., Sandler, S.I., 2005. Global Distribution of Methane Hydrate in Ocean Sediment. Energy & Fuels 19, 459-470.

Kopf, A.J., 2002. Significance of mud volcanism. Rev. Geophys. 40, 1005.

Körber, J.-H., Sahling, H., Pape, T., Dos Santos Ferreira, C., MacDonald, I., Bohrmann, G., submitted. Natural oil seepage at Kobuleti Ridge, eastern Black Sea. Marine and Petroleum Geology.

Kornacki, A.S., Kendrick, J.W., Berry, J.L., 1994. Impact of oil and gas vents and slicks on petroleum exploration in the deepwater Gulf of Mexico. Geo-Marine Letters 14, 160-169.

Korsakov, O., Byakov, Y., Stupak, S., 1989. Gas hydrates in the Black Sea Basin. International Geology Review 31, 1251 - 1257.

Kourogi, M., Kurata, T., Hoshino, J., Muraoka, Y., 1999. Real-time image mosaicing from a video sequence, Image Processing, 1999. ICIP 99. Proceedings. 1999 International Conference on, pp. 133-137 vol.134.

Kozlova, E.V., 2003. Petroleum potential revealed from geochemical study of mud volcano deposits (in Russian). Moscow State University.

Krastel, S., Spiess, V., Ivanov, M., Weinrebe, W., Bohrmann, G., Shashkin, P., Heidersdorf, F., 2003. Acoustic investigations of mud volcanoes in the Sorokin Trough, Black Sea. Geo-Marine Letters 23, 230-238.

Kruglyakova, R.P., Byakov, Y.A., Kruglyakova, M.V., Chalenko, L.A., Shevtsova, N.T., 2004. Natural oil and gas seeps on the Black Sea floor. Geo-Marine Letters 24, 150-162.

Krylova, E.M., Sahling, H., 2010. Vesicomyidae (Bivalvia): Current Taxonomy and Distribution. PLoS ONE 5, e9957.

Kukowski, N., Schillhorn, T., Flueh, E.R., Huhn, K., 2000. Newly identified strike-slip plate boundary in the northeastern Arabian Sea. Geology 28, 355-358.

Kukowski, N., Schillhorn, T., Huhn, K., von Rad, U., Husen, S., Flueh, E.R., 2001. Morphotectonics and mechanics of the central Makran accretionary wedge off Pakistan. Marine Geology 173, 1-19.

Kvenvolden, K.A., 1993. Gas hydrates: geological perspective and global change. Rev. Geophys. 31, 173-187.

Kvenvolden, K.A., Cooper, C.K., 2003. Natural seepage of crude oil into the marine environment. Geo-Marine Letters 23, 140-146.

Kvenvolden, K.A., Rogers, B.W., 2005. Gaia's breath--global methane exhalations. Marine and Petroleum Geology 22, 579-590.

Le Treut, H., Somerville, R., Cubasch, U., Ding, Y., Mauritzen, C., Mokssit, A., Peterson, T., Prather, M., 2007. Historical Overview of Climate Change, in: Solomon, S., Qin, D., Manning, M.R., Chen, Z., Marquis, M., Averyt, K.B., Tignor, M., Miller, H.L. (Eds.), Climate Change 2007: The Physical Science Basis. Contribution of Working Group I to the Fourth Assessment Report of the Intergovernmental Panel on Climate Change. Cambridge University Press Cambridge, United Kingdom and New York, NY, USA.

Leifer, I., Boles, J., 2005. Measurement of marine hydrocarbon seep flow through fractured rock and unconsolidated sediment. Marine and Petroleum Geology 22, 551-568.

Leifer, I., Clark, J.F., Chen, R.F., 2000. Modifications of the Local Environment by Natural Marine Hydrocarbon Seeps. Geophys. Res. Lett. 27.

Leifer, I., Judd, A.G., 2002. Oceanic methane layers: the hydrocarbon seep bubble deposition hypothesis. Terra Nova 14, 417-424.

Leifer, I., MacDonald, I., 2003. Dynamics of the gas flux from shallow gas hydrate deposits: interaction between oily hydrate bubbles and the oceanic environment. Earth and Planetary Science Letters 210, 411-424.

Leifer, I., Patro, R.K., 2002. The bubble mechanism for methane transport from the shallow sea bed to the surface: A review and sensitivity study. Continental Shelf Research 22, 2409-2428.

Lelieveld, J.O.S., Crutzen, P.J., Dentener, F.J., 1998. Changing concentration, lifetime and climate forcing of atmospheric methane. Tellus B 50, 128-150.

Levin, L., A. , Ziebis, W., Mendoza, G.F., Growney, V.A., Tryon, M.D., Brown, K.M., Mahn, C., Gieskes, J.M., Rathburn, A.E., 2003. Spatial heterogeneity of macrofauna at northern California methane seeps: influence of sulfide concentration and fluid flow. Marine Ecology Progress Series 265, 123-139.

Levin, L.A., 2005. Ecology of cold seep sediments: Interactions of fauna with flow, chemistry and microbes, in: Gibson, R.N., Atkinson, R.J.A., Gordon, J.D.M. (Eds.), Oceanography and Marine Biology: An Annual Review,, Taylor & Francis, p. 46.

Levy, E.M., Ehrhardt, M., 1981. Natural seepage of petroleum at Buchan Gulf, Baffin Island. Marine Chemistry 10, 355-364.

Li, C., Clark, A.L., 1991. SeaMARC II study of a giant submarine slump on the northern Chile continental slope. Marine Geotechnology 10, 257-268.

Lichtschlag, A., Felden, J., Wenzhöfer, F., Schubotz, F., Ertefai, T.F., Boetius, A., de Beer, D., 2010. Methane and sulfide fluxes in permanent anoxia: In situ studies at the Dvurechenskii mud volcano (Sorokin Trough, Black Sea). Geochimica et Cosmochimica Acta 74, 5002-5018.

Limonov, A.F., van Weering, T.C.E., Kenyon, N.H., Ivanov, M.K., Meisner, L.B., 1997. Seabed morphology and gas venting in the Black Sea mudvolcano area: Observations with the MAK-1 deep-tow sidescan sonar and bottom profiler. Marine Geology 137, 121-136.

Linke, P., Sommer, S., Rovelli, L., McGinnis, D.F., 2010. Physical limitations of dissolved methane fluxes: The role of bottom-boundary layer processes. Marine Geology 272, 209-222.

Linke, P., Wallmann, K., Suess, E., Hensen, C., Rehder, G., 2005. In situ benthic fluxes from an intermittently active mud volcano at the Costa Rica convergent margin. Earth and Planetary Science Letters 235, 79-95.

Logan, G.A., Jones, A.T., Kennard, J.M., Ryan, G.J., Rollet, N., 2010. Australian offshore natural hydrocarbon seepage studies, a review and re-evaluation. Marine and Petroleum Geology 27, 26-45.

Lorenson, T.D., Collett, T.S., Hunter, R.B., 2011. Gas geochemistry of the Mount Elbert Gas Hydrate Stratigraphic Test Well, Alaska North Slope: Implications for gas hydrate exploration in the Arctic. Marine and Petroleum Geology 28, 343-360.

Lüdmann, T., Wong, H.K., Konerding, P., Zillmer, M., Petersen, J., Flüh, E., 2004. Heat flow and quantity of methane deduced from a gas hydrate field in the vicinity of the Dnieper Canyon, northwestern Black Sea. Geo-Marine Letters 24, 182-193.

Luff, R., Wallmann, K., Aloisi, G., 2004. Numerical modeling of carbonate crust formation at cold vent sites: significance for fluid and methane budgets and chemosynthetic biological communities. Earth and Planetary Science Letters 221, 337-353.

Lurton, X., 2010. An introduction to underwater acoustics - Principles and applications, 2 ed. Springer, Heidelberg.

Luyendyk, B., Kennett, J., Clark, J.F., 2005. Hypothesis for increased atmospheric methane input from hydrocarbon seeps on exposed continental shelves during glacial low sea level. Marine and Petroleum Geology 22, 591-596.

MacDonald, I.R., Bender, L.C., Vardaro, M., Bernard, B., Brooks, J.M., 2005. Thermal and visual time-series at a seafloor gas hydrate deposit on the Gulf of Mexico slope. Earth and Planetary Science Letters 233, 45-59.

MacDonald, I.R., Boland, G.S., Baker, J.S., Brooks, J.M., Kennicutt, M.C., Bidigare, R.R., 1989. Gulf of Mexico hydrocarbon seep communities. Marine Biology 101, 235-247.

MacDonald, I.R., Guinasso, N.L., Jr., Ackleson, S.G., Amos, J.F., Duckworth, R., Sassen, R., Brooks, J.M., 1993. Natural Oil Slicks in the Gulf of Mexico Visible From Space. Journal of Geophysical Research 98, 351-364.

MacDonald, I.R., Guinasso, N.L., Jr., Sassen, R., Brooks, J.M., Lee, L., Scott, K.T., 1994. Gas hydrate that breaches the sea floor on the continental slope of the Gulf of Mexico. Geology 22, 699-702.

MacDonald, I.R., Leifer, I., Sassen, R., Stine, P., Mitchell, R., N. Guinasso, J., 2002. Transfer of hydrocarbons from natural seeps to the water column and atmosphere. Geofluids 2, 95-107.

MacDonald, I.R., Peccini, M.B., 2009. Distinct activity phases during the recent geologic history of a Gulf of Mexico mud volcano. Marine and Petroleum Geology 26, 1824-1830.

MacDonald, I.R., Russell Callender, W., Burke Jr, R.A., McDonald, S.J., Carney, R.S., 1990. Fine-scale distribution of methanotrophic mussels at a Louisiana cold seep. Progress In Oceanography 24, 15-24.

MacDonald, I.R., Sager, W.W., Peccini, M.B., 2003. Gas hydrate and chemosynthetic biota in mounded bathymetry at mid-slope hydrocarbon seeps: Northern Gulf of Mexico. Marine Geology 198, 133-158.

Macgregor, D.S., 1993. Relationships between seepage, tectonics and subsurface petroleum reserves. Marine and Petroleum Geology 10, 606-619.

Manga, M., Brumm, M., Rudolph, M.L., 2009. Earthquake triggering of mud volcanoes. Marine and Petroleum Geology 26, 1785-1798.

Marks, R.L., Rock, S.M., Lee, M.J., 1995. Real-time video mosaicking of the ocean floor. Oceanic Engineering, IEEE Journal of 20, 229-241.

Martin, J.B., Kastner, M., Henry, P., Le Pichon, X., Lallement, S., 1996. Chemical and isotopic evidence for sources of fluids in a mud volcano field seaward of the Barbados accretionary wedge. J. Geophys. Res. 101, 20325-20345.

Maslin, M., Mikkelsen, N., Vilela, C., Haq, B., 1998. Sea-level –and gas-hydrate–controlled catastrophic sediment failures of the Amazon Fan. Geology 26, 1107-1110.

Maslin, M., Owen, M., Betts, R., Day, S., Dunkley Jones, T., Ridgwell, A., 2010. Gas hydrates: past and future geohazard? Philosophical Transactions of the Royal Society A: Mathematical, Physical and Engineering Sciences 368, 2369-2393.

Maslin, M., Owen, M., Day, S., Long, D., 2004. Linking continental-slope failures and climate change: Testing the clathrate gun hypothesis. Geology 32, 53-56.

Mau, S., Heintz, M., Kinnaman, F., Valentine, D., 2010. Compositional variability and air-sea flux of ethane and propane in the plume of a large, marine seep field near Coal Oil Point, CA. Geo-Marine Letters 30, 367-378.

Mau, S., Sahling, H., Rehder, G., Suess, E., Linke, P., Soeding, E., 2006. Estimates of methane output from mud extrusions at the erosive convergent margin off Costa Rica. Marine Geology 225, 129-144.

Mazzini, A., Ivanov, M.K., Nermoen, A., Bahr, A., Bohrmann, G., Svensen, H., Planke, S., 2008. Complex plumbing systems in the near subsurface: Geometries of authigenic carbonates from Dolgovskoy Mound (Black Sea) constrained by analogue experiments. Marine and Petroleum Geology 25, 457-472.

Mazzini, A., Ivanov, M.K., Parnell, J., Stadnitskaia, A., Cronin, B.T., Poludetkina, E., Mazurenko, L., van Weering, T.C.E., 2004. Methane-related authigenic carbonates from the Black Sea: geochemical characterisation and relation to seeping fluids. Marine Geology 212, 153-181.

McGinnis, D.F., Greinert, J., Artemov, Y., Beaubien, S.E., Wüest, A., 2006. Fate of rising methane bubbles in stratified waters: How much methane reaches the atmosphere? Journal of Geophysical Research 111.

McInerney, F.A., Wing, S.L., 2011. The Paleocene-Eocene Thermal Maximum: A Perturbation of Carbon Cycle, Climate, and Biosphere with Implications for the Future. Annual Review of Earth and Planetary Sciences 39, 489-516.

McKenzie, D., Sclater, J.G., 1971. The evolution of the Indian Ocean since the late Cretaceous. Geophysical Journal of the Royal Astronomical Society 24, 437-528.

Meisner, A., Krylov, O., Nemcok, M., 2009. Development and structural architecture of the Eastern Black Sea. The Leading Edge 28, 1046-1055.

Meisner, L.B., Tugolesov, D.A., Khakhalev, E.M., 1996. The Western Black Sea Volcanic Mud Province. Oceanology 36, 119-127.

Mello, U.T., Karner, G.D., Anderson, R.N., 1994. A physical explanation for the positioning of the depth to the top of overpressure in shale-dominated sequences in the Gulf Coast basin, United States. J. Geophys. Res. 99, 2775-2789.

Melsheimer, C., Alpers, W., Gade, M., 2001. Simultaneous observations of rain cells over the ocean by the synthetic aperture radar aboard the ERS satellites and by surface-based weather radars. J. Geophys. Res. 106, 4665-4677.

Meredith, D.J., Egan, S.S., 2002. The geological and geodynamic evolution of the eastern Black Sea basin: insights from 2-D and 3-D tectonic modelling. Tectonophysics 350, 157-179.

Merewether, R., Olsson, M.S., Lonsdale, P., 1985. Acoustically Detected Hydrocarbon Plumes Rising From 2-km Depths in Guaymas Basin, Gulf of California. J. Geophys. Res. 90.

Michaelis, W., Seifert, R., Nauhaus, K., Treude, T., Thiel, V., Blumenberg, M., Knittel, K., Gieseke, A., Peterknecht, K., Pape, T., Boetius, A., Amann, R., Jorgensen, B.B., Widdel, F., Peckmann, J., Pimenov, N.V., Gulin, M.B., 2002. Microbial Reefs in the Black Sea Fueled by Anaerobic Oxidation of Methane. Science 297, 1013-1015.

Mienert, J., Vanneste, M., Bünz, S., Andreassen, K., Haflidason, H., Sejrup, H.P., 2005. Ocean warming and gas hydrate stability on the mid-Norwegian margin at the Storegga Slide. Marine and Petroleum Geology 22, 233-244.

Milkov, A.V., 2000. Worldwide distribution of submarine mud volcanoes and associated gas hydrates. Marine Geology 167, 29-42.

Milkov, A.V., Vogt, P.R., Crane, K., Lein, A.Y., Sassen, R., Cherkashev, G.A., 2004. Geological, geochemical, and microbial processes at the hydrate-bearing Håkon Mosby mud volcano: a review. Chemical Geology 205, 347-366.

Minshull, T., White, R., 1989. Sediment Compaction and Fluid Migration in the Makran Accretionary Prism. J. Geophys. Res. 94.

Minshull, T.A., Keddie, A., 2010. Measuring the geotherm with gas hydrate bottom-simulating reflectors: a novel approach using three-dimensional seismic data from the eastern Black Sea. Terra Nova 22, 131-136.

Minster, J.B., Jordan, T.H., 1978. Present-day plate motions. J. Geophys. Res. 83.

Mitchell, R., MacDonald, I.R., Kvenvolden, K.A., 1999. Estimation of total hydrocarbon seepage into the Gulf of Mexico based on satellite remote sensing images, Transamerican Geophysical Union Ocean Science Meeting Supplement OS242.

Mulder, T., Cochonat, P., 1996. Classification of offshore mass movements. Journal of Sedimentary research 66, 43-57.

Murray, J.W., Jannasch, H.W., Honjo, S., Anderson, R.F., Reeburgh, W.S., Top, Z., Friederich, G.E., Codispoti, L.A., Izdar, E., 1989. Unexpected changes in the oxic/anoxic interface in the Black Sea. Nature 338, 411-413.

Murray, J.W., Top, Z., Özsoy, E., 1991. Hydrographic properties and ventilation of the Black Sea. Deep Sea Research Part A. Oceanographic Research Papers 38, S663-S689.

Murton, B.J.R., I.P.; Millard, N.W.; Flewellen, C.G., 1992. Multisensor, deep-towed instrument explores the ocean floor. EOS, Transactions American Geophysical Union 73, 225.

Naehr, T.H., Stakes, D.S., Moore, W.S., 2000. Mass wasting, ephemeral fluid flow, and barite deposition on the California continental margin. Geology 28, 315-318.

Naudts, L., Greinert, J., Artemov, Y., Staelens, P., Poort, J., Van Rensbergen, P., De Batist, M., 2006. Geological and morphological setting of 2778 methane seeps in the Dnepr paleo-delta, northwestern Black Sea. Marine Geology 227, 177-199.

Naudts, L., Greinert, J., Poort, J., Belza, J., Vangampelaere, E., Boone, D., Linke, P., Henriet, J.-P., De Batist, M., 2010. Active venting sites on the gas-hydrate-bearing Hikurangi Margin, off New Zealand: Diffusive- versus bubble-released methane. Marine Geology 272, 233-250.

Nauhaus, K., Boetius, A., Krüger, M., Widdel, F., 2002. In vitro demonstration of anaerobic oxidation of methane coupled to sulphate reduction in sediment from a marine gas hydrate area. Environmental Microbiology 4, 296-305.

Nicosevici, T., Gracias, N., Negahdaripour, S., Garcia, R., 2009. Efficient three-dimensional scene modeling and mosaicing. Journal of Field Robotics 26, 759-788.

Niemann, H., Losekann, T., de Beer, D., Elvert, M., Nadalig, T., Knittel, K., Amann, R., Sauter, E.J., Schluter, M., Klages, M., Foucher, J.P., Boetius, A., 2006. Novel microbial communities of the Haakon Mosby mud volcano and their role as a methane sink. Nature 443, 854-858.

Nikishin, A.M., Korotaev, M.V., Ershov, A.V., Brunet, M.-F., 2003. The Black Sea basin: tectonic history and Neogene-Quaternary rapid subsidence modelling. Sedimentary Geology 156, 149-168.

Nikolovska, A., Sahling, H., Bohrmann, G., 2008. Hydroacoustic methodology for detection, localization, and quantification of gas bubbles rising from the seafloor at gas seeps from the eastern Black Sea. Geochemistry Geophysics Geosystems 9, 13.

Nisbet, E.G., 1990. The end of the ice age. Canadian Journal of Earth Sciences 27, 148-157.

Olu-Le Roy, K., Caprais, J.C., Fifis, A., Fabri, M.C., Galéron, J., Budzinsky, H., Le Ménach, K., Khripounoff, A., Ondréas, H., Sibuet, M., 2007. Cold-seep assemblages on a giant pockmark off West Africa: spatial patterns and environmental control. Marine Ecology 28, 115-130.

Olu, K., Caprais, J.C., Galéron, J., Causse, R., von Cosel, R., Budzinski, H., Ménach, K.L., Roux, C.L., Levaché, D., Khripounoff, A., Sibuet, M., 2009. Influence of seep emission on the non-symbiont-bearing fauna and vagrant species at an active giant pockmark in the Gulf of Guinea (Congo-Angola margin). Deep Sea Research Part II: Topical Studies in Oceanography 56, 2380-2393.

Olu, K., Duperret, A., Sibuet, M., Foucher, J.P., Fiala-Médioni, A., 1996. Structure and distribution of cold seep communities along the Peruvian active margin: relationship to geological and fluid patterns. Marine Ecology Progress Series 132, 109-125.

Ondréas, H., Olu, K., Fouquet, Y., Charlou, J., Gay, A., Dennielou, B., Donval, J., Fifis, A., Nadalig, T., Cochonat, P., Cauquil, E., Bourillet, J., Moigne, M., Sibuet, M., 2005. ROV study of a giant pockmark on the Gabon continental margin. Geo-Marine Letters 25, 281-292.

Orange, D.L., Greene, H.G., Reed, D., Martin, J.B., McHugh, C.M., Ryan, W.B.F., Maher, N., Stakes, D., Barry, J., 1999a. Widespread fluid expulsion on a translational continental margin: Mud volcanoes, fault zones, headless canyons, and organic-rich substrate in Monterey Bay, California. Geological Society of America Bulletin 111, 992-1009.

Orange, D.L., Angell, M., Lapp, D., 1999b. Applications of multibeam mapping to exploration and production; detecting seeps, mapping geohazards, and managing data overload with GIS. The Leading Edge 18, 495-501.

Orange, D.L., Breen, N.A., 1992. The Effects of Fluid Escape on Accretionary Wedges 2. Seepage Force, Slope Failure, Headless Submarine Canyons, and Vents. J. Geophys. Res. 97.

Orange, D.L., Yun, J., Maher, N., Barry, J., Greene, G., 2002. Tracking California seafloor seeps with bathymetry, backscatter and ROVs. Continental Shelf Research 22, 2273-2290.

Osborne, M.J., Swarbrick, R.E., 1997. Mechanisms for generating overpressure in sedimentary basins; a reevaluation. AAPG Bulletin 81, 1023-1041.

Özsoy, E., Ünlüata, Ü., 1997. Oceanography of the Black Sea: A review of some recent results. Earth-Science Reviews 42, 231-272.

Page, D.S., Boehm, P.D., Douglas, G.S., Bence, A.E., Burns, W.A., Mankiewicz, P.J., 1997. An estimate of the annual input of natural petroleum hydrocarbons to seafloor sediments in prince William Sound, Alaska. Marine Pollution Bulletin 34, 744-749.

Palacas, J.G., Monopolis, D., Nicolaou, C.A., Anders, D.E., 1986. Geochemical correlation of surface and subsurface oils, western Greece. Organic Geochemistry 10, 417-423.

Pape, T., Bahr, A., Klapp, S.A., Abegg, F., Bohrmann, G., 2011. High-intensity gas seepage causes rafting of shallow gas hydrates in the southeastern Black Sea. Earth and Planetary Science Letters 307, 35-46.

Pape, T., Bahr, A., Rethemeyer, J., Kessler, J.D., Sahling, H., Hinrichs, K.-U., Klapp, S.A., Reeburgh, W.S., Bohrmann, G., 2010. Molecular and isotopic partitioning of low-molecular-weight hydrocarbons during migration and gas hydrate precipitation in deposits of a high-flux seepage site. Chemical Geology 269, 350-363.

Pape, T., Blumenberg, M., Seifert, R., Bohrmann, G., Michaelis, W., 2008. Marine Methane Biogeochemistry of the Black Sea: A Review, in: Dilek, Y., Furnes, H., Muehlenbachs, K. (Eds.), Links Between Geological Processes, Microbial Activities and Evolution of Life. Springer Netherlands, pp. 281-311.

Parsons, B.S., Vogt, P.R., Haflidason, H., Jung, W.-Y., 2005. Sidescan and video exploration of the Storegga slide headwall region by submarine NR-1. Marine Geology 219, 195-205.

Paull, C.K., Buelow, W.J., Ussler, W., Borowski, W.S., 1996. Increased continental-margin slumping frequency during sea-level lowstands above gas hydrate–bearing sediments. Geology 24, 143-146.

Paull, C.K., Normark, W.R., Ussler Iii, W., Caress, D.W., Keaten, R., 2008. Association among active seafloor deformation, mound formation, and gas hydrate growth and accumulation within the seafloor of the Santa Monica Basin, offshore California. Marine Geology 250, 258-275.

Paull, C.K., Ussler, W., Borowski, W.S., Spiess, F.N., 1995. Methane-rich plumes on the Carolina continental rise: Associations with gas hydrates. Geology 23, 89-92.

Peckmann, J., Reimer, A., Luth, U., Luth, C., Hansen, B.T., Heinicke, C., Hoefs, J., Reitner, J., 2001. Methane-derived carbonates and authigenic pyrite from the northwestern Black Sea. Marine Geology 177, 129-150.

Pellon de Miranda, F., Marmol, A.M.Q., Pedroso, E.C., Beisl, C.H., Welgan, P., Morales, L.M., 2004. Analysis of RADARSAT-1 data for offshore monitoring activities in the Cantarell Complex, Gulf of Mexico, using the unsupervised semivariogram textural classifier (USTC). Canadian Journal of Remote Sensing 30, 424-436.

Platt, J.P., Leggett, J.K., Young, J., Raza, H., Alam, S., 1985. Large-scale sediment underplating in the Makran accretionary prism, southwest Pakistan. Geology 13, 507-511.

Plaza-Faverola, A., Bünz, S., Mienert, J., 2011. Repeated fluid expulsion through sub-seabed chimneys offshore Norway in response to glacial cycles. Earth and Planetary Science Letters 305, 297-308.

Poort, J., Kutas, R., Klerkx, J., Beaubien, S., Lombardi, S., Dimitrov, L., Vassilev, A., Naudts, L., 2007. Strong heat flow variability in an active shallow gas environment, Dnepr palaeo-delta, Black Sea. Geo-Marine Letters 27, 185-195.

Popescu, I., De Batist, M., Lericolais, G., Nouzé, H., Poort, J., Panin, N., Versteeg, W., Gillet, H., 2006. Multiple bottom-simulating reflections in the Black Sea: Potential proxies of past climate conditions. Marine Geology 227, 163-176.

Popescu, I., Lericolais, G., Panin, N., De Batist, M., Gillet, H., 2007. Seismic expression of gas and gas hydrates across the western Black Sea. Geo-Marine Letters 27, 173-183.

Ranero, C.R., Grevemeyer, I., Sahling, H., Barckhausen, U., Hensen, C., Wallmann, K., Weinrebe, W., Vannucchi, P., von Huene, R., McIntosh, K., 2008. Hydrogeological system of erosional convergent margins and its influence on tectonics and interplate seismogenesis. Geochem. Geophys. Geosyst. 9, Q03S04.

Rangin, C., Bader, A.G., Pascal, G., Ecevitoglu, B., Görür, N., 2002. Deep structure of the Mid Black Sea High (offshore Turkey) imaged by multi-channel seismic survey (BLACKSIS cruise). Marine Geology 182, 265-278.

Reeburgh, S., W., Ward, B., B., Whalen, C., S., Sandbeck, A., K., Kilpatrick, Kerkhof, J., L., 1991. Black Sea methane geochemistry. Pergamon, Oxford.

Reeburgh, W.S., 1976. Methane consumption in Cariaco Trench waters and sediments. Earth and Planetary Science Letters 28, 337-344.

Rehder, G., Brewer, P.W., Peltzer, E.T., Friederich, G., 2002. Enhanced lifetime of methane bubble streams within the deep ocean. Geophysical Research Letters 29.

Rehder, G., Leifer, I., Brewer, P.G., Friederich, G., Peltzer, E.T., 2009. Controls on methane bubble dissolution inside and outside the hydrate stability field from open ocean field experiments and numerical modeling. Marine Chemistry 114, 19-30.

Reitz, A., Pape, T., Haeckel, M., Schmidt, M., Berner, U., Scholz, F., Liebetrau, V., Aloisi, G., Weise, S.M., Wallmann, K., 2011. Sources of fluids and gases expelled at cold seeps offshore Georgia, eastern Black Sea. Geochimica et Cosmochimica Acta 75, 3250-3268.

Rice, D.D., Claypool, G.E., 1981. Generation, accumulation, and resource potential of biogenic gas. AAPG Bulletin 65, 5-25.

Riedel, M., Rohr, K.M.M., 2012. Gas hydrate within the Winona Basin, offshore western Canada. Marine and Petroleum Geology 30, 66-80.

Roberts, J.J., Best, B.D., Dunn, D.C., Treml, E.A., Halpin, P.N., 2010. Marine Geospatial Ecology Tools: An integrated framework for ecological geoprocessing with ArcGIS, Python, R, MATLAB, and C++. Environmental Modelling & Software 25, 1197-1207.

Robinson, A.G., Griffith, E.T., Gardiner, A.R., Home, A.K., 1997. Petroleum geology of the Georgian fold and thrust belts and foreland basins, in: Robinson, A.G. (Ed.), Regional and petroleum geology of the Black Sea and surrounding region. AAPG, Tusla, pp. 347-367.

Robinson, A.G., Rudat, J.H., Banks, C.J., Wiles, R.L.F., 1996. Petroleum geology of the Black Sea. Marine and Petroleum Geology 13, 195-223.

Römer, M., Sahling, H., Pape, T., Bahr, A., Feseker, T., Wintersteller, P., Bohrmann, G., *in press*. Geological control and quantity of gas bubbles emanating from high-flux seep areas in the Black Sea - The Kerch Seep Area. Marine Geology.

Römer, M., Sahling, H., Pape, T., Bohrmann, G., Spiess, V., *submitted*. Methane bubble emission at the Makran continetal margin (offshore Pakistan). Journal of Geophysical Research.

Rosenzweig, C., Karoly, D., Vicarelli, M., Neofotis, P., Wu, Q., Casassa, G., Menzel, A., Root, T.L., Estrella, N., Seguin, B., Tryjanowski, P., Liu, C., Rawlins, S., Imeson, A., 2008. Attributing physical and biological impacts to anthropogenic climate change. Nature 453, 353-357.

Ross, D.A., Degens, E.T., MacIlvaine, J., 1970. Black Sea: Recent Sedimentary History. Science 170, 163-165.

Ross, D.A., Uchupi, E., Prada, K.E., MacIlvaine, J., 1974. Bathymetry and Microtopography of Black Sea, in: Degens, E.T., Ross, D.A. (Eds.), The Black Sea - Geology, Chemistry, and Biology. AAPG, Tulsa, Oklahoma, pp. 1-10.

Rothwell, R.G., Thomson, J., Kahler, G., 1998. Low-sea-level emplacement of a very large Late Pleistocene /`megaturbidite/' in the western Mediterranean Sea. Nature 392, 377-380.

Sahling, H., Bohrmann, G., Artemov, Y.G., Bahr, A., Brüning, M., Klapp, S.A., Klaucke, I., Kozlova, E., Nikolovska, A., Pape, T., Reitz, A., Wallmann, K., 2009. Vodyanitskii mud volcano, Sorokin trough, Black Sea: Geological characterization and quantification of gas bubble streams. Marine and Petroleum Geology 26, 1799-1811.

Sahling, H., Bohrmann, G., Spiess, V., Bialas, J., Breitzke, M., Ivanov, M., Kasten, S., Krastel, S., Schneider, R., 2008a. Pockmarks in the Northern Congo Fan area, SW Africa: Complex seafloor features shaped by fluid flow. Marine Geology 249, 206-225.

Sahling, H., Masson, D.G., Ranero, C.R., Hühnerbach, V., Weinrebe, W., Klaucke, I., Bürk, D., Brückmann, W., Suess, E., 2008b. Fluid seepage at the continental margin offshore Costa Rica and southern Nicaragua. Geochem. Geophys. Geosyst. 9.

Sahling, H., Rickert, D., W. Lee, R., Linke, P., Suess, E., 2002. Macrofaunal community structure and sulfide flux at gas hydrate deposits from the Cascadia convergent margin, NE Pacific. Marine Ecology Progress Series 231, 17.

Sain, K., Minshull, T.A., Singh, S.C., Hobbs, R.W., 2000. Evidence for a thick free gas layer beneath the bottom simulating reflector in the Makran accretionary prism. Marine Geology 164, 9.

Salisbury, J.W., D'Aria, D.M., Sabins Jr, F.F., 1993. Thermal infrared remote sensing of crude oil slicks. Remote Sensing of Environment 45, 225-231.

Sassen, R., Sweet, S.T., Milkov, A.V., DeFreitas, D.A., Kennicutt, M.C., 2001a. Thermogenic vent gas and gas hydrate in the Gulf of Mexico slope: Is gas hydrate decomposition significant? Geology 29, 107-110.

Sassen, R., Sweet, S.T., DeFreitas, D.A., Morelos, J.A., Milkov, A.V., 2001b. Gas hydrate and crude oil from the Mississippi Fan Foldbelt, downdip Gulf of Mexico Salt Basin: significance to petroleum system. Organic Geochemistry 32, 999-1008.

Sauter, E.J., Muyakshin, S.I., Charlou, J.-L., Schlüter, M., Boetius, A., Jerosch, K., Damm, E., Foucher, J.-P., Klages, M., 2006. Methane discharge from a deep-sea submarine mud volcano into the upper water column by gas hydrate-coated methane bubbles. Earth and Planetary Science Letters 243, 354-365.

Schlüter, H.U., Prexl, A., Gaedicke, C., Roeser, H., Reichert, C., Meyer, H., von Daniels, C., 2002. The Makran accretionary wedge: sediment thicknesses and ages and the origin of mud volcanoes. Marine Geology 185, 219-232.

Schmale, O., Beaubien, S.E., Rehder, G., Greinert, J., Lombardi, S., 2010. Gas seepage in the Dnepr paleo-delta area (NW-Black Sea) and its regional impact on the water column methane cycle. Journal of Marine Systems 80, 90-100.

Schmale, O., Greinert, J., Rehder, G., 2005. Methane emission from high-intensity marine gas seeps in the Black Sea into the atmosphere. Geophysical Research Letters 32.

Schmale, O., Haeckel, M., McGinnis, D.F., 2011. Response of the Black Sea methane budget to massive short-term submarine inputs of methane. Biogeosciences 8, 911-918.

Schmaljohann, R., Drews, M., Walter, S., Linke, P., von Rad, U., Imhoff, J.F., 2001. Oxygen-minimum zone sediments in the northeastern Arabian Sea off Pakistan: a habitat for the bacterium Thioploca. Marine Ecology Progress Series 211, 27-42.

Schneider von Deimling, J., Brockhoff, J., Greinert, J., 2007. Flare imaging with multibeam systems: Data processing for bubble detection at seeps. Geochem. Geophys. Geosyst. 8.

Schneider von Deimling, J., Rehder, G., Greinert, J., McGinnnis, D.F., Boetius, A., Linke, P., 2011. Quantification of seep-related methane gas emissions at Tommeliten, North Sea. Continental Shelf Research 31, 867-878.

Schoell, M., 1988. Multiple origins of methane in the Earth. Chemical Geology 71, 1-10.

Scott, C.L., Shillington, D.J., Minshull, T.A., Edwards, R.A., Brown, P.J., White, N.J., 2009. Wide-angle seismic data reveal extensive overpressures in the Eastern Black Sea Basin. Geophysical Journal International 178, 1145-1163.

Selley, R., 1998. Elements of Petroleum Geology, 2 ed. Academic Press, San Diego.

Serié, C., Huuse, M., Schødt, N.H., 2012. Gas hydrate pingoes: Deep seafloor evidence of focused fluid flow on continental margins. Geology 40, 207-210.

Shakhova, N., Semiletov, I., Salyuk, A., Yusupov, V., Kosmach, D., Gustafsson, Ö., 2010. Extensive Methane Venting to the Atmosphere from Sediments of the East Siberian Arctic Shelf. Science 327, 1246-1250.

Shipley, T.H., Houston, M.H., Buffler, R.T., Shaub, F.J., McMillen, K.J., Ladd, J.W., Worzel, J.L., 1979. Seismic evidence for widespread possible gas hydrate horizons on continental slopes and rises. AAPG Bulletin 63, 2204-2213.

Sibuet, M., Juniper, K.S., Pautot, G., 1988. Cold-seep benthic communities in the Japan subduction zones: Geological control of community development. Journal of Marine Research 46, 333-348.

Sibuet, M., Olu, K., 1998. Biogeography, biodiversity and fluid dependence of deep-sea cold-seep communities at active and passive margins. Deep Sea Research Part II: Topical Studies in Oceanography 45, 517-567.

Sibuet, M., Vangriesheim, A., 2009. Deep-sea environment and biodiversity of the West African Equatorial margin. Deep Sea Research Part II: Topical Studies in Oceanography 56, 2156-2168.

Singh, H., Howland, J., Pizarro, O., 2004. Advances in large-area photomosaicking underwater. Oceanic Engineering, IEEE Journal of 29, 872-886.

Sloan, E.D., 2003. Fundamental principles and applications of natural gas hydrates. Nature 426, 353-363.

Solberg, A.H.S., Brekke, C., 2008. Oil Spill Detection in Northern European Waters: Approaches and Algorithms, pp. 359-370.

Solberg, A.H.S., Brekke, C., Husoy, P.O., 2007. Oil Spill Detection in Radarsat and Envisat SAR Images. Geoscience and Remote Sensing, IEEE Transactions on 45, 746-755.

Solomon, E.A., Kastner, M., MacDonald, I.R., Leifer, I., 2009. Considerable methane fluxes to the atmosphere from hydrocarbon seeps in the Gulf of Mexico. Nature Geoscience 2, 561-565.

Sommer, S., Linke, P., Pfannkuche, O., Schleicher, T., Schneider v. Deimling, J., Reitz, A., Haeckel, M., Fl, xf, gel, S., Hensen, C., 2009. Seabed methane emissions and the habitat of frenulate tubeworms on the Captain Arutyunov mud volcano (Gulf of Cadiz). Marine Ecology Progress Series 382, 69-86.

Sommer, S., Pfannkuche, O., Linke, P., Luff, R., Greinert, J., Drews, M., Gubsch, S., Pieper, M., Poser, M., Viergutz, T., 2006. Efficiency of the benthic filter: Biological control of the emission of dissolved methane from sediments containing shallow gas hydrates at Hydrate Ridge. Global Biogeochem. Cycles 20.

Stadnitskaia, A., Blinova, V., Ivanov, M.K., Baas, M., Hopmans, E., van Weering, T.C.E., Sinninghe Damsté, J.S., 2007. Lipid biomarkers in sediments of mud volcanoes from the Sorokin Trough, NE Black Sea: Probable source strata for the erupted material. Organic Geochemistry 38, 67-83.

Stadnitskaia, A., Ivanov, M.K., Poludetkina, E.N., Kreulen, R., van Weering, T.C.E., 2008. Sources of hydrocarbon gases in mud volcanoes from the Sorokin Trough, NE Black Sea, based on molecular and carbon isotopic compositions. Marine and Petroleum Geology 25, 1040-1057.

Staneva, J.V., Dietrich, D.E., Stanev, E.V., Bowman, M.J., 2001. Rim current and coastal eddy mechanisms in an eddy-resolving Black Sea general circulation model. Journal of Marine Systems 31, 137-157.

Starostenko, V., Buryanov, V., Makarenko, I., Rusakov, O., Stephenson, R., Nikishin, A., Georgiev, G., Gerasimov, M., Dimitriu, R., Legostaeva, O., Pchelarov, V., Sava, C., 2004. Topography of the crust–mantle boundary beneath the Black Sea Basin. Tectonophysics 381, 211-233.

Suess, E., 2010. Marine Cold Seeps. Handbook of Hydrocarbon and Lipid Microbiology, in: Timmis, K.N. (Ed.). Springer Berlin Heidelberg, pp. 185-203.

Suess, E., Torres, M.E., Bohrmann, G., Collier, R.W., Goldfinger, C., Linke, P., Heuser, A., Sahling, H., Heeschen, K., Jung, C., Nakamura, K., Greinert, J., Pfannkuche, O., Trehu, A., Klinkhammer, G.P., Whiticar, M.J., Eisenhauer, A., Teichert, B., Elvert, M., 2001. Sea floor methane hydrates at Hydrate Ridge, Cascadia margin, in: Paull, C.K., Dillion, W.P. (Eds.), Natural gas hydrates: occurence, distribution, and detection. American Geophysical Union, pp. 1-15.

Talukder, A.R., 2012. Review of submarine cold seep plumbing systems: leakage to seepage and venting. Terra Nova, no-no.

Taylor, R., Vine, N., York, A., Lerner, S., Hart, D., Howland, J., Prasad, L., Mayer, L., Gallager, S., 2008. Evolution of a benthic imaging system from a towed camera to an automated habitat characterization system, OCEANS 2008, pp. 1-7.

Thrasher, J., Fleet, A.J., Hay, S.J., Hovland, M., Düppenbecker, S., 1996. Understanding geology as the key to using seepage in exploration: spectrum of seepage styles, in: Schumacher, D., Abrams, M.A. (Eds.), AAPG Memoir. AAPG, Tusla, pp. 223-241.

Tissot, B.P., Welte, D.H., 1984. Petroleum Formation and Occurrence, 2 ed. Springer-Verlag.

Topouzelis, K., 2008. Oil Spill Detection by SAR Images: Dark Formation Detection, Feature Extraction and Classification Algorithms. Sensors 8, 6642-6659.

Torres, M.E., Embley, R.W., Merle, S.G., Trehu, A.M., Collier, R.W., Suess, E., Heeschen, K.U., 2009. Methane sources feeding cold seeps on the shelf and upper continental slope off central Oregon, USA. Geochem. Geophys. Geosyst. 10.

Torres, M.E., McManus, J., Hammond, D.E., de Angelis, M.A., Heeschen, K.U., Colbert, S.L., Tryon, M.D., Brown, K.M., Suess, E., 2002. Fluid and chemical fluxes in and out of sediments hosting methane hydrate deposits on Hydrate Ridge, OR, I: Hydrological provinces. Earth and Planetary Science Letters 201, 525-540.

Torres, M.E., Wallmann, K., Tréhu, A.M., Bohrmann, G., Borowski, W.S., Tomaru, H., 2004. Gas hydrate growth, methane transport, and chloride enrichment at the southern summit of Hydrate Ridge, Cascadia margin off Oregon. Earth and Planetary Science Letters 226, 225-241.

Traynor, J.J., Sladen, C., 1997. Seepage in Vietnam — onshore and offshore examples. Marine and Petroleum Geology 14, 345-362.

Tréhu, A.M., Torres, M.E., Moore, G.F., Suess, E., Bohrmann, G., 1999. Temporal and spatial evolution of a gas hydrate–bearing accretionary ridge on the Oregon continental margin. Geology 27, 939-942.

Treude, T., Boetius, A., Knittel, K., Wallmann, K., Jørgensen, B.B., 2003. Anaerobic oxidation of methane above gas hydrates at Hydrate Ridge, NE Pacific Ocean. Marine Ecology Progress Series 264, 1-14.

Tugolesov, D.A., Gorshkov, A.S., Meisner, L.B., Soloviev, V.V., 1985. Tectonics of the Mesozoic-Cenozoic Deposits of the Black Sea Basin (in Russian). Nedra, Moscow.

Tugolesov, D.A., Gorshkov, A.S., Meisner, L.B., Soloviev, V.V., Khakhalev, E.M., 1983. Geolocical structure of the Black Sea basin (in Russian). Akad Nauk SSSR, pp. 440-444.

Tugolesov, D.A., Meisner, L.B., 2002. Evaluation of the rates of sedimentation and tectonic subsidence with reference to the Black Sea basin. Geotectonics 36, 81-88.

Udachin, K.A., Lu, H., Enright, G.D., Ratcliffe, C.I., Ripmeester, J.A., Chapman, N.R., Riedel, M., Spence, G., 2007. Single Crystals of Naturally Occurring Gas Hydrates: The Structures of Methane and Mixed Hydrocarbon Hydrates. Angewandte Chemie International Edition 46, 8220-8222.

Ussler III, W., Paull, C.K., Boucher, J., Friederich, G.E., Thomas, D.J., 2003. Submarine pockmarks: a case study from Belfast Bay, Maine. Marine Geology 202, 175-192.

Valentine, D.L., Blanton, D.C., Reeburgh, W.S., Kastner, M., 2001. Water column methane oxidation adjacent to an area of active hydrate dissociation, Eel river Basin. Geochimica et Cosmochimica Acta 65, 2633-2640.

Van Dover, C.L., Aharon, P., Bernhard, J.M., Caylor, E., Doerries, M., Flickinger, W., Gilhooly, W., Goffredi, S.K., Knick, K.E., Macko, S.A., Rapoport, S., Raulfs, E.C., Ruppel, C., Salerno, J.L., Seitz, R.D., Sen Gupta, B.K., Shank, T., Turnipseed, M., Vrijenhoek, R., 2003. Blake Ridge methane seeps: characterization of a soft-sediment, chemosynthetically based ecosystem. Deep Sea Research Part I: Oceanographic Research Papers 50, 281-300.

Vaughn Barrie, J., Cook, S., Conway, K.W., 2011. Cold seeps and benthic habitat on the Pacific margin of Canada. Continental Shelf Research 31, S85-S92.

von Huene, R., Scholl, D.W., 1991. Observations at convergent margins concerning sediment subduction, subduction erosion, and the growth of continental crust. Rev. Geophys. 29, 279-316.

von Rad, U., Berner, U., Delisle, G., Doose-Rolinski, H., Fechner, N., Linke, P., Lückge, A., Roeser, H.A., Schmaljohann, R., Wiedicke, M., Parties, S.S., Block, M., Damm, V., Erbacher, J., Fritsch, J., Harazim, B., Poggenburg, J., Scheeder, G., Schreckenberger, B., von Mirbach, N., Drews, M., Walter, S., Ali Khan, A., Inam, A., Tahir, M., Tabrez, A.R., Cheema, A.H., Pervaz, M., Ashraf, M., 2000. Gas and fluid venting at the Makran accretionary wedge off Pakistan. Geo-Marine Letters 20, 10-19.

von Rad, U., Rösch, H., Berner, U., Geyh, M., Marchig, V., Schulz, H., 1996. Authigenic carbonates derived from oxidized methane vented from the Makran accretionary prism off Pakistan. Marine Geology 136, 55-77.

von Rad, U., Schulz, H., Sonne 90 Scientific, P., Khan, A.A., Ansari, M., Berner, U., Cepek, P., Cowie, G., Dietrich, P., Erlenkeuser, H., Geyh, M., Jennerjahn, T., Lückge, A., Marchig, V., Riech, V., Rösch, H., Schäfer, P., Schulte, S., Sirocko, F., Tahir, M., Weiss, W., 1995. Sampling the oxygen minimum zone off Pakistan: glacial-interglacial variations of anoxia and productivity (preliminary results, 90 cruise). Marine Geology 125, 7-19.

Wagner-Friedrichs, M., 2007. Seafloor seepage in the Black Sea: mud volcanoes, seeps and diapiric structures imaged by acoustic methods, Faculty of Geosciences. University of Bremen, Bremen.

Wagner-Friedrichs, M., Krastel, S., Spiess, V., Ivanov, M., Bohrmann, G., Meisner, L., 2008. Three-dimensional seismic investigations of the Sevastopol mud volcano in correlation to gas/fluid migration pathways and indications for gas hydrate occurrences in the Sorokin Trough (Black Sea). Geochem. Geophys. Geosyst. 9, Q05012.

Westbrook, G.K., Thatcher, K.E., Rohling, E.J., Piotrowski, A.M., Pälike, H., Osborne, A.H., Nisbet, E.G., Minshull, T.A., Lanoisellé, M., James, R.H., Hühnerbach, V., Green, D., Fisher, R.E., Crocker, A.J., Chabert, A., Bolton, C., Beszczynska-Möller, A., Berndt, C., Aquilina, A., 2009. Escape of methane gas from the seabed along the West Spitsbergen continental margin. Geophys. Res. Lett. 36, L15608.

Wettle, M., Daniel, P.J., Logan, G.A., Thankappan, M., 2009. Assessing the effect of hydrocarbon oil type and thickness on a remote sensing signal: A sensitivity study based on the optical properties of two different oil types and the HYMAP and Quickbird sensors. Remote Sensing of Environment 113, 2000-2010.

Whelan, J., Eglinton, L., Cathles Iii, L., Losh, S., Roberts, H., 2005. Surface and subsurface manifestations of gas movement through a N-S transect of the Gulf of Mexico. Marine and Petroleum Geology 22, 479-497.

White, R.S., 1982. Deformation of the Makran accretionary sediment prism in the Gulf of Oman (north-west Indian Ocean). Geological Society, London, Special Publications 10, 357-372.

White, R.S., Klitgord, K., 1976. Sediment deformation and plate tectonics in the Gulf of Oman. Earth and Planetary Science Letters 32, 199-209.

Whiticar, M.J., 1999. Carbon and hydrogen isotope systematics of bacterial formation and oxidation of methane. Chemical Geology 161, 291-314.

Wiedicke, M., Neben, S., Spiess, V., 2001. Mud volcanoes at the front of the Makran accretionary complex, Pakistan. Marine Geology 172, 57-73.

Wilson, R.D., Monaghan, P.H., Osanik, A., Price, L.C., Rogers, M.A., 1974. Natural Marine Oil Seepage. Science 184, 857-865.

Wyrtki, K., 1973. Physical oceanography of the Indian Ocean, in: Zeitschel, B. (Ed.), Ecological Studies. Springer, Berlin, pp. 18-36.

Yun, J.W., Orange, D.L., Field, M.E., 1999. Subsurface gas offshore of northern California and its link to submarine geomorphology. Marine Geology 154, 357-368.

Zhang, J., Lee, J.W., 2008. Enhanced Kinetics of CO2 Hydrate Formation under Static Conditions. Industrial & Engineering Chemistry Research 48, 5934-5942.

Zillmer, M., Flueh, E.R., Petersen, J., 2005. Seismic investigation of a bottom simulating reflector and quantification of gas hydrate in the Black Sea. Geophysical Journal International 161, 662-678.

Zonenshain, L.P., Pichon, X., 1986. Deep basins of the Black Sea and Caspian Sea as remnants of Mesozoic back-arc basins. Tectonophysics 123, 181-211.

Acknowledgements

I could not have written this thesis without the support and contributions, whether being technical, scientific or mental in nature, of other people. First, I would like to thank Prof. Dr. Gerhard Bohrmann for providing me the opportunity to work on this PhD project in his working group. During the last three years Gerhard enabled me to develop my ideas and use unconventional methods in marine geology. I greatly benefited from the research cruises I participated in and Gerhard's support allowed me to develop towards a marine geoscientist.
Further, I would like to thank Prof. Dr. Heinrich Villinger for reviewing this thesis as a second reviewer.
I am thankful to Dr. Heiko Sahling who had many of the initial ideas this work is based on. Heiko spent a lot of time on reviewing manuscripts, discussing data, and methods. Thank you for keeping my focus on the 'scientific results'!
Further, I am grateful to Dr. Thomas Pape for the countless '5 minutes' during which he patiently unveiled geochemical and gas hydrate-related aspects of marine geology to me. Also, I greatly benefited from his thorough reviews of my abstracts or manuscripts.
I also thank Dr. Christian Melsheimer from the Department of Environmental Physics at the University of Bremen for being part of my thesis committee and for linking satellite remote sensing engineers with users.
Without the technical support with respect to hydroacoustic data and data processing by Christian dos Santos Ferreira and Paul Wintersteller I often would have remained puzzled. Also, without their work most of the bathymetry data which is presented in this work would not have been available. Thank you for all the great seafloor images!
I thank my PhD student colleagues (now Post-docs) David Fischer and Miriam Römer, and my former office-mates Stephan Klapp and Markus Brüning who helped me a lot and provided me a warm welcome in the beginning of my project. David deserves special thanks for enlightening me on various (bio)geochemical processes. I am grateful to Yann Marcon, with whom I shared the office for the longest time of my PhD project. Thank you for all the scientific and non-scientific discussions we had through the years, for being patient with my ventilation-mania, sharing the interest in technical aspects of science, and the passion for filter coffee. I would also like to thank Jiangong Wei, Tobias Himmler, Henry Wu, Michal Tomczyk, Tingting Wu, and Morten Iversen who made it a pleasure come to work every day. It is often the small talks and short breaks from work which make a day! I would like to give an extra big 'Thank you' to our secretaries Angelika Rinkel and Greta Ohling who do all the administration and keep the research group together. Without your support I would have gone lost in bureaucracy!
Special thanks go to Prof. Dr. Ian MacDonald and Dr. Oscar Garcia-Pineda for hosting me at Florida State University and sharing their knowledge on satellite image analysis with me.

I am indebted to my parents who did not only allow and encourage me to do what I want throughout my life, but also *enabled* me to do everything. If you had not shown me the world from earliest childhood on, I would probably not have developed my curiosity for nature. Without your constant support, especially during the last years, I could not have done this work!

Finally, my biggest thanks go to Heta for her absolute support. I am grateful for the hours and days you spent on proofreading, listening to the problems I might have faced, and worries I had. Thank you for comforting me and keeping up the faith in me. There are no words that could describe how much your love helped me during the last years and how much energy it is giving me every day! Home is where you are!

Jan-Hendrik Körber
Vorstraße 39
28359 Bremen

Erklärung

Gemäß § 6 Abs. 5 der Promotionsordnung der Universität Bremen für die mathematischen, natur- und ingenieurwissenschaftlichen Fachbereiche versichere ich hiermit, dass ich

1. die Arbeit ohne unerlaubte fremde Hilfe angefertigt habe,

2. keine anderen als die von mir angegebenen Quellen und Hilfsmittel benutzt habe und

3. die den benutzten Werken wörtlich oder inhaltlich entnommene Stellen als solche kenntlich gemacht habe.

Bremen, den 30.07.2012

Jan-Hendrik Körber